Biogenic volatile organic compounds in tropical, temperate and boreal forest ecosystems

Dissertation
zur Erlangung des Grades
"Doktor der Naturwissenschaften"
im Promotionsfach Chemie

am Fachbereich Chemie, Pharmazie und Geowissenschaften
der Johannes Gutenberg-Universität Mainz

Vorgelegt von
Gunter Eerdekens
geboren in Neerpelt, Belgien

Mainz, 2010

Tag der mündlichen Prüfung: 9. Dezember , 2010

ABSTRACT

Biogenic volatile organic compounds (BVOC) are emitted in large quantities into the lower troposphere primarily from terrestrial ecosystems, in particular forests. Surface fluxes of BVOCs are important in tropospheric chemistry because of their role in ozone and aerosol formation. The temporal and spatial variation of BVOC emissions and their role in the formation and the growth of aerosol particles remain uncertain.

Within this dissertation, data gathered using a proton transfer reaction mass spectrometry (PTR-MS) on three separate field campaigns is presented. The campaigns were located in tropical, temperate and boreal forests. The main advantage of the PTR-MS technique is the high measurement frequency which permits changes caused by transport, mixing and chemistry to be monitored on-line. PTR-MS measurements have been performed twice at ground based sites and once from a research jet aircraft.

In Chapter 3 the PTR-MS data collected by aircraft over the tropical rainforest is presented. The study highlighted, by comparison with a Single-Column, chemistry climate Model (SCM), the importance of the boundary layer dynamics on the distributions of tracers. The diurnal cycle of isoprene showed an average between 14:00 - 16:15 LT of 5.4 ppbv at canopy level and 3.3 ppbv above 300 m, indicating the role of turbulent exchange in diluting as well as the high reactivity of isoprene towards the oxidants OH and O_3. After correction for chemistry and entrainment fluxes, a maximum surface flux of 8.4 mg isoprene $m^{-2}h^{-1}$ has been estimated for the tropical rainforest in the Guyana region under partially clouded conditions with a mixing height up to ~1880 meter. This corresponds to a daily emission flux of 28.0 mg isoprene per square meter between 9:00 and 15:00.

The Single Column, chemistry climate Model used to support the analysis, is able to reproduce the diurnal profile provided that the temporal and vertical resolution within the model is sufficiently high to ensure a good representation of the boundary layer dynamics.

In Chapter 4 measurements made at a temperate latitude hill site in Southern Germany are presented. At this location, the boundary layer sank below the station's altitude at night, isolating the station from the ground based emissions. Trapped night time emissions within the boundary layer were observed at the station in the morning as the boundary layer rose again over the station. Clear increases in volatile organic species were characterised when air masses were transported to the site over the Munich metropolitan area. Data from this campaign have been used to examine changes in mixing ratios of volatile organic species associated with the passage of warm and cold fronts, as well as rain events.

Chapter 5 details PTR-MS measurements from a ground station in the boreal forest. Strong nocturnal inversions with low wind speeds trapped the nearby pine forest emissions leading to high night time VOC mixing ratios. Daytime and night time particle events during the campaign have been analysed in detail. The night time particle event occurred synchronously with huge increases in monoterpenes, while the second event type involved nucleation and was anti-correlated with sulphuric acid. Monoterpene mixing ratios of up to 16 ppbv are quite extraordinary for this time of the year. Low wind speeds and back trajectories suggest an intensive source nearby Hyytiälä. Optical stereoisomery of monoterpenes has confirmed the source to be unnatural as the ratio of [(+)-α-pinene]/[(−)-α-pinene] is much higher than the natural monoterpenes emissions reflect.

ZUSAMMENFASSUNG

Biogene flüchtige organische Verbindungen (BFOV) werden in großen Mengen aus terrestrischen Ökosystemen, insbesondere aus Wäldern und Wiesen, in die untere Troposphäre emittiert. Austausch-Flüsse von BFOVs sind in der troposphärischen Chemie wichtig, weil sie eine bedeutende Rolle in der Ozon- und Aerosolbildung haben. Trotzdem bleiben die zeitliche und räumliche Änderung der BFOV Emissionen und ihre Rolle in Bildung und Wachstum von Aerosolen ungewiss.

Der Fokus dieser Arbeit liegt auf der in-situ Anwendung der Protonen Transfer Reaktions Massenspektrometrie (PTR-MS) und der Messung von biogenen flüchtigen organischen Verbindungen in nordländischen, gemäßigten und tropischen Waldökosystemen während drei unterschiedlicher Feldmesskampagnen. Der Hauptvorteil der PTR-MS-Technik liegt in der hohen Messungsfrequenz, wodurch eine eventuelle Änderung in der Atmosphäre durch Transport, Vermischung und Chemie online beobachtet werden kann. Die PTR-MS-Messungen wurden zweimal am Boden aus und einmal von einem Forschungsflugzug durchgeführt.

In Kapitel 3 werden die PTR-MS-Daten, gesammelt während der Flugmesskampagne über dem tropischen Regenwald, vorgelegt. Diese Studie zeigt den Belang der Grenzschichtdynamik für die Verteilung von Spurengasen mittels eines eindimensionalen Säule - Chemie und KlimaModells (SCM). Der Tagesablauf von Isopren zeigte zwischen 14:00 und 16:15 Uhr lokaler Zeit einen Mittelwert von 5.4 ppbv auf der Höhe der Baumspitzen und von 3.3 ppbv über 300 m Höhe. Dies deutet darauf hin, dass sowohl der turbulente Austausch als auch die hohe Reaktionsfähigkeit von Isopren mit den Oxidantien OH und Ozon eine wichtige Rolle spielen. Nach dem Ausgleich von chemischen Verlusten und Entrainment (Ein- und Ausmischung von Luft an der Grenzschicht), wurde ein Fluss von 8.4 mg Isopren $m^{-2}h^{-1}$ unter teilweise bewölkten Bedingungen für den tropischen Regenwald in der Guyanregion abgeschätzt. Dies entspricht einem täglichen Emissionsfluss von 28 mg Isopren pro Quadratmeter.

Im Kapitel 4 werden die Messungen, welche auf einer Hügellage in gemäßigter Breite in süddeutschland stattgefunden haben, diskutiert. Bei diesem Standort ist die Grenzschicht nachts unter die Standorthöhe abgefallen, was den Einsatzort von Emissionen abgesondert hatte. Während die Grenzschicht morgens wieder über die Höhe des Einsatzortes anstieg, konnten die eingeschlossenen nächtlichen Emissionen innerhalb der bodennahen Schicht beobachtet werden. Außerdem wurde ein deutlicher Anstieg von flüchtigen organischen Verbindungen gemessen, wenn die Luftmassen über München geführt wurden oder wenn verschmutzte Luftmassen aus dem Po-Tal über die Alpen nach Deutschland transportiert wurden. Daten von dieser Kampagne wurden genutzt, um die Änderungen in dem Mischungsverhältnis der flüchtigen organischen Verbindungen, verbunden mit dem Durchfluss von warmen und kalten Wetterfronten sowie bei Regen zu untersuchen.

Im Kapitel 5 werden PTR-MS-Messungen aus dem nördlichen Nadelwaldgürtel beschrieben. Starke nächtliche Inversionen mit einer niedrigen Windgeschwindigkeit fingen die Emissionen von nahegelegenen Kiefernwäldern und andere BFOV-Quellen ab, was zu hohen nächtlichen BFOV-Mischverhältnissen führte. Partikelereignisse wurden für Tag und Nacht detailliert analysiert. Die nächtlichen Partikelereignisse erfolgten synchron mit starken extremen von Monoterpenen, obwohl das zweite Ereignis Kernbildung einschloss und nicht mit Schwefelsäure korrelierte. Die Monoterpen Mischungsverhältnisse von über 16 ppbv waren unerwartet hoch für diese Jahreszeit. Niedrige Windgeschwindigkeiten und die Auswertung von Rückwärtstrajektorien deuten auf eine konzentrierte Quelle in der Nähe von Hyytiälä hin. Die optische Stereoisomerie von Monoterpenen hat bestätigt, dass die Quelle unnatürlich ist, da das Verhältnis von [(+)-α-pinen]/[(−)-α-pinen] viel höher ist als das natürliches Verhältnis der beiden Enantiomeren.

TABLE OF CONTENTS

Important remark:

Chapter 3 has been published in Atmospheric Chemistry and Physics, 9, 4207-4227, 2009. However, new insights have been obtained by further analysis after publication. It is therefore recommended to refer to the chapter in this dissertation in scientific publications.

1 Introduction

The atmosphere is a dynamic system in which biogenic and anthropogenic gaseous and particulate constituents can be introduced, transported, as well as physically and chemically transformed. In general, the spatial and temporal variability of any atmospheric tracer is determined by the balance between the rate at which it is introduced into the atmosphere (its source), and the rate at which it is removed from the atmosphere (its sink). Eq. 1-1 represents the total change in the concentration *c* of an atmospheric tracer *i* as function of time as a combination of the different processes that affect its concentration such as emission, transport, chemistry and deposition to name the most important processes.

$$\frac{\partial c_i}{\partial t} = \left[\frac{\partial c_i}{\partial t}\right]_{EMISSIONS} + \left[\frac{\partial c_i}{\partial t}\right]_{TRANSPORT} + \left[\frac{\partial c_i}{\partial t}\right]_{CHEMISTRY} + \left[\frac{\partial c_i}{\partial t}\right]_{DEPOSITION} + \ldots \qquad \text{E 1-1}$$

These processes will be explained in Chapter 1 with regards to volatile organic compounds (VOCs), the atmospheric tracers of interest in this study. Volatile organic compounds are a variety of compounds composed primarily of carbon and hydrogen, and are described as volatile because of their tendency to evaporate at normal pressures and temperatures.

VOCs are generally present at relatively low concentrations (pmol/mol - nmol/mol or pptv - ppbv) and have short atmospheric residence times (hours to days). All VOCs together are emitted daily and in relatively large quantities into the atmosphere from both anthropogenic and natural sources. Globally the biogenic source (~1300 TgC, Guenther et al., 2006, 1Tg C= $x10^{12}$ g C) of VOCs outnumbers the anthropogenic (~150 TgC, Müller, 1992, Fuentes et al., 2000).

Since most VOCs are emitted directly into the planetary boundary layer the structure and temporal variability of this layer is described in detail in Chapter 1 and the sources and chemistry of the main VOC species investigated here are described in this comprehensive introduction. Despite their low concentration in the atmosphere VOCs can have a profound effect on ozone and thereby on the Earth´s oxidative capacity and radiative budget. The underlying chemistry is summarized within this introductory chapter.

Chapter 2 describes Proton Transfer Reaction Mass Spectrometry (PTR-MS), the instrument and its principle of operation used for quantification of the VOCs. Such instrument has been deployed on all three field campaigns presented in this dissertation. This chapter includes the campaign instrumental settings as inlet configurations for each campaign.

The focus of this work has been on assessing the source characteristic of various vegetation types (tropical forest - chapter 3, temperate forest - chapter 4, and boreal forest - chapter 5).

Chapter 3 presents the results of measurements made from an aircraft covering N 3 - 6 °, W 50 - 58° and generally up to 7 km over the tropical rainforest. The results from 8 flights during the GABRIEL 2005 campaign are used to assess the diel, vertical and horizontal variations in VOC and in the boundary layer height and concludes by estimating the fluxes of isoprene, methanol and acetone.

Chapter 4 covers the analysis of ground-based campaign data from an Observatory located in southern Germany (N 47° 48', E 11° 00'). This HOHPEX04 campaign was conducted within a forest at temperate latitudes and was subject to multiple rain associated frontal passages. In this chapter the impact of these

events on the mixing ratios of the VOCs is examined with particular focus on oxygenated organic compounds.

Chapter 5 covers the ground-based measurements during the BACCI4-QUEST–campaign which took place in spring 2005 in the boreal pine forests of southern Finland (N 61°51', E 24°17'). Variations in the observed VOC mixing ratios are examined as a function of meteorological parameters, height above the surface, back trajectories, and boundary layer height. Interestingly, during this period of measurement several aerosol "events" took place. The VOC measurements have been used in this study to distinguish two distinct forms of aerosol production and to identify a strong nearby source that periodically will affect the measurement site

The final chapter summarises the findings by examining the relationship of acetone and methanol from Equator and Arctic.

1.1 Biogenic emissions

The terrestrial biosphere plays a critical role in the global carbon cycle as green plants sequester carbon dioxide from the atmosphere and convert it into organic compounds by using solar energy through photosynthesis and releasing oxygen as a by product (121 PgC/yr, 1 Pg=$1x10^{15}$g). Through the processes of respiration, solar energy conserved during photosynthesis and stored as chemical energy in organic molecules, is released. Respiration, which leads to the return of 60 PgC/yr, is essential for growth and maintenance of all plant tissues, and plays an important role in the carbon balance of individual cells, whole-plants and ecosystems.

Vegetation is the principal VOC source to the atmosphere. Direct plant emissions may include isoprenoids, terpenoids and various oxygenated compounds (oVOCs) such as aldehydes, organic acids, esters and alcohols. Many biogenic molecules consist of at least one olefinic double bond thus making the VOC extremely reactive towards atmospheric oxidising agents (OH, O_3, NO_3) which eventually oxidise the VOC to CO_2. See next section for details.

Although in plants, trace gas exchange is clearly dominated by the emission and uptake of carbon dioxide, water vapour and oxygen, they also produce and emit a class of trace gases collectively termed biogenic volatile organic compounds (BVOCs). These emissions can be a significant fraction of the carbon budget of a forest, and make up ~1.3 Pg C/yr globally.

1.1.1 Biogenic volatile organic compounds

Some of these BVOCs have important roles in plant physiology and signalling, in plant-herbivore relationships, and in defence against micro organisms (Roshchina and Roshchina, 1993). A major activity within atmospheric chemistry besides identifying compounds and studying their reactivity has been the determination of emission and deposition fluxes from natural systems.

BVOC emission from plants is limited by both physiological and physicochemical factors. The physiological factors determine the availability of BVOC precursors and rate-controlling enzymes. The physicochemical factors limit the volatility (temperature, air-phase partial pressure, aqueous- and lipid-phase concentrations), the diffusion within gaseous, aqueous and lipid phases of organic compounds within the leaves, and the gas-phase diffusion at the leaf-atmosphere interface (Niinemets et al., 2004).

BVOCs can enter the atmosphere by diffusion through the stomata, followed by diffusion through the laminar leaf boundary layer, transport by turbulence through the canopy layers and into the overlying surface layer (Baldocchi et al., 1995). Some of these BVOCs are emitted in surprisingly large amounts and have high enough chemical reactivity to represent one of the most important ways in which plant processes influence the composition and functioning of the atmosphere (Harley et al., 1999; Fuentes et al., 2000; Lerdau et al., 1997). These BVOCs function as ozone precursors and therefore indirectly as absorbers of radiation (Trainer et al., 1987; Chameides et al., 1988).

BVOC emission also depends on sunlight, ambient CO_2 concentration, genetics, leaf development, and phenological events. BVOCs emission rates are species specific, which can vary by as much as four orders of magnitude depending upon plant species. Variation in biomass density and physiological status of vegetation may also affect emission. Accordingly, BVOC emission from vegetation is sensitive to land cover changes (plant species composition and dominance) and environmental conditions.

It is important to understand the factors that determine the strength of VOCs sources, and the subsequent impact of transport and chemistry on their ambient concentration. In this regard in-situ observations are essential, ideally in conjunction with model results to verify the emission and transformation algorithms. Figure 1-1 summarises the key processes in which the BVOCs are involved. It should be borne in mind that many of the processes depicted are still poorly understood.

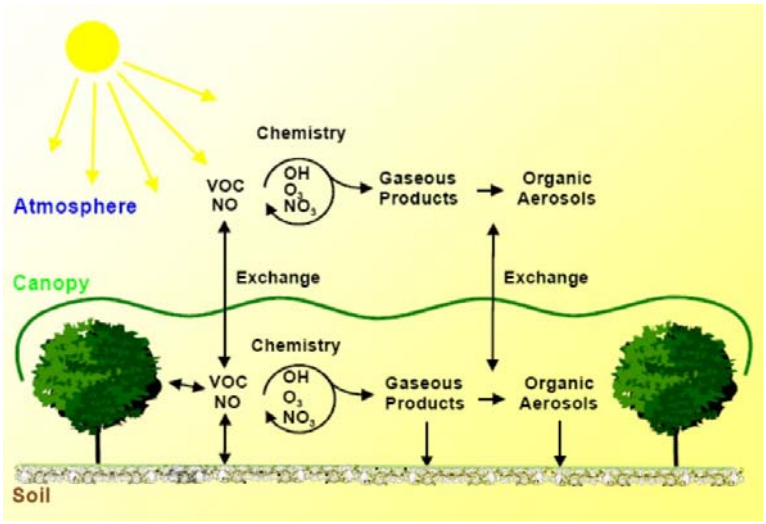

Figure 1-1 Schematic on the emission and chemical transformation of biogenic volatile organic compounds in and above a forest canopy.

Leaf, canopy and ecosystem flux measurements are needed to develop and validate regional and global VOC emission models. Over the past 20 years, studies of BVOC emissions from vegetation have used various types of enclosure systems to capture the emissions of individual leaves, branches or entire plants, and estimate emission rates from the increase in concentration over time. These enclosure systems determined which BVOC emissions occur and their relative contribution for many plant species. Enclosure studies continue to be the prime source of emission factors and emission algorithms used in BVOC emission models. As enclosure studies may in some cases exert an influence on the emissions (e.g. different BVOC from plants under stress; measurement uncertainties), current studies continue to refine and improve existing measurement techniques and extend them into new landscapes and new chemical species. With increased understanding of additional environmental controls over BVOC emissions, enclosure studies are utilized to develop new algorithms that account for a more complete set of driving variables.

The most significant advancement is the capability for direct measurements of BVOC fluxes using eddy covariance (e.g., Guenther and Hills, 1998; Karl et al., 2001b). These setups not only provide more accurate flux estimates but also enable continuous measurements and the ability to look at a wider range of BVOCs including oxygenated volatile organic chemicals (oVOCs) which have been found to be ubiquitous components of the global troposphere (Singh et al., 2001).

Eddy covariance systems are now being used as the primary means of establishing area average emission factors in regions with high species diversity, such as tropical rainforests (Rinne et al., 2002), where it is difficult to characterize the emission characteristics of all of the tree species present.

Current biogenic emissions models are parameterised and used to quantify net terrestrial biosphere emission of BVOCs into the atmosphere. Examples of such emission models are "Biogenic Emissions Inventory System" (BEIS) (Lamb et al., 1993), "A global model for natural volatile organic compounds" introduced by Guenther et al., (1995), and the more recent "Model of Emissions of Gases and Aerosols from Nature" (MEGAN) (Guenther et al., 2006). MEGAN is designed for both global and regional emission modelling and has global coverage with ~1 km^2 spatial resolution. The MEGAN emission algorithm used in chapter 3 to describe the emissions of isoprene still requires a full operating model that deals with the other important processes as chemistry, transport. The annual global emission estimated depends on the driving variables that are used. Global emissions from plants are estimated to be very large, ~1300 Tg C yr^{-1}. Evidence by Guenther et al., (1995) and Fall, (1999) suggested that, in addition to isoprene and monoterpenes, plants emit on the order of ~529 Tg C yr^{-1} of other VOCs. ~260 Tg C yr^{-1} of organic reactive volatile compounds and the remainder of ~260 Tg C yr^{-1} is formed by other volatile compounds. Biogenic emissions exceed anthropogenic emissions of organic compounds by an order of magnitude.

Nowadays, research not only focuses on quantifying the present day emissions but also tries to predict VOC emissions under future conditions due to climate change (e.g. temperature extremes, elevated CO_2 and O_3 mixing ratios) and to validate the currently assumed emission algorithms for climate extremes.

1.1.2 **Isoprene**

Isoprene (2-methyl 1,3-butadiene, C_5H_8) is principally released by deciduous trees as a by-product of photosynthesis and/or photorespiration (Fehsenfeld et al., 1992; Guenther et al., 1994; Zimmerman et al., 1988) and is instantaneously produced in chloroplasts from photosynthetically fixed carbon (Delwiche and Sharkey, 1993; Monson and Fall, 1989). Foliage temperature and intercepted photosynthetic active radiation (PAR) exert the greatest environmental influence on the release of isoprene from vegetation, and emission rates increase with increasing temperatures and light. Temperature regulates the enzymatic (isoprene synthase) activity responsible for isoprene biosynthesis (Silver and Fall, 1991), whereas PAR mediates the increased metabolite substrates required to form isoprene (Loreto and Sharkey, 1993). Because phytogenic hydrocarbons such as isoprene are linked to photosynthesis (Monson and Fall, 1989; Sharkey et al., 1991), they also constitute a source of atmospheric carbon and can thus play a key role in the global carbon budget and cycling. There's still a great deal of uncertainty on why plants release isoprene, although current thinking is that many plants emit isoprene as a mechanism to cope with thermal stress (Sharkey and Singsaas, 1995).

When measured in a forest, isoprene concentrations generally follow a pattern of steady increase throughout the morning, responding to radiation and temperature, followed by a peak concentration around mid-afternoon, with slow decay throughout the afternoon (see also chapter 3). This emission pattern has been studied in depth and emission algorithms derived (Guenther et al., 2006; Guenther et al., 1995). These are then used to model the global trace gas emissions from terrestrial vegetation. Isoprene emissions are estimated to be half of the total global BVOC emissions. The annual global emission estimated based on the MEGAN algorithm ranges from about 500 to 750 Tg isoprene (or 38 - 57%) depending on the driving variables that are used and can differ by more than a factor of 3 for specific times and locations.

The emission rate is dependent on the plant species, considerably complicating the characterisation of biogenic emissions from biodiverse tropical forests (with more than 5,000 different species per 10,000 km^2). Although most studies have been performed in a bottom-up approach, scaling up from leaves to trees or from trees to ecosystem, there is need for flux measurements on a region scale to validate models as will be discussed in Chapter 3.

1.1.3 **Terpenes**

Monoterpenes (consisting of two isoprene units) are a large class of biogenic $C_{10}H_{16}$ hydrocarbons and may be linear (acyclic) or contain rings (mono- or bicyclic). This latter group includes the commonly observed species α-pinene, Δ^3-carene and ß-pinene. Monoterpenes are emitted from conifers as well as broad-leaved trees (Kesselmeier and Staudt, 1999). Their emissions can be strongly dependent on light as well as temperature, and represent a significant fraction of the total VOC flux from the biosphere to the atmosphere (120–480 Tg C y^{-1} or 10 - 42% of the total VOC emissions, Guenther et al., 1995). The mechanisms for their formation (Fall, 1999) and rates of emission, plus their roles in atmospheric chemistry (Fehsenfeld et al., 1992) have been studied extensively. Monoterpenes are highly reactive and can be oxidised by ozone, as well as the hydroxyl and nitrate radicals, with lifetimes that range from days to minutes (Fuentes et al., 2000).

Less well characterised and quantified are the emissions of sesquiterpenes (consisting of three isoprene units, $C_{15}H_{24}$). These compounds have been identified to play an important role in defence and communication mechanisms (chemically mediated plant–insect interactions) of injured plants. Substantial uncertainties in sesquiterpene emission rates arise from the lack of proven analytical techniques for sesquiterpene identification and from their losses to walls of canisters and inlet tubes. They are far more reactive than isoprene and monoterpenes. Sesquiterpenes atmospheric lifetimes from their reactions with ozone, and the OH and NO_3 radicals have been estimated to be only a few minutes (Shu and Atkinson, 1995).

Measurement of the atmospheric concentrations and biogenic emission rates of the monoterpenes and related VOCs are necessary if their roles in plant biochemistry, plant physiology, atmospheric chemistry and aerosol formation are to be understood and quantified. Both monoterpenes and Sesquiterpenes contribute to aerosol nucleation and growth (Bonn and Moortgat, 2002, 2003; Koch et al., 2000; Bonn et al., 2007a), which will be examined in Chapter 5 of this dissertation. These nucleation processes can occur within the canopy compromising many commonly used above canopy flux measurements. Therefore, in order to estimate landscape fluxes for many of these compounds, it is necessary to measure emissions at the leaf or branch level and scale these values to the canopy level by using detailed information on leaf and canopy characteristics.

1.1.4 **Oxygenated VOCs**

Methanol (CH_3OH) and acetone (CH_3COCH_3) have been identified as a natural emission product from various plants (Fall and Benson, 1996) and as biological decomposition products of decaying plant matter (Warneke et al., 1999). A major fraction of methanol emissions arise in the cell walls of plants as a byproduct of the pectin (a polysaccharide) methylesterase reaction, an enzymatic process that occurs in the apoplast, the free diffusional space outside the plasma membrane. Methanol is in direct contact with leaf air spaces and is released from plants primarily by transport in the transpiration stream with exit from leaf surfaces via stomatal pores and thus stomatal conductance affects the emissions (Fall and Benson, 1996).

Studies have reported typical mixing ratios of 1–10 ppbv in the continental boundary layer and 0.1–1 ppbv in the remote troposphere (Singh et al., 1995; Goldan et al., 1997; Holzinger et al., 2001; Schade and Goldstein, 2001). Unless measured very close to their sources, the mixing ratios of the classic plant emissions isoprene and monoterpenes are generally smaller due to their short atmospheric lifetimes. Only compounds such as formaldehyde and acetaldehyde whose atmospheric sources are dominated by secondary formation, sometimes rival the methanol and acetone abundance. Methanol emissions represent approximately 6% of the identified terrestrial biogenic organic carbon sources to the atmosphere (Heikes et al., 2002; Fall, 1999) and is the second most abundant hydrocarbon in the atmosphere after methane.

Formaldehyde (HCHO) and acetaldehyde (CH_3CHO), the most ubiquitous aldehydes in the environment, can be directly emitted from plants. Within leaves, acetaldehyde can be enzymatically oxidized to acetate and metabolically consumed (Fall, 2003), and as a result exchange with the atmosphere is bi-directional, with the net flux determined by temperature and light levels, by the ambient acetaldehyde concentration, and by stomatal conductance (Jardine et al., 2008; Kesselmeier, 2001). Rottenberger et al., (2004) concluded from their study that the tropical forest acts rather as a sink than as a direct source for formaldehyde and acetaldehyde. They have concluded that the diel cycles of ambient air concentrations and ratios of formaldehyde and acetaldehyde above the canopy suggest photochemical oxidation of biogenically or pyrogenically emitted precursor compounds as the major sources for short-chain aldehydes in the tropical atmosphere.

Formaldehyde is formed naturally in the troposphere during the OH and O_3 oxidation of hydrocarbons e.g. methane, or isoprene. The largest source of atmospheric acetaldehyde is thought to be photochemical degradation in air of VOCs such as $>C_1$ alkanes and $>C_2$ alkenes (Atkinson et al., 2006b). Acetaldehyde is also produced in surface waters from photo-degradation of dissolved organic matter (Kieber et al., 1990), and subsequently emitted to the atmosphere (Sinha et al., 2007b). Acetaldehyde plays an important role in the atmosphere as a source of ozone, peroxyacetyl nitrate (PAN) (Roberts, 1990) and HO_x radicals (Singh et al., 2004). Sources of atmospheric acetaldehyde are poorly understood. Contributions may also come from isoprene and ethanol oxidation. Ethanol is of particular interest as a renewable alternative to fossil fuel. Ethanol combustion emissions consist largely of unburned ethanol itself (Jacobson, 2007) which is then oxidized to acetaldehyde.

Known primary, anthropogenic emissions of oVOCs include sources of e.g. acetone from solvent usage, acetaldehyde from combustion, methanol from biofuel. Secondary emission occurs as byproducts of atmospheric oxidation of hydrocarbon species such as ethane and propane. The atmospheric lifetimes of oxygenated VOCs are relatively short (<24 h–14 days), controlled by a combination of chemical, photolytic and physical removal processes. These relatively short lifetimes have proven difficult to reconcile with the presence of some oVOCs (acetaldehyde) at both high altitudes and in remote locations.

The biogenic sources of other C_1-C_3 oxygenated VOCs are relatively large but not as large as those of methane and isoprene. Global estimates of 38-105 Tg C/yr (methanol), >25-59 Tg C/yr (acetone) and 44-88 Tg C/yr (acetaldehyde) have been summarised by Fall, (2003).

Recent evaluation of global acetaldehyde sources and sinks by Millet et al., (2009) using a 3D model of atmospheric chemistry (GEOS-Chem), using an ensemble of observations (including our results from field campaigns discussed in chapter 3, 4 and 5) concluded that hydrocarbon oxidation provides the largest acetaldehyde source in the model (128 Tg /yr), mainly from alkanes, alkenes, ethanol, and isoprene. Sea-to-air acetaldehyde flux calculations on the basis of measured photoproduction rates from dissolved organic matter have resulted in a net ocean emission is 57 Tg /yr, the second largest global source of acetaldehyde. Terrestrial acetaldehyde sources include direct emissions from live and decaying plants (36 Tg/yr), biomass burning (3.3 Tg /yr), and anthropogenic sources (2.0 Tg /yr). The principle sink of atmospheric acetaldehyde appears to be reaction with OH, giving an atmospheric lifetime on the order of one day (Atkinson et al., 2006a). Other sinks include photolysis (Sander et al., 2006) and wet and dry deposition (Custer and Schade, 2007; Karl et al., 2004b; Warneke et al., 2002).

1.1.5 **VOC emissions due to plant wounding and stress**

When VOCs accumulate in specialised organs of leaves, stems or trunks, they can be released rapidly in large amounts after wounding. Plant wounding has been recognised recently as a tropospheric source of acetaldehyde (e.g. Karl et al., 2001a). Some studies mentioned the release under various physiological conditions, including during normal photosynthesis and transpiration (Kesselmeier and al., 1997) and after root flooding (Kreuzwieser et al., 2001).

Wounding emissions are thought to act as a powerful deterrent against pathogens and herbivores, and to contribute to wound sealing.

Wounded or drying plant leaf material can emit numerous VOCs (Fall et al., 1999). Typical wound C_6-VOCs from leaves including (cis and trans) hexenals, hexenols, and hexenyl acetates, are produced via several steps following enzymatic breakdown of membrane lipids following chloroplast disruption and has been reviewed in-depth by Hatanaka, (1993). Another family of wound compounds, including carbonyls and HCN, arises from the breakdown of cyanogenic glycosides by enzymes when a cell is ruptured (Conn, 1991; Custer et al., 2002). A different emission pattern has been observed by Fall et al., (2001) when a variety of leaves were subject to freeze–thaw damage. Here, C_6-VOCs were accompanied by comparable amounts of C_5-VOCs like 1-penten-3-ol and 1-penten-3-one (Fishera et al., 2003 and references therein).

Wounded needles, either illuminated or darkened, massively release monoterpenes contained in the ducts (Loreto et al., 2000) and are emitted in different proportionalities (Yassaa and Williams, 2007).

1.2 Anthropogenic VOCs and biomass burning

The most important sources of anthropogenic hydrocarbons are: fossil fuel combustion; direct release from industry, and industrial processing of chemicals and waste. The global estimated anthropogenic hydrocarbon flux is approximately 100 Tg C yr^{-1} (Singh and Zimmerman, 1992; Müller, 1992; Piccot et al., 1992) which amounts to only 10% of the total global BVOC emission. Regionally the proportions can be different, for example European anthropogenic and biogenic VOC are more comparable in magnitude; biogenic VOC emissions are estimated at ~14 Tg C yr^{-1}, and man-made around 24 Tg C yr^{-1} (Simpson et al., 1999).

Aromatic hydrocarbons, like benzene (C_6H_6) and toluene (C_7H_8) which have mainly anthropogenic sources, are of great interest especially in urban areas, not only because of their high ozone-forming potential (e.g., Derwent et al., 1996) but also because of their direct health effects. They constitute a substantial fraction of VOC emission from traffic (Singh et al., 1985). Atmospheric concentrations of benzene and toluene have been observed at several remote locations of the world ranging in latitude from inside the Arctic Circle to the South Pole. (Rasmussen and Khalil, 1983). In the northern hemisphere benzene and toluene are observed to be most abundant during winter and least abundant during summer. Based on the limited data available, such cycles are not observed in the tropics. These findings are consistent with the expected latitudinal and seasonal variations of OH radicals. The observed concentration distribution and variability are consistent with the atmospheric lifetime of the order of weeks for benzene and days for toluene

The difference in atmospheric lifetimes between two species emitted from a common source can be exploit to determine the extent of photochemical processing that a given airmass has undergone prior to measurement (Clarkson et al., 1996). After prolonged photochemical degradation of an air mass, the benzene:toluene ratio increases as the more reactive toluene is preferentially removed. (Atkinson, 1990). However, ‘fresh’ anthropogenic pollution contains considerably higher levels of toluene than benzene (>~4:1) a result of emission profiles at source. Dispersion and dilution processes also occurring during transport affect both species equally, having no impact on the change in ratios observed. Such approaches are employed in chapter 4 and 5 to assess the photochemical age in the boundary layer.

In many areas throughout the world wood combustion / biomass burning is one of the most important sources of a large number of pollutants including oVOCs, benzene, toluene and xylenes (BTX) (Christian et al., 2004), but also polycyclic aromatic hydrocarbons (PAHs), and particulate matter.

Frey et al., (2009) has recently shown for residential wood combustion that fine particle emissions strongly depend on combustion air supply as well as the log and batch size. Poor operation in log-wood combustion leads to a low burning temperature and insufficient oxidation of the flue gases causing

smouldering combustion which increases the particulate emissions significantly, about 3 times the normal combustion conditions. Related to low burning temperatures are the formation of oxygenated compounds and CO. Better combustion air supply and a higher combustion temperature in normal combustion decreases the release of organic carbon in comparison to elemental carbon.

Biomass burning, as well as the natural direct emission of biogenic compounds is significant source of oxygenated compounds (Singh et al., 1994; Jacob et al., 2002; Holzinger et al., 1999). The emissions of oxygenated volatile organic compounds such as methanol, acetonitrile, acetaldehyde, acetone, acetic acid, furan, acetol, pyrazine, 2,3 butadione, phenol, furylaldehyde, benzaldehyde, and terpenes may even dominate during the heating of the vegetation (Greenberg et al., 2006).

Acetonitrile (CH_3CN) is emitted into the atmosphere as a byproduct of combustion processes. The main global source of this compound is from biomass burning, with an additional minor contribution from are automobile exhaust gases (Holzinger et al., 2001). Thus, acetonitrile can be used as an indicator for biomass burning influenced emissions. Holzinger et al. (1999; 2001) analysed by relative enhancements of e.g. acetonitrile in biomass burning plumes and indicated that contributions of around 10 % of acetone and 15 % of methanol can occur to the atmospheric burden. Reported tropospheric acetonitrile mixing ratios range between approximately 20 and 8000 pptv, but a global average value has been estimated to be 82 pptv (Hamm and Warneck, 1990). Measurements of acetonitrile are used in chapter 3 and 5 to determine the extent of biomass burning influence at each site.

1.3 Organic Aerosol particles

Aerosol research became in the recent decade a major branch in atmospheric science, mainly due to the high importance but also high uncertainty related to particle processes in the atmosphere and in the climate system.

Some gas phase organic species can, following emission to the atmosphere transform into aerosol. This gas-to-particle conversion may proceed via different pathways and contribute to the growth of pre-existing particles or to the formation of new particles. In addition to this secondary organic aerosol production, direct emission of primary organic or inorganic particles may occur (see Figure 1-2).

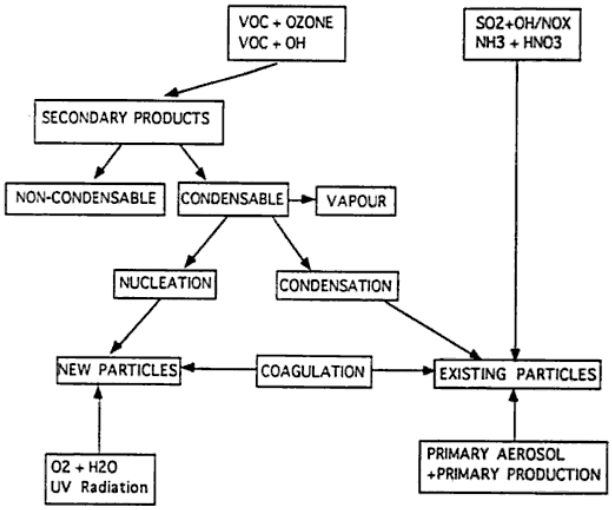

Figure 1-2 Principle pathways for particle production from organic and inorganic traces gases.

New particle formation events have been observed to occur over large spatial scales, implying that the processes driving these events are regional, rather than local, in nature (Vana et al., 2004). Several investigators have observed spontaneous new particle formation events in the continental boundary layer of remote boreal forests (Mäkelä et al., 1997; Kulmala et al., 1998, chapter 5) coastal environments in Europe (O'Dowd et al., 1998) and forested ecosystems in mountainous regions (Weber et al., 1997).

These events are characterised by the observation of ultra-fine particles detected at a few nanometres in size and subsequent condensational growth to the 100 nm size range within 1 to 2 days (Kulmala et al., 2004) leading to a characteristic “banana-shaped” evolution of the particle size distribution (as shown in chapter 5).

Despite extensive research efforts, both experimental and theoretical, many aspects of the mechanism for atmospheric new particle formation remain elusive. Known, favourable conditions for nucleation include a strong source of condensable vapour, high UV radiation intensity, low ambient aerosol surface area, high relative humidity, low temperature, and atmospheric mixing processes.

Perhaps the most widely accepted theory for nucleation events (Kulmala et al., 2000) postulates that ternary nucleation of sulphuric acid, ammonia and water explains the appearance of thermodynamically stable clusters in the 1–2 nm size range. However, the concentrations of sulphuric acid are generally too low to allow the clusters to grow beyond the 3 nm detection limit of modern aerosol instruments before they are scavenged during collisions with large aerosol particles. Co-condensation of H_2SO_4 and BVOC oxidation products are required to explain the observed growth dynamics. Theoretical calculations have identified that the formation of an unusually stable aromatic acid–sulphuric acid complex likely leads to a reduced nucleation barrier. The results imply that the interaction between organic and sulphuric acids promotes efficient formation of organic and sulphate aerosols in the polluted atmosphere because of emissions from burning of fossil fuels, which strongly affect human health and global climate (Zhang et al., 2004).

Atmospheric aerosols often contain a substantial fraction of organic matter but the incorporation of these organics into aerosols can occur in many different ways, many of which are not well understood because, at present, comprehensive information about the organic species participating in the nucleation process is not available. The chemical analysis of aerosol particles is a very challenging task. Organic species are often present at trace levels, the number of compounds present in the particles is extremely large, and the chemical and physical characteristics of the compounds vary a great deal.

While turbulent vertical fluxes of several trace gases between ecosystems and the atmosphere are occasionally measured, the direct measurement of aerosol particle fluxes is more challenging. In order to study biosphere/atmosphere interactions with regard to particles, detailed information on particle formation and transformation as well as turbulent particle exchange is required. Needed are time-resolved measurements of specific organic marker compounds in order to get a more detailed understanding of such issues. The understanding is required to predict how these reactions affect particles' abilities to participate in further reactions, take up water, act as cloud-condensation nuclei and grow. Quantitative measurements of aerosol formation and growth rates have required the recent developments in instrumentation for measuring size distributions down to sizes as small as 3 nm in diameter (McMurry, 2000). However, the phase change between vapour and liquid will occur at still smaller sizes, typically around 1 nm in diameter, which cannot be measured by Differential Mobility Particle Sizer systems, which have cut off sizes of 3 nm. It is suspected that the vapours causing the condensational growth of the clusters to observable sizes are low vapour pressure organic species whose exact chemical nature is unknown. Only recently, combined measurements with DMPS and ion spectrometers can be used to study formation and growth of aerosol particles focusing particularly in the initial steps of the growth. In principle the initial steps of the growth can occur via several ways: condensation of nucleating vapours, activation of soluble vapours, heterogeneous nucleation or ion mediated particle formation (Yu and Turco, 2000). In recent years aerosol mass spectrometry has become available as a powerful tool for the on-line chemical characterization of individual aerosol particles (Murphy, 2007) or small aerosol ensembles (Canagaratna et al., 2007).

Recently de Gouw and Jimenez, (2009) have reviewed the latest results from field studies on the sources of organic aerosol and concluded that urban SOA formation could be a much larger source than

previously recognised at northern mid latitudes and that biomass burning is possibly the largest source of SOA on a global scale. They also stress the further research on many of these aspects is needed.

Estimates of global organic aerosols formed through BVOC oxidation range from 19 Tg yr^{-1} to 270 Tg yr^{-1}. These estimates are quite uncertain because the emission rates of certain particle producing gas-phase BVOCs, such as sesquiterpenes, are poorly known. In addition, these estimates do not consider changes in all of the relevant environmental variables that affect secondary organic aerosol formation.

Besides being a sink of VOCs, organic aerosol can be a source of oxidised VOCs. Organic matter in aerosols affects their water uptake potential and in turn on cloud condensation nuclei (CCN) property. This has impactions for cloud formation and climate as secondary organic material is found to significantly absorb solar radiation in the tropospheric actinic window ($\lambda > 300$ nm). The ensuing photolysis of SOA constituents modifies the SOA chemical composition and leads to emission of small volatile molecules back into the gas-phase which then have the potential to change the oxidative capacity of the surrounding environment (Kwan et al., 2006).

Aerosol events will be a focus of chapter 5 in which aerosol particle events observed over the boreal forest are discussed.

1.4 Transport and mixing

Nearly all the energy which drives the large scale weather and general atmospheric circulation comes through the planetary boundary layer, the lowermost layer of the Earth's atmosphere (Arya, 1988). These large scale phenomena are being fed by the energy involved in small scale processes which are therefore important in determining the evolution of atmospheric constituents. Knowledge on the PBL height is of special importance to local and regional air studies as it hinders mixing of air and as a result of strong gradients in trace constituents can develop and will therefore be more specially addressed for each measurement location in Chapters 3, 4, and 5 of this dissertation. We therefore introduce here the most important processes that influence the distribution of trace gases in the troposphere.

1.4.1 Planetary Boundary Layer

The planetary boundary layer (PBL), the lowest part of the troposphere (<1-2 km), is directly influenced by the presence of the Earth's surface, and responds to surface forcings with a time scale of about an hour or less (Stull, 1988). Its depth or height varies significantly with time of a day (see Figure 1-3 for a diel evolution), latitudinal position and with meteorological conditions. The PBL height, corresponding to an inversion under clear sky conditions which is a strong barrier for the transport of heat, momentum and matter from or to the earth's surface.

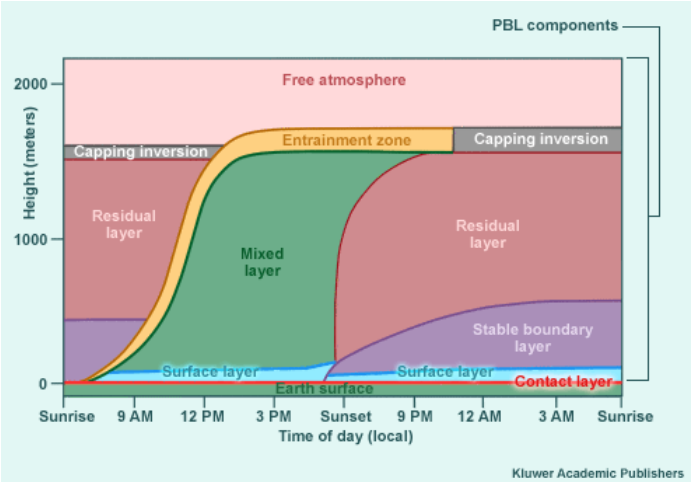

Figure 1-3 A typical evolution of layers within the planetary boundary layer

Two physical processes drive the structure of the lower troposphere:

i) Long wave radiative cooling and heating of the surface are stronger than at higher levels in the atmosphere since the principal sources and sinks of heat are at the surface. Solar heating of the surface causes thermal plumes to rise, transporting moisture, heat, gases and aerosols. The plumes rise and expand adiabatically until a thermodynamic equilibrium is reached at the top of the atmospheric boundary layer (unstable conditions). The depth of this layer grows rapidly in the morning, and more slowly throughout the rest of the day, principally through entrainment at the top of the layer. The mixed layer is capped by an inversion where the potential temperature rapidly increases. Above the inversion the stratification is stable.

The concentration profile of gaseous constituents including water vapour originating from the surface strongly depends on the mixing height. During daytime the mixing height over land increases and reaches a maximum value in situations with constant synoptic conditions. Some of the most reactive BVOCs have lifetimes that are similar to the turnover time of the CBL (15-30min) and thereby, the relationship between turbulence and chemistry becomes an important issue.

In the evening solar radiation rapidly falls and so the surface begins to cool through outgoing long wave radiation. With the change in the surface heat flux, the primary source of turbulent kinetic energy in the PBL is removed and so the turbulence rapidly decays. This leads to a stable layer near the surface, known as the nocturnal boundary layer (NBL) with an inversion developing above it. On top of it remains the residual layer characterized by weak sporadic turbulence and initially uniformly mixed potential temperature and pollutants remaining from the mixed layer of the previous day.

ii) Secondly the wind flowing over the surface becomes mechanically turbulent by the vertical wind shear in the boundary layer. The turbulence acting to ‘stir’ the air by irregular swirls close to the ground has an important impact on the transport of heat, moisture, chemicals and aerosols from the surface higher into the atmosphere. These irregular swirls or eddies are accompanied by fluctuations in temperature and humidity on similar timescales. The vertical component of wind is important on the scales at which turbulence acts. Trace gases emitted near the surface can accumulate close to the ground influencing the vertical profiles of reactive species.

The breakup of the NBL in the morning under influence of incoming radiation and entrainment air from elevated layers usually causes accumulated trace gas and aerosol concentrations at the ground and in the CBL to chance (e.g. Trainer et al., 1995).

The atmospheric boundary layer height variation over a region has theoretical, experimental and practical implications as this height controls the vertical extent, the concentration and transformation of trace gases and aerosols in the lower troposphere. As for gases, the shorter the lifetime of a compound, the slighter the effect of vertical transport on its concentrations will be, while the compound is removed during the transport by other processes such as chemical reactions. The effect of vertical transport is notable on ozone, since its tropospheric lifetime depends on the altitude (as it is subject to surface deposition), but negligible for OH with a lifetime shorter than a second. The oxidative capability of the atmosphere therefore is not simply a function of chemistry.

Modellers have shown that different PBL schemes can yield very different vertical profiles of simulated parameters, including temperature, water vapour mixing ratio, and horizontal winds, particularly during the daytime growth of the mixed-layer (Berman et al., 1999; Zhang et al., 2001). These parameters exert a strong influence on the formation, spatial distribution, and removal of airborne chemical species in the atmosphere (Alapaty and Mathur, 1998). In photochemical model simulations, three important boundary-layer parameters for studying air pollution events are the mixing height, ventilation coefficient, and cloud cover (Rao et al., 2003).

To obtain a representative evolution of the CBL height over course of a day, a sufficient number of profiles are needed. Several methods have been exploited but the potential temperature and specific humidity profiles are often used in estimating the CBL mean height. Usually, the CBL height is indicated by a sudden potential temperature increase or specific humidity drop with height but it's not always as easy to identify these locations especially when clouds are present, as discussed in chapter 3. Clouds, precipitation and frontal systems have left their marks on the observations discussed in chapter 4.

1.4.2 **Pressure systems and fronts**

When analysing data on atmospheric tracers, back trajectories are commonly used to get insight in the source areas that have been encountered also known as the air mass history. The longer air remains stagnant over its source region, the more likely it will acquire properties of the surface below.

In order for a huge air mass to develop uniform characteristics, its source region should be generally flat and of uniform composition with light surface winds. In nature, such situation often gets disturbed by landscape and orographic elements, large water bodies. Furthermore, high and/or low pressure systems drive the movement of the air. Dry air in regions of excess pressure (H) sinks to the Earth and moves toward regions of deficit pressure (L) where moist air rises. Such vertical air motion is largely responsible for the organization of precipitation as clouds develop.

Clouds play important roles in atmospheric chemistry and climate, and yet their effects and feedbacks on tropospheric chemical and meteorological processes are poorly understood. In following of the previous section, convective clouds transport pollutants vertically, allowing an exchange across the inversion at the top of the boundary layer to the free troposphere. Buoyantly-driven updrafts and downdrafts within clouds rapidly transport heat, water vapour, momentum, and pollutants between the lower and upper atmosphere. Precipitation produced by clouds rapidly removes water and other soluble contaminants from the atmosphere. Condensed water in clouds scatters radiation, reducing the rates of photochemical reactions in the lower troposphere, while also redirecting incoming solar radiation away from the Earth's surface. Aqueous-phase chemical reactions also occur in clouds, changing the chemical reactivity of the atmosphere. Clouds can also affect gas-phase chemistry by attenuating solar radiation below the cloud base which has a significant impact on the photolysis reactions.

Often, two air masses, especially in the mid-latitudes, develop a sharp boundary or interface, where the temperature difference between them becomes intensified. Such an area of intensification is called a front. A moving front is named according to the advancing air mass, e.g., cold front is the leading edge of a relatively cold air mass, which moves so that it replaces the warmer air. A warm front is the boundary zone between retreating cold air and the advancing warm air. The warm air, being more buoyant, overrides the cooler air, forming clouds and precipitation. However, rain or showers, rather than storms, characterize the weather at such warm fronts. There will be a temperature and humidity increase with the passage of a warm front. Because the slope of the warm front is not as steep as the cold front, showers form more gradually, preventing latent energy, the energy transferred from the earth's surface to the atmosphere through the evaporation and condensation processes, from reaching high altitudes. The structure of a warm front appears therefore to be favourable for investigating the removal of trace gases by rain, as the rain droplets fall out of the through the underlying colder air. On its way down, rain droplets are exposed to the “pollutants”, and absorption of both particles and gases into liquid droplets can occur. Such frontal systems are particularly prevalent in the temperate latitudes of the Earth.

1.5 Chemical and physical removal of VOCs from the atmosphere

Volatile organic compounds all share the same major atmospheric removal mechanisms, which include the following: photolysis, photochemical oxidation by hydroxyl radicals, reaction with other reactive species such as nitrate radicals and ozone, and wet and dry deposition to the earth’s surface. These

mechanisms determine the atmospheric residence time of the VOCs which are generally short, varying from few hours to months. These processes will be briefly discussed in the following subsections.

1.5.1 **Photolysis**

Tropospheric chemistry is driven by the production of radicals from photolysis of trace gases. Thus, important photolysis processes must be considered quantitatively for an understanding of VOC photochemistry. The basic ingredients for the formation of hydroxyl are NO and NO_2, water vapour, ozone and radiation at wavelengths shorter than 315 nm.

The most important tropospheric photolysis processes is that of O_3 yielding electronically excited $O(^1D)$ atoms (Levy, 1972). Photolysis of ozone by ultraviolet light in the presence of water vapour is the main source of hydroxyl radicals in the troposphere (Ehhalt et al., 1991; Levy, 1974) (see radical generation in Figure 1-5).

The fraction of $O(^1D)$ atoms that form OH is dependent on the concentrations of H_2O, for example in the marine boundary layer about 10% of $O(^1D)$ formed go onto generate OH. Hydroxyl radical concentrations not only decrease with altitude but also decrease with latitude since both the water vapour concentrations and sunlight intensity decrease towards the poles.

The oxygen atom $O(^3P)$, the exited state of the oxygen atom has the ability to oxidize unsaturated hydrocarbons and other gases containing a double bond in the upper troposphere.

While VOCs are removed extensively by the photochemically produced OH, certain species can themselves absorb actinic radiation and photolyse themselves. Atmospheric filtration of short wavelength radiation ($\lambda \leq 290$ nm), means that carbonyl (aldehydes and ketones) are the most susceptible VOC species. These carbonyl compounds are common oxidation products and are ubiquitous components of the troposphere. Thus the atmospheric loss processes of VOC include photolysis, and reaction with OH radicals.

1.5.2 **Photochemistry (OH-chemistry)**

The steady-state mixing ratio of OH is extremely low (max. of about 1 - 10 molecules OH in 10^{13} molecules of air). Since VOCs react directly with the OH radical they may influence the oxidation capacity of the atmosphere by prolonging the lifetime of methane in the atmosphere, or in other words, the capability of the atmosphere to clean itself (Houweling et al., 1998; Lelieveld et al., 2004; Roelofs and Lelieveld, 2000). The initial reaction of the OH radical with a VOC generally leads to the abstraction of a hydrogen atom and the generation of water molecule and an alkyl radical that reacts almost exclusively with O_2 to produce peroxy radicals. These peroxy radicals may react further with HO_2, NO or themselves to yield various stable compounds (hydroperoxides, alkoxy radicals, nitrates, carbonyls, alcohols etc.). The alkoxy radicals can react with themselves to generate hydroxyl peroxy radicals, fragment to smaller alkyl radicals or react with molecular oxygen to form a carbonyl compound and HO_2 as is shown in Figure 1-4. The gas phase oxidation can continue until the VOC compound in question is ultimately converted into CO_2 and H_2O. Without an efficient chemical cleansing process such as this, the levels of emitted trace gases would rise indefinitely. Reaction with OH-radicals forms the main sink for VOCs with an extractable hydrogen atom and the same is true for organic gases with an unsaturated bond with which the OH radical undergoes an addition reaction

Because the photochemical production of OH is favoured by sunlight and high humidity, its formation rate varies diurnally. Strong seasonal variations in atmospheric VOC concentrations can occur due to variation in the source strengths and in the main sink the OH radical. The removal of VOCs by OH is maximal in the summer period when the photolysis source of OH radicals is highest. Minimal concentrations of anthropogenic VOCs and maximum concentrations of biogenic are therefore observed in summer. In the winter, the opposite occurs, which results in maximum concentration of anthropogenic

VOCs and minimum concentration in biogenic VOCs. This produces harmonic seasonal variations of VOC concentrations. Minimum OH levels are found at high latitude during winter in association with significant reduced removal rates for many trace gases.

In summary, atmospheric VOCs rapidly react with hydroxyl radicals, ozone, and nitrate radicals to generate a multitude of intermediate, secondary chemical species. A schematic diagram of the OH oxidation routes is given in Figure 1-4.

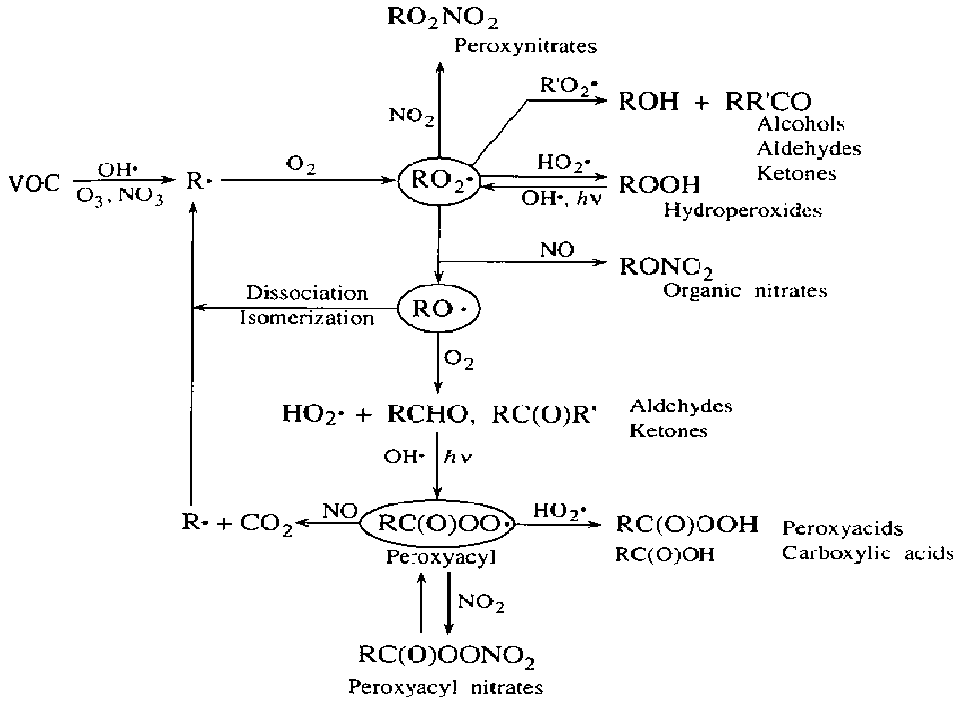

Figure 1-4 Organic radicals and products in the photo-oxidation of an organic molecule (Seinfeld and Pandis, 1998)

1.5.3 **Ozone chemistry**

Ground level ozone is considered to be an important environmental threat affecting human health negatively and causing damage to vegetation. Ozone has a detrimental health effect on humans, and plants and is a significant greenhouse gas. Ozone is produced from nitrogen oxides (NO_x) and volatile organic compounds (VOC) in the presence of sunlight (Haagen-Smit and Bradley, 1953). The concentration of ozone is balanced by in situ photolysis and by dry deposition at the Earth's surface. As a result of these processes, the concentration of ozone in the troposphere is in the order of 10-40 ppb in clean remote sites and about 100 ppb in polluted urban areas. The only way to reduce ozone is to reduce the emissions of the precursors.

Two different ozone producing chemical regimes in the troposphere are often distinguished and referred to as low and high NO_x chemistry. At low VOC to NO_x ratios (< about 4 to 1), ozone production is considered to be VOC-limited; whereas at high VOC to NO_x ratios (> about 15 to 1), ozone production is considered to be NO_x limited.

Unsaturated oxygenated VOCs including aldehydes, ketones, alcohols, ethers and esters are oxidized by ozone in reaction involving the electrophilic addition to the C=C bond and also they can react with OH and NO_3 radicals. Even though unsaturated VOCs react with ozone when NO is present, there is a net production of O_3 from the whole process. This net O_3 production is due to the reaction of RO_2 and HO_2 formed from VOCs with NO and the subsequent conversion to NO_2 which lead to O_3 formation (Atkinson and Arey, 2003) as summarized in Figure 1-5.

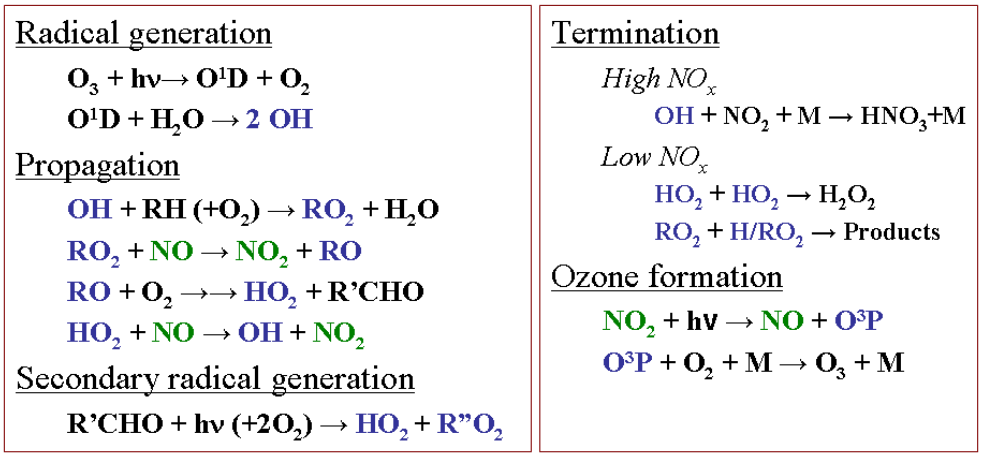

Figure 1-5 Photochemical oxidation of organic compounds in the troposphere: formation of ozone. Each VOC has its own atmospheric lifetime, its own chemical mechanism and its own tendency to form ozone.

The reaction with ozone is of particular interest because it produces carboxylic acids and other polar compounds which are soluble in water. These polar compounds may play a preponderant role in the troposphere influencing the hygroscopic properties of aerosols (Grosjean and Grosjean, 1999).

1.5.4 **Night time chemistry**

Photolytic reactions producing OH during the day, are absent at night. However, the NO_3 radical, which is rapidly photolysed during the day becomes an important sink for VOC species. Nitrate radicals are formed from the reaction of ozone with nitrogen dioxide. Nocturnal chemistry and physics can play an important role in the conversion and removal of VOCs, which would otherwise be available for daytime ozone formation. Nitrate radicals abstract an H-atom from alkanes to form nitric acid (HNO_3) and alkyl radicals ($R^{\bullet}$), which react with the oxygen and form peroxy radicals $RO_2^{\bullet}$. NO_3 adds also to the double bonds of unsaturated organic compounds and can form peroxy nitrates after addition of O_2. All peroxy species, emerging from OH, NO_3 or ozone reactions undergo complex reaction sequences in the atmosphere with O_2, HO_2, RO_2, NO or NO_2 leading to alcohols, aldehydes, nitrates and carboxylic acids.

1.5.5 **Dry and wet deposition**

Dry and wet depositions are ultimate pathways for many gases and particles to leave the atmosphere to terrestrial and aquatic ecosystems. Thus, deposition plays an important role in controlling the concentration of species in the atmosphere and providing essential nutrients or depositing hazardous compounds to ecosystems.

Dry deposition is the process by which gaseous and particulate pollutants are adsorbed or uptaken by e.g. plant foliage, aerosols and other solid surfaces in the absence of liquid water. The rate at which this occurs depends on the 'deposition velocity' which is affected by (a) meteorological variables (e.g., wind speed, temperature, terrain, atmospheric stability, and humidity); (b) surface variables (e.g., surface aerodynamic roughness and structure, pH, surface charge, hydrophobicity, porosity); (c) properties of the depositing material (e.g., chemical reactivity, solubility, diameter, surface charge, and shape). Hence, large temporal and spatial differences in dry deposition rates are to be expected due to the large variety in the biological, chemical and physical properties of the surface cover.

Wet deposition involves the absorption of pollutants, both particles and gases, into liquid droplets or ice crystals. Substances with low aqueous phase affinity are mostly converted via oxidation into relatively soluble products, which in turn can be more efficiently removed from the atmosphere (washed out) by precipitation. Washout refers to the process in which during rain, falling rain droplets washes out

atmosphere below the raining cloud. This is different from the process in which pollutants become incorporated to cloud droplets are wet deposited when cloud rains, this is known as rainout. Pollutants can be incorporated into droplets in one place and the cloud can rain in another location. Both processes probably occur simultaneously during a wet deposition event (Pena et al., 2002). Large uncertainties exist on the quantification of the removal of components by rain. The complexness of the whole makes validation by field experiments difficult. Although the quantification of the removal of oVOCs was not a goal during the HOHPEX04 campaign, the topic is only raised here as a matter of interest and as a line of thought for future investigations.

Washout of (semi-) volatile organic compounds (and aerosol particles) is an important removal mechanism from the atmosphere and an important loading mechanism to terrestrial and aquatic systems i.e. vegetation and surface waters, especially with respect to pesticides (Simcik, 2004). Pesticides usually are less abundant and have much higher molecular weights than the oVOCs such as formaldehyde, methanol, acetaldehyde and acetone discussed in this study. Compared to pesticides, these oVOCs can be considered as harmless.

The efficiency of removal of gaseous compounds by rain droplets depends on the surface and the matrix characteristics of the droplets. It is therefore different from the wet removal of aerosol particles. As aerosol particles mostly are removed by collision with the rain droplets both the size distribution of the droplets and the aerosol particles are decisive. For the removal of gaseous compounds, droplet size does matter but removal is based on physical (condensation, coagulation, adsorption and absorption) and chemical processes in the droplet and at the droplet's surface. This is very difficult to assess in the field.

Factors which might affect the removal of oVOC by precipitation include the molecular weight (the solubility of VOCs decreases with increasing number of carbons), the solubility expressed by the Henry´s law constant (see Table 4-4, data compiled from Sander, (1999)), the total concentration of compounds in particular in the rain droplets or more precisely the equilibrium between the amount of VOCs between the liquid phase and the gas phase.

Most theories assume an equilibrium between a component in the droplet (the liquid phase) and the air surrounding it (the gas phase). Henry's law should be applicable because chemical equilibrium for absorption processes in the atmosphere is on the time scale of one second. Gas scavenging, therefore, is reversible, while aerosol scavenging is an irreversible process.

The equilibrium is a rather instant phenomenon whereas the internal droplet concentration depends on the history of the airmass in which the clouds have been formed and on the airmass through which the rain droplet falls. The latter also influences the equilibrium processes. It is incorrect to assume uniform conditions between the cloud base and the drop zone (area of impact of the droplets). Solubility which is a temperature dependent process and the transport of compounds towards the surface of the droplet are also important. Furthermore, the removal might depend on the type and amount of precipitation (droplet size distribution, intensity and density (drizzle, light, moderate, heavy...), duration of interaction (persistency of the rain and the distance between the cloud base and the ground) (Smith, 2003). Recording rain droplet size distributions is recommended.

Table 4-4 shows that solubility and reactivity are not coupled. For example, isoprene is very reactive but not soluble; formaldehyde is very soluble but not so reactive. The life time of OH-radicals under rainy conditions is assumed to be short because the high possibility of collision with the droplets. Although chemical reactivity remains the most dominant removal process we will qualitatively examine in the following paragraphs the extent to which the relationships between the oVOCs mirror the relationship of the Henry law coefficients.

Based on their vapour pressure, short chained oVOCs are expected to exist almost entirely in the vapour phase in the ambient atmosphere. The dominant chemical loss process for these compounds is by

reaction with the hydroxyl radical. Washout due to rain is expected to be significant due to the water solubility of compounds like formaldehyde and methanol.

There have been relatively few measurements focussing on the removal of ambient oVOC during rainfall, probably due to the complexness of the events. The ideal situation in the field would be to monitor the effects of washout that occurs when rain falls through an air mass that has been characterised before and after the rain event, without synchronous changes in the air mass associated with the frontal change. Such a situation can arise with an approaching warm front. The measurement site remains in a single airmass as the warm front approaches and the warmer air within the warm sector rises up the warm front eventually forming nimbostratus or cumulonimbus clouds. When rain falls from these clouds the water can fall through the airmass and cease prior to the arrival of the front.

In the case of a cold front the rainfall is normally more closely associated with the front. In this case of a warm front, precipitation falls through the air mass that has been monitored before and would therefore be an ideal situation to study the impact of wet deposition on trace gasses.

The equivalent of a warm front in experimental terms could be an equilibrator which is a vertical column (recommended several dozens of meters) with a larger shower head for which physical (droplet size, rain fall rate and duration) and chemical (composition, surface tension, pH) parameters of the droplets can be controlled and the dependency of the removal of VOCs on certain parameters can be studied. Likewise, the gas phase composition can be controlled as well as the throughput or flow rate to control the time of interaction. The rate of removal of VOCs could then be calculated from monitoring the concentration in the gas and liquid phase influents and effluents.

The amount of removal of a vapour may be calculated from the air-to-water partition coefficient (i.e., Henry's law constant), which is found to be temperature dependent. As a consequence, the solubility of gases generally decreases with increasing temperature. A significant fraction of VOC will only reside in the aqueous phase if its Henry's law constant exceeds ~50 $mol_{aq}/(m^3_{aq}.Pa)$, which suggests that VOCs with Henry's law coefficients between ~10 and ~100 $mol_{aq}/(m^3_{aq}.Pa)$ can be classified as moderately soluble (Seinfeld and Pandis, 1998). Overall, wash-out is a rather minor removal process for vapour-phase chemicals, since the majority are quite volatile and/or are hydrocarbons which have low Henry's law coefficients.

As the characteristics of rain events can differ substantially from each other, quantification of the removal of VOCs by field experiments may suffer from a low degree of reproducibility. It therefore seems more appropriate to conduct controlled experiments with a large shower-head type equilibrator in the laboratory first in which many parameters can be controlled for the gas phase and the liquid phase. These results may then be converted into a model (e.g. Naresh et al., 2006) and compared to the in situ observations.

Lopez et al., (1989), although they were limited in quantifying compounds of sub-nanomole amounts of solute material, have found a good agreement between theory (parameterised model by Walcek and Pruppacher, 1984) and experiments for droplets with seizes of about 0.33 mm. The uptake by larger droplets was computed to be slower and requires including an eddy diffusivity factor which is compound specific. Details of the physics of the scavenging process can be found in Schwartz and Slinn, (1992) but are beyond the scope of this study.

Hydrophobic volatile organic compounds are usually found in rainwater with higher concentrations than the values determined from Henry's law partitioning (Sato et al., 2006). However, there have been studies which concluded that despite the high solubility of formaldehyde, ambient concentrations predicted via Henry's Law coefficient from the concentration of formaldehyde in rain have been found to be significantly lower than the measured values by factors ranging from 5 to 30 (Levsen et al., 1990; Hopkins et al., 2003; Baez et al., 1993). Very poor or no correlation was found between formaldehyde concentrations and rainfall rate by Dong and Dasgupta, (1986).

1.5.6 **Isoprene and its oxidation products**

Isoprene oxidation by OH has been widely studied in laboratory based chamber experiments. First order oxidation products are known; namely formaldehyde ($H_2C=O$), methyl vinyl ketone ($CH_3C(=O)CH=CH_2$), methacrolein ($O=CHC(CH_3)=CH_2$) and the dependence of these product yields on NO_x have been determined. The relative yields of these species are determined by the site of the OH addition to isoprene. Lee et al., (2005) suggested that under low NO_x conditions reactions of some of the hydroperoxides and hydroxycarbonyls produced from the OH-initiated oxidation of isoprene may be a significant source of methyl vinyl ketone and 3-methylfuran in the atmosphere. Primary oxidation products of isoprene are still reactive as they contain an unsaturated carbon-carbon bond (Atkinson, 2000). This rate of production and yield of these oxidation products is examined in chapter 5.

The atmospheric lifetime of isoprene under standard daytime conditions (1013.25hPa, 25°C) with an OH concentration of $5x10^6$ molec. OH cm^{-3} and $1.2x10^{12}$ molec. O_3 cm^{-3} (=50 ppbv) is 32 minutes. The night-time lifetime of isoprene against NO_3 is on the order of 20 hours. Several investigators (Biesenthal et al., 1998; Yokouchi, 1994; Goldan et al., 1995; Hurst et al., 2001) have observed surface isoprene decay at rates 5-10 times faster than this. Other possible night-time sinks include ozone and hydroxyl radicals.

1.5.7 **Terpenes and their oxidation products**

Monoterpenes have lifetimes with respect to OH and O_3 that range from days to minutes (Fuentes et al., 2000). The reaction of e.g. α-pinene with ozone begins with the formation of two radicals, which stabilizes or rearranges to give more stable products. These products include: pinonaldehyde, norpinonaldehyde, pinoic acid, norpinoic acid, pinic acid, norpinic acid and oxo-pinoic acid (Kamens and Jaoui, 2001) as well as formaldehyde, acetaldehyde and acetone. The first series of products have low vapour pressures and their identification in atmospheric aerosol samples serves as direct evidence for aerosol formation from monoterpenes under ambient conditions (Jianzhen et al., 1999).

1.5.8 **Chemistry of Oxygenated VOCs**

In recent years, oxygenated volatile organic chemicals like acetone have been recognized as important atmospheric constituents due to their ability to sequester reactive nitrogen in the form peroxyacetyl nitrate (PAN) and to be a source of hydroxyl radicals (HOx) in critical regions of the atmosphere. Atmospheric modelling studies and measurements indicate that acetone and other oxygenated hydrocarbons can cause HOx formation in the remote troposphere (Singh et al., 1995; Arnold et al., 1997; Colomb et al., 2006). This in turn contributes to ozone production in the upper troposphere, at altitudes where ozone is an important greenhouse gas. However, significant uncertainties remain regarding the budget, fate and impacts of these oxygenated and other organic compounds on the remote troposphere extending to the global scale.

Methanol directly reacts with hydroxyl radicals in gas and aqueous phases. The reaction products are a subsequent source of formaldehyde and CO (Riemer and al., 1998; Palmer et al., 2003), hydrogen radicals, and ozone. Methanol is produced in the atmosphere to minor extend by reactions of the methylperoxy (CH_3O_2) radical with itself and with higher organic peroxy (RO_2) radicals (Tyndall et al., 2001). The CH_3O_2 and RO_2 radicals are produced in the atmosphere by oxidation of VOCs.

The atmospheric lifetimes (methanol: ~3 days and acetone: 13 days), as well as that of acetaldehyde (~4 hours), are controlled by a combination of chemical, photolytic and physical removal processes. Consequently, methanol and acetone are transported globally (Singh et al., 2000; Singh et al., 2001) and are proposed to have a role in tropospheric oxidant photochemistry (e.g., Fehsenfeld et al., 1992; Monod et al., 2000). Atmospheric sources and sinks of methanol have been discussed in four recent publications by Galbally and Kirstine, (2002), Heikes et al., (2002), Tie et al., (2003), and Singh et al., (2004).

Methanol and acetone are ubiquitously present throughout the atmosphere in all seasons, with highest levels in summer and lowest levels in winter as they have sources in the terrestrial biosphere (Jacob et al., 2002; Galbally and Kirstine, 2002) and photochemical production from hydrocarbon precursors. Often, the acetone to methanol ratio is observed to be the highest during fall and winter, probably a result of secondary acetone production from diffuse anthropogenic sources. This ratio will be examined further at the end of this dissertation in sight of the results from all three campaigns.

Singh et al., (2000) estimated the global sources of acetone to range between 37 and 80 Tg acetone/year. Secondary formation for acetone from the oxidation from precursors as propane, isobutane, isobutene were believed to be the largest source (50%) followed by biomass burning and direct biomass emissions and only very little coming from direct anthropogenic emissions.

Recently, Marandino et al., (2005) demonstrated that the net flux of acetone is into, rather than out of the oceans and seems to be around 48Tg/yr globally. Furthermore, investigations by Blitz et al., (2004) have recently updated the photolysis rate of acetone to about half of what has been previously thought. The total loss of acetone changes from 96 Tg/year given by Jacob et al., (2002) now totals to 101Tg/year by Koppmann, (2007).

1.6 Uncertainties in volatile organic compounds

Updates on sources and sinks, such as mentioned in the previous section on acetone, could imbalance former widely accepted atmospheric budgets often used in many computer simulations, suggesting that verification processes involving VOCs remain essentially important as computer models have to rely on them to simulate budget and climate scenarios.

Figure 1-6 summarises schematically many of the aforementioned oxidation processes by HOx, Ox, NO_x. However, there still is a great deal of uncertainty concerning the sources and sinks of the VOCs. For example, diurnal and seasonal variability, night time and residual layer chemistry, and chemistry under low NO_x (remote atmosphere) (related chapter 3, aircraft-based campaign over the Tropics of South America, between 3 - 6 °N and 50 - 58°W), dry and wet deposition (related chapter 4, ground-based campaign in Southern Germany at Hohenpeißenberg, 47°N, 11°E) and the role of organics in new particle formation and growth (related chapter 5, ground-based campaign in Southern Finland at Hyytiälä, 61°N, 24°E) to name a few.

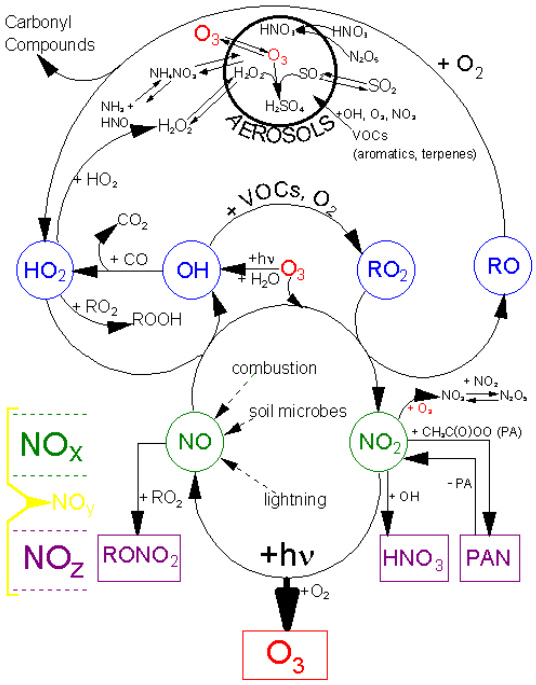

Figure 1-6 The chemical degradation through a free radical chain oxidation of volatile organic compounds by reactive species (HO_x, O_x, NO_x) produces a variety of products, which play a role in the contribution to tropospheric ozone and other oxidants (such as peroxides) and the formation of secondary organic aerosols (SOA).

The uncertainties on these aspects can be reduced by making in situ and laboratory measurements and combining them with an evaluation of these findings against our current understanding of each aspect incorporated in computer models. These models should be evaluated for each of the key processes involved, starting from a very limited domain before scaling it up to e. g. regional or global scales.

2 Experimental

Low abundances, rapid changes in concentration, and the complex mixture of trace gases in ambient air make atmospheric measurements a significant analytical challenge. One of the most powerful techniques available to the atmospheric chemist is mass spectrometry which can detect very small quantities of material very specifically.

When analysing a mixture of organics, like an air sample with a mass spectrometer, the mass spectra can, depending on the ionisation energy used, be complex and therefore of limited use for quantitative analysis (Lagg et al., 1994). Chemical ionisation mass spectrometry (CIMS) uses much lower ionisation energies compared to conventional ionisation methods with the result that a lot less fragmentation of the molecules occurs Harisson, (1992). This reduced fragmentation allows these techniques to be used for on-line measurements of atmospheric trace substances and this in a very sensitive and reasonably selective way. Modern mass spectrometers have also become, fairly robust and compact, and have been deployed in a variety of field settings, including ground stations, lorries, ships, and research aircrafts. Numerous chemical ionisation schemes have been exploited for atmospheric measurements.

Proton Transfer Reaction Mass Spectrometry (PTR-MS) is an emerging technique for the measurement and monitoring of volatile organic compounds at low concentrations in gaseous samples in approximately real time. This specific form of chemical ionisation uses H_3O^+ ions as a reagent, and it combines the desirable attributes of high sensitivity and short integration times with good precision and accuracy. Here, the principles of operation of the PTR-MS are described, its advantages and disadvantages discussed, its inherent uncertainties highlighted, its use in atmospheric sciences reviewed, and the specific details of how it was operated in the course of this doctoral dissertation given.

2.1 Proton Transfer Mass Spectrometry (PTR-MS)

The PTR-MS is a technological innovation, suitable for analysing gas mixtures because it allows for direct and real time monitoring of VOCs measurements with reasonable sensitivity, in the sub-ppbv (parts-per-billion) range (Lindinger et al., 1998). On-line monitoring of the diel variations of VOCs in the troposphere has demonstrated the present sensitivity of PTR-MS to be in the range of a few tens of pptv (de Gouw and Warneke, 2007; Blake et al., 2009). PTR-MS is well-suited for studying the atmospheric chemistry of organic compounds, because it allows many important hydrocarbons of both natural and man-made origin to be measured along with their oxidation products (e.g. Warneke et al., 1999). The fast time response of only seconds or less makes it possible to study compounds with a very short lifetime or to monitor rapidly changing conditions like aircraft measurements (e.g. Colomb et al., 2006; de Gouw et al., 2003b) or eddy covariance flux measurements (Karl et al., 2002). Three major parts can be distinguished in the instrument as shown in Figure 2-1 . Each part of the instrument will be addressed in the following section individually.

2.1.1 System configuration

Figure 2-1 shows the different parts of the PTR-MS including the ion source, the reaction chamber, the analyser and the detector. Each of these parts will be discussed in the following sections.

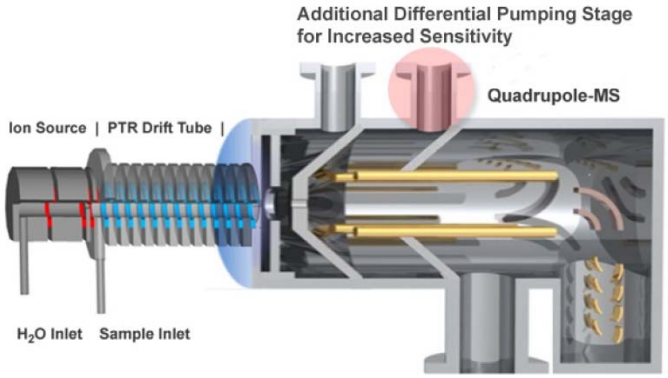

Figure 2-1 Scheme of the proton transfer reaction mass spectrometer

2.1.1.1 Ion source

The hollow cathode discharge in the ion source is a specific form of glow discharge. The plasma is produced when the electrons within the cathode have enough energy to generate visible light by excitation collisions. The glow can be produced by applying a potential difference between two electrodes in a gas.

The discharge plasma can be used as a source for gas ion beam production due to its high stability and good uniformity. The cathode spacing in the PTR-MS is a few millimetres and the prevalent pressure in the ionisation region remains above 0.01 mbar. A cylindrical hollow cathode discharge region acts as an ion source producing an ion current, which is substantially comprised of H_3O^+ ions. For this purpose water vapour is ionised, whereby various ions (O^+, OH^+, H^+, H_2^+,…) are also formed. These ions are extracted by means of a weak electric field into a region, located outside of the ionisation region. This space between the ionisation region and the reaction region makes up the Small Drift (SD) region.

The SD region has an aperture in one of the walls, through which a gas flow can be maintained in the direction from the ionisation region to the reaction region. Intermediate pumping-down between the regions is also conceivable and possible.

Ions are kept in the SD region until those ions, initially differing from H_3O^+, have also been converted into H_3O^+-ions in secondary reactions. In the SD region and/or in a region adjoining thereon, the ion current is guided through an electric field of which the field strength is of adequate magnitude such that $H_3O^+(H_2O)_n$ cluster ions have gained sufficient kinetic energy in order for these collisions to be largely dissociative. $H_3O^+(H_2O)_n$ cluster ions are formed through association reactions between two successive collisions with neutral collision partners. The build-up of such cluster ions is thereby prevented or largely cancelled. To improve these dissociation reactions, an additional gas (buffer gas), such as Ar, Kr, N_2 or air, which serves as a collision partner for the cluster ions but does not enter into chemical reactions with the H_3O^+ ions can also be added to the H_2O. In the reaction chamber, conventionally known as the drift tube, the primary H_3O^+ ion current is allowed to react with a sample gas in which the organic trace gases are present, and the reaction products formed through ion-molecule reactions, in particular proton transfer reactions are analysed in a mass spectrometer (Hansel et al., 1995; Lindinger et al., 1998).

Although at a relatively low concentration the existence of NO^+ and O_2^+-ions can make interpretation of the PTR mass spectra more complicated due to their reaction with VOCs and the production of fragment ions. Therefore the formation of NO^+ and O_2^+-ions should be suppressed both in the ion source and in the drift tube i.e. less than 5%.

2.1.1.2 Reaction Chamber

The drift tube, a sequence of ring electrodes arranged along the central axis, is continuously flushed with the air to be analysed. The drift tube (length ca. 10 cm and diameter varying from 1-5 cm)

maintained at a constant gas pressure (2 to 2.5 mbar) with the air to be analysed acting as the buffer gas. Smaller volumes of the drift tube result in a shorter residence times which can be advantageous particularly for sticky gases such as ammonia. The fixed length of the drift-tube provides a fixed reaction time for the ions as they pass along the tube.

Any gas mixture containing the trace constituents to be analysed can be used as a buffer gas. Along the central axis drift tube, an electric field is applied at fixed E/N, where E stands for the applied electric field and N corresponds with the buffer gas density. Primary H_3O^+ ions move under the influence of this linear potential gradient and collide with molecules they come across on their way to the ion detection system, as can be seen in Figure 2-2. There drift velocity v_d is controlled by the ratio E/N and will be discussed in detail under section 2.1.3 Distribution of cluster ions in the drift tube.

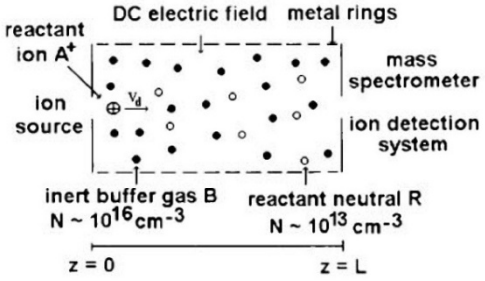

Figure 2-2 Schematic representation of the drift tube (Hansel et al., 1995)

2.1.1.3 Ion analyser and detection system

The H_3O^+ and product ions are extracted from the gas flow out of the drift tube and the neutrals are led away by the main flow to a turbo molecular pump. Ion optic lenses just in front of the quadrupole rods are important to accelerate and focus the ions through an aperture into the downstream quadrupole mass spectrometer (QMS). This mass analyser filters charged particles only by electric fields and separates them according to their mass over charge ratio (m/z) and are then counted with an electron multiplier located at the end of the quadrupole mass filter. Combined direct current (DC) and radio frequency (RF) potentials on the quadrupole rods can be set to pass only a selected mass-to-charge ratio. All other ions do not have a stable trajectory through the quadrupole mass analyzer and will collide with the quadrupole rods, never reaching the detector. Furthermore, a high-vacuum-system of $<2.10^{-5}$ mbar is needed to let the ions reach the detector.

The instrument may be operated in either the full scan mode or the selected ion-monitoring mode. For the measurements in this work, only the selected ion-monitoring mode is used. In this mode, a time resolution of a few seconds may be achieved. The combination of (1) an intense source of H_3O^+ primary ions, giving typically 10^7 counts per second of primary ions; (2) a cross-section for proton transfer which ensures unit conversion efficiency of primary ions to secondary ions on every collision; (3) a mass analyser which selects the ion peaks specific to the trace compounds present in the air to be analysed; (4) an electron multiplier detector operated in pulse counting mode with single particle detection efficiency are the key features of the PTR-MS analyser.

2.1.2 The principle: ion molecule reactions - proton transfer reactions

An ion/molecule reaction (IMR) can be described as an interaction of a charged species with an electrically neutral reactant to produce either chemically different species or changes in the internal energy of one or both of the reactants. High sensitivity of a CI system is obtained when the ratio between the product ion signal $i(R^+)$ and the density of the neutral compound [R], is high. Hence, high sensitivity is achieved in CI when the primary ions have ample time to react with the neutral compounds to be measured and therefore producing high signals $i(R^+)$. This works well as long as the response is linear in the concentration of R. Over the last decade, the specificity and sensitivity of mass spectrometry has

been used to detect organic compounds in gases directly without trapping, allowing on-line monitoring of gas-phase compounds in the atmosphere at a high time resolution.

The PTR-MS technique is based on the IMR of H_3O^+ ions that interact with any ambient species with a proton affinity greater than water. Because of the lower ionisation energy compared to conventional ionisation methods, a lot less fragmentation of the molecules occurs and in general, each compound can be detected at its protonated mass, which is one mass unit higher than the nominal mass. For these reasons, PTR-MS is an attractive technique for analysing VOCs. If energetically allowed, this proton transfer reaction (R2-1) takes place between the H_3O^+ and the trace gas R.

$$H_3O^+ + R \xrightarrow{k} RH^+ + H_2O \qquad \text{R 2-1}$$

R is a combination of C, O, N, S, H and k the rate coefficient of the reaction.

These reactions are exothermic if the proton affinity (PA) of molecule RH^+ is higher than the PA of water (691 kJ mol $^{-1}$ or 7.16 eV, see Table 2-1), in which case the reaction proceeds at a rate close to the collision rate of a few times 10^{-9} cm^3 molecule^{-1} s^{-1}. Fortunately the H_3O^+ ions undergo non-reactive collisions with many of the common components in air (N_2, O_2, Ar, CO_2,…), since their PAs are lower than the PA of water (Hunter and Lias, 1998).

Table 2-1: The proton affinity of selected inorganic and organic compounds

Compound	Formula	kJ mol^{-1}	Compound	Formula	kJ mol^{-1}
oxygen	O_2	421.0	methanol	CH_4O	754.3
hydrogen	H_2	422.3	acetaldehyde	C_2H_4O	768.5
nitrogen	N_2	493.8	ethanol	C_2H_6O	776.4
nitric oxide	NO	531.8	acetonitrile	C_2H_3N	779.2
carbon dioxide	CO_2	540.5	toluene	C_7H_8	784.0
methane	CH_4	543.5	propanal	C_3H_6O	786.0
carbon monoxide	CO	594.0	n-propylbenzene	C_9H_{12}	790.1
ethane	C_2H_6	596.3	p-xylene	C_8H_{10}	794.4
propane	C_3H_8	625.7	o-xylene	C_8H_{10}	796.0
acetylene	C_2H_2	641.4	methacrolein	C_4H_6O	808.7
sulphur dioxide	SO_2	672.3	acetone	C_3H_6O	812.0
ethylene	C_2H_4	680.5	m-xylene	C_8H_{10}	812.1
water	**H_2O**	**691.0**	isoprene	C_5H_8	826.4
sulphuric acid	H_2SO_4	699.0	dimethyl sulphide	C_2H_6S	830.9
hydrogen sulphide	H_2S	705.0	benzaldehyde	C_7H_6O	834.0
formaldehyde	CH_2O	712.9	methyl vinyl ketone	C_4H_6O	834.7
benzene	C_6H_6	750.4	1,3,5-trimethyl-benzene	C_9H_{12}	836.2
nitric acid	HNO_3	751.4	atyrene	C_8H_8	839.5

Most VOCs have proton affinities higher than water and in this case a collision with the H_3O^+ ion will result in a proton transfer. Note that many oxygenated species of atmospheric interest can be detected, although the PTR-MS is blind to species such as alkanes.

If the proton affinity (PA) of a compound R is only slightly higher than the PA of water (e.g. formaldehyde), then the reverse of reaction (R2-1) can play a role in PTR-MS complicating quantification:

$$RH^+ + H_2O \longrightarrow H_3O^+ + R \qquad \text{R 2-2}$$

As reaction (R2-2) is endothermic, the rate coefficient is much smaller than for the forward reaction (R2-1). However, the concentration of water in the drift tube is much larger than the concentration of R, and therefore, the forward and backward reactions may be of similar importance. Moreover, the ion kinetic energy is elevated in the PTR-MS, and endothermic reactions are thus more important than based solely on the reaction enthalpy. The backward reaction (R2-2) was shown to be significant in the case of formaldehyde (HCHO; PA = 712.9 kJ mol^{-1}) (Hansel et al., 1997).

Although lower ionisation energies (soft ionisation) lead to a lot less fragmentation of the molecules in the reaction chamber, dissociation still occurs in some cases, especially with alcohols in the following way:

$$H_3O^+ + ROH \longrightarrow R^+ + 2\,H_2O \qquad \text{R 2-3}$$

In addition to reaction (R2-3), the H_3O^+ (and RH^+) ions can cluster with water molecules in the sampled air:

$$H_3O^+ + n\,H_2O \longleftrightarrow H_3O^+(H_2O)_n \ . \qquad \text{R 2-4}$$

These cluster ions could present a problem since their presence will complicate the interpretation of the mass spectra. In PTR-MS, however, cluster ion formation is effectively prevented by increasing the average kinetic energy of the ions using an electric field over the entire length of the drift tube. Depending on the electric field and pressure in the drift tube, however, $H_3O^+(H_2O)_n$ cluster ions can be present in the drift tube and react by:

$$H_3O^+(H_2O)_n + R \longrightarrow RH^+ + (n+1)H_2O \qquad \text{R 2-5}$$

$$\longrightarrow H_3O^+(H_2O)_{n-1}R + H_2O \qquad \text{R2-5b}$$

Since the proton affinities of $(H_2O)_n$ water clusters are higher than that of H_2O, the proton-transfer reaction (R2-5a) is more selective than reaction (R2-1): some organic trace gases do react with H_3O^+ but not with $H_3O^+(H_2O)_n$ ions (Warneke et al., 2001b).

The rate of the ligand-switching reaction (R2-5b) depends on the dipole moment of R: ligand-switching for polar molecules can be as efficient as proton transfer, whereas for non-polar compounds, reaction (R2-5b) does not occur. The cluster ions formed by reaction (R2-5b) are in most cases less strongly bound than the $H_3O^+(H_2O)_n$ clusters, which means that they will dissociate in the drift tube leading to formation of RH^+ and $RH^+(H_2O)$. Therefore both reactions (R2-5a) and (R2-5b) can lead to formation of RH^+ ions, but since the cluster ion distribution may depend on the concentration of water vapour in the drift tube, the detection efficiency can be humidity dependent (Warneke et al., 2001b) as discussed in the following section.

2.1.3 **Distribution of cluster ions in the drift tube**

The fixed length of the drift tube provides a fixed reaction time for the ions as they pass along the drift tube. The reaction time can be measured or it can be calculated from ion transport properties. If the proton donor (H_3O^+) is present in large excess over the acceptor molecules, then a measurement of the ratio of donor/protonated acceptor ion signals allows the concentration of the acceptor molecules to be

calculated. This calculation is straightforward and requires only the rate constant for proton transfer, which may be available experimentally or which can readily be estimated using tried and tested theoretical models (Su and Chesnavich, 1982). Drift tube E/N (and thus the mean collisional energy between reactant ions and neutrals) has a profound effect on both reagent and product ion distribution and abundance. Ions in the drift tube obtain an increased velocity v_d under influence of an the electric field (E) (Mason and McDaniel, 1988) given by:

$$v_d = \mu \times E \qquad \text{E 2-1}$$

The ion mobility μ has been determined for various ions in different buffer gases, including for H_3O^+ ions in nitrogen (Dotan et al., 1976; Viehland and Mason, 1995). The reduced mobility μ_0 is generally reported as:

$$\mu_0 = \left(\frac{p}{p_0}\right)\left(\frac{T_0}{T}\right)\mu = \left(\frac{N}{N_0}\right)\mu \qquad \text{E 2-2}$$

in which N is the number density of the gas, p the pressure and T the temperature in the drift tube. The parameter N_0 is the gas number density at standard pressure p_0 (1 atm) and temperature T_0 (273.15 K). Substituting (E2-2) into (E2-1) shows that the drift velocity is a function of the parameter E/N

$$\upsilon_d = \mu_0 N_0 \left(\frac{E}{N}\right) \qquad \text{E 2-3}$$

in units of Townsend (1 Td = 10^{-17} Vcm^2). Selective heating of the ions by the electric field causes the temperature of the ions T_{coll} to be higher than the drift-tube temperature T. The average centre-of-mass kinetic energy of collisions between ions and neutrals in a buffer gas KE_{cm} is given by:

$$\left\langle KE_{cm} \right\rangle = \frac{(m_i + m_b)m_n}{2(m_i + m_n)}\upsilon_d^2 + \frac{3}{2}k_B T = \frac{3}{2}k_B T_{coll} \qquad \text{(Wannier expression)} \qquad \text{E 2-4}$$

where m_i, m_b and m_n are the masses of the reagent ion, the buffer gas and the neutral, respectively, and k_B the Boltzmann's constant.

For collisions with the buffer gas itself (in this case air) $m_n = m_b$ and (E2-4) reduces to:

$$\left\langle KE_{cm} \right\rangle_{buffer} = \frac{1}{2}m_b \upsilon_d^2 + \frac{3}{2}k_B T = \frac{3}{2}k_B T_{eff} \qquad \text{E 2-5}$$

The effective temperature T_{eff} depends only on E/N; and describes the internal energy of the ion reactants (here H_3O^+) and the degree of clustering with water molecules in the drift tube (Viggiano and Morris, 1996).

Clustering of H_3O^+ ions with water molecules is prevented in PTR-MS by the enhanced kinetic energy of the ions in the drift tube. Depending on the operating conditions, however, there can be a significant number of $H_3O^+(H_2O)_n$ ions in the drift tube as can be seen in Figure 2-3.

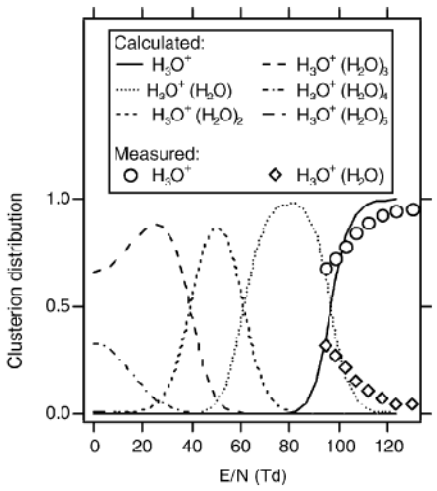

Figure 2-3 Distribution of $H_3O^+(H_2O)_n$ cluster ions in the drift tube of a PTR-MS instrument as a function of the parameter E/N (de Gouw et al., 2003a)

The distribution of $H_3O^+(H_2O)_n$ cluster ions in the drift tube can be calculated depending on the parameter E/N and the concentration of water in the drift tube. It can be seen that the overall cluster size decreases with increasing E/N until all ions are converted into H_3O^+ at approximately 120 Td. Measurements of the cluster ion distribution may give significantly different results from the calculated for instance due to collision-induced dissociation of the water cluster ions in the intermediate chamber between the drift tube and quadrupole chamber. The potentials in this intermediate chamber can be chosen such that collision-induced dissociation is minimised. The agreement is in general much worse at lower E/N values. At an E/N of 120 Td, the effect of humidity is minimal. At 100 Td, the fraction of H_3O^+ ions strongly depends on the humidity, whereas at 90 Td most of the reagent ions are cluster ions.

The density of H_3O^+-ions after traversing the drift tube with the reaction time t can be described as

$$\left[H_3O^+\right]_{\Delta t} = \left[H_3O^+\right]_0 \exp\left(-k[R]\Delta t\right) \qquad \text{E 2-6}$$

$[H_3O^+]_0$ is the density of reagent ions injected from the ion source, k is the rate coefficient for the proton-transfer reaction typically ca. $1.5*10^{-9}$ cm^3 s^{-1} and Δt is constant.

The ion count rates $[RH^+]$ are to a first approximation a direct measure for the ion density of different VOCs measured simultaneously.

[R] is the concentration of trace gas R. It is assumed that the only loss of reagent ions occurs through reaction (R2-1). In reality, the radial diffusion of ions and collisions with the wall of the drift tube leads to additional losses. It can be shown, however, that such losses are relatively small in the PTR-MS under the operating conditions that are normally used. Also, in equation (E2-6) it is assumed that there is only one trace gas R reacting with H_3O^+. If there are more, as in any air sample, the term $k[R]\Delta t$ in (E2-6) has to be replaced with $-k_i[R_i]\Delta t$, where the summation is made over all the different trace gases present. The density of RH^+ ions produced from reaction (R2-1) is given by

$$\left[RH^+\right] = \left[H_3O^+\right]_0 \{1 - \exp(-k[R]\Delta t)\} \approx \left[H_3O^+\right]_0 k[R]\Delta t \qquad \text{E 2-7}$$

The approximation in (E2-7) is justified if $k[R]\Delta t$ is small, and thus only a small fraction of H_3O^+-ions reacts in the drift tube. Equation 2-7 shows that under these conditions the density of RH^+ ions at the end of the drift tube is proportional to the concentration of the trace gas R. If [R] is too high, then the approximation in (E2-7) is no longer justified and the production of RH^+ ions is non-linear in [R], which should be avoided. The reaction time Δt is determined by the ion drift velocity v_d and the length L of the

drift tube, the reduced mobility μ_0 of H_3O^+ (2.76 $cm^2\ V^{-1}\ s^{-1}$), the buffer gas density N and is inversely proportional to the ratio E/N:

$$\Delta t = \mathrm{L}\mu_0 \mathrm{N}\left(\frac{E}{N}\right)^{-1} \qquad \text{E 2-8}$$

Therefore, the agreement between the measured and calculated reaction times is good for E/N above 100 Td, where H_3O^+ is indeed the most abundant ion in the drift tube (see Figure 2-3). At lower E/N values, the higher $H_3O^+(H_2O)_n$ clusters dominate. These have lower mobilities, and hence the calculation according to (E2-7) underestimates the measured reaction time.

Warneke et al., (2001) measured the drift velocity of ions in the drift tube of the PTR-MS, and found that the velocity is the same for all the $H_3O^+(H_2O)_n$ cluster ions. The residence time of ions in the drift tube is calculated using (E2-7). Ions have different ion mobilities, but the association and dissociation reactions (R2-2) are in equilibrium: the number of ligands attached to an individual ion changes many times during its residence time in the drift tube.

The fraction of H_3O^+-ions that is converted into RH^+ ions can be expressed as

$$\frac{\left[RH^+\right]}{\left[H_3O^+\right]_0} = [R]\frac{kL}{\mu_0 N_0}\left(\frac{E}{N}\right)^{-1} = VMR\frac{kL}{\mu_0 N_0}\left(\frac{N^2}{E}\right) \qquad \text{E 2-9}$$

where VMR is the volume mixing ratio of trace gas R.

From (E2-9) we can obtain the sensitivity, defined as the signal of RH^+ ions obtained at a VMR of 1 ppbv and normalised to a H_3O^+ signal of 10^6 counts s^{-1}:

$$Sensitivity = 10^{-3}\frac{kL}{\mu_0 N_0}\left(\frac{N^2}{E}\right)\left(\frac{T_{RH^+}}{T_{H_3O^+}}\right) \qquad \text{E 2-10}$$

The sensitivity is expressed in units of normalised counts s^{-1} $ppbv^{-1}$ (ncps $ppbv^{-1}$). In (E2-10) the factors $T_{(RH+)}$ and $T_{(H3O+)}$ are the detection efficiencies for RH^+ and H_3O^+ ions, respectively. The differences in these factors are determined by the mass-dependent transmission of the mass filter and to a lesser extent by the electrostatic lenses, which focus the ions onto the quadrupole entrance. The ratio $T_{(RH+)}/T_{(H3O+)}$ has to be determined experimentally, for instance by adding a single compound R and by measuring the decrease in the H_3O^+-signal simultaneously with the increase in RH^+ signal.

Equation (E2-9) shows that the sensitivity depends on the pressure squared; whereas both the reaction time and the frequency of reactions between H_3O^+ and trace molecules depend linearly on the pressure. However, at a constant value of E/N, the sensitivity depends linearly on the pressure.

Reasons for discrepancies in sensitivity may include (1) the dependence of the transmission factor on the pressure in the drift tube, and (2) the dependence of the proton-transfer reaction on the kinetic energy, which is not a constant in the measurement at constant electric field.

From (E2-9) it is clear that the sensitivity can be improved by increasing the pressure and the length of the drift tube. In practice, the pressure in the PTR-MS is limited by the pumping speeds of the system. Moreover, operating the system at a higher pressure means that the electric field must also be increased in order to operate at the same E/N value. A discharge of the electric field over the length of the drift tube starts to become possible at higher fields and pressures. Increasing the length means that the potential of the ion source has to be multiplied by a similar factor, which may be difficult to achieve in practice.

Analytical sensitivities and detection limits are ultimately a function of the ratio of signal to noise (S/N). Decrease the noise, the sensitivity is increased. The sensitivity of PTR-MS depends on many different factors, including (1) the current of H_3O^+ ions from the ion source, (2) the reaction efficiency of H_3O^+ ions with VOCs in the drift tube, (3) the collection and detection efficiency of reagent and product ions by the quadrupole mass spectrometer

Very important in the study of trace gases in the atmosphere is to determine the background signal of the instrument, particularly while measuring in the low mixing ratio (pptv) range. Background impurities in the system can vary from a few to a few hundred pptv depending on the mass. These background levels have to be subtracted from the measured signals to obtain the correct mixing ratios in the air sample. In all PTR-MS measurements described in this study, the background levels are determined by diverting the sample flow through a catalytic converter. The converter consists of a stainless steel chamber with platinum-coated quartz wool (Shimadzu) heated to 380 ºC, which efficiently removes the VOCs from the sample. The key motivation for using a catalytic converter is that it does not remove water vapour from the sample, as opposed to other filter materials such as activated charcoal. This is important because the background impurities may depend on the humidity of the sampled air.

Because of variations in the intensity of the ion source and the humidity of the sample air, the signals of $[H_3O]^+$ and $[H_3O]^+(H_2O)$ are not constant. To account for the varying primary ion signals, the product ion signals are normalised to a standard primary ion signal using the following equation:

$$normalized \quad ion \quad signal = 1000 \times \frac{i([RH]^+)}{i([H_3O]^+) + X_R \times i([H_3O]^+(H_2O))} \qquad \text{E 2-11}$$

where $i([H_3O]^+)$ and $i([H_3O]^+(H_2O))$ are the ion signals of $[H_3O]^+$ and $[H_3O]^+(H_2O)$ measured and $i(RH^+)$ is the product ions measured. The normalised ion signal is given in units ncps (=normalised counts per second). The factors X_R are compound specific and reflect both the mass dependent detection efficiency for $[H_3O]^+$, $[H_3O]^+(H_2O)$ and R, and the difference in rate coefficient for the $[H_3O]^+$ + R and $[H_3O]^+(H_2O)$ + R proton transfer reactions. Values for X_R are determined by measuring constant mixing ratios of each VOC at varying humidity, which changes the ratio of $[H_3O]^+$ and $[H_3O]^+(H_2O)$ (Warneke et al., 2001b; de Gouw et al., 2003a).

In principle, the response of the PTR-MS instrument with respect to specific VOCs can be calculated from the instrumental conditions and the rate coefficient for the proton transfer reaction with $[H_3O]^+$ (Lindinger et al., 1998). Because the uncertainties in the rate coefficient can be substantial (50%) and to a lesser extent to account for possible inlet losses, calibration measurements are performed to achieve greater accuracy

2.1.4 **Validation of VOC measurements by PTR-MS**

PTR-MS has emerged as a useful tool to measure volatile organic compounds, including many oxygenated VOCs, in the atmosphere. In PTR-MS due to the quadrupole filter, only the mass of the ions produced in the instrument is determined, which is a useful but not a unique indicator of the identity of a VOC. PTR-MS instruments employed here to measure several mass over charge ratios (m/z) among which 33, 42, 45, 47, 59, 69, 71, 79, 93, 107, 121, 137 have been attributed to protonated methanol, acetonitrile, acetaldehyde, ethanol, acetone, isoprene, MACR+MVK, benzene, toluene, C_2- and C_3-benezenes and sum of monoterpenes, respectively. The compounds listed above are thought to be the predominant compounds on these m/z's but contributions from other compounds or compound fragments e.g. contributions of propanal to m/z 59 or from a fragment of 3-pentene-2-ol to m/z 69 may have occurred.

A significant limitation of that method is that it cannot distinguish between sometimes important isobaric species, such as methyl vinyl ketone / methacrolein (products of isoprene oxidation) and acetone

/ propanal (products of propane oxidation). Fragments of ions at m/z 87 (e.g. 3-pentene-2-ol) may contribute to m/z 69.

One solution is to operate the PTR-MS in parallel with the slower but more specific technique of gas chromatography as was done in this dissertation. Another possibility is to use hyphenated techniques as GC-PTR-MS (Eerdekens, 2002; Warneke et al., 2003; de Gouw et al., 2003a).

Alternatively, identification would be possible using PTR- Ion Trap -MS (Warneke et al., 2005; Prazeller et al., 2003; Warneke et al., 2004) or PTR- Linear quadrupole Ion Traps (Hager, 2002). Recently, the combination of proton transfer reaction chemical ionisation with a time-of-flight mass spectrometer (Blake et al., 2004) has become commercially available. The PTR-TOF-MS instrument enables the complex interplay between many trace gas components to be determined in real-time measurements. The ability of PTR-TOF-MS to capture the complete mass spectrum on a short time scale makes it possible to take a holistic view of important transient phenomena.

2.1.5 **Accuracy, precision in measurements and calibrations**

Measurement of any physical quantity produces results that have errors. Various factors can introduce experimental errors and the overall quality of a measurement can be discussed in terms of precision and accuracy. Accuracy is defined as the difference between a measured value and a true value. The overall accuracy may be affected by a combination of statistical errors (precision) and systematic errors (bias) that are due to sampling and analytical operations. Statistical errors sometimes can be improved (reduced) by making many repeated measurements so that the data distribution is narrower. Systematic errors are common to every measurement and examples include calibration errors and offsets. Systematic errors are generally avoidable or correctable, though it is not always apparent when such an error exists. Often statistical analysis of the data reveals a mistake as a subset of data that is not consistent with other data (Bevington and Robinson, 2002.)

The precision or statistical uncertainty in the volume mixing ratio was calculated conservatively using the Gaussian error propagation. The overall accuracy of the determination depends on the accuracy of each signal used in the calculation and their respective systematic errors. Reported values should be accurate to within 5-10 % assuming no unaccounted-for systematic errors are present and using the stated accuracy of the calibration standard and measurements of calibrated instrument response.

In practice for PTR-MS measurements, higher signals, and therefore more precise signals, can be obtained by observing the ion count rate at a given mass-to-charge ratio for a longer period of time (e.g., increasing the dwell time for each m/z ratio). The percent uncertainty $dCPS_i$ (a measurement of precision) in the measured count rate of a compound due to counting statistics is defined as:

$$if\ dt > 1s\ then\ \mathrm{d}CPS_i = \sqrt{\frac{CPS_i}{dt_i}} * dt_i \quad if\ dt \leq 1s\ then\ dCPS_i = \sqrt{CPS_i * dt} * \frac{1}{dt} \qquad \text{(E15)}$$

in which CPS_i is the count rate, in counts per second and dt, the dwell time. There are diminishing returns in reducing uncertainty as dwell time is increased. For trace gas measurements, there are also lower limits to the dwell time since the smallest signals are often those of greatest interest (e.g., signal must be higher than the noise). A balance must be found between sensitivity and time resolution that is satisfactory for a given experimental situation.

When the final quantity to be determined, such as the volume mixing ratio VMR, is derived by combining more than one measurement, the statistical uncertainty in VMR can be estimated using the rule of propagating errors. The general method of getting formulas for propagating errors involves the total differential of a function. Suppose that VMR = f(p1, p2, p3, ...) where the variables / parameters p_1, p_2, p_3, etc. must be independent variables. The total differential is then

$$dVMR = \left(\frac{\partial f}{\partial p_1}\right) dp_1 + \left(\frac{\partial f}{\partial p_2}\right) dp_2 + \left(\frac{\partial f}{\partial p_3}\right) dp_3 + \ldots \qquad \text{E 2-12}$$

and dp_i is treated here as the error in parameter p_i. The numerical values of the partial derivatives are evaluated by using the average values of p_1, p_2, p_3 etc. The general results are

$$\Delta VMR^2 = \left(\frac{\partial f}{\partial p_1}\right)^2 \Delta p_1{}^2 + \left(\frac{\partial f}{\partial p_2}\right)^2 \Delta p_2{}^2 + \left(\frac{\partial f}{\partial p_3}\right)^2 \Delta p_3{}^2 + \ldots \qquad \text{E 2-13}$$

Using this equation assumes that the errors are small perturbations from the measured quantities and that errors of independent variables are uncorrelated (knowing one error does not tell you anything about any other error).

The method used in this study for the calibration of the PTR-MS-system employs serial dynamic dilution of synthetic standards over a certain mixing ratio interval using the same parent standard. The accuracy of calibration standards is therefore important because all data will be measured in reference to the standard. Dilutions are prepared by mixing amounts of standard with (purified) synthetic air over mass flow controllers. All flows are checked against a primary standard airflow calibrator (Gilibrator System from Gilian). These tests are used to confirm the linearity of the detector over the range required and the accuracy of the sample dilution procedure. The uncertainty of the calibration factor can be determined using error propagation to combine the uncertainties in the counting statistics with the other sources of uncertainty in the calculation of the calibration factor. The uncertainty in the concentration accuracy of the standard mixture was ≤5% (Apel-Riemer Environmental Inc.), the uncertainty of the mass flow controllers or the airflow calibrator used to prepare the different dilution series need to be taken into account.

2.1.6 **Campaign instrumental settings**

Table 2-2 summarises the PTR-MS experimental settings followed by a description of the inlet configurations as applied during each field campaign.

One PTRMS instrument was upgraded with an additional pumping stage between the reaction chamber and the detector. The old (2 stage) system will be referred to as PTRMS_W and the newly configured (3-stage) as PTRMS_Q. Further modifications were applied to the ion source - drift tube. There was a minor change in the reaction and electrical length of the drift tube (PTRMS_W: 9.2 cm, PTRMS_Q: 8.7 cm) but the volume of the drift tube was reduced by a factor of 4.5 (radius PTRMS_W: 2.5 cm versus PTRMS_Q: 0.6 cm) in order to shorten the residence time of the air in the drift tube. Changing the radius of the drift tube has an effect on the buffer gas velocity, the kinetic energy of the H_3O^+ions, the centre of mass energy of H_3O^+ with air and the reduced mobility. Changing the reaction length affects the reaction time, the reduced mobility, E/N, and the sensitivity (see Table 2-2).

Instrument 2 clearly has a better sensitivity as a higher number of primary ions H_3O^+ has been counted throughout all field campaigns.

Table 2-2: overview of the PTR-MS instrumental settings for each campaign.

	Instrument 1		Instrument 2	
	HOHPEX04	GABRIEL	HOHPEX04	BACCI QUEST IV
differential pumping	2-stage	3-stage (upgraded)	3-stage	3-stage
Radius Drift tube [cm]	2.5	0.6	0.6	0.6
Gas flow [cm³/min]	30.0	27.6	27.6	27.6
pressure [mbar]	2.00	2.10	2.10	2.20
drift voltage [V]	600	600	600	600
temperature [°C]	40	42	40	40
reaction time [µs]	88	87	87	92
reduced mobility	2.76	2.76	2.76	2.76
reaction length [cm]	9.2	8.7	8.7	8.7
electric field [V/cm]	65.2	69.0	69.0	69.0
E/N [Td]	141.0	142.8	142.0	135.5
ion velocity [cm/s]	1.05E+05	1.00E+05	9.96E+04	9.50E+04
Buffer gas velocity [cm/s]	12.9	196.2	196.2	187.3
Kinetic energy of H_3O^+ [eV]	0.31	0.28	0.28	0.26
H_3O^+ (cps, campaign average)	9.40e+05	5.98e+06	1.27e+07	2.55e+07
$H_3O^+(H_2O)$ (cps, campaign average)	7.90e+04	2.39e+05	1.22e+06	1.15e+06

2.1.6.1 GABRIEL

During the GABRIEL campaign measurements were performed on board of a Learjet (35A) to monitor the distribution of species vertically (300m - 10 km), and horizontally (range ca. 1800 km) by day. Morning-, noon- and afternoon-time flights were conducted to obtain data following latitudinal and longitudinal grid patterns within the boundary layer and the free troposphere.

A second PTR-MS was sited in the forest approximately central in the measurement region (Brownsberg, Suriname) to provide 24 hour ground level data for comparison with the aircraft (Sinha et al., 2008).

2.1.6.1.1 Airborne PTR-MS

A main flow of more than 10 l min^{-1} was drawn through a 9 mm I.D forward facing Teflon fast flow inlet (length ~30 cm) coupled inside the aircraft to a 6.35 mm I.D (length 1 m) Teflon tube. From the fast flow inlet, the PTR-MS system drew a flow of between 1.5 L min^{-1} at ground level to 150 ml min^{-1} at 10 km, through 2.5 m of 3.18 mm I.D. Teflon tubing. A fraction of this flow was sampled at between 25-30 ml min^{-1} directly into the drift tube. Measurements were performed under isobaric and isothermal conditions for the drift tube. The drift tube pressure was set at 2.2 mbar and was automatically adjusted to its set point value in flight. The drift tube was temperature controlled to 40 ºC when the cabin air was sufficiently cool. However, under the extremely hot cabin temperatures which were often experienced at the end of the flights this was not possible. Under such circumstances the drift tube temperature has been assumed to be equal to the cabin for the calculation of concentration. Data were obtained from 8 of the

10 flights. The time resolution was almost 30 s with dwell times of 0.9-2 s per mass. The average airspeed of the Learjet above the rainforest was ~128 ± 6 m/s.

The drift tube pressure was automatically adjusted to its set point value in flight during the GABRIEL campaign. The drift tube was temperature controlled to 40 ºC when the cabin air was sufficiently cool. However, under the extremely hot cabin temperatures which were often experienced at the end of the flights this was not possible. Under such circumstances the drift tube temperature has been assumed to be equal to the cabin temperature for the calculation of concentration. Data were obtained from 8 of the 10 flights. The time resolution was almost 30 s with dwell times of 0.9-2 s per mass. The average airspeed of the Learjet above the rainforest was ~128 ± 6 m/s.

Humidity controlled calibrations were performed in the laboratory subsequent to the campaign. The corrections for humidity driven sensitivity changes led to a small decrease in the mixing ratios for isoprene (2.7% to 9.1%), MACR+MVK (6.1 %-12.3%), methanol (19.3 % to 28.5%) and acetone (<1%). Although the calibration factor for methanol over humidity interval 20% - 100% changed only a little, for dry conditions its calibration factor was substantially lower. The effect was smaller for acetonitrile (5.5 to 7 %). Similar effects were found for the ground-based instrument.

The total measurement error (calculated as the geometric sum of accuracy and precision) for the airborne instrument for isoprene ranged from 25 % (at 0.5 ppbv), and 8 % (at 6 ppbv). For MACR+MVK volume mixing ratios between 0.4 and 2.5 ppbv the corresponding total measurement errors were between 20 % and 9 %. For acetone the total measurement errors were 25 - 10 %, for measurements ranging between 0.4 - 1.5 ppbv; and 50 - 20 % for methanol between 2 - 6 ppbv. If noise at each channel is taken as the signal observed upon sampling zero air (sampling with a catalytic converter in-line), the detection limits for the unsmoothed data using a threshold signal-to-noise ratio of three were 0.27 ppbv (methanol), 0.07 ppbv (acetonitrile), 0.09 ppbv (acetone), 0.10 ppbv (isoprene) and 0.09 ppbv (MVK).

2.1.6.1.2 Ground-based PTR-MS

The ground based site (Brownsberg National Park, Suriname) was approximately central to the operational area of the aircraft, which ranged from 6°-3.5°N and 57°-50°W. The Brownsberg measurement site (4 ° 53´ N, 55° 13´ W, ~500 m) was situated on the Mazaroni Plateau ca. 450 m above the surrounding lowlands and adjacent to a 55x40 km² lake situated east of the measurement site. Upwind from the site is 250 - 300 km of pristine rainforest before the coast of French Guyana.

An existing radio communication tower situated in a jungle clearing served as a stand for the inlet line. A membrane pump pulled down air sampled at canopy top level (~35m) through a 50 m PFA tubing (6.35 mm I.D.) towards the instrument operated at 2.1 mbar, 45°C for the drift tube. The main flow was restricted to 5 L min^{-1} mainly by a 5µm Teflon filter. The PFA tubing was shrouded with black tubing to minimise the potential of photochemically induced artefact signals. Continuous monitoring of the aforementioned BVOCs by PTR-MS (time resolution of 2 min.) at the ground based site was only possible for ~3 days starting from the 3rd of October until the 6th of October from midday to midday.

2.1.6.2 HOHPEX04

For this ground based campaign in southern Germany, the sample air was taken to both PTR-MS instruments from a rooftop sampling platform down to the laboratory by a pump, generating a main flow of 1 L/min through a 1/8" PFA tube of 11 m. This time delay was taken into account for each of the two instruments.

The minimum time resolution was 70 s with dwell times of 1.5-2 s per mass. Due to computational memory problems, the time resolution gradually rose to 114 s for the same list of 50 compounds.

The total measurement error for PTR-MS_Q for α-pinene ranged from 60 % (at 0.10 ppbv) to 10.0 % (at 1.30 ppbv); for methanol from 32% (at 0.50 ppbv) to 4% (at 8.00 ppbv); acetone 9.0 % (at 0.8 ppbv)

to 9% (at 2.60 ppbv); acetonitrile 100% (at 0.10 ppbv) to 30% (at 0.18 ppbv); acetaldehyde 60% (at 0.10 ppbv) to 7.7% (at 1.20 ppbv), and for toluene from 60 - 11% for volume mixing ratios between 0.10 - 0.70 ppbv.

The total measurement error for PTR-MS_W for α-pinene ranged from 100 % (at 0.14 ppbv) to 32.0 % (at 0.80 ppbv); for methanol from 41% (at 0.84 ppbv) to 7.5% (at 7.50 ppbv); acetone 16 % (at 0.7 ppbv) to 7% (at 2.6 ppbv); acetonitrile 100% (at 0.07 ppbv) to 32% (at 0.28 ppbv); acetaldehyde 100% (at 0.15 ppbv) to 17% (at 1.20 ppbv), and for toluene from 80 - 19% for volume mixing ratios between 0.10 - 0.60 ppbv.

2.1.6.3 BACCI QUEST IV

The VOC measurements were made at heights of 2.1, 4.6, 8.2 and 11.8 m above the forest floor. While the lowermost level was below the leaved branches, the 8.2 m level was in the centre of the foliage and the uppermost inlet was located in the canopy crown. The tree tops were generally around 14-16 meters. A single main pump was used to draw ambient air through six parallel PFA Teflon inlet lines. The length of each 6.35 mm i.d. inlets was 25 m to ensure identical residence times. Each inlet line was shrouded with black tubing to minimise any potential light induced artefacts within the lines. To prevent condensation, the lines were insulated. The flow per inlet line was restricted to a continuous 4.3 standard L min^{-1} resulting in inlet residence times of air of ~11 seconds. Each of the VOC measurement techniques is described briefly in the following sections.

At a rate of approximately 50 seconds per measurement cycle and 40 measurement cycles per level, the PTRMS sampling interval per level was ~30 minutes from April 17 to April 24. The PTR-MS sequentially monitored at all the aforementioned measuring heights, whereas the TD-GCMS and NMHC systems sampled from 8.2 m. From 24 April to 29 April all 3 instruments sampled from the 8.2 m level only.

The PTRMS calibration factors have been corrected for humidity dependence. The time resolution for the PTR-MS was 50 s with dwell times of 2 s per mass. The total measurement error for α-pinene ranged from 40 % (at 0.15 ppbv) to 4.3 % (at 15.0 ppbv); for methanol from 50% (at 0.7 ppbv) to 14% (at 5.0 ppbv); acetone 14 % (at 0.4 ppbv) to 5% (at 2.5 ppbv); acetonitrile 100% (at 0.05 ppbv) to 40% (at 0.14 ppbv), and for toluene from 50 - 10% for volume mixing ratios between 0.1 - 0.45 ppbv.

If noise at each channel is taken as the signal observed upon sampling zero air (sampling with a catalytic converter in-line), the detection limits for the unsmoothed data using a threshold of 3 signal-to-noise ratio were 60 pptv (α-pinene), 200 pptv (methanol), 42 pptv (acetone), 18 pptv (acetonitrile), and 24 pptv (toluene).

2.2 Auxiliary measurements

This section describes all other methods applied in support of the PTR-MS analysis.

2.2.1 **GABRIEL**

Details on the airborne instrumentation for the measurements of CO_2, H_2O, CO, O_3, NO, JNO_2, H_2O_2, total peroxides, OH, HO_2, HCHO, besides VOCs can be found elsewhere (Stickler et al., 2007; Martinez et al., 2008). The measurement of volatile organic compounds by the airborne proton transfer reaction mass spectrometer (PTR-MS) have been described previously, whereas VOCs measured with Thermo Desorption-Gas chromatography - Mass Spectrometry (TD-GCMS) and halogenated VOC canister GC-MS analysis are described by Williams et al., (2007) and Gebhardt et al., (2008), respectively.

2.2.1.1 TD-GCMS

Sampling for isoprene and monoterpenes over the tropical rainforest was performed using a custom built 18-cartridge sampling device installed within a standard aircraft wing pod. Within the wing pod,

outside air was drawn by a metal bellows pump into the system. The sample tubes were fitted into the flowpath approximately 80 cm after the pump with Swagelok Ultra-Torr stainless steel fittings and sealed with 2-way electromagnetic valves at the entrance and the exit. To minimise the sample contamination from airport air, the pump was generally started 15 minutes after take-off. The sample tubes were fitted into the flow path after the pump and sealed with 2-way electromagnetic valves at the entrance and the exit.

Calibrated mass flow-controllers regulated the air flow through the system and a custom made processor was used to set the parameters and record the sampling processes. All pertinent sampling and analysis parameters and further details on the Thermo Desorption-GCMS system can be found in (Williams et al., 2007). Briefly, a stainless steel, two-bed sampling cartridge (Carbograph I & II) was filled every 10 minutes for 5 minutes continuous sampling (at least one blank was flown i.e. cartridge that was not opened in flight).

Prior to flight, the cartridges were cleaned (flushed at high temperature with clean Helium 6.0) within the Thermo-conditioner. Laboratory multipoint calibrations showed good linearity within the concentration ranges measured. Blanks, namely cartridges that were flown but not opened, were taken regularly and showed no high levels for the compounds discussed. One-point calibrations of VOC and of a terpene standard (both Apel-Riemer Environmental, Inc., Denver, USA, stated accuracy 5 %) were carried out at the beginning and the middle of each flight analysis. The total measurement uncertainties were around 15 % and the detection limit ranged from 0.5 pptv to 5 pptv.

2.2.2 **HOHPEX04**

For details on the long-term VOC (Plass-Dülmer et al., 2002) ,OH radical (Berresheim et al., 2000) and other measurements at the site, the reader is referred to the aforementioned publications. These measurements have been complemented by short term campaign-type studies focussing on e.g. particle and oxidant formation processes e.g. (Birmili et al., 2000; Birmili et al., 2002; Handisides et al., 2003).

Regarding the HOHPEX04-campaign in particular, Acker et al., (2006) addressed a strong daytime production of OH from HNO_2. Bartenbach et al., (2007) used a variability-to-lifetime relationship of the short-lived VOCs to estimate a daytime mean OH-concentration of $5.3\pm1.4\times10^6$ molecules OH cm^{-3}, which compares well to the OH concentrations measured at the site, $3.2\pm2.3\times10^6$ molecules cm^{-3}. Here, the salient characteristics of the gas chromatographic and the chemiluminescence techniques for measuring VOCs are given. All instruments except the ombrometer, described briefly in the following sections, sampled from the same sampling platform under the MOHp radar tower.

2.2.2.1 GCxGC-MS

Sample air for the GCxGC-MS was taken by sub sampling the fast flow from the main inlet (3.2 L min^{-1}, approx. 15m, 1/2" Teflon tube) at a rate of 50 ml min^{-1} for 1 hour over a cold trap (Tenax TA/Carbograph) . The trap was purged with helium for 10 min to remove traces of water vapour, and then heated up to 200 °C to inject the focussed compounds onto the column. For complete desorption, this temperature was maintained for 5 min. Two dimensional chromatograms were obtained after separation over two GC columns with different polarity: a non-polar DB-5 (Agilent,Waldbronn, Germany) in the first dimension and a polar BPX-50 (SGE Deutschland, Darmstadt, Germany) in the second dimension. These columns were housed in a GC/MS 6890/5973 system from Agilent Technology, USA) which has been modified from the commercial version for analysis of low-level ambient air samples and is comprehensively described in (Xu et al., 2003 and Bartenbach et al., 2007). The system was calibrated against a 74 compound VOC standard (Apel-Riemer, CT, USA). A custom integration procedure was written to calculate the volume of each peak and allow semi-automatic data analysis processing of selected substances (Bartenbach, 2005).

2.2.2.2 GC-FID

Automated on-line long-term VOC measurements are performed routinely at the DWD, Hohenpeißenberg (since 1998). In brief, in on-line operation mode, ambient air is continuously flushed through a 10 m x 4 cm I.D. glass (Duran, Schott Glaswerke, Mainz, Germany) at 1 m^3 min^{-1} using a fan installed at the downstream end of the tube. The air intake is at 10 m above ground level, which is comparable in height to the nearby tree canopies. Samples are transferred, after passing through an ozone trap, to two Gas Chromatographic systems from the centre of the air inlet flow through a silica-lined stainless steel tubes at 30–50 cm^3 min^{-1} through a permeation dryer with a counter flow of ultrahigh pure nitrogen or helium and a stream selector valve. A first system (cryotrap: glass beads (85 K / 473 K) + Varian 3600CX: Al_2O_3/KCl, 50m x 0.53 mm column, FID) focuses on C_2-C_8 Hydrocarbons and a second system (adsorption trap TenaxTA/Carboxen (303 K / 473 K) + Varian 3400CX: BPX-5, 50 m x 0.22 mm column, MS/FID) focuses on C_5-C_{14} hydrocarbons, halocarbons and oxygenated VOCs. These systems are described in detail in e.g. (Plaß-Dülmer et al., 2002). Measurements are performed at 1:00 and 13:00 CET ca. 80 VOCs with detection limits between 1 ppt and 10 ppt and a measurement accuracy for C_2-C_9 hyrocarbons of 5-25 %, and 20-40 % for terpenes.

2.2.2.3 Formaldehyde

A slightly modified analyser (model AL 4021, Aerolaser GmbH, Germany) was used to determine formaldehyde (HCHO) mixing ratios sampling though a 1/8" Teflon tube. The measurements are based on the fluorescence technique first described in Kelly and Fortune, (1994). Formaldehyde, after being quantitatively stripped into the liquid phase (0.025 M H_2SO_4) at 10 °C in a stainless steel stripping coil, reacts with an amine and 2,4-pentadione (acetylacetone) at a regulated low pH (CH_3COOH, 100% p.a. in a second temperature stabilized stainless steel coil at 65 °C to form alpha,alpha'-Dimethyl-beta,beta'-diacetyl-pyridine (Hantzsch reaction) which is excited at 400 nm with an Hg lamp. This produces a fluorescence radiation detected 90° off-axis at 510 nm with a photomultiplier tube (PMT) (H957-01, Hamamatsu Photonics, Germany). A low pH with SO_4^{2-} is used to prevent SO_2, a possible interferent, from entering the stripping solution.

2.2.2.4 Precipitation measurements

A precipitation sensor was installed on the sampling platform for establishing the start and end of precipitation events (Eigenbrodt, Germany). Its output is 1 (one) for a closed electrical circuit and 0 (zero) for an open electrical circuit. The precipitation sensor does not provide an indication of how much rain is falling but has the advantage of been a high frequency measurement. The sampling platform was located about 25 m higher and about 125 metres NW of the open meteorological measurement field where permanent precipitation measurements are performed. These include an ombrometer (also called micro pluviometer) (Attmannspacher and Riedl, 1973). This type of rain gauge is capable of measuring very small amounts of precipitation. The duration of the precipitation is determined by a separate precipitation sensor, determining the start and the end of the precipitation with an accuracy of one minute (similar to the sensor on the platform). The amount of precipitation is measured by two sensors, uniform artificial formed drops and a tipping bucket. The accuracy of measurement in case of the artificial drop is 0.005 mm, in case of the tipping bucket 0.1 mm precipitation. We assume both the sampling platform and the open meteorological measurement field to be co-located.

2.2.3 **BACCI-QUEST IV**

At the SMEAR II station in Hyytiälä, a 74 metre high mast is used for long-term measurements of meteorological, physical, and chemical parameters as a function of height (4.2, 8.4, 16.8, 33.6, 50.4, and 67.2 m). These measurements include trace gases such as NO, NO_2, SO_2, CO, CO_2 and O_3; temperature, humidity, wind speed and wind direction and radiative measurements. A more detailed description of the site is given in Hari and Kulmala, (2005). For the VOC measurements, a smaller mast was constructed circa 100 m from the aforementioned main SMEAR II measurement tower and circa 25 m from where the aerosol measurements were made. Gas phase sulphuric acid measurements were made from another nearby cottage. All these measurements were conducted within 100 m radius of the SMEAR II tower. Thus, for the interpretation of the observations all the three inlets are considered to be co-located. VOCs

were quantified using a Proton Transfer Reaction Mass Spectrometer (PTR-MS), a Thermo Desorption - Gas Chromatography Mass Spectrometer (TD-GC-MS) and a Methane & Total Non Methane Hydrocarbon (NMHC) analyser.

2.2.3.1 TD-GCMS/SPME

On-line adsorption/thermal desorption was conducted using a gas chromatograph (GC 6890A) coupled to a Mass Selective Detector (MSD 5973 *inert*), both Agilent Technologies. The TD-GC-MS as used during this campaign is described elsewhere Williams et al., (2007). The MSD was operated in scan mode (20-250amu) for the identification of compounds and in SIM mode for their quantification. Monoterpenes which differ from one another only in the way the atoms are oriented in space and consequently are non-superposable mirror-images of one another, better known as chiral monoterpenes or enantiomeric monoterpenes were separated using a beta-cyclodextrin capillary column (Cyclodex-B, 30 m-long, 0.256 mm I.D., 0.25 μm film thickness) supplied by J & W Scientific (Folsom, CA, USA). The internal coating was composed of a permethylated β-cyclodextrin dissolved into a cyanopropyl-dimethyl polysiloxane liquid. The overall analysis time was 52 minutes with a precision error of 5-10% and accuracy against a monoterpene gas standard of 5% (Apel-Riemer Environmental, Inc., Denver, Colorado, USA). Retention time confirmation of individual enantiomeric and non-enantiomeric monoterpenes was performed by analyzing pure standards under the same conditions. The elution order of enantiomers was further confirmed by comparison with previous work (Yassaa and Williams, (2005) and from the literature. Subsequent experiments designed to study the enantiomeric composition of monoterpenes in the emission of natural and damaged Scots pine have been conducted with solid-phase microextraction (SPME) combined with dynamic branch enclosure cuvettes and enantioselective GC-MS (for details see Yassaa and Williams, 2007) simultaneously with TD-GC-MS.

2.2.3.2 CH_4 & NMHC

Methane and total non-methane hydrocarbons were measured using a commercial gas chromatograph equipped with a flame ionization detector (Model 55C, Thermo Electron Corporation, Massachusetts, USA). Upon complete elution of methane in ~17 seconds, the GC column is back flushed by the carrier gas (N_2) and the non methane hydrocarbons are carried to the flame ionization detector (FID) for detection. The signal of the FID NMHC-channel is calibrated for propane and reported in propane equivalents, which can then be converted to parts per billion carbon (ppbC). The analysis time is 70 seconds while the accuracy and precision is ± 2 % of the measured value. The detection limit is 20 ppb for methane and 150 ppbC for the non-methane hydrocarbons. Methane measurements conducted with this instrument in the boreal and tropical forests have been described in Sinha et al., (2007)

2.2.3.3 H_2SO_4

Gaseous sulphuric acid measurements were performed by MPIK Heidelberg (Fiedler et al., 2005) using a chemical ionization mass spectrometer (CIMS) instrument developed and built by MPIK, Heidelberg. Reagent ions of the type $NO_3^-(HNO_3)_n$ (n mostly 1) are produced in the ion source and subsequently introduced into the flow reactor. Instrumental details have been described elsewhere (Hanke et al., 2002). H_2SO_4 molecules in the ambient air, are passed through the flow reactor, undergo ion-molecule reactions and the mass spectrometer measures the abundance ratio of product and reagent ions. The detection limit of H_2SO_4 was 2×10^5 cm^{-3} corresponding to an atmospheric mole fraction of 8 ppqv. The time resolution of the H_2SO_4 measurements is better than 10 s, but the H_2SO_4 concentrations presented here were integrated over 200 s to reduce statistical error. The measurements bear an uncertainty of ±30 % to the actual reading (Fiedler et al., 2005).

2.2.3.4 Aerosols

Aerosols at Hyytiälä were measured by numerous instruments operated by the University of Helsinki. An aerodynamic particle sizer, (TSI3321) was used to count aerosol particles in the size range 0.7μm to 20μm while a Differential Mobility Particle Sizer (DMPS) instrument described by Aalto et al., (2001)

measures the number of particles in the diameter range 3 nm to 850 nm. The total aerosol number concentration refers to the integrated $dN/dlogD_p$ over the DMPS-measurement range. The precision for the DMPS-measurements was calculated to be 4 - 10 % on the total aerosol number concentration and include counting statistics, flow rate errors, detection efficiency errors, the differential mobility analyser dimension errors, and errors for temperature and pressure.

2.2.3.5 Other trace gases

H_2O and CO_2 concentrations were measured on all levels at SMEAR II with an infrared light absorption analyser (URAS 4); O_3 concentration with ultraviolet light absorption analyser (TEI 49C) and CO with infra red absorption (Horiba APMA 360). The trace gases SO_2 and NO_x were measured by UV fluorescence (TEI 43CTL) and chemiluminescence (TEI 432CTL), respectively. The time resolution was 1 minute for all analysers. Thus within 30 minutes, parameters were measured 5 times at each height. For a detailed description see Kulmala et al., (2001). The measurement precision is expressed as the standard deviation (1σ) of the signal while sampling calibration gas and amount to ~0.05 g H_2O/m^3, ~0.1 ppm CO_2, ~0.5 ppb; O_3, ~0.05 ppb SO_2, ~0.05 ppb NO_x, and ~6 ppb of CO. The measurement accuracy amounts to 0.5 g/m^3 for H_2O, 5 ppm for CO_2 , 1 ppb for O_3, 0.1 ppb for SO_2, 0.1 ppb for NO_x, and 10 ppb for CO. These values are based on the observed changes of the signal offsets between successive calibration checks. Relative humidity was calculated as the ratio between the measured H_2O concentration (converted to vapour pressure) and the saturation vapour pressure (dew point temperature was only measured at 23.3m) calculated from the measured air temperature with an accuracy of 2% absolute to the actual reading (P. Keronen, 2009 Personal communication).

3 Flux estimates of isoprene, methanol and acetone from airborne PTR-MS measurements over the tropical rainforest during the GABRIEL 2005 campaign

This chapter has been published in Atmospheric Chemistry and Physics, 9, 4207-4227, 2009 www.atmos-chem-phys.net/9/4207/2009/

New insights have been obtained by further analysis after publication. It is therefore recommended to refer to the chapter given below in scientific publications.

3.1 Introduction

Tropical forest ecosystems are important sources and sinks for many gas and aerosol species, producing almost half of the estimated 1.3 Pg C yr^{-1} globally emitted biogenic volatile organic compounds (BVOCs) (Guenther et al., 1995; Guenther, 2002) comprising 44 % of isoprene, 11 % of monoterpenes, 22.5 % of other reactive VOCs and 22.5 % of other VOCs (e.g. methanol and acetone). Global atmospheric chemistry models rely on emission inventories to provide accurate fluxes of BVOCs. Such emissions vary as a function of many parameters e.g. temperature, light, species, age etc. (e.g. Monson et al., 1992; Kesselmeier and Staudt, 1999) and hence are subject to large uncertainty due to enormous species diversity, uncharacterised landscapes and limited datasets.

Recently a new parameterised inventory named the Model of Emissions of Gases and Aerosols from Nature (MEGAN) (Guenther et al., 2006), has been developed to better quantify net terrestrial biosphere BVOC emissions. Leaf area index and plant functional type are among the driving parameters within MEGAN. The annual global isoprene emission estimated with MEGAN ranges from about 500 to 750 Tg C yr^{-1} depending on the driving variables used. Estimated emissions can, however, vary by more than a factor of 3 for specific times and locations. This applies not only to isoprene but also to biogenic oxygenated compounds such as acetone and methanol which will be introduced in future versions of the inventory. Both these compounds are strongly emitted by terrestrial vegetation but their budgets are currently not well constrained (Galbally and Kirstine, 2002; Jacob et al., 2002). Therefore comparisons of modelled and measured values are essential to assess our current understanding of BVOC fluxes. A further motivation for such comparisons is that the oxidation chemistry of BVOCs over low NO_x tropical ecosystems is currently not well understood (Lelieveld et al., 2008).

In this study we present *in situ* airborne measurements of BVOCs for the long dry season in October 2005, monitored by a Proton Transfer Reaction Mass Spectrometer (PTR-MS) together with other trace gases over Guyana's tropical rainforest. Most notable within the context of this study are the observations of hydroxyl (OH) and hydroperoxy (HO_2) radicals, reactive oxidized nitrogen (NO_x) and ozone (O_3), during the GABRIEL (Guyana's Atmosphere-Biosphere exchange and Radicals Intensive Experiment with the Learjet) campaign. The GABRIEL campaign was a successor to the LBA/CLAIRE (Large-scale Biosphere-Atmosphere experiment) which was conducted in the short dry season in March 1998 (e.g. Williams et al., 2001). The main focus of GABRIEL was to concurrently quantify OH and key BVOC species over the Amazonian rainforest and to compare these values to those simulated by state of the art models. Ten flights were performed between 300 m to 10km altitude, at different times of day and extents of rainforest influence, providing a data set suitable for studying horizontal, vertical and diurnal profiles over the pristine rainforest. This large scale approach is inherently less prone to scaling errors

than single leaf or tower based studies (Greenberg and Zimmerman, 1984; Rinne et al., 2002; Greenberg et al., 2004a; Karl et al., 2004a). The spatial and temporal distribution of isoprene, its oxidation products methacrolein and methyl vinyl ketone, methanol and acetone during the GABRIEL campaign were used together with an empirically derived convective boundary layer (CBL) height (or ‘‘mixing height’’) to estimate their emission fluxes as a function of time.

Profiles and inferred fluxes are compared directly with data derived from a Single-Column atmospheric chemistry and climate Model (SCM) (described in detail elsewhere Ganzeveld et al., (2008) and references therein). It is important to compare *in situ* measurements and empirically derived fluxes with those predicted by (chemistry-transport) models. There are few such comparisons available in the literature to date and as such this research is a first attempt to determine the model uncertainties in representing the physical and chemical processes. There is evidence for large discrepancies reported between measured and modelled isoprene concentrations from these regions (Ehhalt and Prather, 2001; von Kuhlmann et al., 2004; Jöckel et al., 2006). These discrepancies seem to occur in all these model simulations despite the use of well established isoprene emission algorithms (Guenther et al., 2006; Guenther et al., 1995). Application of the SCM, deemed to be representative for the simulated atmospheric chemistry in these chemistry-transport models, also facilitates interpretation of the observations by providing information regarding unmeasured processes and parameters.

This chapter is structured as follows: first we examine the specific boundary layer dynamics and meteorology of the region since this is essential for the interpretation of BVOC observations. The vertical and diurnal profiles of mixing ratios are then examined and related to chemical and mixing timescales. Finally the measurements are used to calculate a flux from the rainforest using several approaches, the results of which are compared and discussed.

3.2 Site description and meteorology

Meteorological conditions over the northeast coast of South America are strongly influenced by the annual migration of the Inter-Tropical Convergence Zone (ITCZ). Two rainy and two dry seasons can be distinguished and the long dry season takes place from mid August till end November. In October 2005 the ITCZ was located north of Suriname at approximately 10-15°N. Although geographically in the northern hemisphere, the Guyana’s lie in the atmospheric southern hemisphere at this time, under the influence of the south-easterly trade winds. At the surface the trade winds advect clean marine boundary layer air westwards over the pristine tropical rainforests of French Guyana and Suriname.

Despite the fact that GABRIEL was conducted during the dry season, meteorological observations indicate that the region was still relatively moist with almost daily rain showers subsequent to the development of shallow cumuli in the afternoon and increasing cloudiness towards the evening. The low level cloud base over land during the GABRIEL-campaign varied from 300-550 m in the morning, to 900-1200 m in the afternoon (based on visual, civil aircraft and satellite observations) and the cloud coverage has been comparable over Suriname and French Guyana during this campaign; generally up to 3/8, occasionally 5/8 in the afternoon (Scheeren et al., 2007). Cloud shadows reduce the upward heat flux from the surface into the atmosphere (Schumann et al., 2002) as well as the light-dependent trace gas emissions. The average surface temperature for October 2005 was 33°C and the relative humidity generally varied between ~70 % (morning) and ~50 % (afternoon) with surface easterlies of 5-6 m/s.

3.3 Comparison PTR-MS - GCMS

The number of PTR-MS data points that could be averaged over 5 minutes around the centred sampling time of the cartridges varied because of the unequal sampling rates among the flights and because the PTR-MS periodically measured background values through the aforementioned catalytic converter. Therefore, a minimum threshold of 5 PTR-MS data points per cartridge was imposed for the intercomparison with the TD-GC-MS as presented in Figure 3-1. The error bars indicate the total

measurement uncertainty for isoprene. The y-axis error bars are calculated by the root mean square of the total measurement errors of all PTRMS data points within each interval. These total errors were found to be less than 16 % for values higher than the median mixing ratios measured by the PTR-MS and 15 % for the TD-GC-MS.

The orthogonal distance analysis expresses a linear relationship between the PTRMS and the TD-GCMS with a slope of 0.81 and an off-set of 34 pptv (R^2=0.895). From all the diagnostic information we have on both measurement systems, no irregularities have been found. Since GC-PTR-MS measurements were not performed, the relative contributions from known and unknown interferants (protonated molecules, or fragments e.g. from m/z 87 to m/z 69) could not be determined. Such interferences are assumed to be minor as isoprene will be most abundantly present over the tropical rainforest and the furan interferences from biomass burning were low.

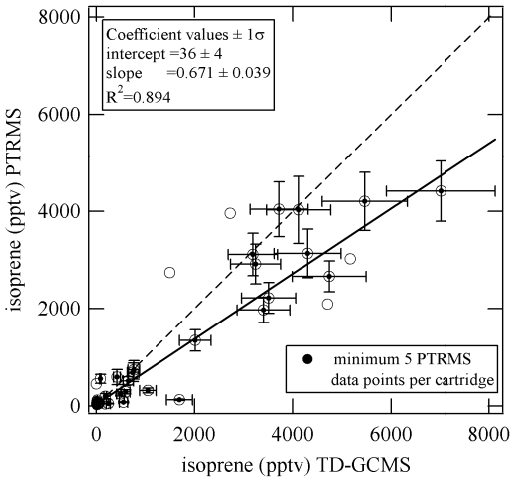

Figure 3-1: Orthogonal distance regression of PTR-MS vs TD-GCMS. Error bars represent the total measured uncertainty for each measurement technique within each interval of comparison.

The intercept is approximately zero in contrast to the isoprene inter-comparison for the LBA/CLAIRE campaign in 1998 (Warneke et al., 2001a). In 2005, the cartridges were analysed immediately after each flight in order to minimise possible storage time artefacts. Storage tests on alkenes including isoprene captured in canisters have shown that the concentration of these species tend to grow after storage (Colomb et al., 2006), possibly explaining the larger 1998 offset. The high pumping rate through the wingpod system prevented the testing of sample integrity with a gas standard. If a reactive compound such as isoprene had been destroyed in the pump then isoprene would have been underestimated by the TD-GCMS analysis against PTR-MS and this was not observed.

As the inter-comparison of the GC and the PTR-MS is just within the stated uncertainty, we do not correct the PTR-MS data in our subsequent calculations.

3.4 SCM Model

Since the Single-Column, chemistry climate Model is described elsewhere (Ganzeveld et al., (2008) and references therein), only the salient features of the model are summarised below.

The SCM includes an explicit representation of atmosphere-biosphere trace gas exchanges using a multi-layer canopy exchanges model, distinguishing a crown- and understorey layer. It accounts for exchange processes and turbulence within the canopy as a function of the SCM's meteorological, hydrological and atmospheric chemistry parameters. In the default version processes are resolved using, similar to the commonly applied vertical resolution of global models (e.g. ECHAM4/5), 19 layers (hereafter referred to as L19 version) from the surface up to 10 hPa with 5 layers representing the

daytime CBL. However, because of the demonstrated impact of a higher vertical resolution on tracer transport (Ganzeveld et al., 2008), the measurements are also compared with a 60 layer (L60) version of the SCM with 13 layers in the CBL.

The SCM's chemistry scheme is based on the CBM4 mechanism (Roelofs and Lelieveld, 2000 and references therein and has been modified to include the oxidation of terpenes by ozonolysis (Ganzeveld et al., 2006) and H_2O_2 production through the formation and decomposition of long-chain hydroxyalkyl-hydroperoxides (Valverde-Canossa, 2004). For more details on the NO_x and ozone chemistry during the GABRIEL campaign we refer to Ganzeveld et al., (2008).

Model simulations have been performed in the "Lagrangian mode" which implies that during the simulations, the air column is advected from the Atlantic Ocean over the Amazon rainforest along a transect along 4.5°N from 45°E to 60°E at a speed of the average PBL wind speed (~6 m/s) based on the observations (see Figure 2 in Gebhardt et al., (2008) for the vertical profiles for the wind direction and wind speed for the whole campaign). Modelled air masses are first advected over the ocean (1 day, 2nd of October) and then for 2 days over land (3-4th of October), simulating the response of the column to changes in surface cover properties including the transition from atmosphere-ocean to the atmosphere-land-biosphere exchanges properties. The land cover properties, NO and VOC emission factors are determined by the distribution of the 72 ecosystem classes of the Olson, (1992) ecosystem database. Biogenic NO emissions are calculated according to Yienger and Levy, (1995) whereas isoprene emissions are simulated using the recent MEGAN (Model of Emissions of Gases and Aerosols from Nature) algorithm (Guenther et al., 2006). All other biogenic fluxes, including terpenes and oxygenated VOCs are based on alternative algorithms (see Ganzeveld et al., 2008 and references therein).

The North Atlantic Oceanic vertical profiles of methanol and acetone have been used to initialise the model at 45°E up to 4 km (see Figure 3-2). Since isoprene mixing ratios over the ocean were close to or below the detection limit, its vertical initialisation profile was set to zero on all levels in the SCM.

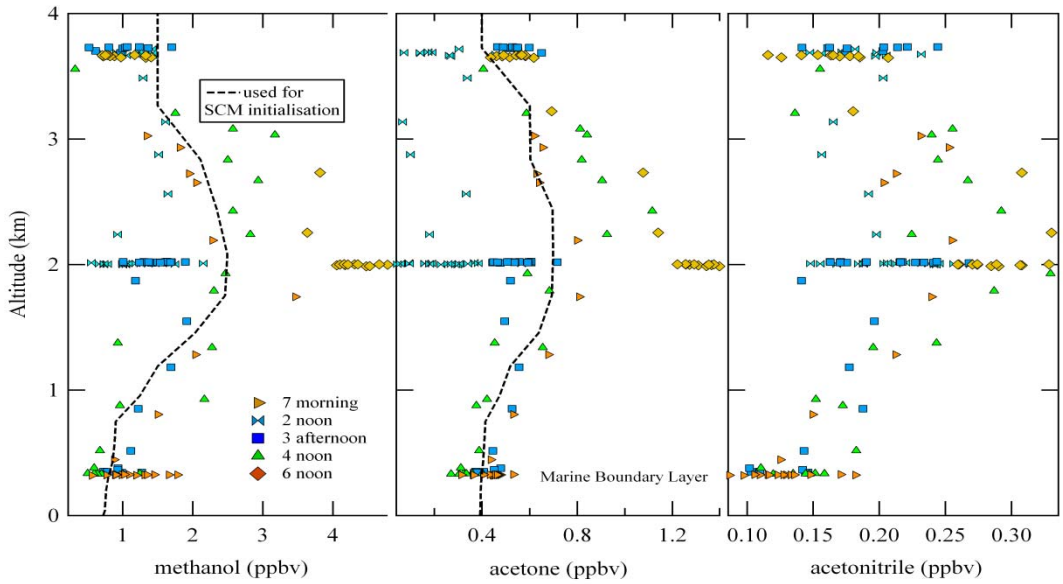

Figure 3-2: Oceanic vertical profiles for methanol, acetone and acetonitrile used for SCM-model initialisation.

The SCM calculates the isoprene fluxes separately online from the simulated micrometeorology according to the MEGAN emission algorithm (Guenther et al., 2006). In this way, a maximum of 14 mg isoprene $m^{-2}h^{-1}$ has been obtained on the first day over land as shown in Figure 11 of Ganzeveld et al., (2008). The isoprene emission flux for the second day over land is simply lower because of the simulated clouds. From the data presented in this paper (see Section 3.5.5) we have inferred an emission flux which

is apparently a factor 2 smaller than that calculated with default SCM configuration (L19) including the state-of-the-art emission algorithm MEGAN. This reduction does not imply that the MEGAN fluxes are incorrect. Consequently, to focus on the role of CBL transport and chemistry we compare our results to SCM simulations with a factor 2 decrease in simulated emissions.

Since bi-directional exchanges for methanol and acetone have been reported in the field (Karl et al., 2004a), biogenic exchanges in the SCM are described using a compensation point approach in which a balance between emission and deposition is defined. The reader is referred to Ganzeveld et al., (2008) and references therein for further details.

3.5 Results and discussion

3.5.1 Observations and simulations of the CBL

At the outset of this study it is important to characterise the evolution and structure of the CBL over the tropical forest. This is of particular importance when estimating trace gas concentrations and fluxes from the forest since the boundary layer dynamics control the dilution and vertical turbulent transport of the chemical species (see also Vilà-Guerau de Arellano et al., 2009).

Surface winds were rather constant (surface easterlies of 5-6 m/s) throughout the campaign, which is consistent with stable trade wind conditions. Figure 3-3 shows the characteristic thermodynamic vertical profiles during GABRIEL in 5-95 percentile box and whisker plots with highlighted means and medians (13-15 local time, LT=UTC-3) for the virtual potential temperature (θ_v) and the specific humidity (q). θ_v is calculated according to Bolton, (1980) from the static air temperature and q is calculated from the measured water vapour mixing ratio using an NDIR absorption spectrometer (Gurk, 2003). The observed morning profiles of θ_v are typical for dry convective boundary layers without clouds and strong persistent winds above the CBL (marked by clear differences in temperature and humidity). The exchange of compounds with the layer above occurs particularly when the CBL develops. The growth may continue in the afternoon or the CBL height may stabilize, depending on the synoptic conditions and the amount of surface buoyancy flux.

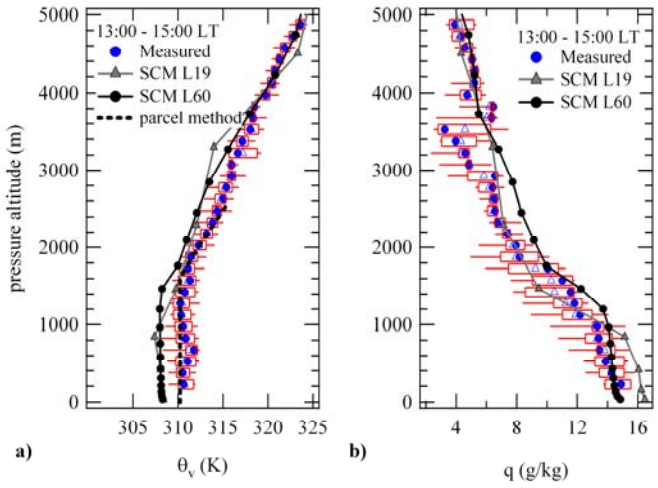

Figure 3-3: Virtual potential temperature and specific humidity profiles between 13:00 and 15:00 gathered from several flights above the Guyana's rainforest in comparison to their SCM simulated profiles.

In the course of a day, as clouds are being formed, the profiles of θ_v over the rainforest show a conditionally unstable layer caused by the high moisture content, above the first virtual temperature inversion (see below). The sub-cloud layer buoyancy is driven by upward thermals, and in the cloud layer the positive buoyant motions are due to the release of latent heat by the condensation process. Both

sub-layers are components of the CBL or mixed layer. As a result, chemical compounds are transported to higher vertical heights compared to clear sky conditions, causing the CBL mixing ratios of emitted compounds to change (Schumann et al., 2002; Vilà-Guerau de Arellano et al., 2005). Clouds also reduce radiation dependent biogenic emissions, photolysis rates and photochemical processes underneath (Lelieveld and Crutzen, 1991; Tang et al., 2003).

To support our observational analysis and to verify the occurrence of clouds, we have used a parcel method calculation. In short, we release a parcel with initial surface values θ_v=310.2 K and q_t=16 g/kg which follows a dry adiabatic until it condensates at the lifting condensation level (LCL: 1590 m). After this level the parcel follows a moist adiabatic. The results are shown in Figure 3-3a indicating a well-mixed sub-cloud layer below the LCL. By comparing the slope of the observed virtual potential temperature gradient with the moist adiabatic, we can conclude that the stratification is conditionally unstable, characteristic for shallow cumuli. The analysis does not show a clear limit of free convection (LFC), which may indicate that the cloud extension could be higher than 5000 m. We are aware that this situation is not in a steady-state and other important processes like horizontal and vertical advection are not included. However, the parcel method allows us to gain a better impression of the boundary layer dominated by clouds (Siebesma et al., 2003; Vilà-Guerau de Arellano, 2007).

In order to determine the CBL height over the rainforest as a function of time of day we have used inversions (fluctuations) in the static air temperature measured on-board the aircraft. An example of one such capping inversion (at 941 m) is shown in Figure 3-4a, and those from the entire dataset in Figure 3-4b. Data from coastal areas, (25 km from the coastline), were omitted in these estimates (see next section for further details of data filters). Note there are several inversions present in most vertical profiles and these inversions generally occur at comparable levels above the rainforest for a particular time in the day.

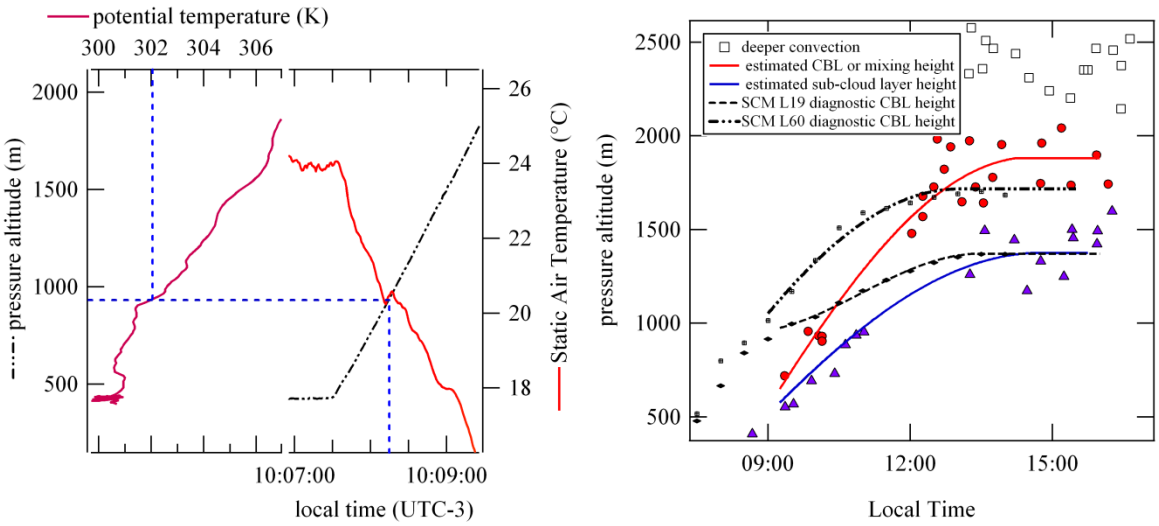

Figure 3-4: (a) Fluctuation of the Static Air Temperature (SAT) upon constant climbing of the aircraft; (b) estimate of the sub-cloud layer and the CBL or mixing height evolution for the dry season (Ocober) over the Guyana rainforest as explained in the text in comparison to that simulated by the (L19 and L60) SCM for the 1st day over land.

We determine empirically that between 9 and 15 LT the boundary layer over the forest grows from ~500 to ~1450 m (bottom curve in Figure 3-4b) by applying a sinusoidal fit and a 5th order polynomial fit for undisturbed conditions. Both fits have been found to equally well reproduce a diurnal profile of the boundary layer height with realistic boundary layer growth rates. The uncertainty on the boundary layer height estimate is directly related to the scatter and the number of observed temperature inversions. Nonetheless, in many cases several inversions occurred beyond the 1st inversion above the rainforest, marking a 2nd inversion with maxima at around 1880 m and another at around 2550 m (open squares in

Figure 3-4b) in the afternoon. These inversions are assumed to represent cloud tops. The volume below the 1st inversions is then called the sub-cloud layer.

It is important to note that due to the partial cloud cover (~3 oktas), the mixing height, the height of the atmosphere above the ground, which is well mixed due either to mechanical turbulence or convective turbulence, may not have been equal over the entire domain. Weather observations by Scheeren et al., (2007) report higher altitude scattered clouds which could be passive remnants that are no longer connected to the boundary layer and occasionally there may have been uninterrupted clouds to the 2.5 km level.

The observationally inferred evolution in height of the sub-cloud layer compares reasonably well with the findings for undisturbed conditions by Krejci et al., (2005), for the same area during LBA-CLAIRE 1998 and by Martin et al., (1998), who investigated the regions of Manaus further inland. They have reported boundary layer heights of 1200-1500 m and a cloud base of 1600-1800 m altitude.

By comparing the observed to the SCM simulated boundary layer evolution for the first day over land, we conclude that the simulated boundary layer growth rates for both the L19 and L60 version were larger in the early morning and smaller between 9 and 14LT compared to the observations (see Ganzeveld et al., (2008) for details on its boundary evolution and its driving modelling parameters). The dissimilarities in the boundary layer representation are most likely caused by inaccurate potential temperature lapse rates. Observations namely show a 3-4 K higher virtual potential temperature including a specific humidity that remained between 14 and 16 g/kg throughout the day below 1000 m. Both the L19 and L60 version simulate higher boundary layer moisture contents (16-17 g/kg) which does not decrease in the L19 version but which decreases by almost 2 g/kg in the L60 version over the course of the day. The water vapour is transported deeper in the L60 troposphere, resulting in an improved agreement between the simulated and observed moisture content. However, it results in a slightly wetter and cooler layer above 1.5 km and below 3.5 km. The sensitivity of the boundary layer evolution to the potential temperature lapse rate for the GABRIEL conditions is discussed by Vilà-Guerau de Arellano et al., (2009).

The depth of the marine boundary layer (MBL) is not expected to vary much over the course of the day. The observed inversions occurred at ~460 m pressure altitude at 08:30, around 575m around noontime, and at ~500 m around 15:15. The observed MBL depth was thereby a little less compared to the simulated MBL depth (~640 m).

3.5.2 **Data selection criteria**

BVOC emissions are inherently highly variable, being a function of plant type, solar intensity, temperature and other factors. In order to present the flight data as clearly as possible and to ensure interpretation of pristine tropical forest exchange fluxes and a fair comparison with the simulated fluxes and CBL concentrations, a number of geographical, temporal and altitude filters have been applied. The intention is to reduce the possibility masking trends in the dataset. Details of each filter applied are presented below.

Biogeographical filter: a vegetation map of South-America (Eva et al., 2004) was used to filter only data collected over rainforested regions for analysis. The northernmost 100 km of Suriname is covered along the coast by mangrove forest), fresh water swamp forest (wetland forest) and cultivated crops and non-forest land cover (UNEP-WCMC). Data from this region have been filtered out so as to leave only rainforested areas under analysis (see Figure 3-5). The total rainforested area under investigation was approx. 775 km by 220 km.

Vertical filter: data were also filtered for the time evolution of the CBL height as discussed in the section on the 3.5.1. Hereafter, only data within the mixed layer are retained.

Temporal filter: to ensure fluxes were derived from airmasses that had spent the entire daylight period over the rainforest, the "startpoint" of the measured air parcel at sunrise (ca. 6:25) was calculated based on the specific wind direction and wind speed measured by the aircraft. If the airmass at dawn, for a certain data point measured in flight, was situated above the Atlantic Ocean or the coastal periphery, the data point was not considered.

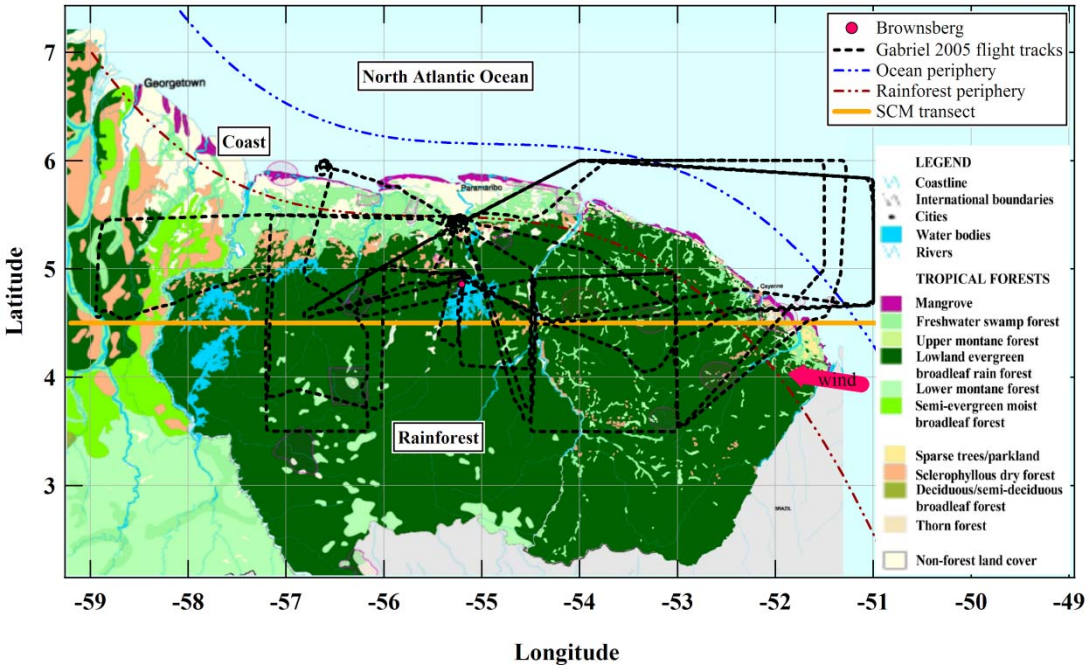

Figure 3-5: Flighttracks of the GABRIEL campaign superimposed onto a vegetation map (UNEP-WCMC, 2000).

The remaining data points are therefore deemed to reflect the role of rainforest emissions in air masses which crossed land between dawn and the moment of measurement and are characterised by their Forest Contact Time (FCT) with the Guyana's rainforest. The FCT has been defined as the time an air parcel spends in the CBL above the rainforest starting from the rainforest's periphery near the east coast of French Guyana. For this study, we focus on a transect which corresponds to the distance over the rainforest covered by an air mass between sunrise and sunset. The column of air was advected with an average speed of 5.4 m/s over the rainforest, being exposed to the surface emissions between the east coast of French Guyana and the eastern shore of the reservoir (54.9 W). This transect will be referred to as "the first day over land". Filtered data are used to infer the diurnal cycle of BVOCs above the rainforest and will be compared to the simulated diurnal cycle for the 3rd of October.

3.5.3 Isoprene chemistry

Isoprene is oxidised in the air, primarily by OH. The main sources of HOx (OH + HO_2) are photolysis of ozone, formaldehyde and higher aldehydes, whereas the main sinks are the reaction with CO, methane and isoprene emitted from the rainforest. The reaction of OH with isoprene forms methacrolein (MACR), methyl vinyl ketone (MVK) and formaldehyde as first order products (Carter and Atkinson, 1996).

Low-NO_x chemistry is still poorly understood for crucial species like isoprene (Paulson and Seinfeld, 1992) but several studies e.g. (Montzka et al., 1993; Goldan et al., 1995; Biesenthal et al., 1998; Stroud et al., 2001) have shown that ambient NO_x levels can influence the relationship between isoprene and MACR+MVK. Laboratory studies have shown that in the absence of NO oxidation product yields of MACR and MVK are 22 % and 17 % respectively and 34 % for formaldehyde in addition to organic hydroperoxides (Miyoshi et al., 1994; Benkelberg et al., 2000). Slightly different but comparable yields

for MACR / MVK were obtained by Ruppert and Becker, (2000) (17.8 % / 15.3 %) and Lee et al., (2005) (19.0 % / 14.4 %). Ruppert and Becker, (2000) indicates that small amounts of methanol may be formed as a primary product from the OH-initiated oxidation of isoprene under low NO_x. As NO was found to be generally less than 40 pptv during the GABRIEL campaign (Ganzeveld et al., 2008) isoprene oxidation is expected to produce MACR and MVK with a yield resembling that for the low NO_x studies. This is essential to this analysis in which the isoprene flux is inferred from the CBL mixing ratios of the chemically conservative tracer. For this empirical study, a summed MACR and MVK product yield of 39 % is assumed whereas the chemistry scheme in the SCM assumes a 55 % yield.

3.5.4 **Mixing ratio vertical profiles**

Isoprene and MACR+MVK mixing ratios decreased with increasing altitude reflecting the role of photo-oxidation chemistry and mixing (Figure 3-6a and b). The vertical profile shows that the isoprene was well mixed in the boundary layer with average mixing ratios of 3.2±1.0 (1σ) ppbv for isoprene and 1.5±0.3 ppbv for MACR+MVK between 14 and 17 LT below 1.5 km.

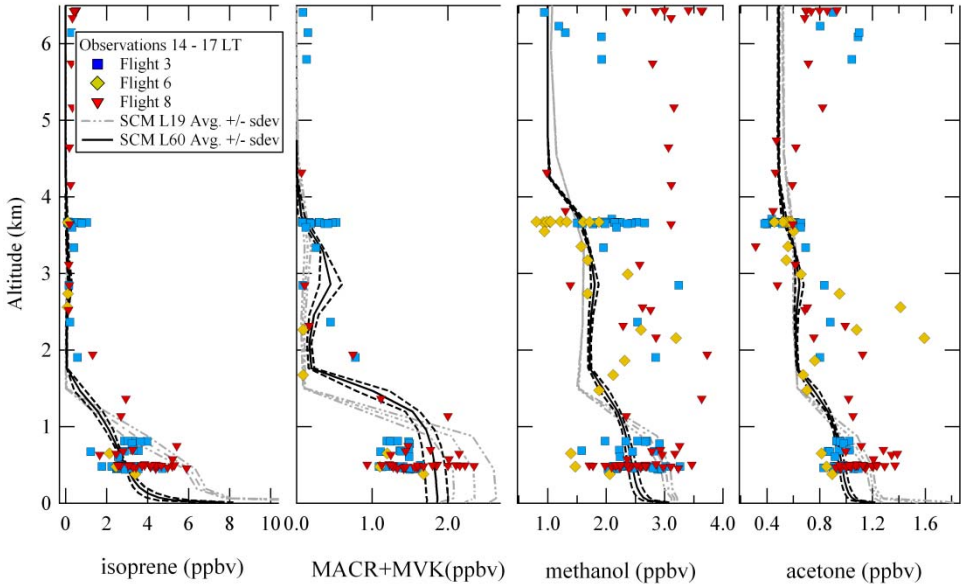

Figure 3-6: Measured and modelled vertical profiles for isoprene, the sum of methacrolein and methyl vinyl ketone, methanol and acetone over the rainforest for the first day over land.

Enhanced isoprene and MACR+MVK mixing ratios observed above ~1500 m altitude are most likely a result of convection associated with shallow cumulus clouds as discussed in a paper by Vilà-Guerau de Arellano et al., (2009). This indicates that the timescale of mixing for GABRIEL is presumably shorter than the chemical lifetime of isoprene (see below). The MACR+MVK vertical profile suggest even more effective transport but the mixing ratios remains directly related to isoprene. During flight 6 the upward transport appears to be limited to a smaller vertical domain compared to the other flights possibly due to differences in land-atmosphere interactions and cloud cover conditions

The mixed layer average isoprene afternoon mixing ratio for GABRIEL is comparable to the 3.3 ppbv obtained by Warneke et al., (2001) over the southern part of Suriname during LBA-CLAIRE 1998. It is less than observed further inland at Manaus (5.2 ppbv) reported by Karl et al., (2007) or 6.7 ppbv measured in the mixed layer over Jaru (Rondônia) reported by Greenberg et al., (2004). The latter has also reported mixed layer mixing ratios of 2.9 ppbv over Balbina also situated in Brazil.

In order to compare surface layer data, mixed layer isoprene mixing ratios need to be corrected for chemical loss as discussed below.

Figure 3-6 shows the effect of increasing the vertical resolution in the SCM from 5 (L19) to 13 (L60) layers on the distribution of BVOCs within the simulated CBL. Most remarkable is that L19 SCM version clearly underestimates the vertical mixing within the CBL and overestimates surface layer mixing ratios. The mixing ratios simulated with the L60 version results are in better agreement with observations. Furthermore, enhanced resolution results in well mixed profiles and convective transport beyond the clear sky boundary layer height (~1450m). The discrepancies between the model simulated and observed profiles are much smaller in the morning and early afternoon when convection is not as strong as in the afternoon and clouds have not yet being formed (see diurnal profiles in next section). Furthermore, the agreement in the morning is also due to a better agreement between simulated and observed OH-concentration in the PBL due to relatively large NO_x mixing ratios associated with the nocturnal accumulation of soil-biogenic NO.

Less steep mixing ratio profiles have been observed for methanol and acetone as they are less reactive towards OH and O_3 and can consequently serve to interpret the role of transport in and above the CBL for conditions with no significant contributions from biomass burning. There were no frequent influences of biomass burning on the airmasses encountered during this campaign (Lelieveld et al., 2008 also confirmed by acetonitrile mixing ratios which generally varied from 100 to 300 pptv with the exception of flight 6 and 7 for which local acetonitrile mixing ratios reached a maximum of 450 pptv between 2-3 km. During these flights, acetonitrile mixing ratios were also slightly elevated between 1 and 3.5 km over the ocean as shown in Figure 3-2. Because of the relative long lifetime it is also important to consider the background oceanic methanol and acetone mixing ratios for the initialisation of the SCM. This initialization results in simulated acetone and methanol in reasonable agreement with the observations after more than one day of transport over the ocean before arriving at sunrise at the coast (~51.5°E). Decreases of the observed mixing ratios within the marine boundary layer (~500 m) are probably due to an oceanic uptake of methanol (Sinha et al., 2007b; Williams et al., 2004), acetone (Marandino et al., 2005) and acetonitrile (de Gouw et al., 2003c; Hamm et al., 1984).

Model simulations have also shown that the free troposphere oceanic profiles, used to initialise the model, not only influence the free tropospheric mixing ratios throughout the 4-day simulation but also the morning mixing ratios above the rainforest as these compounds get mixed into the growing CBL.

Figures 6c and d show well mixed methanol and acetone profiles over the rain forest reflecting surface emissions and turbulent transport in the boundary layer. The average mixing ratios below 3 km were 2.4±0.5 (1σ) ppbv for methanol and 1.0±0.2 ppbv for acetone between 14 and 17 LT. The methanol values reported here are therefore significantly higher than the average value of 1.1 ppbv from the 1998 LBA-CLAIRE campaign over the same height range (0-3 km). In contrast, the 2005 acetone data reported here are significantly lower than the 2.7±0.8 ppbv reported for 1998.

The simulated vertical profiles, in particular those for the L60 version, are in good agreement with the observations as a consequence of the deeper CBL and more efficient upward transport compared to the L19 version. Increasing the vertical resolution within the boundary layer of the model effectively reduced the boundary mixing ratios by about 30 % between 9 and 16 LT.

The simulated vertical profile of ozone, relevant to the interpretation of the HO_x concentration profiles, is in reasonable agreement with the observations though the SCM underestimates the ozone mixing ratios between 2 and 3.5 km. The OH and HO_2 profiles in Figure 3-7 show that the measured values exceed the modelled OH-concentrations by an order of magnitude. Increasing the vertical resolution within the SCM and consequently influencing the transport of trace gases and water vapour lead to an increase in OH and HO_2. The production of HO_2 and OH (and its recycling) is much stronger in the boundary layer (and up to 3km) and is discussed in more detail in Ganzeveld et al., (2008) and in Kubistin et al., (2008).

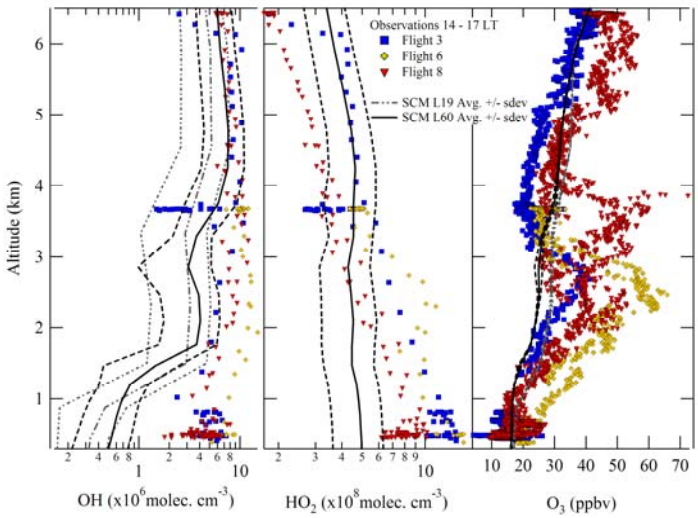

Figure 3-7: Measured and modelled vertical profile of OH, HO2 and O3 over the tropical rainforest.

3.5.5 **Mixing ratio diurnal cycles**

To assess the area average diurnal profiles of the BVOCs in the rainforest mixed layer we have used the entire aircraft dataset, filtered according to the data selection criteria, see section 3.5.2. Restricting the dataset to the first day over land has the advantage of avoiding influences of residual layers from previous days (discussed in next section and in Ganzeveld et al., (2008). Median values of the quarter hourly 5p-95p box and whisker plots have been fitted to both a 5th order polynomial fit and a sinusoidal fit. Such fits have been also applied in combination with the CBL depth to infer surface fluxes from mixing ratio observations as discussed in section 3.5.7. The green vertical lines indicate the time interval for which the vertical profiles were taken.

Airborne and ground-based observations of isoprene mixing ratios show a distinct diurnal variation, being very low in the morning, reaching peak concentrations during mid-afternoon, and decreasing towards the evening along with temperature and sunlight. Strong gradients in isoprene from the canopy source to the top of the mixed layer are responsible for the large span of values measured at any given time in the diurnal plot. Furthermore, since the aircraft sampled over undulating terrain (particularly south of 5 °N, with maximum height of 1280 m asl), sampling occurred at various heights above surface. Therefore the height above ground has been considered (calculated with SRTM3 digital elevation model data) rather than the pressure altitude. The ground-based measured values (25p / avg. / 75p / 95p: 3.3 / 4.3 / 5.4 / 6.2 ppbv,14-16:15LT) are higher than those taken in the mixed layer above 300 m (25p / avg. / 75p: 3.0 / 3.3 / 3.7 ppbv~,14-16:15LT), indicating the role of turbulent exchange in diluting as well as the high reactivity of isoprene towards the oxidants OH and O_3. K34 tower measurements near Manaus in July 2001 (beginning of the dry season, LBA-CLAIRE-2001 campaign) by Kuhn et al., (2007) displayed lower mean canopy level daytime mixing ratios of 3.4 ppbv with a maximum of 6.6 ppbv for isoprene. Higher mean noontime surface layer isoprene mixing ratios of 7.8 ± 3.7 ppbv with peak values up to 15 ppbv were obtained during the TROFFEE campaign on the Z14 tower in September 2004 (end of the dry season). Accompanying mixed layer mixing ratios between 0.6 and 6.7 ppbv with a mean of 5.2 ppbv have been observed by Karl et al., (2007). These results are comparable, yet slightly higher than the mixing ratios reported here.

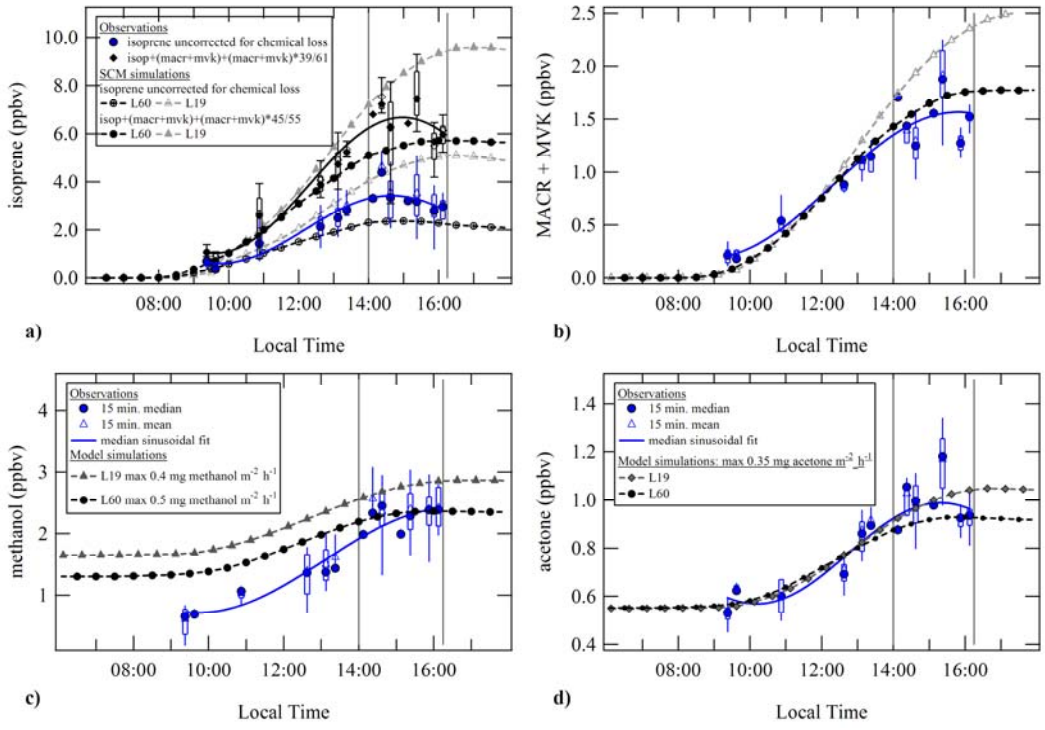

Figure 3-8: Mixed layer diurnal cycles for isoprene and its oxidation products, methanol and acetone over the Guyana's rainforest (first day over land).

Figure 3-8b indicates that mixed layer MACR and MVK mixing ratios show less variability compared to isoprene as they are formed aloft in the well-mixed boundary layer and have significantly longer chemical lifetimes. Their average summed median mixing ratio was 1.4 ppbv, ranging between 1.2 - 1.8 ppbv (25p-75p) and similar to the observations reported e.g. 2.1 ppbv by Karl et al., (2007), 2.5 ppbv by Warneke et al., (2001)a whereas the observations by Kuhn et al., (2007) were substantially smaller (~0.5 ppbv).

Figure 3-8 shows that both the L19 and L60 model simulations reproduce the diurnal mixed layer profiles of the BVOCs before 14LT reasonably well and that afterwards, only the L60 simulations are in better agreement with the observations, meaning that the discrepancy between the modelled and the observed BVOC mixing ratios can potentially to some extend be related to a misrepresentation of turbulent and convective mixing including cloud formation processes (transport of water vapour), also affecting surface emissions and photolysis. Furthermore, Figure 9 shows that increasing the vertical resolution in the SCM from L19 to L60 does lead to an increase in OH. However, differences in simulated turbulent and convective mixing apparently do not adequately explain the discrepancy between the modelled and the measured OH-concentrations. The best agreement is obtained between 9 and 9:30 LT when isoprene is still low and simulated NO_x concentrations are relative large. This reflects the release of NO_x, accumulated in the nocturnal inversion layer, out of the canopy into the mixed layer. Later in the day the discrepancy increases, pointing at a potential misrepresentation of the afternoon sources and/or sinks reactive tracers and OH. One proposed misrepresented process is OH and HO_2-recycling involved in the isoprene oxidation mechanism as explored in detail by Lelieveld et al., (2008) and Butler et al., (2008).

The Brownsberg canopy levels of MACR+MVK (25p / avg. / 75p: 5.0 / 6.4 / 8.0 ppbv, 14-17LT) were slightly higher but comparable to the average noontime mixing ratios of 2.3 ppbv reported by and 2.5 ppbv by Karl et al., (2007). Measured OH data exhibited a much less pronounced diurnal variation in the mixed layer over the rainforest than in the model (see Figure 3-9a).

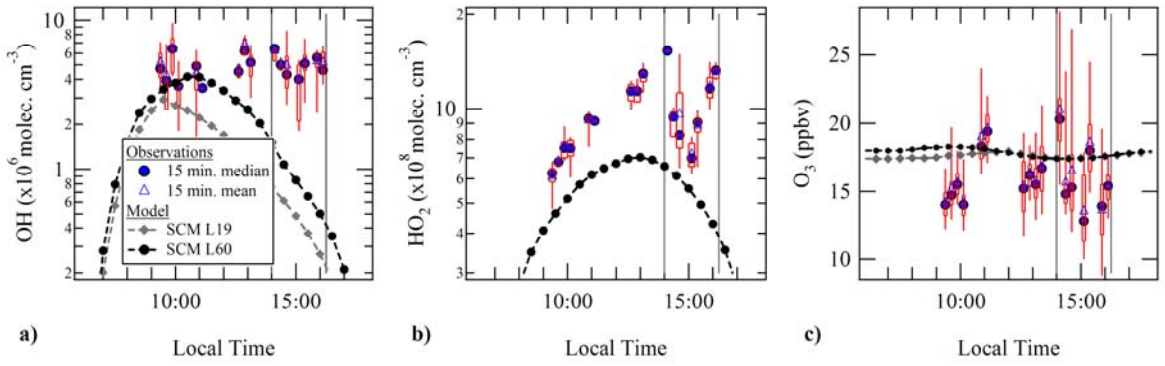

Figure 3-9: Measured and modelled diurnal profiles of OH, HO_2 and O_3 above the rainforest for October 2005.

Figures 5-8c and 5-8d show strong increases in both methanol and acetone in the mixed layer as a function of time of day. The observed morning mixing ratios for acetone and methanol are ~0.6 ppbv. The diurnal increase in methanol is larger compared to that in acetone. Afternoon methanol mixing ratios increased to 2-3 ppbv and those for acetone to 0.9 and 1.1 ppbv, and 0.18-0.20 ppbv for acetonitrile.

In the absence of significant anthropogenic activity and low biomass burning influences, the observed increases in acetone and methanol were attributed to direct biogenic emission from the rainforest ecosystem and from secondary production. The average simulated acetone mixing ratios agree well with the measurements whereas methanol mixing ratios are overestimated by the model by about 0.6 ppbv for the 3rd day of the SCM L60 simulation despite a model initialisation above the ocean in accordance with the measurements. This difference may be caused by the variation in the free troposperic methanol mixing ratios present in the advected air. The paper by Ganzeveld et al., (2008) shows that the model underestimates the mixing as well as the nocturnal deposition of all tracers discussed here. This issue is very important in the comparison of data further land inward.

3.5.6 **Chemical and mixing time scales**

The photochemical age *t* or the extent of chemical processing of isoprene in the encountered air masses can be judged from solving Eq.(1) for *t* using the ratio of [product] to [precursor], based on the reactions R1,R2,R3, assuming pseudo first order reactions and a dominance of the OH sink:

$$\frac{MACR + MVK}{ISOP} = \left(\frac{\gamma_{MACR} k_1}{(k_2 - k_1)}\right)\left(1 - e^{((k_1 - k_2)[OH]t)}\right) + \left(\frac{\gamma_{MVK} k_1}{(k_3 - k_1)}\right)\left(1 - e^{((k_1 - k_3)[OH]t)}\right) \quad \text{E 3-1}$$

$$ISOP + OH \xrightarrow{k_1 = k_{isop,OH}} \gamma_{MACR}\ MACR + \gamma_{MVK}\ MVK \quad \text{R 3-1}$$

$$MACR + OH \xrightarrow{k_2 = k_{macr,OH}} products \quad \text{R 3-2}$$

$$MVK + OH \xrightarrow{k_3 = k_{mvk,OH}} products \quad \text{R 3-3}$$

γ_{macr} and γ_{mvk} are the OH oxidation yields for MACR and MVK respectively under low NO_x, the reaction rate constants were taken accordingly as $k_{isop,OH}$=2.7E-11*exp(390/T); $k_{macr,OH}$=8E-12*exp(389/T) and $k_{mvk,OH}$=2.6E-12*exp(610/T) (IUPAC, 2007a, b, c) and [OH] as measured over the rainforest.

The ratio of [MVK+MACR]/[isoprene] has been studied elsewhere e.g. (Biesenthal et al., 1998; Stroud et al., 2001; Apel et al., 2002) and has shown a NO_x dependency. Here we compare the observed vertical (14-17LT) and diurnal profile to the model simulation for the surface and the mixed layer in Figure 3-10a and b.

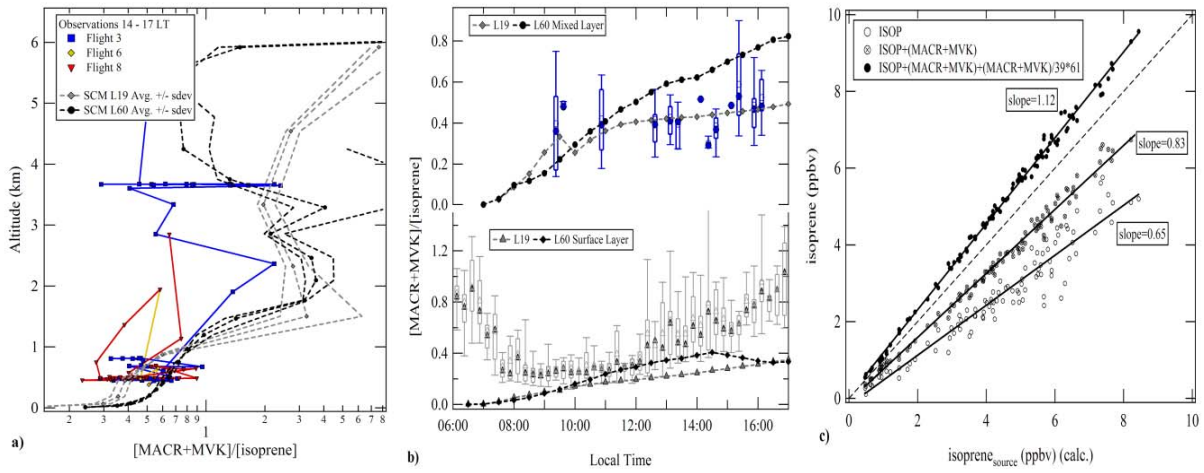

Figure 3-10: Comparison of the measured to the modelled vertical (a, 14-17LT) and diurnal profile (b) of [MACR+MVK]/[isoprene] (first day over land). (c) Comparison of conserved tracer isoprene+MACR+MVK+others in the mixed layer to isoprene calculated for the surface layer (as discussed in the text).

The observed profile is comparable to the one obtained for the TROFFEE campaign by Karl et al., (2007). However, [MVK+MACR]/[isoprene] varied over a large range and drawing conclusions from the ratio is not straightforward since it depends on the history of the air mass (forest contact time), on vertical mixing and on chemistry (dominated by OH as O_3 mixing ratios were low (10-20 ppbv)). The OH concentrations measured during GABRIEL (Figure 3-7 and Figure 3-9) were on average of 5.0×10^6 molec. cm^{-3} in the mixed layer and ~8.1×10^6 molec. cm^{-3} between 2 and 5 km and which is substantially higher than the OH concentrations used by Karl et al., (2007) and Kuhn et al., (2007) in a convective boundary layer budget analysis. The observed [MVK+MACR]/[isoprene] ratios above the CBL height are higher compared to those in the CBL reflecting low mixing ratios of isoprene and upward transport of oxidation products.

Surface layer data from Brownsberg revealed a diel pattern in the ratio [MACR+MVK]/[isoprene] that drops at sunrise from ~0.8 to ~0.3 around 8 LT, then remains rather constant at ~0.3 until noon, followed by an increase until sunset (see Figure 3-10b, lower panel). The drop in ratio in the morning hours cannot be explained with certainty by the breakup of the nocturnal boundary layer and mixing in of residual layer air. Too little information is available to clarify this and to investigate the fate of the MACR and MVK during night. Nevertheless, the model assumes a constant latitude transect (at 4.5 °N) exclusively above the ocean before sunrise and consequently the bottom panel of Figure 3-10b shows an almost constantly increasing ratio between sunrise and sunset in the surface layer. In addition, the simulated [MACR+MVK]/ [isoprene] ratio is lower for L19 than for L60 version but both are lower than observed also reflecting the fact that the model calculates lower OH concentrations.

Differences in measured and modelled product-precursor ratio suggests a much shorter "measured" photochemical age of isoprene (19 and 27 minutes) than the simulated age (0.5 to ~2 hours). It should be noted that solving Eq.(1) for t using high NO_x rather than low NO_x branching yields results in 23 % longer photochemical ages.

We calculate for the GABRIEL boundary layer conditions, atmospheric lifetimes for isoprene, MACR, and MVK with respect to OH and O_3 of on average 0.5, 2 and 2.75 hours, respectively. For acetone and methanol, we calculate atmospheric lifetimes of 13.5 and 2.5days, respectively. Due to the misrepresentation of OH and the different mixing in the model, the atmospheric lifetime of isoprene is much shorter above the rainforest as modelled (1 to 3.5 hours before 14 LT to 6 hours and more afterwards.

In order to compare the mixing and chemistry timescale we estimate the convective timescale, i.e. the time scale for the air to circulate between the surface and the top of the mixed layer (large Eddy). We assume here typical parameter values for the tropics (as observed during the TROFFEE campaign in September 2004, T. Karl, personal communication) to estimate the timescale for convective mixing (t*) based on the convective velocity scale (w*) and the boundary layer height (z_i). We used a maximum sensible heat flux ~200 W m^{-2} (also simulated by the SCM) before noon declining to ~100 W m^{-2} in the afternoon (due to cloud cover) and a surface temperature diurnal profile as observed at Brownsberg (24-26 °C). In this way we obtain a maximum convective velocity scale of 2 m/s which is in range of the convective velocity scale obtained for the TROFFEE campaign. This results in an inferred convective time scale between 8 minutes in the morning, to 16 minutes in the afternoon which is substantially shorter compared to the chemical time scale and the photochemical age calculated above.

3.5.7 **Flux calculations**

The emission surface flux is retrieved from the airborne measurements over the rainforest by the CBL budgeting approach based on E 3.2. This CBL budgeting approach assumes a quasi-stationary steady state for the vertical profiles, and as a result vertical linear flux profiles are obtained. It uses the natural integrating properties of the well-mixed atmospheric boundary layer, allowing average surface fluxes to be obtained over relatively larger regions.

Vilà-Guerau de Arellano et al., (2009) discusses this method and addresses the quantitative importance of each of the four terms. In short, the surface emission flux (Fs) is inferred from observations using:

$$F_s = h\left[\frac{\partial\langle S\rangle}{\partial t} + \left(U\frac{\partial\langle S\rangle}{\partial x} + V\frac{\partial\langle S\rangle}{\partial y}\right) - R\right] + F_e \qquad \text{E 3-2}$$

This method is time dependent reflecting the role of chemistry and the mixing (vertical transport). We assume that the tendency term ∂<S>/∂t (the change in the median concentration of a BVOC as function of time, taken from the inferred diurnal profile) within a boundary layer and mixing volume (h, determined in section 3.5.1) results in the net flux of the tracer. Although this term is mainly important in the early morning, the contribution for chemical loss term (R) is imperative during the day. The longer the atmospheric lifetime, the smaller the contribution chemical losses term will be and for inert species concentration changes with time are only due to the surface emission/deposition and entrainment of free troposphere air masses while neglecting the advection term.

As a consistency check, CO_2 data measured on board of the Learjet during GABRIEL have been used to determine the daytime uptake of CO_2. Assuming a sub-cloud layer up to ~1450 m and a CBL up to ~1880 m due to shallow cumuli, maximum value of 2.3 g CO_2 m^{-2} h^{-1} and 2.6 g CO_2 m^{-2} h^{-1} has been found from the median values after correction for entrainment. This is in good agreement with the daytime CO_2 uptake measured under high irradiance state of 2.53–3.01 g CO_2 m^{-2} h^{-1} over an old-growth tropical forest in Para, Brazil from July 2000 to July 2001 using an eddy covariance technique by Goulden et al., (2004).

For chemical reactive species like isoprene the reactivity term (R) needs to be taken into account. We propose here two different ways to calculate R:

1) In case OH has not been measured, we estimate isoprene at the canopy level by summing up the precursor and product concentrations as follows

$$R_1 = \frac{\partial\langle isoprene + (MACR + MVK) + (MACR + MVK)/39 * 61\rangle}{\partial t} \qquad \text{E 3-3}$$

based on the low NO_x oxidation yield. Note that although formaldehyde has been measured, it cannot exclusively be attributed to the oxidation of isoprene.

2) In case that OH has been measured, isoprene mixing ratios can be inferred according to:

$$R_2 = \frac{\partial\left\langle \frac{[isop]_t}{\exp\left(\left(-k_{isop,OH}[OH] - k_{isop,O_3}[O_3] + 0.5\left(k_{macr,OH} + k_{mvk,OH}\right)[OH] + 0.5\left(k_{macr,O_3} + k_{mvk,O_3}\right)[O_3]\right)t\right)}\right\rangle}{\partial t} \quad \text{E 3-4}$$

in which *t* corresponds to the photochemical age as discussed earlier.

In this way, we can study the sensitivity of the surface emission to different chemical mechanism. Figure 3-10c shows the isoprene mixing ratios calculated using the two reaction terms R_1 and R_2. From the linear slope of 1.12 we conclude that both methods provide comparable estimates of isoprene at the canopy level.

Ideally, to examine oxidation one should follow the same air mass as it traverses the landscape as is done by the SCM. Practically, only relatively short (few hours), discontinuous periods (spread over 14 days) of airborne measurements were available for analysis. The rather constant boundary conditions in terms of the key meteorological drivers in exchange and chemistry and little day-to-day variability during GABRIEL 2005 support the use of this method. By limiting ourselves to the first day over land we have eliminated the influence of residual layer air which complicates interpretation of daytime BVOC exchanges (Ganzeveld et al., 2008). We therefore neglect the second (advection) term on the right hand side of Eq. (2) as we inherently assume that the emissions occur into clean air advected from the ocean during the previous night. Empirically, we use a sinusoidal and 5th polynomial fits through the median values of 15 minute binned concentrations presented in Figure 3-11 to calculate the mixed layer fluxes for the first day over land. Both fits have been of equal merit for interpolation.

As the mixed layer mixing ratios are determined by the surface and the entrainment flux we calculate first a diurnal profile of Fs-Fe directly from the measurements before correcting for chemical loss and entrainment.

Methods to determine the importance of entrainment often (i) are based on a distinct concentration jump (ΔS) across the CBL like e.g. $F_e = -w_{entr}(C_{CBL}-C_{FT})$ with w_{entr} being the boundary layer growth on time as used in e.g. Goulden et al., (2004) or (ii) relate the overshoot and exchange of heat, moisture and compounds driven by the thermals $F_e=K_e*dC/dz$, where the exchange coefficient K_e is proportional to the convective velocity scaling and inversely proportional to dT/dz. It can be questioned if these methods, which are strictly speaking valid under clear sky conditions, are applicable to clouded boundary layers with a less pronounced concentration jump. This discussion is further pursued in Vilà-Guerau de Arellano et al., (2009).

Overshoots beyond the clear sky boundary layer height due to shallow cumuli clouds (as indicated in Figure 3-4b) are important, but the transport level is not uniform over the entire domain due to partial cloud cover. Therefore, maximum surface emission fluxes have been calculated taken a 3/8 cloud cover into account as summarised in Table 3-1. Based on the concentration jump method we roughly estimate a maximum detrainment flux (Fe) after correction for chemical loss of 1.5 mg isoprene $m^{-2}h^{-1}$ for a boundary layer that grows to 1450 m. Consequently, we obtain a surface flux (Fs) of 6.5 mg isoprene $m^{-2}h^{-1}$. Considering the upper estimate of the CBLh to 1880 m, the detrainment flux for isoprene after correction for chemical loss has been 2.3 mg isoprene $m^{-2}h^{-1}$ and the surface flux 8.4 mg isoprene $m^{-2}h^{-1}$.

Estimating the entrainment flux for methanol is more complicated as the concentration difference between the mixed layer and the free troposphere was less pronounced as for acetone. Several processes may have been involved increasing their concentrations above ~1450m involve the deeper convective transport of these compounds through shallow cumuli clouds and the eventual contribution from biomass burning to the free tropospheric air. However, both processes affect also acetone. We note in particular possible contributions to acetone from terpene oxidation (α-pinene oxidation yield of 15% in absence of NO (Nozière et al., 1999)) and methanol may be formed in the mixed layer as secondary products from

the isoprene oxidation under low NO_x (e.g. from the photolysis of glycolaldehyde, lifetime against OH of 6 hours), as well as from the self-reaction of alkyl peroxy radicals.

Data show entrainment in the early morning (<10LT) for acetone, methanol and acetaldehyde with lower concentration in the boundary layer than above, however, its importance could not be quantified. The maximum entrainment flux of oxygenated compounds has been 0.22 mg acetone $m^{-2}h^{-1}$, 0.06 mg methanol $m^{-2}h^{-1}$ and 0.12 mg acetaldehyde $m^{-2}h^{-1}$.

The CBL budgeting approach applied here inherently rejects outliers by using median values over distinct time spans (here 15 minutes) but remains sensitive to changes in concentrations e.g. due to biomass burning plumes. Such events have not been considered in the methanol and acetone flux calculation and resulted in a maximum surface layer flux (Fs) of 0.76 mg methanol $m^{-2}h^{-1}$, 0.77 mg acetone $m^{-2}h^{-1}$ and 0.27 mg acetaldehyde $m^{-2}h^{-1}$as shown in Figure 3-11 and summarised in Table 3-1.

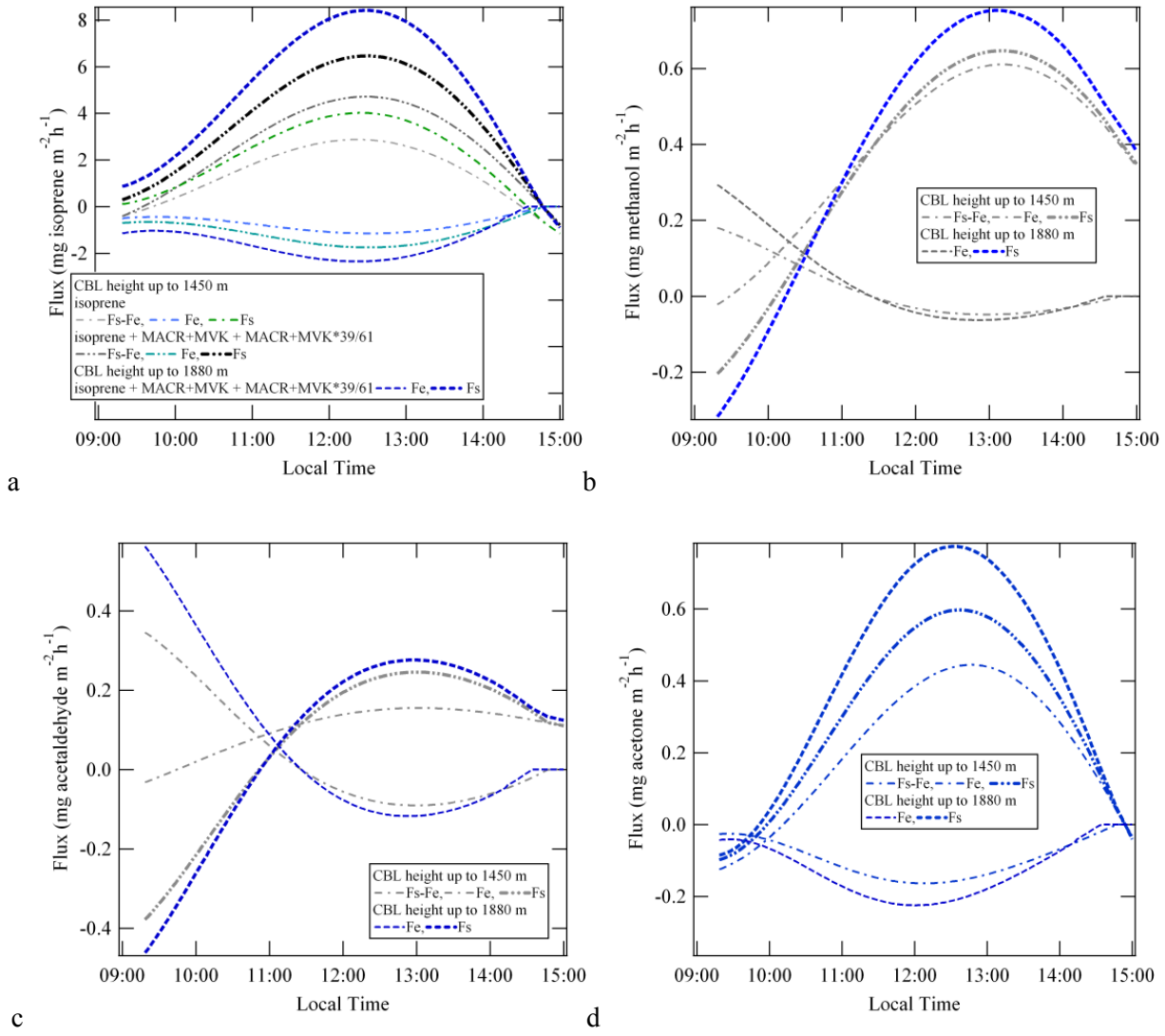

Figure 3-11: Comparison of the mixed layer median fluxes for isoprene (before and after correction for chemical loss), methanol, acetaldehyde and acetone.

It should be noted from Table 3-1 that before correction for detrainment/entrainment, Fs-Fe has been higher for methanol than for acetone. After correction, Fs for acetone and methanol are estimated to be equal to each other. This is due to a smaller detrainment flux for methanol based on the concentration difference between the boundary layer and the free troposphere than has been observed or acetone. This

suggests additional sources of methanol above the boundary layer. In contrast to isoprene, these oxygenated compounds have primary and secondary sources. They are produced during oxidation of other hydrocarbon. Methanol is formed together with formaldehyde during methane oxidation and isoprene oxidation under low NO_x conditions. Acetone is produced from monoterpenes oxidation, and acetaldehyde has many secondary sources. In addition, oVOCs are predominantly released during biomass burning (Christian et al., (2004)), often with stronger emission of methanol over acetone, although for this campaign, the impact of biomass burning was low.

Table 3-1: maximum median observed mixed layer and surface layer emission fluxes under cloudless and 3/8 cloud cover for isoprene methanol and acetone

	Mixed layer		Brownsberg
(mg m^{-2} h^{-1})	**Fs-Fe**	**Fs**	**Fs**
isoprene	2.88 - 3.27	4.02 - 5.28	3.73 – 4.23
isoprene + MACR&MVK	3.97 - 4.51	4.72 - 7.15	6.43 – 7.40
isoprene + MACR&MVK + MACR&MVK*39/61	4.72 - 5.35	6.46 - 8.42	8.22 – 9.46
methanol	0.60 - 0.68	0.65 - 0.76	0.50 - 0.56
acetone	0.44 - 0.50	0.60 - 0.77	0.50 - 0.56
acetaldehyde	0.16 - 0.18	0.25 - 0.27	0.37 – 0.41
	1450 m – 1880 m with 3/8 cloud cover		

Putting our findings in the context of previous tropical forest emission studies, as listed in Table 3-2, we conclude that the isoprene fluxes obtained here are higher than e.g. mean REA-measured isoprene fluxes of 2.5 mg isoprene $m^{-2}h^{-1}$ which were measured under cloudy conditions in Costa Rica in October 1999 by Geron et al., (2002). Similarly, Karl et al. (2004) observed on average 1.72 (max. 2.5 mg isoprene $m^{-2}h^{-1}$) for a drought-stressed Costa Rican ecosystem in April-May, 2003. These results suggest that sub-tropical rainforest of Costa Rica seems generally to emit less isoprene compared to the Amazon rainforests.

The number of studies reporting methanol and acetone fluxes from the tropical rain forest is very limited. To what extend the methanol and acetone emissions from the Guyana rainforest are comparable to the emissions from Costa Rica's rainforest remains an open question, keeping in mind the large difference in the maximum isoprene emission flux.

Table 3-2: Overview of midday BVOCs emission fluxes in the literature for the tropical rainforests of South-America.

Flux (mg $m^{-2}h^{-1}$)	isoprene		Location, year, (season)
This study Airborne PTR-MS	Median: 6.9 - 8.4		French Guyana + Suriname October 2005 (dry)
Karl et al., 2007 EC, tower, + airborne	Avg: 7.8±2.3 Max: 12.1±4.0		Manaus September, 2004 (dry)
Karl et al., 2004a DEC, tower, PTR-MS	Avg: 1.72 Max: 2.50		Heredia, Costa Rica April & May, 2003 (dry)
Geron et al., 2002 REA, cartridge, GC-FID	Avg: 2.50 Max: ~11		Heredia, Costa Rica October, 1999 (dry)
Kuhn et al., 2007 REA, tower, cartridge, GCMS	Avg: 2.36		Manaus, Brazil, July, 2001 (dry)
Rinne et al., 2002 DEA, tower, cartridge, FIS	Max:~2.40		Tapajós, Brazil July, 2000 (end of wet)
Greenberg et al., 2004a Blimp, cartridge, GCMS	Max: 2.2*		Tapajós, Brazil February, 2000 (wet)
Greenberg et al., 2004a Blimp, cartridge, GCMS	Max: 5.3*		Balbina, Brazil March, 1998 (wet)
Greenberg et al., 2004a Blimp, cartridge, GCMS	Max: 9.8*		Rondônia, Brazil February, 1999 (wet)
	methanol	acetone	
This study airborne	Med: 0.60 - 076	Med:0.44 -0.77	French Guyana, Suriname October 2005 (dry)
Karl et al., 2004a DEC, tower, PTR-MS	Avg: 0.13 Max:0.50	Avg: 0.09 Max:0.36	Heredia, Costa Rica April & May 2003
Geron et al., 2002 REA, cartridges, GC-FID	Avg: 1.41	Avg: 2.25	Heredia, Costa Rica October, 1999

* estimated from a box model by Guenther et al., 1999

Karl et al., (2007) describes how an average eddy covariance surface flux of 8.3 ± 3.1 mg isoprene $m^{-2}h^{-1}$ or an average mixed layer gradient surface flux of 12.1 ± 4.0 mg isoprene $m^{-2}h^{-1}$ was obtained nearby the centre of the Amazon (Manaus). These measurements have also been conducted under partially cloudy sky for a boundary layer which was defined to be ~1200 m deep corresponding to the bottom of the developing cloud layer which is different to our definition discussed earlier.

Kuhn et al., (2007) reported a mean midday isoprene flux of 6.2 mg isoprene $m^{-2}h^{-1}$ using the mixed layer gradient method for a mixed layer depth of ~1100 m near Manaus in July 2001. They state that this

flux was on average about a factor two higher than the fluxes derived from tower-based measurements reported in the same study.

Karl et al., (2007) and Kuhn et al. (2007) also used the mixed box technique to estimate the OH concentration over the tropical rainforest (assuming an entrainment term). In contrast, we have measured all parameters on the right hand side of equation 4 (including OH).

$$F_s - F_e = \frac{C}{\tau} z_i = \left(k_{isop,OH}[OH]_r + k_{isop,O_3}[O_3]_r\right)[ISOP]_r z_i \qquad \text{E 3-5}$$

We obtain values for Fs-Fe that range, for the well mixed afternoon conditions in the sub-cloud layer, between 16 and 25 mg isoprene $m^{-2}h^{-1}$ (25p-75p) and a median of around 20 mg isoprene $m^{-2}h^{-1}$ for this region. Such flux values are much higher than we have obtained following the mixed layer budget approach and much higher than observed by both studies mentioned. Furthermore, their deduced OH-concentrations over the rainforest ($1.3\pm0.5x10^6$ molecules cm^{-3} and $2.5\pm1.5x10^6$ molecules cm^{-3}, respectively for both studies) are substantially lower than measured during GABRIEL (on average ~$5x10^6$ molecules OH cm^{-3}).

For L19 and L60 SCM simulations, after compensation for chemical loss (by the sum of parent and product concentrations), we calculate mixed layer maximum values for Fs-Fe of 6.0 and 4.6 mg isoprene $m^{-2}h^{-1}$ respectively at 12:00 and 13:00, each with respect to their own simulated boundary layer evolution.

Due to their different CBL growth rates, we calculate entrainment maximum detrainment fluxes for conserved isoprene of 0.70 and 0.54 mg isoprene $m^{-2}h^{-1}$ for the L19 and L60 version respectively following the concentration jump method. In the L60 version this maximum occurs around 10:00 whereas in the L19 version the maximum detrainment occurs at 12:00 which matches better in timing to the observations.

Though we calculate maximum surface layer fluxes of 6.6 and 6.1 mg isoprene $m^{-2}h^{-1}$ for the L19 and L60 version, respectively, they reflect the result from a simulated isoprene emission flux which has been scaled down by a factor 2 to arrive at daytime peak fluxes in agreement with the "observed" emission flux. Reducing the isoprene emission flux in the SCM does lead to higher OH concentrations, however, the isoprene mixing ratios then fall well below the measured values.

As the surface diurnal profiles of methanol and acetone have been fairly synchronous, the fluxes are considered to be predominantly due to emissions from plants and only a relatively small fraction of these fluxes would be attributable to abiotic decay assuming the emission rate determined by Warneke et al., (1999), and the leaf litter fall (which is larger during the dry season) as described by Martius et al., (2004). In absence of CO measurements, only acetonitrile and acetaldehyde mixing ratio have been used to filter the Brownsberg data for eventual biomass burning influences. For both methanol and acetone, we obtain maximum median surface fluxes of 0.36 mg $m^{-2}h^{-1}$, without correction for en/detrainment. These fluxes are comparable to the maximum surface layer fluxes of 0.36 mg acetone $m^{-2}h^{-1}$ and 0.5 mg methanol $m^{-2}h^{-1}$ reported by Karl et al., (2004) and higher than the average flux of 0.09 mg acetone $m^{-2}h^{-1}$ and 0.13 mg methanol $m^{-2}h^{-1}$ observed during these 3 weeks of disjunct eddy covariance measurements in Costa Rica. Values are nevertheless not as high as the mean REA fluxes of 2.25 mg acetone $m^{-2}h^{-1}$ reported by Geron et al., (2002) for October 1999.

Applying Eq.(5), results in very low fluxes for species like acetone and methanol due to their long atmospheric lifetimes, even though the observed changes in their mixing ratios are not particularly low.

Alternatively, the fluxes of acetone and methanol can also be estimated from their longitudinal concentration gradient in the boundary layer as function of the time over land (TOL). This gradient of fairly unreactive species builds up as the emissions accumulate in the air traversing the rainforest. TOL has been calculated along the back trajectories of the air parcels as discussed by Gebhardt et al., (2008).

In contrast to the halogenated compounds, methanol and acetone do express a diurnal cycle. By interpreting the observations in a Lagrangian sense, i.e. with increasing TOL (max 14 hours = sunset to sunrise), time of the day and consequent to the CBL height, fluxes can be determined. In this admittedly cruder approach as less data points remain after filtering, the obtained mixed layer fluxes are ~0.42±0.05 mg methanol $m^{-2}h^{-1}$ and ~0.28±0.04 mg acetone $m^{-2}h^{-1}$ and are thereby comparable but slightly lower than obtained previously. The errors taken into account for the Orthogonal Distance Regression are the total measurement uncertainty on the PTR-MS measurements and an uncertainty of 20 % on the time over land. Interestingly, this method also indicates a mixed layer methanol flux which is higher than observed for the ground-based measurements.

Airborne data have covered only the period of most intense surface emissions between 9LT and 15LT, lacking the emissions before and after. Nevertheless, the emissions during these 6 hours already account for 28.0 mg isoprene, 2.76 mg methanol, 2.37 mg acetone and 0.82 mg acetaldehyde per square meter considering a mixing height up to ~1880 meter over the Guyana rainforest during the dry season as from Figure 3-11.

To estimate the surface flux for Brownsberg, we assume same CBL evolution as used for the airborne data. Since OH concentrations were not measured within the canopy, we compensate for chemical loss by using (ISOP+MACR+MVK+ (MACR+MVK)*61/39). After taking a 23% and 27% entrainment flux in analogy to the airborne measurements, a maximum surface flux ranged between 8.22 and 9.46 mg isoprene $m^{-2}h^{-1}$.

Meteorological data at Brownsberg have shown that wind blew land inward from a constant direction before 15:00LT, afterwards, the situation becomes complicates as the wind blew land outward transporting more aged air towards the site and can therefore not be considered as representative for this campaign. The period between 6:45 LT and 15:00LT covers almost the emission from an entire day in the dry season and accounts for 38.0 mg isoprene m^{-2} under partially clouded conditions. When generalised and assuming that the wet season isoprene emission flux is one fifth of the dry season emission flux (concluded from the TROFFEE and the AMAZE campaigns around Manaus), 2.8 Tg C is emitted per year as isoprene by the Guyana rainforest (0.38 million km²). For 7.2 million km² of Amazonian rainforest on the South-American continent, a suggestive 52.8 Tg C per year is emitted as isoprene. However, as shown in Fig 1 of Müller et al., (2008), the Guyana and other coastal rain forests are not as strong in emitting isoprene as further land inward.

3.6 Conclusion

The presented analyses of airborne and ground-based observations of BVOC mixing ratios, complemented by the simulated tropical forest chemistry in a single column chemistry and climate model, in combination with OH measurements, show that the OH-concentrations above the tropical rainforest have been higher than currently modelled. These high OH concentrations led to fast oxidation of the emitted BVOCs in a convective boundary layer, the development of which was also influenced by shallow cumulus convection.

The campaign average mixed layer depth has been assessed based on the occurrences of the first potential temperature inversions to rise from ~500 m in the morning (09:00) to ~1450 m in the afternoon. It has been shown that the deeper transport through clouds (increasing the mixing layer up to ~1880m) also affects the distribution of reactive tracers like isoprene and accordingly of MACR+MVK to higher altitudes. Methanol and acetone mixing ratio vertical profiles are less steep but suggest mixing throughout a higher vertical domain. The importance of deeper transport through clouds is directly related to the cloud cover which increased over the course of a day.

The mixed layer diurnal profile of isoprene showed low mixing ratios (ca. 0.5 ppbv) in the morning increasing to about 3.5 ppbv in the afternoon. Mixing ratios measured from the aircraft were significantly lower than those measured at the surface since the transported air has been impacted by chemical oxidation and by mixing in of air from above.

Mixed layer isoprene diurnal profiles can be used to empirically determine the emission flux provided that other influences such as boundary layer dynamics and chemistry can be taken into account. A maximum surface layer flux of 6.46 - 8.42 mg isoprene $m^{-2}h^{-1}$, 0.65 - 0.76 mg methanol m^{-2} h^{-1}, 0.6 - 0.77 mg acetone m^{-2} h^{-1} and 0.29 - 0.32 mg acetaldehyde m^{-2} h^{-1} was determined. The daytime maximum surface emission flux of 6.69 - 8.73 mg isoprene $m^{-2}h^{-1}$ obtained at Brownsberg is in good agreement with the isoprene emission flux obtained for the mixed layer.

Model simulations (Guenther et al., 2006) show that the isoprene emission rate increases further land inward and therefore the total amount of carbon from the tropical rainforest will in all probability be higher. However, our obtained surface flux is about 2 times lower than the default surface flux calculated for this area by SCM using the implementation of the MEGAN BVOC emission algorithm.

From this study and Ganzeveld et al., (2008) we have demonstrated by comparing simulated and measured vertical and diurnal profiles of trace gases that the issues of mixing and radical recycling in the SCM need to be further investigated to unravel the higher isoprene mixing ratios and underprediction of OH (Ganzeveld et al. 2008). The applied scaling factor in SCM L19 could be reduced by 30% through increase of the vertical resolution and the processing time in the column.

The reason to prescribe the modelled fluxes was to obtain the best fit to the measured concentration values in order to diagnose the likely cause for model/measurement disagreement. The model's dynamics (vertical transport of water, heat and tracers) and in particular chemistry are most likely the cause for the discrepancy

Higher resolved boundary layer schemes in the SCM (and other state-of-the art atmospheric chemistry and transport models) compared to default resolution of 5 layers in the CBL are required in order more realistically simulate the vertical distribution of water and energy, BVOCs and other tracers over the course of a day. A vertical resolution of 13 layers within the boundary layer effectively reduced boundary mixing ratios by circa 30 % and increased the OH concentration by almost 50% between 9 and 16 LT.

As the SCM's default resolution is commonly used in global chemistry-transport models, such increase could affect the prediction of the oxidation capacity of the atmosphere above tropical rainforests.

Additional regional scale observations of BVOC concentrations and fluxes are needed over tropical continents in combination with high resolution boundary layer meteorological measurements to better constrain the budget of BVOCs emitted by the different tropical ecosystems. Furthermore in-depth investigation of the underlying low NO_x, organic oxidation chemistry in the remote troposphere is needed to improve current atmospheric models.

4 Characterising summertime variations in oVOCs at a temperate latitude site: Hohenpeissenberg

4.1 Introduction

European land cover has been intensively modified by man resulting in an extremely patchy landscape of rural and urban character. This leads to a high degree of spatial variability in the emission of VOCs. When these VOCs oxidise in the presence of NO_x and sunlight, ozone and a multitude of oxygenated products can form (Atkinson and Arey, 2003). These compounds have an impact on human health (Fenger, 1999), and on the oxidizing capacity of the troposphere. Aged air masses, enriched in oxygenated volatile organic compounds (oVOCs), may potentially include ketones, organic hydroperoxides, peroxyacyl nitrates, aldehydes, organic acids, alkyl nitrates, alcohols or even polyfunctional compounds. In addition to photochemical formation of oxygenates, several oVOCs may be directly emitted from biomass. In recent years there has been considerable progress in understanding the biogenesis of e.g. three major C_1- C_3 oVOCs (methanol, acetaldehyde and acetone) that are abundantly present in the troposphere (Fall, 2003). Yet many uncertainties remain both in the sources (photochemical and direct) and in the sinks (in particular wet and dry deposition).

The multitude of processes in which OVOC are involved has complicated the assessment of their atmospheric chemistry. OVOC can have sufficiently low vapour pressures to influence secondary organic aerosol growth. On the other hand laboratory and field studies have also suggested that oxidation of organic aerosols can be a source of oVOCs (Kwan et al., 2006). OVOCs can be more efficiently removed from the atmosphere by wet deposition and dry deposition to wet surfaces (e.g. removal into dew in the morning) compared to their less polar precursors. Night time dry deposition and wet deposition of VOCs are not well characterised. There have been few measurements focussing on the removal of ambient oVOC during rainfall.

The focus of the HOHPEX04 field study was to investigate photochemistry and emissions of oVOCs in the semi-rural, continental, temperate latitude, atmosphere. HOHPEX04 (Hohenpeissenberg OH-Interkomparison and Photochemistry EXperiment) was conducted in summer 2004 at the Meteorological Observatory Hohenpeissenberg (MOHp) in the countryside of Bayern, southern Germany. This station is part of the Global Atmospheric Watch (GAW) network and also functions as meteorological monitoring site for the German Weather Service (Deutscher Wetterdienst, DWD) with the objective to perform long term measurements and investigate seasonality of emissions. Additional interim measurements during the HOHPEX04 campaign were in support of the atmospheric trace gases to better characterise the site. Particularly for VOCs, several techniques were applied and a first intercomparison for short-lived compounds can be found in (Bartenbach, (2005); Bartenbach et al., (2007)). Here, we focus on the relatively short-chained oVOCs.

4.2 Site description

The HOHPEX04 campaign was conducted from June 21 to July 14, 2004 at the Meteorological Observatory Hohenpeissenberg (47°48'4.50"N, 11° 0'35.00"E), labelled H in Figure 4-1. This southern-German observatory is located on a hilltop (elevation of 980 m asl) in a rural agricultural and forested area, about 40 km north of the Zugspitze in the Alps. It is elevated some 200-300m above the surrounding countryside with the slopes mostly covered by coniferous forest, some beeches in most directions (~30%) and agricultural pastures or meadows dominating in the valley below (~70%). From a source inventory point of view depicted in Figure 4-1, air advected from the sector 225-315° very likely

advects low levels of pollution from surrounding countryside to the station. Higher levels of pollution were expected from the Munich metropolitan area (350° - 80° including the city Munich (1.33 million inh., 4205 inh./km²) and Augsburg (63.300inh., 1787 inh./km²) at distances of about 55-63 km). Under certain meteorological circumstances (as shown in section 4.4.5), pollution from South (e.g. the Po-basin) can be advected to the site. The village of Hohenpeissenberg is located at the foot of the mountain and within a radius of 25 km there are no motorways and the average population density is around 155 inh./km². To the West, the predominant wind direction during this campaign, there are 2 motorways (>50km) but mostly main roads connecting towns and cities (~600 - 1000 inh./km²).

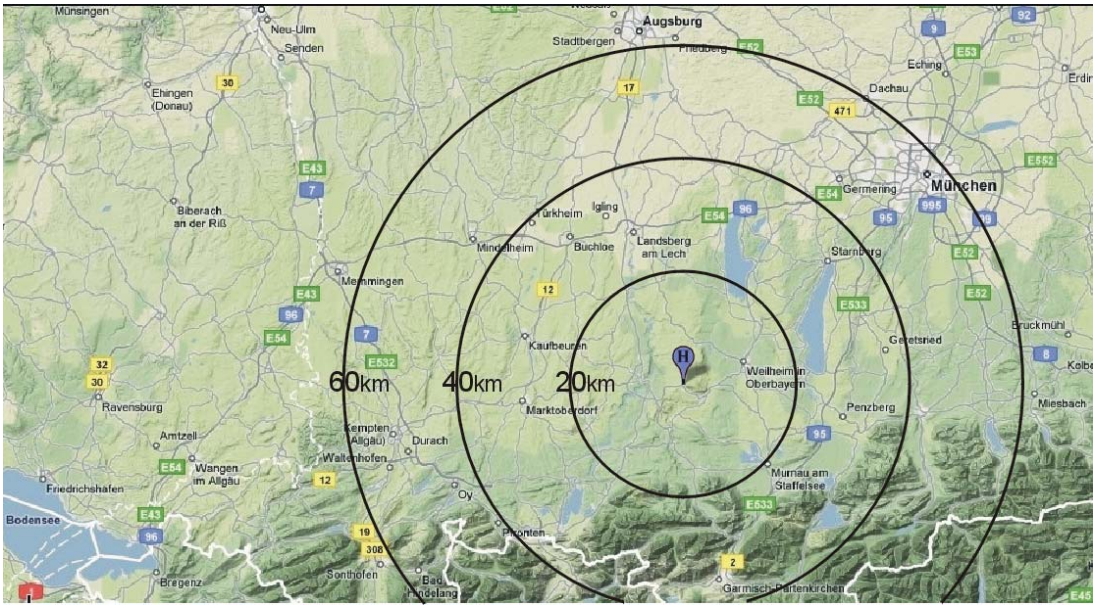

Figure 4-1: Map of the area centred on the Meteorological Observatory Hohenpeißenberg.

4.3 General meteorology and boundary layer dynamics

Trace gas analysis at the observatory Hohenpeissenberg is complicated by the diel variation in height of the planetary boundary layer (PBL) on top of the atmospheric turbulence caused by the hilly terrain and prevailing meteorology (e.g. Handisides et al., 2003). Detailed analysis of the PBL dynamics are beyond the scope of this study. The general meteorology and the occurrences of temperature inversions are important for the analysis and are discussed in relation to the data shown in Figure 4-2. During the nights before July 10, the height of stable nocturnal boundary layer often dropped below the altitude level of station, cutting off the station from its local surroundings and leaving it in the residual layer under the influence of air masses from the previous day. Local emissions trapped under the inversion layer can build up during the night. At the onset of the convective boundary layer convective currents transfer heat and gases upwards, lifting the nocturnal inversion and the airmass gets diluted by mixing in of residual layer and possibly even free tropospheric air. Signatures of this transition have been perceived in trace gas concentrations at mid-morning hours with significant advection of VOCs from both anthropogenic and biogenic emissions.

Higher than average wind speeds after July 10 may have prevented the nocturnal inversion layer from developing. Night time VOC mixing ratios were lower and more variable. From about noontime to 17 LT, MOHp was situated in the well-mixed CBL, and during this time transport processes played an important role for VOC mixing ratios measured at the station.

The predominant wind direction (200° - 300°) for the period between June 28 and July 14 as presented together with many other meteorological parameters in Figure 4-2 was associated with low temperatures and turbulent weather. Periods of abnormal wind direction readings are noticeable in the beginning (28-30 June) and in the middle of the HOHPEX campaign (6-8 July). The daytime temperature varied

between 11 - 18 °C (25p-75p) with only a few degrees difference between the average day and night temperatures. Temperatures were mostly below the campaign average of 15°C after July 9th.

The precession of (dew point & ambient) temperature, pressure and relative humidity indicate the passage of synoptic features crossing the region. Weather maps indicate that a sequence of high and low pressure systems have controlled the weather during this period. Wind speeds generally varied between 1.8 - 3.4 m/s (25p-75p) and were on average 2.6 m/s. More gusty winds of 6 m/s or higher occurred when fronts passed through. In fact, cold, warm, and occluded fronts, passed over the station clearly influencing the campaign weather. Over a period of 14 days, 94 mm (=L/m²) of rain fell, varying in intensity and duration.

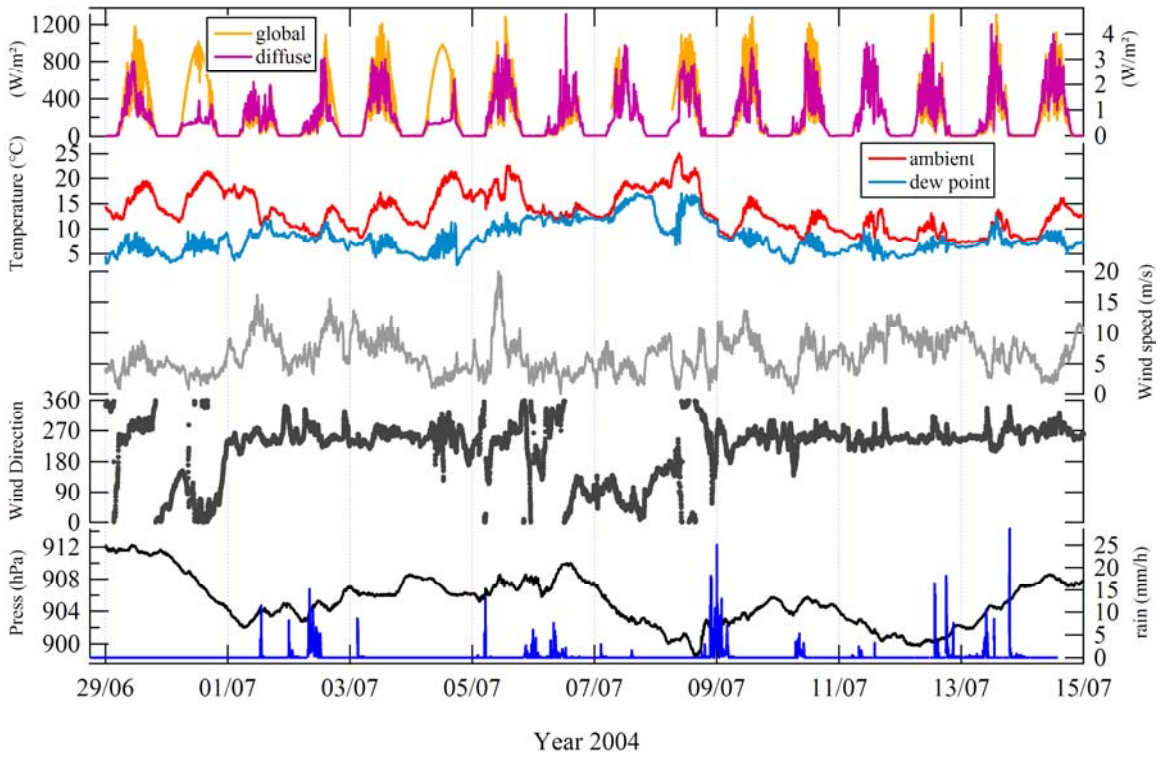

Figure 4-2: Basic meteorological parameters for the period of measurements

Here we examine 2 cyclones that have affected the weather over central Europe. In both cases, Southern Germany has been situated in the warm sector of the low pressure system. The warm sector is the region of air that lies between the warm and cold front early in the lifetime of a depression. Generally for such a cyclonic frontal system, the faster moving cold front forces air from the warm sector up the warm front, producing clouds and often giving significant amounts of precipitation.

On the 1st of July, a low pressure system centred south of Iceland with its occluded front and cold front reaching out to Spain divided Central Europe into two: the East encountering warm air, the West encountering cold air.

On the 7th of July, a low pressure system moved north along the French Atlantic Coast and stalled over Brittany influencing the weather over Western Europe. Weather maps indicate that these frontal boundaries have crossed the region around Hohenpeißenberg on July 7th with a warm front crossing shortly after noon (Figure 4-3a) followed by a cold front on 8 July in the evening (Figure 4-3b).

The general circulation of air towards the site was analysed using 4 day back trajectories (airmasses below 700 hPa). Between the end of June and the 5th of July, airmasses arrived mainly from the West following a path across central France with their origin above the North Sea and the North Atlantic.

Back trajectories indicate that the air masses has stayed closer to the ground during the days before arrival and have crossed France and Germany on 6 and 7 (noon) of July and Austria and Northern Italy on 7 (afternoon) and 8 July enhancing the chance of strong pollution from the Po-Valley and Milan area (Figure 4-3c and d). On the days that followed, air masses have descended from higher altitudes and originated from southern France. During the colder days, 10th to 14th of July, airmasses originated from over Ireland and Scotland.

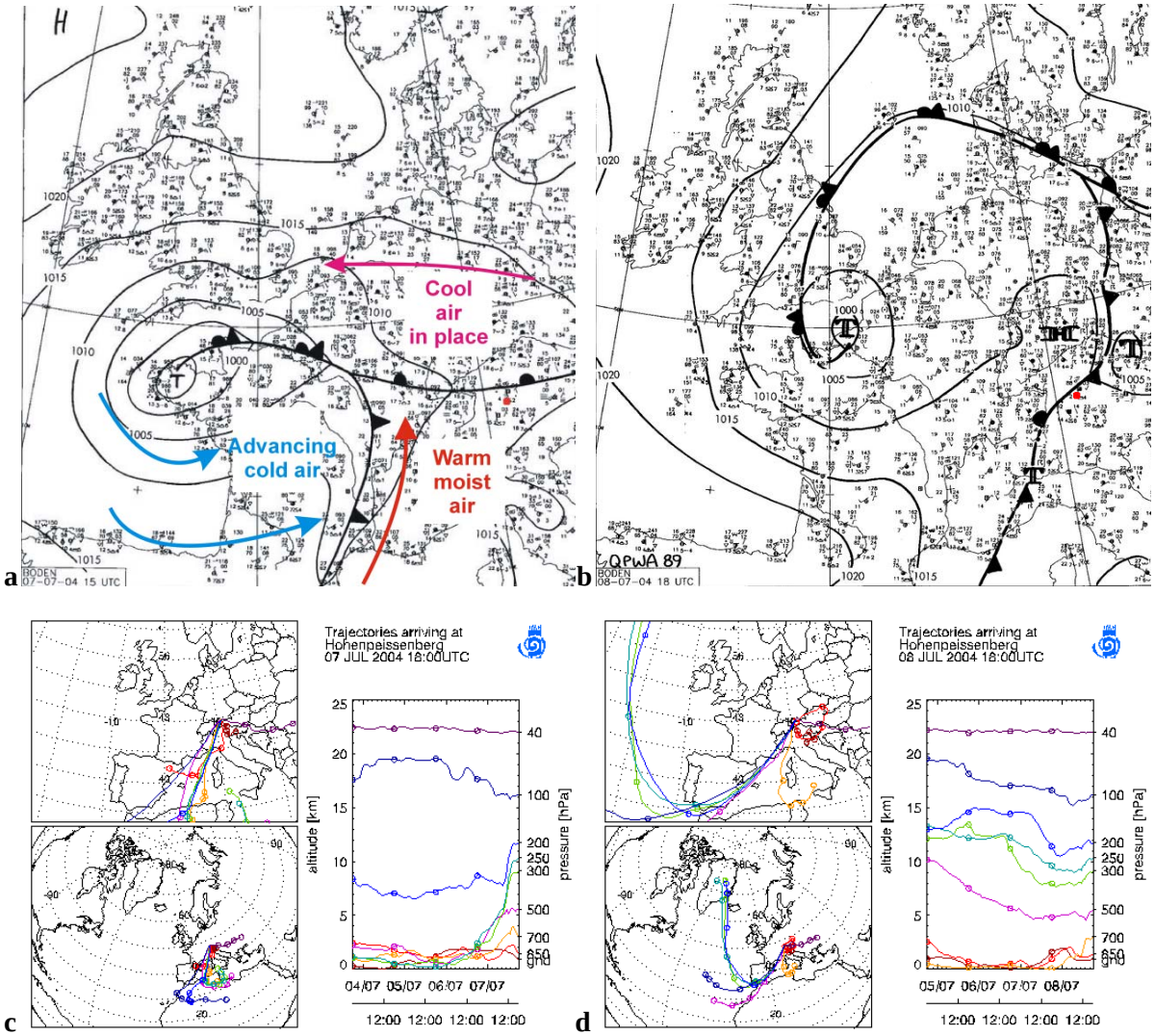

Figure 4-3: Synoptic charts for 7 July (15:00LT, a) and 8 July (18:00LT, b). Region of Hohenpeißenberg is indicated by the small red dot on the right. Panel c and d show 4 day back trajectory maps for these days.

4.4 Results

In the first part of the results section the parallel measurements of the same species made by different techniques are compared for consistency. This is done by averaging the highest resolution data around the centred measurement time of the low resolution data considering its sampling time.

4.4.1 Intercomparison PTRMS-PTRMS

In this campaign two PTRMS systems were operated for comparison. One system was equipped with three vacuum pumps and the second two only two. A significant improvement in sensitivity was expected through the installation of the third sampling pump. Both PTRMS systems described in section

2 were calibrated against the same standard (VOC mixture Apel-Riemer, stated accuracy 5%) with synthetic air as dilution gas. Each instrument was equipped with its own catalytic converter. The interpolated signal between the frequently measured background signals was subtracted from the sample signal to determine the mixing ratios present in the analysed air or the calibration mixture (range 0.5 - 4.0 ppbv). Both systems were calibrated 3 times in 3 days measuring one mixture to check on the reproducibility of the measurements and to evaluate the PTRMS instrumental improvements. The results of these calibrations are summarised in Table 4-1 for all compounds in the mixture.

Table 4-1: Summary of the mean calibration factors and offset values ± the standard deviations for 3 calibrations and the instrument's detection limit.

N=3				
PTRMS_W	(cps/ppbv)	(ncps/ppbv)	Offset (ppbv)	LOD (ppbv)
methanol	19±1	8.15±0.90	0.86±0.79	1.62±0.77
acetonitrile	36±2	15.94±0.79	0.40±0.74	0.19±0.2
acetaldehyde	39 ±1	18.09±1.11	-1.61±0.88	0.44±0.17
acetone	43±3	19.44±0.52	-0.67±1.13	0.31±0.11
DMS	14±1	6.31±0.29	-0.79±0.95	1.82±0.89
isoprene	19±2	8.48±0.99	-0.18±0.23	0.19±0.06
metacrolein	32±3	14.24±1.41	-0.92±0.45	0.16±0.05
butanone	43±2	19.30±1.13	-1.42±1.70	0.23±0.08
benzene	27±2	11.97±0.93	-0.87±0.84	0.30±0.15
toluene	27±2	11.85±1.03	-0.97±0.42	0.11±0.04
o-xylene	26 ±3	11.73±1.51	-2.40±1.22	0.23±0.08
1,3,5-TMB	20±2	8.99±1.40	-2.77±1.52	1.00±0.39
α-pinene	5±1	2.40±0.56	-0.22±0.29	0.43±1.51

PTRMS_Q	cps/ppbv	(ncps/ppbv)	Offset (ppbv)	LOD (ppbv)
methanol	108±23	4.60±0.96	0.74±0.84	0.65±0.18
acetonitrile	229±14	9.92±0.19	-0.32±0.36	0.04±0.01
acetaldehyde	223±10	9.73±0.20	-0.09±0.18	0.18±0.05
acetone	215±20	9.54±0.25	-0.57±0.25	0.15±0.06
DMS	116±16	5.06±0.79	-0.37±0.62	0.21±0.06
isoprene	86±6	3.74±0.08	-0.01±0.08	0.09±0.03
metacrolein	188±10	8.17±0.35	-0.62±0.25	0.06±0.02
butanone	204±11	8.80±0.16	-0.52±0.23	0.11±0.03
benzene	112±6	4.84±0.04	-0.19±0.09	0.04±0.01
toluene	114±8	4.95±0.09	-0.55±0.24	0.05±0.01
o-xylene	128±7	5.53±0.29	-1.01±0.12	0.12±0.04
1,3,5-TMB	125±12	5.42±0.50	-1.31±0.17	0.09±0.03
α-pinene	39±2	1.68±0.04	-0.21±0.10	0.09±0.03

Raw calibration factors (counts per second/ppbv) for PTRMS_Q, the upgraded 3-stage differentially pumped system, have been on average 5.6 times higher than for PTRMS_W which has a much lower

primary ion signal of ~1E6 cps against ~13E6 cps for PTRMS_Q. Signals of H_3O^+ and $H_3O^+.H_2O$ have been used for normalisation. The m/z 33 signal is directly influenced by the signal of O_2^+ at m/z 32 in both systems for which a correction was applied by considering the natural abundance of the O^{17}-isotope. Despite this correction, m/z 33 has the largest standard deviation in the calibration factor (10-20% of the obtained calibration factor for both systems). For all other masses, the standard deviation on the calibration factors for PTRMS_W varied between 3 and 15% whereas for PTRMS_Q this is on the order of 1-5%.

The limit of detection (LOD) has been calculated as three times the standard deviation of the background signals regularly obtained from air scrubbed over the catalytic converter during the calibration. The average value after conversion into volume mixing ratios has been listed in Table 4-1. It shows that the precision was much better and the detection limit was much lower for the 3-stage than for 2 stage differentially pumped PTRMS.

Note that during the campaign both PTRMS instruments have been calibrated under dry conditions (synthetic air) whereas the ambient conditions where more humid (see meteorology section for the ambient conditions and Warneke et al., (2001b) for a discussion on the humidity dependence of PTRMS calibration factors). This dependence has been determined afterwards for each instrument by laboratory experiments and has been taken into account for the VOC mixing ratios discussed below. A comparison has been made between mixing ratios calculated using the dry calibration factors and mixing ratios corrected for the humidity dependence. For compounds, like acetaldehyde, benzene, toluene, o-xylene, calibration factors decreased with increasing humidity resulting in increases in their volume mixing ratios by 9, 11, 7 and 2 % respectively for PTRMS_W and by 8, 13, 11 and 4 % respectively for PTRMS_Q. For compounds like methanol, acetonitrile, isoprene, MACR, calibration factors increased with increasing humidity resulting in resulting in decreases in their volume mixing ratios by 23, 6, 5 and 7 % respectively for PTRMS_W and by 15, 3, 11 and 6 % respectively for PTRMS_Q. Mixing ratios of acetone and alpha-pinene changed by less than 2 % with respect to the dry calibration.

Here we compare the in situ measurements between June 28 and July 7 of the two PTRMS instruments corrected for humidity dependence. The data above LOD have been synchronised (centred measurement time) with correction for sampling time delays based on internal volume and flow rate through the sampling line and the PTRMS inlet system. A more precise synchronisation using the analogue output of both quadrupole mass spectrometers has not been considered. Data (time resolution 70s-120s) have been averaged over 5 minutes. The total measurement uncertainty of each of the instruments as described in section 2 has been taken into account in the orthogonal distance regression (ODR) in Table 2-1.

Table 4-2: Intercomparison of in situ measured VOCs monitored by 2 PTRMS systems by orthogonal distance regression.

m/z	Slope	Intercept	R^2
33	1.00 ± 0.01	0.27 ± 0.04	0.827
42	0.18 ± 0.02	0.08 ± 0.00	0.105
45	0.76 ± 0.03	0.16 ± 0.01	0.558
59	1.16 ± 0.01	-0.05 ± 0.02	0.860
69	1.16 ± 0.06	0.03 ± 0.01	0.684
71	1.06 ± 0.05	0.04 ± 0.01	0.703
73	0.78 ± 0.04	0.15 ± 0.01	0.583
79	0.13 ± 0.07	0.06 ± 0.01	0.040
93	0.88 ± 0.06	0.05 ± 0.01	0.479
107	0.52 ± 0.10	0.05 ± 0.01	0.190
121	0.03 ± 0.01	0.05 ± 0.00	0.017
137	0.77 ± 0.05	0.07 ± 0.01	0.279

A generally good agreement has been obtained for many compounds, but Table 4-2 lists poor correlations for those compounds with low abundance during this campaign. For compounds such as acetonitrile, C_2- & C_3-benzenes and benzene mixing ratios sometimes barely have been above detection limit and have been shown to vary only over a small range of mixing ratio values during the entire period of intercomparison. PTRMS_W data have been more scattered, influencing the average values taken and contributing to higher measurement uncertainties leading towards worse regression coefficients.

4.4.2 **Intercomparison to GC-MS/FID and GCxGC-MS**

PTRMS_Q data have been averaged over the sampling time of the GC-MS/FID (30min) and GCxGC-FID (20min) systems and the results are summarised in Table 4-3. Such comparisons have the potential to indicate systematic errors or the reduced selectivity of the PTRMS (see also Eerdekens, 2002; Warneke et al., 2003; de Gouw et al., 2003a).

PTR-MS signals at m/z 71, 107, 121 and 137 are compared to the summed signal of the corresponding, individually quantified compounds present in the calibration mixtures analysed with the GC-systems. Compounds listed between brackets were not quantified by the GC-MS/FID system of the DWD.

Table 4-3: A comparison of PTRMS_Q results (Y-axis) to those of GC-MS/FID and GCxGC-MS (X-axis) considering orthogonal distance regression including the total measurement uncertainty.

	PTRMS vs	**GCxGC-MS, MPCh**		**GC-MS/FID, DWD**	
m/z	**compound**	**Slope**	**offset (pptv)**	**Slope**	**offset (pptv)**
59	acetone	1.13 ± 0.03	364.5 ± 31.8	1.87 ± 0.05	320.8 ± 33.5
69	isoprene	1.68 ± 0.14	22.1 ± 9.3	1.72 ± 0.15	20.9 ± 9.56
71	MACR+MVK	2.20 ± 0.25	4.9 ± 13.4	2.46 ± 0.04	9.5 ± 2.09
73	MEK	3.23 ± 0.39	161.8 ± 26.4	4.36 ± 0.71	160.1 ± 35.8
79	benzene	1.61 ± 0.34	-7.5 ± 17.1	1.61 ± 0.34	-7.7 ± 17.2
93	toluene	1.54 ± 0.16	-15.5 ± 15.3	1.54 ± 0.16	-15.4 ± 15.3
107	C_2-benzenes*	1.27 ± 0.17	0.6 ± 10.8	1.28 ± 0.18	1.8 ± 11.5
121	C_3-benzenes**	1.94 ± 0.96	23.3 ± 16.4	1.45 ± 0.54	23.0 ± 12.5
137	monoterpenes***	1.49 ± 0.11	1.87 ± 13.0	1.62 ± 0.12	-1.7 ± 14.4

* ethylbenzene + p-xylene + m-xylene + o-xylene (+ benzaldehyde)
** 1,3,5-trimethylbenzene + 1,2,4-trimethylbenzene + 1-ethyl,3-methyl-benzene + 1-ethyl,4-methyl-benzene (+ propylbenzene)
*** α-pinene + ß-pinene + sabinene + camphene + limonene + δ-3-carene + (α-terpinene + ß-phellandrene + α-phellandrene + myrcene)

It should be noted that the intercomparison as presented in Bartenbach, (2005) does not include a humidity dependent sensitivity correction for the PTRMS nor involves the uncertainties on the mixing ratios on both instruments.

The total measurement uncertainty on each GC system has been set at 15% of the measured value throughout the entire campaign whereas for the PTRMS data, the total measurement uncertainty for each data point has been calculated implementing the instrumental conditions and counting statistics. Eventual effects of humidity on the performance of the GC-analysis (trapping and purging efficiency of dry versus more humid samples onto the columns) have not been evaluated.

In Table 4-3, the slopes of all compounds in the inter-comparison with the chromatographic techniques have been consistently greater than unity. A possible explanation could be the contribution of additional compounds either as protonated compounds or as fragments of heavier compounds. After all, the PTRMS is less selective towards VOCs. Not all compounds collectively measured by the PTRMS systems are measured by the GC systems. However, when analysing ambient air in general, compounds like benzene and toluene usually don't have interfering compounds or fragments at m/z 79 and m/z 93 in contrast to e.g. acetone at m/z 59 or isoprene at m/z 69. More remarkable is that both GC-systems express similar correlations (similar slopes) to the PTR-MS except for ketones. Using PTR-MS as a reference, we note that the GC-MS/FID system (DWD) underestimates the concentration of acetone (m/z 59), MACR+MVK (m/z 71), and MEK (m/z 73), more than the GC-MS (MPCh) does.

Contributions of anthropogenic interfering tracers are expected to be lower from the West i.e. in this case the dominant wind direction. Isolating these data has in some cases resulted in significant different slopes than generally observed for all the data. In case of m/z 59, a slope of 1.63 has been found in contrast to 1.87 for all data. Similarly for MEK, a slope of 3.23 has been obtained for data from the West in contrast to a slope 4.1 for data isolated in the warm sector of the low pressure system (see below for more details) or to the slope of 4.35 obtained for all data. In case of MEK measurements by PTRMS, humidity is an issue. The signal at mass m /z 73 may incorporate contributions from the 3rd water cluster ($H_3O^+.(H_2O)_3$). PTRMS data under higher humidity show steeper slopes compared to less than average ambient humidity.

Interestingly, toluene also showed a lower slope for data from the West (1.26) compared to 1.52 for all data. The slopes for benzene and MACR+MVK hardly changed.

In conclusion we emphasize the necessity of comparing PTR-MS measurements to GC or other more selective techniques in combination of meteorological parameters.

4.4.3 **Variation in atmospheric constituents in time**

Figures 4-4 and 4-5 show the variation with time for aerosol particles and trace gases in connection to some basic meteorological parameters temperature and rain intensity. The unstable, unsettled, campaign weather has caused considerable changes in the mixing ratios of all trace gasses in the air by changes in temperature and by the varied history of the encountered air masses.

In brief, back trajectories indicate that the air had been transported over France (28 June) and the Benelux & UK (29 - 30 June) before arrival in Southern-Germany. Thereafter, air masses below 500hPa approached the site between 1 and 5 July from a Westerly direction, between 5-9 July from a southwestly - southerly direction, between 9 and 13 July Westerly to Southwesterly direction, and on 13 and 14 July from a Northwesterly to northerly direction.

Methanol, acetone, formaldehyde and acetaldehyde have been abundant in ambient air with fairly strong fluctuations. Their mixing ratios (campaign 5p - 95p) significantly varied between 1.10 - 3.95 ppbv for methanol, 1.05 - 3.17 ppbv for acetone, 0.33 - 2.07 ppbv for formaldehyde and 0.16 - 0.76 ppbv for acetaldehyde as shown in Figure 4-4. The mixing ratios of these oVOCs were generally higher at higher temperatures, though the dependence is less pronounced than found for isoprene (0.018 - 0.259 ppbv) and monoterpenes (0.026 - 0.439 ppbv) during this campaign.

Biogenic sources of acetone include direct emissions from vegetation, decaying organic material and secondary production by the oxidation of biogenic hydrocarbons (e.g. monoterpenes). However, acetone is also formed through the oxidation of anthropogenic hydrocarbons like propane, isobutane and isopentane (among other linear and branched alkanes and alkenes) for which higher mixing ratios were observed between July 7 and July 8. Data clearly show elevated levels of e.g. isopentane together with acetone during these days. Though, there have been clear peaks in isopentane without peaks in acetone and vice versa suggesting other sources in the area. The low time resolution of the GC-MS/FID (1 sample every 2 hours) did not yield in a clear wind direction dependence.

As mentioned previously VOCs are of great significance to atmospheric chemistry since upon photo-oxidation in the presence of NO_x they rapidly lead to the formation of important smog components such as ozone and peroxyacetylnitrate (PAN). NO mixing ratios have shown a clear diurnal profile with higher values before noon (up to 1.4 ppbv) and lower in the afternoon (<0.6 ppbv). For the entire campaign, NO mixing ratios varied between 0.1 ppbv and 0.4 ppbv (25p-75p) between 06:00 LT and 19:30 LT. NO_2 mixing ratios have generally fluctuated between 0.5 ppbv and 3 ppbv over the course of a day. Mixing ratios have on average been higher in the morning. Although, NO_2 occasionally has been much higher, regardless of the time of the day with peaks up to 20 ppbv as shown in Figure 4-5. Ozone levels peaked at almost 80 ppbv in the beginning of this campaign when the wind blew from the north to northeast. Thereafter, levels generally varied between 21.6 and 70.4 ppbv. PAN was also highest in the beginning of the campaign reaching 1 ppbv, while average mixing ratios were 0.4 ppbv.

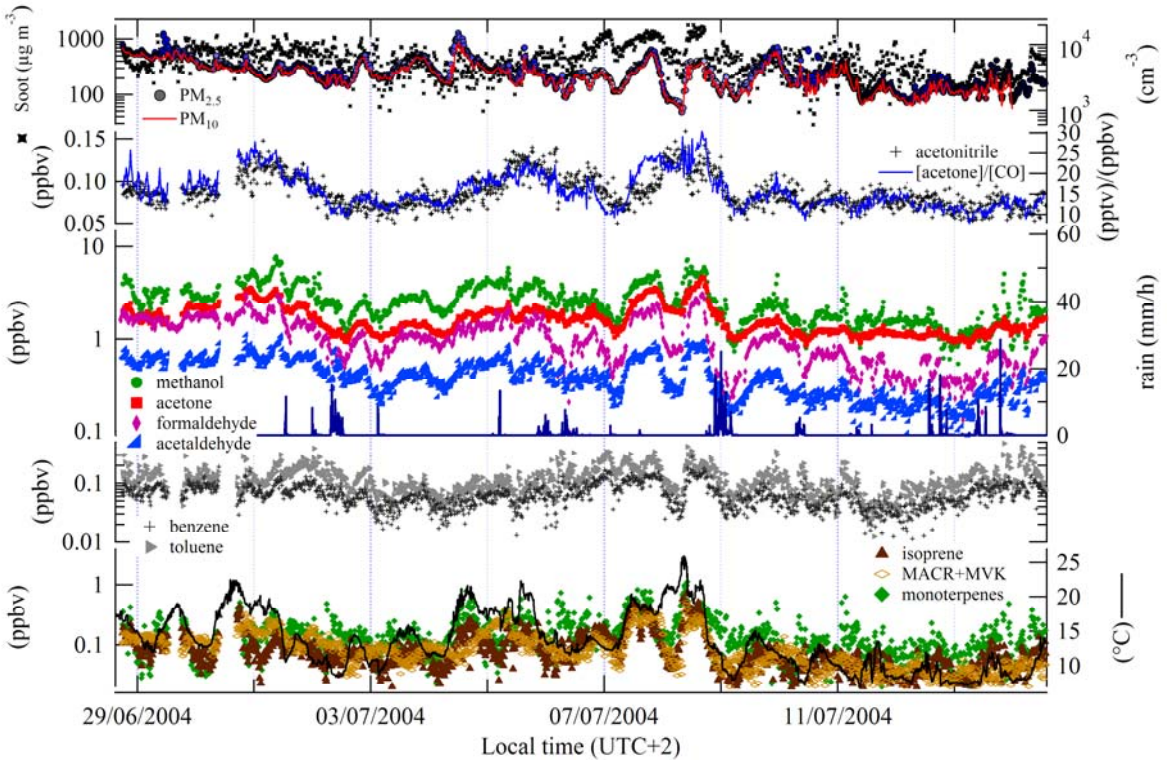

Figure 4-4: HOHPEX timeline for particles, selected VOCs, rain intensity and temperature.

The level of biomass burning monitored by acetonitrile was generally low (avg. 88 ± 22 pptv). Slightly elevated levels of acetonitrile of 100 to 150 pptv were observed on 29 June and 1, 5, 6 and 8 July. No correlation between elevated acetonitrile mixing ratios and a particular wind direction has been found.

Occasionally higher levels of soot particles have been found together with higher levels of oVOCs and acetonitrile. Between July 6 around 15:00 and July 9 around 03:00 significantly more soot particles have been measured by the aethalometer. Concentrations peaked at about 1.2 to 1.8 µg soot m^{-3} which is several times the sustained background soot particle concentration of 0.5 µg m^{-3} measured before and

after the above mentioned timeframe (Figure 4-4). A substantially lower amount of soot particles was observed in the air during the nights in between as a result of the drop of the NBL below the station's altitude.

Clear peaks in the particle concentration on top of the declining background concentrations have been observed at different times of a day. Occasionally, significantly stronger increases in the $PM_{2.5}$ particle number concentration over the PM_{10} concentration have been observed during sunny weather suggesting new particle formation. This has been investigated previously by e.g. Birmili et al., (2002); Birmili et al., (2000) for this site. New particle formation will be addressed in the next chapter for the boreal forest.

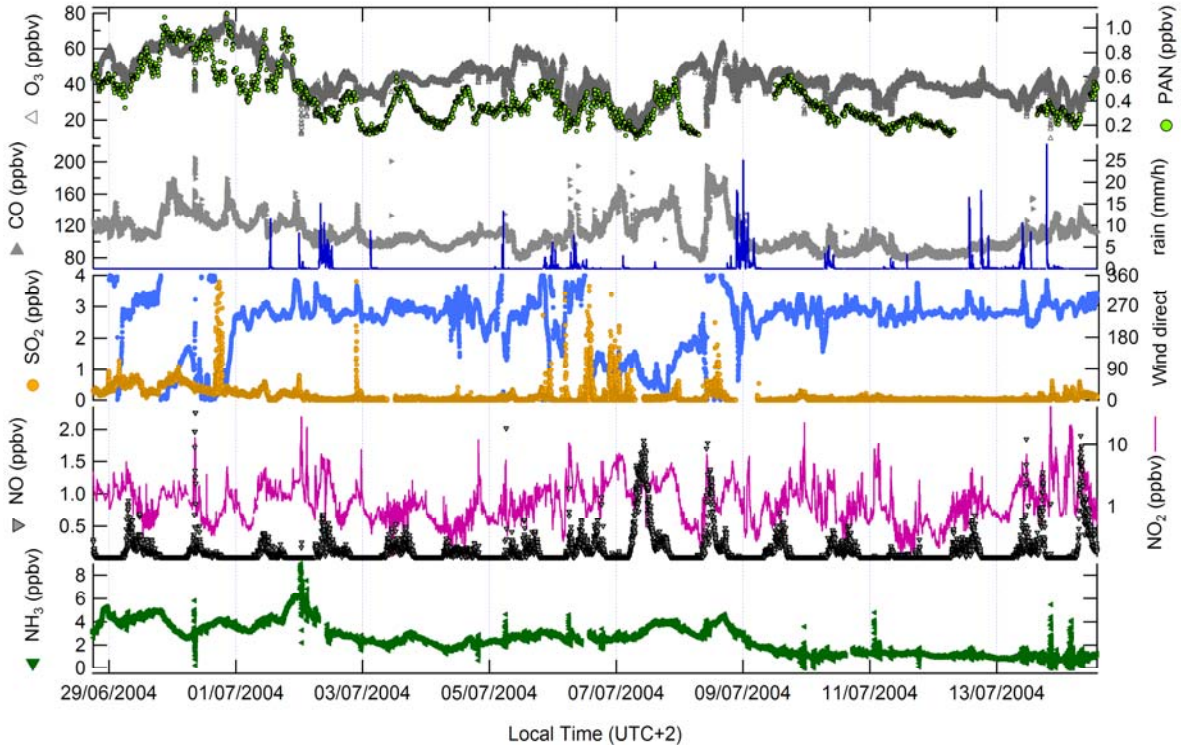

Figure 4-5: other trace gases in relation to some basic meteorological parameters

Occasionally strong SO_2 loaded plumes (with up to 4 ppbv of SO_2) have occurred especially between 6 and 9 July. These peaks mostly did not coincide with elevated NO_x. Clear episodes of anthropogenic pollution are seen in the mixing ratios of toluene. Further indication of anthropogenic pollution comes from observed peaks of e.g. naphthalene (not shown) on 8 July.

Mixing ratios of NH_3 generally decreased over the course of the campaign from about 4 to less than 1 ppbv more or less varying with temperature. Direct volatilisation from synthetic fertilizers may be expected as ammonias main source, the decomposition and volatilisation of animal wastes as a minor source.

In the following sections, mixing ratios will be analysed according to wind direction followed by OVOC correlation analysis. In summary, specific episodes of increased mixing ratios will be investigated.

4.4.4 Variation in atmospheric constituents according to wind direction

Previous figures have indicated clear differences in the wind direction at the start and in the middle of the campaign period. Data analysis has shown distinct features for airmasses approaching the site from the SE sector which are not observed for larger data sets and will be addressed in the following sections. Considering the low contribution of this wind-sector, these observations can be designated as abnormal

and not representative for this site. Distinct but not abnormal are those observations for which the observatory has been cut off from its surroundings by the drop of the NBL below the station's altitude.

Wind rose plots in Figure 4-6 and Figure 4-7 present the statistics for data between 09:00 and 18:00 LT over the period 28 June and 14 July. Statistics show 95, 75 and 25 percentiles (lines), median and mean (markers) per 30° intervals of the wind direction. Figure 4-6 shows the daytime statistics for wind speed, inorganic trace gases and aerosol particles on the radius axis and Figure 4-7 shows the statistics for temperature and organic trace gases.

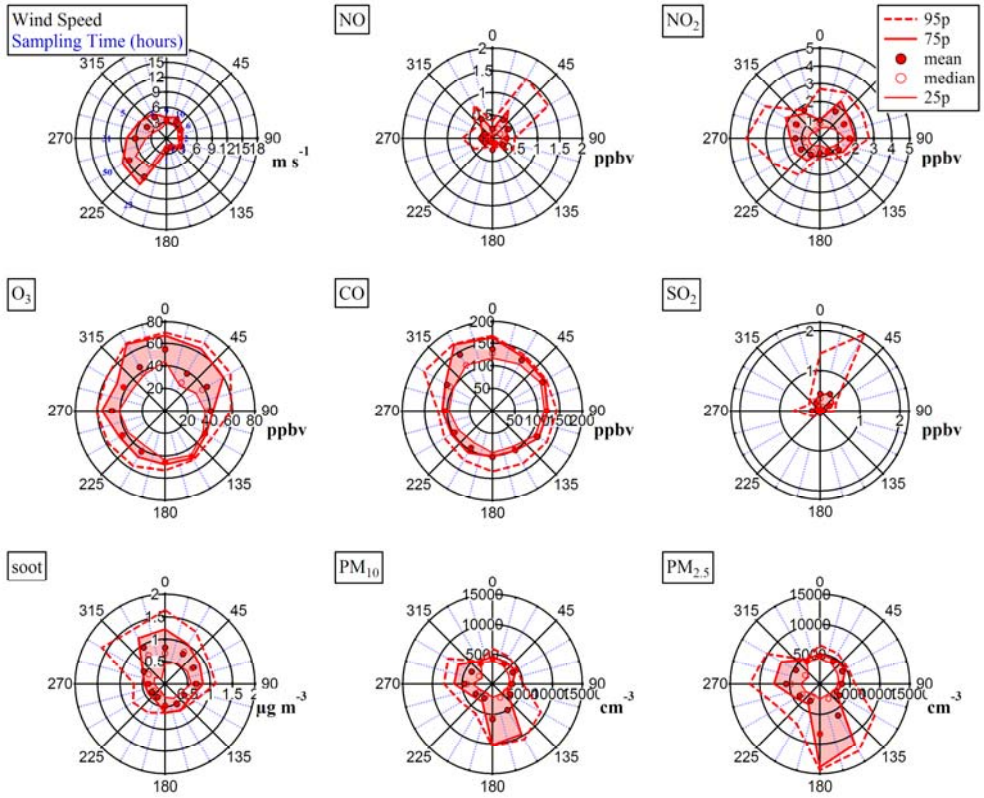

Figure 4-6: Daytime wind rose plots for wind speed, tracers and aerosol particles from 28 June to 14 July. Statistics calculated over 30° intervals. Blue numbers indicate the number of hours the wind blew from each particular interval upon sampling these tracers.

These analyses prove that the campaign period can be divided into 3 flow regimes: 1) relatively clean air from the westerly prevailing wind direction, 2) more polluted air from the north corresponding to the influence of the larger cities, 3) a strong biogenic and particulate source to the south - south east.

For air masses that arrived via the NNW to E i.e. the urban area between Augsburg and Munich, the degree of air pollution has been higher, indicated by elevated levels of NO, NO_2, O_3, CO, SO_2, benzene, toluene and C_2-benzenes and soot particles. However, daytime mixing ratios for NO an NO_2 have also been elevated when the wind blew from the West compared to the other sectors. Increased levels of CO, aromatic hydrocarbons and O_3 have been observed during episodes when the wind blew from north-westerly to northerly direction and these do not coincide with the directions from which higher levels of NO, NO_2 or SO_2 were advected. Nitrous acid (HNO_2) and nitric acid (HNO_3) (not shown) both have been characterised by a diel profile with higher mixing ratios during the day. HNO_3 mixing ratios have been clearly wind direction dependent with higher values from the North, the East-Northeast and the Southeast. HNO_2 mixing ratios have been higher for wind from the North-Northwest to East and from the West.

Slightly stronger sources of soot particles have been observed from the Northern sector whereas higher particle number concentrations of $PM_{2.5}$ over PM_{10} (measured by a TSI3025A and a TSI3762 from GAW) have been observed for the section 135° to 315° and but to a lesser extend in the North-easterly sector corresponding to the Munich metropolitan area.

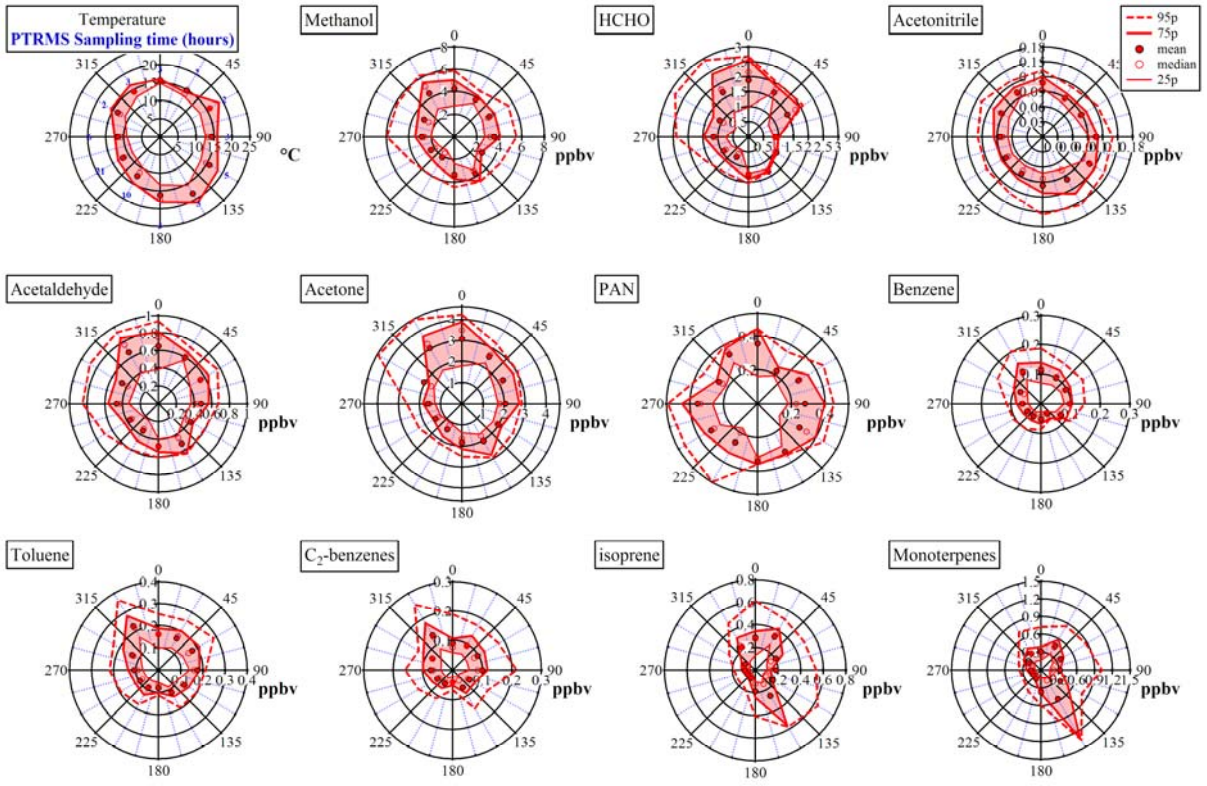

Figure 4-7: Daytime wind rose plots (continued) for temperature and organic trace gases.

Higher mixing ratios of isoprene and monoterpenes have been observed during higher ambient temperatures. The monoterpenes measured during this campaign are discussed in detail more by Bartenbach, (2005); Bartenbach et al., (2007), showed a clear diel profile with higher mixing ratios during day. Half hourly averaged mixing ratios have been below 0.6 ppbv but during sunny spells occasionally went up to 1.4 ppbv.

Formaldehyde, methanol, acetaldehyde and acetone are shown to be wind direction dependent. Elevated mixing ratios of these OVOCs have been observed in the anthropogenic sector (NNW-E), but also slightly enhanced values in the sector with enhanced biogenic VOC concentrations (SE). In contrast, their mixing ratios have been found to be lower for the predominant south westerly wind direction corresponding low anthropogenic emissions and therefore low secondary production from the oxidation of anthropogenic VOC. Furthermore, wet and rainy conditions are more frequently encountered in this sector.

4.4.5 Influence of synoptic features on VOC mixing ratios

As fronts are boundaries that separate air masses with different densities and compositions, their position and movement influence the mixing ratios of trace gases observed at the station. In addition rain events associated with these fronts can further influence the sampled mixing ratios. On July 1st, a cold front originating from a low pressure cell situated just south of Iceland, extended from northern Germany to Spain, and crossed the site at 12:00 causing temperature to drop by 5 °C and methanol, acetone, formaldehyde and acetaldehyde mixing ratios to drop by 3.5 ppbv, 1 ppbv, 1.4 ppbv and 0.46

ppbv, respectively in 2 hours time followed by rain which continued for 1 hour. These changes corresponding to a reduction of the mixing ratios by 38-45%, happened 1 hour prior to, and are far bigger than (10-30 % depending on the compound, see Table 4-6) observed during the rainfall. Similar decreases of about 43% have been observed for isoprene and monoterpenes during the passage of the front. These changes are likely caused by a change in airmass that the front separates as discussed in Bethan *et al.* (1998). Almost immediately after the rain, mixing ratios of methanol rapidly increased by 2.00 ppbv in almost 4 hours whereas over the same time period e.g. acetone increased only by 0.49 ppbv, acetaldehyde by 0.14 ppbv, and formaldehyde by 0.67 ppbv. Mixing ratios of biogenic tracers isoprene and monoterpenes, but also those of MACR+MVK, hardly changed even though temperatures rose by 3 °C.

Figure 4-8 shows the response of the mixing ratios of methanol, acetone, acetaldehyde and formaldehyde (a), isoprene, MVK+MACR and monoterpenes (b), and of NO, NO_2, O_3 and CO (c) due to boundary layer dynamics and synoptic features that have crossed at the site and have controlled the weather for days (as discussed in connection with Figure 4-3). Clouds developed along with the approaching warm front lead to a suppression of temperature controlled emissions long before the front passed the site at ground level. At the moment the warm front passed through at the ground on 7 July around 14:30 LT, light rainfall occurred for half an hour.

Interestingly, mixing ratios of formaldehyde, methanol, acetaldehyde and acetone have shown to increase between sunrise and sunset, whereas the mixing ratios of isoprene, MACR+MVK and monoterpenes went temporarily down at 14:30LT. Formaldehyde mixing ratios fluctuated more, probably due to emissions and photolysis (variable solar radiation due to partial cloud cover). The second most fluctuating compound in this short list of oxygenated VOCs was methanol.

Although the ambient temperature hardly declined at midnight, the relative humidity declined substantially (from ~92% on 7 July, 22:30LT to ~50% on 8 July, 2:00LT) along with the mixing ratios of all VOCs, NO_x and CO. Only the mixing ratios of ozone went up (Figure 4-8c). Mixing ratios of all these tracers including ozone have been found to be relatively constant until 06:00LT. Immediately after 06:00 LT the ambient temperature increased to 23.5 °C at 8:00LT and further to 25°C at 9:15LT as can be seen in Figure 4-8b. Mixing ratios of isoprene, monoterpenes and methanol increased in a similar manner over the course of time and reduced around 10:15 LT as clouds appeared. The strong increase in temperature during a short period of time conjectures the passage of a warm conveyer belt within the warm sector. However, a warm conveyer belt is relatively narrow flow of air that transfers significant amounts of heat, moisture, and momentum from lower latitudes towards the poles. Meteorological observations show the area of Hohenpeißenberg to be dry, under constant ambient low pressure (900 hPa), declining wind speeds from 4 to 0 m/s and clear sky conditions.

Mixing ratios of both methanol and acetone have been equal to ~2 ppbv around 8:00 LT, methanol mixing ratios have increased much faster than those of acetone reaching 7.5 and 3.6 ppbv respectively at the moment temperature has dropped and relative humidity increased around 10:00LT. Methacrolein and methyl vinyl ketone behaved like acetone, acetaldehyde and formaldehyde all of which are oxidation products of biogenically emitted compounds.

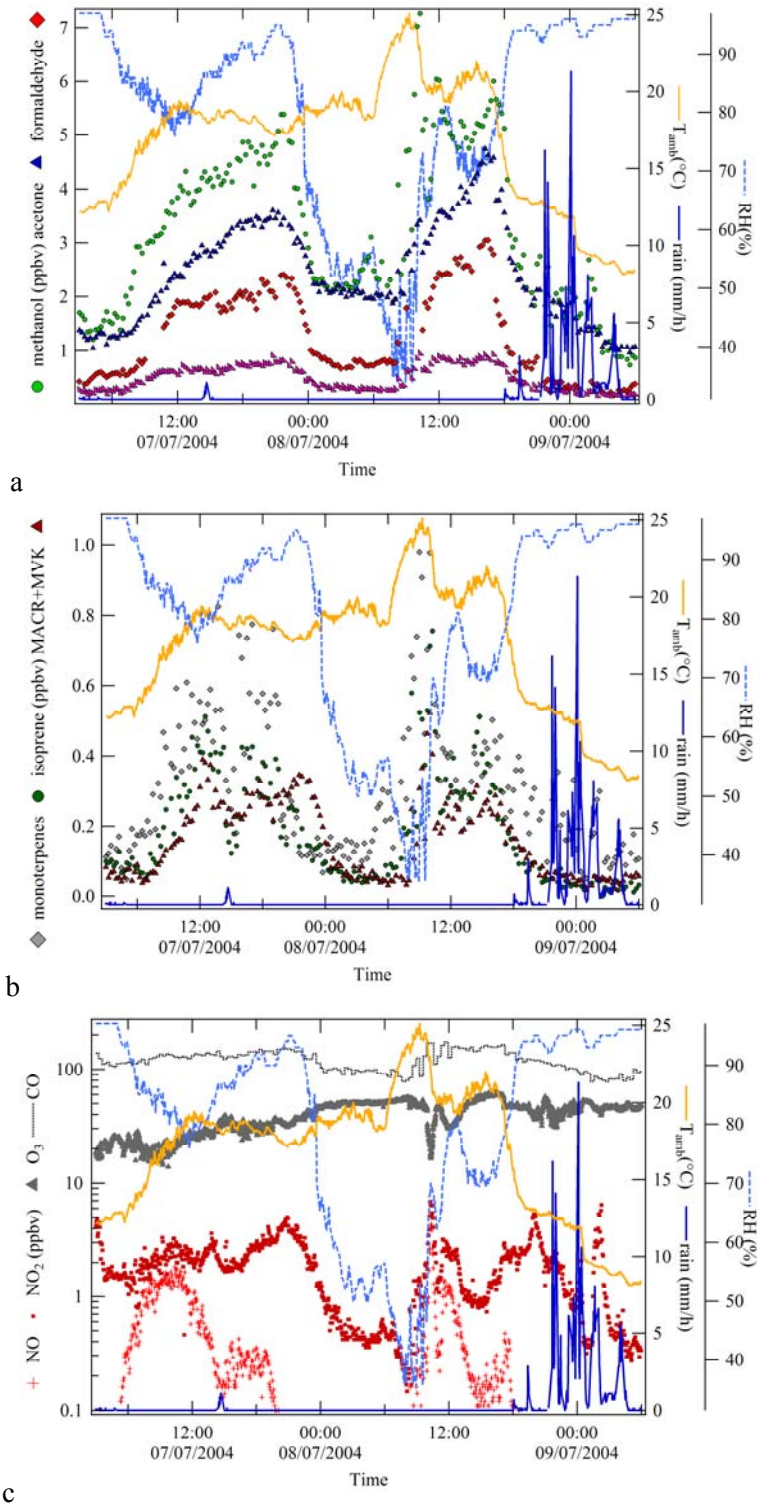

Figure 4-8: Time line for (a) methanol, acetone and formaldehyde and (b) isoprene, MACR+MVK and the sum of monoterpenes and (c) NO, NO_2, O_3 and CO together with ambient temperature and diffuse radiation and rain.

The nocturnal boundary layer break up on a hill site usually implicates rather complex atmospheric issues. After 10:30, the region remained in the warm sector until around 18:00LT when the cold front connected to the low pressure system passed the site causing, analogously to the cold front on 1 July, strong decreases of 50-57% in the mixing ratios of all VOCs before the showers and thunderstorm set in. Mixing ratios fluctuated during the thunderstorm but have finally been lower than before the rain event.

4.4.6 **VOC correlations**

In this section the correlations between oVOCs, ozone and CO will be examined with a view to elucidate common sources and sinks and differences in the prevailing air mass regimes. These analyses are used to highlight particular campaign episodes during which the region has encountered air masses with distinct characteristics e.g. from the South - Southeast (see Figure 4-5).

The correlation between acetone and ozone as shown in Figure 4-9a has been used to develop filters to identify particular chemical characteristics. As a first selection criterion, an arbitrary partition equation ([acetone]-0.9)/([O_3]+0.02) greater than 0.061 has been used to capture the exceptional circumstances marked by grey squares. These data points involve high concentrations of acetone and correspond to 7 and 8 July 2004 but exclude the data of the night in between i.e. from midnight until 9:30 8 July (green diamonds). Applying this partition filter does include some of the data points belonging to the first episode between noontime 30 June and noontime 1 July. This episode is marked in Figure 4-9a by blue triangles and has mainly been characterised by generally higher concentrations in ozone compared the rest of the campaign.

Data from the previous night (21:30 on 6 July - 9:30 on 7 July) have been characterised by lower ozone and acetone mixing ratios i.e. lesser than 28 ppbv and 1.95 ppbv, respectively. Data obtained after applying the latter selection criterion are indicated by yellow hourglass markers also include very brief episodes during the breakup of the NBL on several days (2, 10, 11, 13 and 14 July), when residual air or even free tropospheric air possibly gets mixed in. It suggests that during this night, the station has been cut off from its surroundings by the NBL exposing it to residual layer air.

Figure 4-9b shows using the same markers as discussed before how acetaldehyde and acetone have been correlated to each other. Here, an arbitrary partition equation [acetaldehyde] + 0.45)/[acetone] lesser than or equal to 0.43 has been used as a proxy to separate data from 30 June to 1 July and 7 July to 8 July from the rest. Additionally captured data points in the afternoon of 6 July correspond to the moment of change in the wind direction to the East - Southeast.

Strong emissions of acetone and acetaldehyde suggest high levels of anthropogenic pollution. Therefore, the concentration ratio of [toluene]/[benzene] has been analysed (campaign average of 2.14 ± 2.31, not shown). High ratios measured in the boundary layer reflect fresh toluene from fossil fuel combustion. Ratios of up to 6:1 have regularly but briefly been observed in the morning and evening caused by fresh commuter traffic pollution. Higher than average ratios over the course of a night suggests local, fresh pollution trapped under inversions just above the observatory. Lower than average ratios might occur during entrainment in the morning in absence of commuter traffic related fresh pollution. Variations in the concentration ratios have also been observed during some rain events which are related to the mixing in of air with different characteristics rather than the more efficient removal of one compound over the other as they both have similarly low values for Henry's law constant. The average [toluene]/[benzene] concentration ratio on 30 June and noontime 1 July has been 1.75 ± 0.78 before and 2.38 ± 0.80 after the passage of the cold front for the rest of this day. Data between 6 and 8 July clearly show a diel profile with the lowest concentration ratios between noon and five o'clock (1.57 ± 0.40), elevated concentration ratios at night (2.0± 0.65) and the highest concentration ratios in the evening (up to 2.4) and in the morning (up to 3.0). Morning ratios usually fluctuated much more due to entrainment.

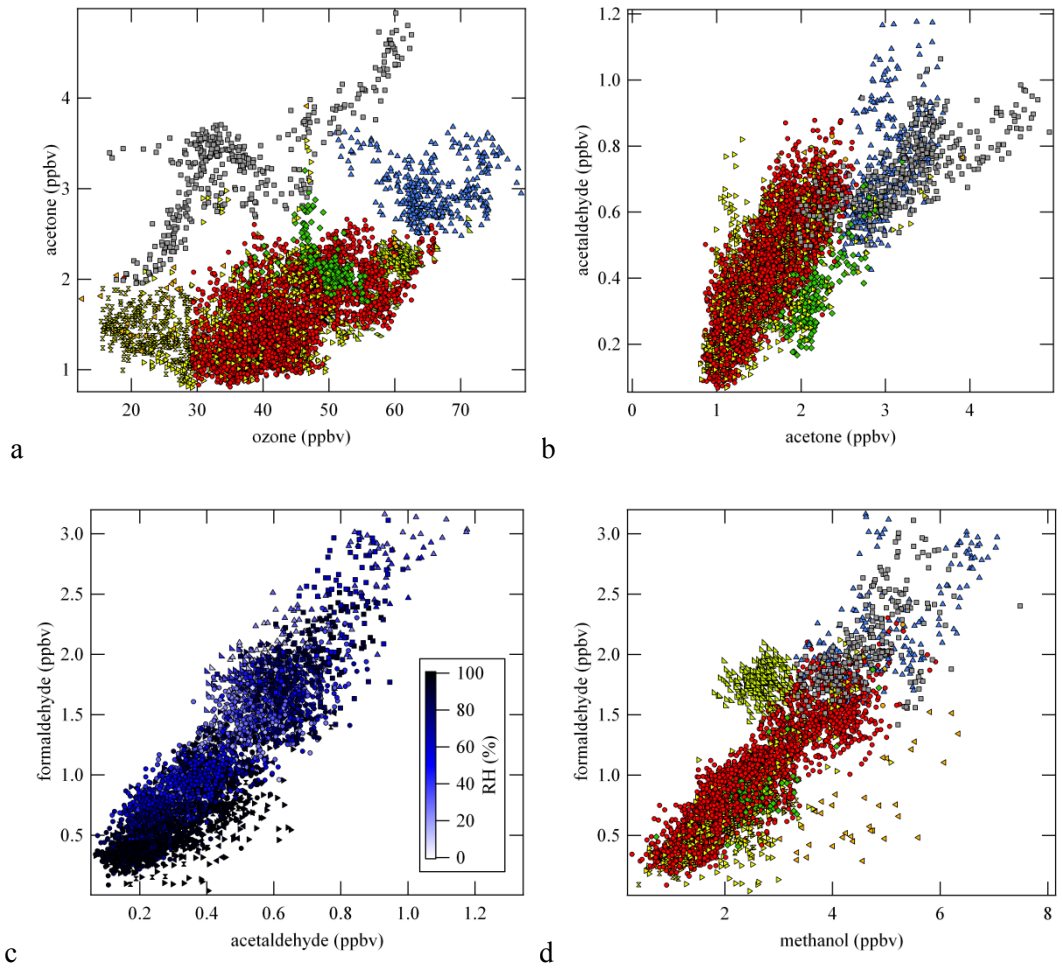

Figure 4-9: Correlation among VOCs and other tracers. Different markers are described in the text.

Acetaldehyde with a photochemical lifetime of 3.5 hours is more reactive than formaldehyde (τ ~6.5 hours), and far more reactive than methanol (τ ~2.5 days) or acetone (τ~2 weeks) which is in agreement with their abundances in atmosphere which is dominated by the source strength of each compound.

Acetaldehyde is less affected by wash-out than formaldehyde as it has a much lower (212 times) value for the Henry's law constant (listed in Table 4-4) and therefore much less efficiently removed by rain or clouds. The Henry's Law constant of methanol is 15.6 times that of acetaldehyde but 13.6 times smaller that of formaldehyde. Formaldehyde in turn should be less affected by wash-out than nitric acid (HNO_3) as it has a much lower (163 times) value for the Henry's law constant. Although these compounds were not linearly correlated during dry periods, clearly much lower HNO_3 mixing ratios are to be associated with wet periods.

Wet removal is assumed to play a subordinate role against photochemical removal. However, oxidising radicals are easily removed from the air by rain, prolonging the lifetime of these tracers.

Table 4-4 Henry's Law Constants for inorganic and organic trace gases for this campaign (25p-75p) and their reaction rate and lifetime against OH in brackets for standard conditions (25°C)

Substance	25p - 75p k_H [a] [mol/m^{3}Pa]	k^{Θ}_{H} [a] [mol/m^{3}Pa]	k^{Θ}_{OH} [b] [cm^3 molec^{-1} s^{-1}]
nitric acid	492.1 - 956.2	2072.5	$1.5x10^{-13}$
formaldehyde	10.1 - 16.6	29.6	$8.5x10^{-12}$
methanol	0.92 - 1.37	2.17	$8.9x10^{-13}$
acetonitrile	0.17 - 0.27	0.524	$2.2x10^{-14}$
acetone	0.11 - 0.17	0.297	$1.75x10^{-13}$
acetaldehyde	0.05 - 0.08	0.139	$1.5x10^{-11}$
propanal	0.05 - 0.08	0.129	$2.0x10^{-11}$
acetonitrile	0.17 - 0.27	0.524	$2.2x10^{-14}$
sulphur dioxide	0.007 - 0.009	0.011	$1.3x10^{-12}$
benzene	0.0008 - 0.001	0.0019	$1.23x10^{-12}$
toluene	0.0008 - 0.001	0.0016	$5.96x10^{-12}$
isoprene	0.00006 - 0.00009	0.0003	$1.03x10^{-10}$

[a] data from Sander, 1999 [b] data from Atkinson et al., 2006b

Figure 4-9c shows that formaldehyde and acetaldehyde have been linearly well correlated (R^2=0.796, slope=2.77). However, even after applying the selection criteria discussed so far, a delineation of the data with humidity is still apparent in the formaldehyde/acetaldehyde plot where lower formaldehyde and acetaldehyde data clearly are associated with wet periods (rain ~RH>95%). This becomes clear after evaluating the slope in the linear correlation which varied from 1.43 for RH>95%, 2.60 for 80%<RH<95%, and 2.72 for 70%<RH<80%. A similar effect has been observed in the relation between methanol and acetaldehyde. Excluding data under rainy conditions (yellow triangles) results in a slope of 2.35 with R^2= 0.798 as summarised in Table 4-5 for all oVOC relationships discussed here.

Figure 4-9d shows green right-angled triangular data points corresponding to dry conditions which have been characterised by higher mixing ratios of formaldehyde compared to methanol than commonly observed during this campaign. Under these conditions on 29 and 30 June, formaldehyde varied only little (1.67 ± 0.20 ppbv) in contrast to methanol (2.74 ± 1.24 ppbv). After removing these data, the slope in the relation between formaldehyde and methanol was 0.378, the intercept = 0.03 and R^2 = 0.798.

Figure 4-10 shows the acetone / methanol plot for daytime (10:00LT- 17:30 LT, a) and nighttime (21:00LT- 05:00 LT, b). Time has been used to separate the data coloured according to the prevailing temperature. The same marker symbols have been used as previously addressed in connection to Figure 4-9, only their seizes have been scaled according to the measured level of CO. Warm sector air has been enriched day and night in CO, probably due to strong hydrocarbon oxidation. Additionally, the distinct correlation for the warm cloudless period has been highlighted and has been characterised by a slope of 0.273 and the highest offset of 1.428 observed during this campaign.

Night time data clearly show the effect of the warm sector as ambient temperatures remain at 20°C and more. These two plots exclude data in the evening and in the morning when the NBL has been formed or resolved by the newly formed CBL.

Distinct groups of datapoints have become apparent by examining the correlations shown above. The average daytime acetone / methanol concentration ratio has been 0.345 with an intercept of 0.641 ppbv whereas for the warm sector, a slope of 0.890 and an atypical intercept of -0.789 have been found. This indicates the presence of very significant sources of acetone which could have been primarily emitted or secondarily formed during transport.

Acetone is measured at m/z 59 by the PTRMS but may also include other compounds. Propanal which is far more reactive towards OH than acetone, is a likely candidate. The oxidation of butanal to form

propanal is not likely to be an important source as its concentrations were low (GC analysis). Although the intercomparison with both gas chromatographic systems does not show a straightforward relationship from which the relative contribution could be estimated (see Table 4-3), we assume acetone to be the predominant compound. The substantial difference in the day and night time slope suggests contributions of photo-oxidation products with a clear diel cycle, but a strong direct source which is active during daytime is also plausible.

The campaign average nighttime acetone / methanol concentration ratio outside the period of 7 and 8 July has been 0.296 with an intercept of 0.781. During this particular period, nighttime warm sector data have been characterised by a steeper slope of 0.376 and an offset which is significantly larger, namely 1.348 ppbv. The ratio between acetone and methanol was higher during the night than during the day and may fluctuated stronger (spiking upwards) during breakup of the NBL (mixing in of air with different characteristics). Upward spikes in the ratio of acetone over methanol have also been observed during rainfall due the stronger washout of methanol.

4-day backward trajectories shown in section 4.3, indicate transport originating from the Mediterranean and close to the surface crossing northern Italy, known for high levels of anthropogenic pollution (Seibert et al., 1998) . Other periods mostly have air masses rapidly advected from the W and NW Atlantic.

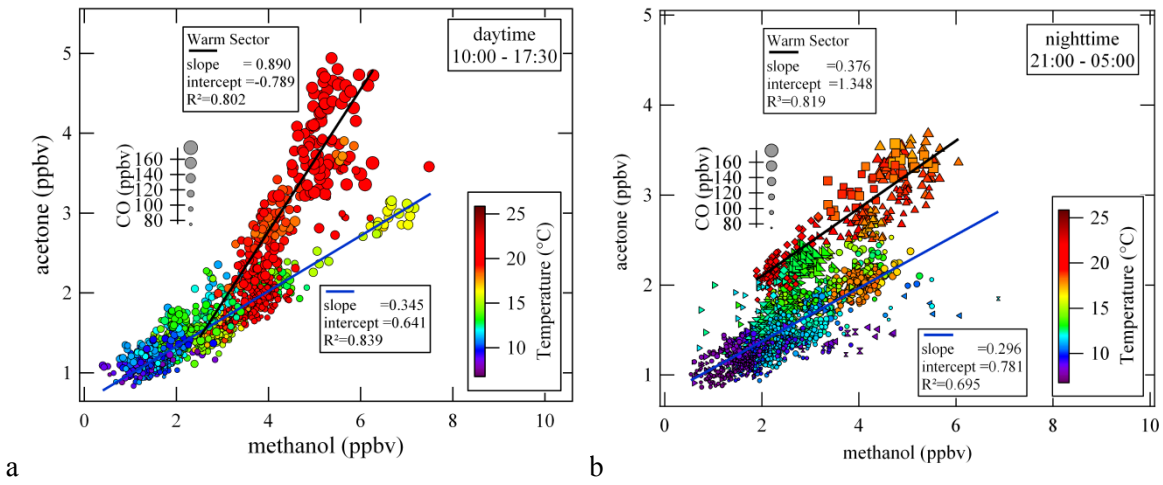

Figure 4-10: Daytime (a) and night time (b) correlation between acetone and methanol as function of temperature.

The long atmospheric lifetime of methanol and acetone complicates the situation as distant sources may also contribute to the observed mixing ratios. Methanol emissions from plants are known to be directly correlated to temperature (Hüve et al., 2007) and this can be clearly seen from Figure 4-10 if one does not take the warm sector data into consideration. We may therefore speculate that methanol measured here originated mostly from the meadows largely surrounding the station. However, methanol has a very long lifetime and contributions of sources further away cannot be ruled out. Some of the very high mixing ratios in acetone and methanol correlate with higher levels of CO, NO_x and low levels of O_3.

This section is concluded by .Table 4-5, listing the linear regression analysis for the most abundant oVOCs during this campaign.

Table 4-5: Common correlation between several oVOCs measured during HOHPEX04.

	slope	intercept	R^2
acetaldehyde vs acetone	0.343	-0.135	0.706
Formaldehyde vs methanol	0.377	0.028	0.798
Acetone vs methanol	0.352	0.628	0.793
Formaldehyde vs acetaldehyde	2.352	0.076	0.783

4.4.7 **Wet removal by wash out**

During this campaign as shown in Table 4-6, data for various compounds has been gathered in rain events. Here the changes in the various species concentrations are examined more closely, by comparing the percentage change in the concentrations of oVOCs during individual rain events with respect to the concentration at the start of the rain fall. The signal of the rain gauge has been used to select the initial concentration and the final concentration of a compound in the air. There often has been a decline in the concentration preceding the rain due to the change in air mass the passage of a front. The rain fall rate listed in the Table 4-6 equals the average rain fall rate for each event. Also included in Table 4-6 is the kind of synoptic feature involved. As addressed in section 1.5.5, warm fronts should purely in point of view of analysis be the most suitable synoptic situation to study oVOC removal.

Table 4-6: Percentage loss rate of several oVOCs during rain events.

Date	Duration (hh:mm)	rain rate (mm/h)	HNO_3	HCHO	CH_3OH	CH_3COCH_3	CH_3CHO	CH_3CN	SO_2	Synoptic
1/7/'04 12:58	00:38	2.75	64	22	33	-7	9	8	77	CF
2/7/'04 10:01	05:31	2.68		43	56	34	23	19	72	WF
3/7/'04 03:05	00:26	2.52		15	19	10	12	11	55	WF
5/7/'04 23:38	00:51	1.97	26	51	33	15	33	1	34	WF
6/7/'04 08:27	01:01	2.25	24	57	18	13	14	-24	-1	SF
9/7/'04 01:06	07:46	3.09	85	52	56	44	40	27		OC
10/7/'04 08:44	03:47	1.19	88	51	46	18	8	14	45	CF
12/7/'04 13:47	00:36	2.42		30	15	2	13	5	31	WF
12/7/'04 18:33	01:18	2.94	-59	6	-21	-8	-38	2	-213	WF
13/7/'04 09:33	02:07	2.09	-738		-38	-18	-68	7	-199	L
13/7/'04 13:02	00:27	2.52	-120	-99	-67	-33	-18	-30	-189	L

WF= warm front; CF=coldfront; SF= stationary front; OC=occluded front; L= Low pressure cell

From table Table 4-6 we conclude that the inorganic soluble species are more depleted during rain events (60-80%). Formaldehyde and methanol have behaved similarly during the main rain events lasting longer than 3 hours and are depleted by ca. 50%. Compounds such as acetone, acetaldehyde and acetonitrile have been depleted significantly less than methanol and formaldehyde. All these results are generally consistent with the relative values of Henry's law constant.

Negative values indicate that the concentration right after the shower of rain has been higher than at the start and have been related to emission plumes or airmass changes but may as well be cause by mixing in of air richer in organic compounds from above. As has been shown previously airmass changes often produce mixing ratios changes larger than the rain events shown above. Uncertainties in downward mixing during the rain events as well as possible airmass changes associated with fronts embedded in the rain events preclude any further meaningful analysis on such loss rates. However, these results serve to indicate the importance of wet deposition to all examined compounds and that any surface site affected by rainfall should show perturbations of the aforementioned compounds which correspond to the relative Henry Law coefficients.

4.5 Discussion and conclusions

The results of the HOHPEX04 campaign have shown that the 3 stage differentially pumped PTR-MS system provided less scattered data and proved to be 5 times more sensitive with a 2.5 lower limit of detection than the 2 stage-differentially pumped PTR-MS. Data from the recommended 3 stage differentially pumped PTR-MS have therefore been used in the comparison with other measurement techniques.

Dry calibrations have demonstrated to differ sometimes substantially from slightly humidified calibration. It is recommended to humidify synthetic purified air for dilution of the calibration standard. If possible, one should accurately control the humidity over the entire ambient RH-range. If not, one should use scrubbed ambient air for dilution of the calibration standard rather than synthetic air.

The quality of the correlations for the ambient PTR-MS measurements were rather mixed. Only for methanol, acetone, isoprene and macr+mvk, the correlation was good. For compounds like acetaldehyde, toluene and the sum of monoterpenes, the agreement was reasonably good. But for acetonitrile, benzene and substituted benzenes the correlations were bad. The latter can to some extent be explained by the large scatter in the signals for compounds at very low concentration, highlighting the superiority of the three pump system..

The variety of compounds emitted in the region around Hohenpeißenberg is large and thus PTR-MS measurements require the support of more selective measurement techniques. The comparison of PTR-MS with the gas chromatographic measurements has shown PTR-MS data to be consistently higher. In particular,, for ketones there has been a substantial overestimation by the PTR-MS or an underestimation by the GC.

Oxygenated VOC correlations for Hohenpeißenberg have clearly shown periods with distinct characteristics. These episodes have their origin in the air mass history, boundary layer dynamics and rainfall all of which are driven by the synoptic features crossing the site. The contribution to the level of anthropogenic from the metropolitan area of Munich can be substantial. However, fresh pollution from traffic and industry in between neighbouring towns and villages can be often significant. The level of pollution can also be temporarily significant at the breakup of the NBL during which the observatory, when situated in the residual layer due to an inversion, is exposed to convective currents transferring heat and accumulated pollution upwards. Under certain circumstances low pressure systems can force heavily polluted North-Italian air masses to be transported north. Furthermore, due to the continuously higher ambient temperatures and more generally cloud free conditions within the warm sector, biogenic emissions remain high.

Rain events have been analysed as a matter of interest. The results have not shown a clear proportionality between the strength of the Henry's law constant and intensity of removal of oVOCs, though a general agreement can be seen. The quantification of the removal of VOCs from the atmosphere by scavenging below the clouds clearly requires a focussed campaign and preferably high time resolution measurements in both the aqueous phase of the rain droplets and the air surrounding them. It is recommended to setup a detailed model based on the findings from equilibrator experiments evaluating all physical and chemical factors influencing the uptake to tracers by the droplets. Very recently a detailed model has been discussed by Elperin et al., (2010) but this work does not report on the removal of volatile organic compounds.

5 VOC measurements within a boreal forest during spring 2005: on the occurrence of elevated monoterpene concentrations during night time intense particle concentration events

This chapter is published in Atmospheric Chemistry and Physics 9, 1-21, 2009. www.atmos-chem-phys.net/9/8331/2009/

5.1 Introduction

Boreal coniferous forests ring much of the region immediately south of the Arctic Circle and are comparable in size (15 million km^2) to that of global rainforest (17 million km^2). They have been shown to profoundly influence regional atmospheric chemistry through the emission of reactive trace gases such as monoterpenes e.g. (Spanke et al., 2001; Bäck et al., 2005; Räisänen et al., 2009). During the atmospheric oxidation of monoterpenes, products with low vapour pressure such as organic acids can be produced, which can in turn condense to the aerosol phase. The role of these organics in new particle formation has been the subject of considerable research activities in recent years (e.g. Yu et al., 1999; Anttila et al., 2005; Tunved et al., 2006; Bonn et al., 2008a and references therein), but is not fully understood. There are only a few studies reporting on night time new particle formation events (e.g. Junninen et al., 2008; Lee et al., 2008). In terms of chemical composition, newly formed ultrafine atmospheric aerosols are poorly characterized and there is currently insufficient information concerning organic species participating in secondary aerosol formation (e.g. Shimmo et al., 2004).

It has been established that the aerosols affect the radiative budget of the region (Kurten et al., 2003; Tunved et al., 2006) and the boreal forest in Finland has been reported to sustain ca. 1000-2000 particles/cm^3 by gas to particle conversion in the climatically relevant size range of 40 - 100 nm.

The process of atmospheric particle production through nucleation and subsequent condensation growth has been shown to occur all over the world (Kulmala et al., 2004; Kulmala and Kerminen, 2008). The different environmental conditions and locations include e.g., in the free troposphere (Raes et al., 1997; Weber et al., 1999), in coastal zones (O'Dowd et al., 2002), in the continental boundary layer (Birmili et al., 2002), and in particular, over boreal forests e.g. (Kulmala et al., 2001b; Dal Maso et al., 2005). These nucleation events occur on a large horizontal scale in the order of several hundreds of kilometres, and have been detected simultaneously at sites 2000 km apart (Vana et al., 2004). A limited number of field studies on newly formed particles (3–5 nm) e.g. (Kulmala et al., 2001b) have concluded that the observed particles were primarily composed of high molecular weight oxidised organic species, such as cis-pinonic acid and pinic acid, produced by ozone induced oxidation of monoterpenes. Sulphate/organic mixtures have also been implicated in such new particle formation (Marti et al., 1997). The results of a study by Zhang et al., (2004) imply that the interaction between organic and sulphuric acids promotes efficient formation of organic and sulphate aerosols. It remains an open question whether organics are only involved in the growth of stable clusters, or if they can also influence the cluster formation.

In this study we present measurements of trace gases and aerosols made in a boreal forest during the "Biosphere - Aerosol - Cloud - Climate Interactions - Quantification of Aerosol Nucleation in the European Boundary Layer (BACCI/QUEST IV) intensive field campaign in Hyytiälä, Finland in April-May, 2005. The measurement period marked the transition from cold winter temperatures to more temperate spring temperatures. This is a particularly interesting period to examine and to compare with previous measurements, since most previous measurements have been taken in the summer e.g. (Hakola

et al., 2003; Rinne et al., 2005; Haapanala et al., 2007). Several aerosol nucleation events have been analysed by Riipinen et al., (2007) for this campaign and the authors concluded that the main process limiting the observable particle formation was the competition between the growth of the freshly formed particles and their loss by scavenging, rather than the initial particle production by nucleation of sulphuric acid. Other particle formation events, in which sulphuric acid and water vapour are not key components, occurred synchronously with rapid and unexpectedly strong increases in monoterpenes. In this study, we examine the variations of VOC and particles during the spring campaign and identify two distinct types of aerosol production at the Hyytiälä site. Additionally, the enantiomeric determination of monoterpenes emitted by boreal trees (Yassaa and Williams, 2007) has been used to identify the source type.

5.2 Site description

The data presented here were collected at the "Station for Measuring Forest Ecosystem-Atmosphere Relations" (SMEAR II) at Hyytiälä (N 61°51', E 24°17'), in southern Finland (see Figure 5-1). The site is 230 km north of Helsinki, 180 m above sea level and surrounded by boreal forest (Vesala et al., 1998; Hari and Kulmala, 2005). The predominant tree species is Scots pine (*Pinus sylvestris*) with some spruce (*Picea abies*), aspen (*Populus sp.)* and birch (*Betula sp.*). Anthropogenic influences at the site are generally low, particularly when the wind comes from the sparsely populated northern sector. Incidental pollution from forest management activities is possible. The main road passing a few kilometres from the station to the southwest, and the cities of Tampere (pop. ~205,000; 391 inh./km² (2005), 49 km to the south west) and Jyväskylä (pop. 84,500; 91 inh./km² (2005), 88 km to the north-east) can sometimes influence the site (see Figure 5-1). Minor influences were expected from the few nearby settlements with low population densities (generally < ~17 inh./km²).

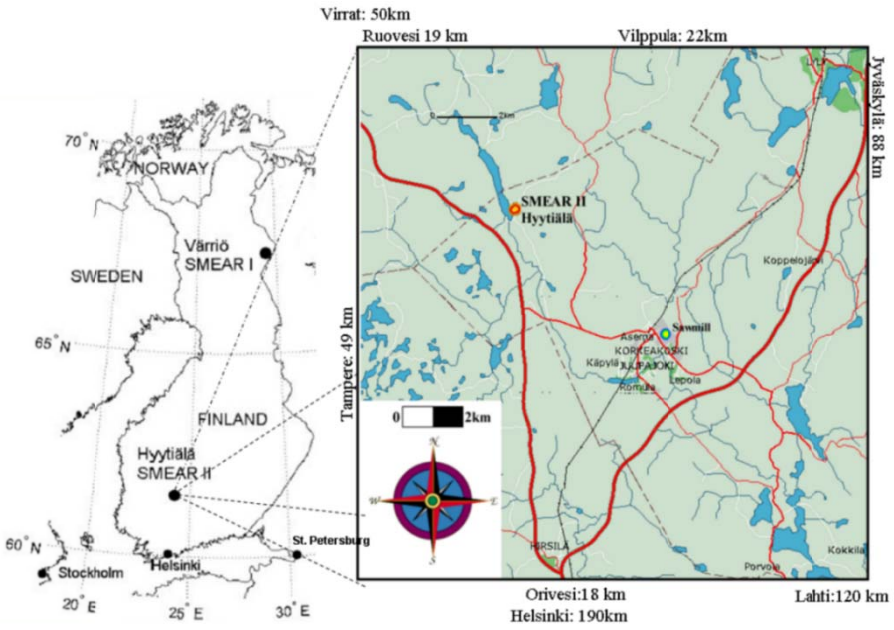

Figure 5-1: Location of Hyytiälä on the map with its surrounding settlements and cities.

5.3 General meteorology

Figure 5-2 shows the basic meteorological parameters measured at the SMEAR II main mast during the campaign, along with the particle number concentration (black solid line). Gaps in the data are due to occasional failures in the data logging system of SMEAR II. During April the wind blew predominantly from the relatively unpopulated north (15–24 April and 29 April–2 May) and from the southeast (26–28 April). The temperature varied from +5 to +13°C by day and from −5 to +5 °C by night, while the humidity ranged from 25 to 100%. These conditions are typical of springtime in Finland. Lower

temperatures were associated with periods of unvarying Arctic winds (higher wind speeds on all levels), whereas somewhat higher temperatures and pressures were reached during weak south-easterly winds. The precession of temperature and pressure indicate that a series of synoptic features have crossed the site in this period, only a few short-term precipitation events were observed during the campaign (19-22 April, occasionally snow, no rain). From Figure 5-2, a gradual rise in temperature throughout the campaign can be ascertained, and a slow thawing of the ground and the ice covered lakes was observed in this time.

Balloon soundings of temperature and pressure made at the site between 23 and 30 April, mostly in the early morning and early evening, indicated clear nocturnal inversions. Although the development of the nocturnal boundary layer (NBL) was not examined by the balloon soundings, the height of the NBL after midnight was to grow from ~70m at 20:00 (Local Time = UTC+2) to ~160m at ~05:45 LT determined by the earliest winching.

5.4 Results

This study focuses on the variations of the VOCs and particles during the spring campaign in Hyytiälä. In the first section, the VOC mixing ratios and particle concentrations are characterised as a function of time, meteorological parameters, diel cycle and height above ground. Subsequently in section 5.4.4 and 5.4.5, two distinct particle burst events are selected and analysed using the VOC and gas phase H_2SO_4 measurements in order to investigate the probable cause of each event.

5.4.1 General variation in VOC and aerosol concentrations

From Figures 2 and 3 it can be seen that the mixing ratios of many VOCs (e.g. acetone, methanol, acetaldehyde and monoterpenes) were observed to be higher during the warmer period of this campaign (23 April - 30 April) than during the colder period (18 April - 23 April). During the latter period, few VOCs showed a diel variation in their mixing ratios except for monoterpenes and methanol. Interestingly, monoterpenes were observed at mixing ratios between 0 and 16 ppbv with a campaign average of 0.32 ppbv, and thereby comparable to the mixing ratios reported by Sellegri et al., (2005a); Sellegri et al., (2005b) and by (Ruuskanen et al., 2009) for the same site.

The mixing ratios of acetone (median = 1.27 ppbv) and methanol (median = 1.62 ppbv) are in agreement with values reported from similar latitudes by Taipale et al., (2008) and Ruuskanen et al., (2009). However, while acetone values reported here (0.75-1.40 ppbv) are in good agreement with previous measurements from the same location for March 2003 (Sellegri et al., 2005a), methanol values recorded in this study (0.60-2.10 ppbv) are markedly higher. Table 5-1 summarises the mixing ratios measured during this campaign with other literature values reported for Hyytiälä.

Table 5-1 Summary of VOC mixing ratios for April 2005 compared to other spring time measurements of VOCs observed at Hyytiälä, Finland.

	(ppbv)	This study colder period	This study warmer period	Sellegri et al., 2005b	Hellén et al., 2004	Ruuskanen et al., 2009
m/z	**Compounds**	**25p - 75p**	**25p - 75p**	**25p - 75p**	**mean**	**5p - 95p**
33	Methanol	0.64 - 1.00	1.23 - 2.01	0.23 - 0.42		0.31 - 1.74
42	Acetonitrile	0.03 - 0.05	0.05 - 0.07	0.05 - 0.10		0.02 - 0.06
45	Acetaldehyde	0.14 - 0.21	0.21 - 0.32	0.02 - 0.05	0.18	0.21 - 0.39
59	Acetone	0.74 - 0.96	1.21 - 1.40	1.09 - 1.66	0.52	0.40 - 1.31
69	Isoprene	0.04 - 0.08	0.05 - 0.10			0.02 - 0.10
71	MACR+MVK	0.01 - 0.03	0.02 - 0.04			0.03 - 0.13
79	Benzene	0.08 - 0.12	0.08 - 0.13			0.06 - 0.11
93	Toluene	0.01 - 0.04	0.03 - 0.07			
137	Monoterpenes	0.06 - 0.18	0.17 - 0.64	0.19 - 0.40		0.03 - 0.20

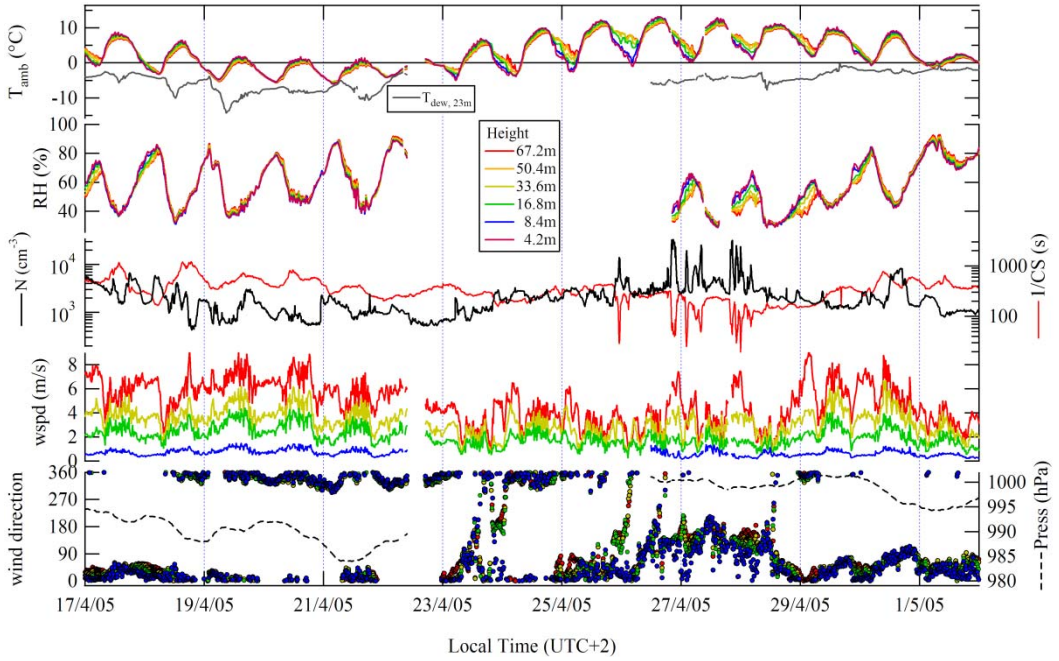

Figure 5-2: Time series of basic meteorological parameters from the SMEAR II main mast (74m) and aerosol total number concentration over the measurement range of the DMPS-analyser (left) and 1/Condensational Sink (right).

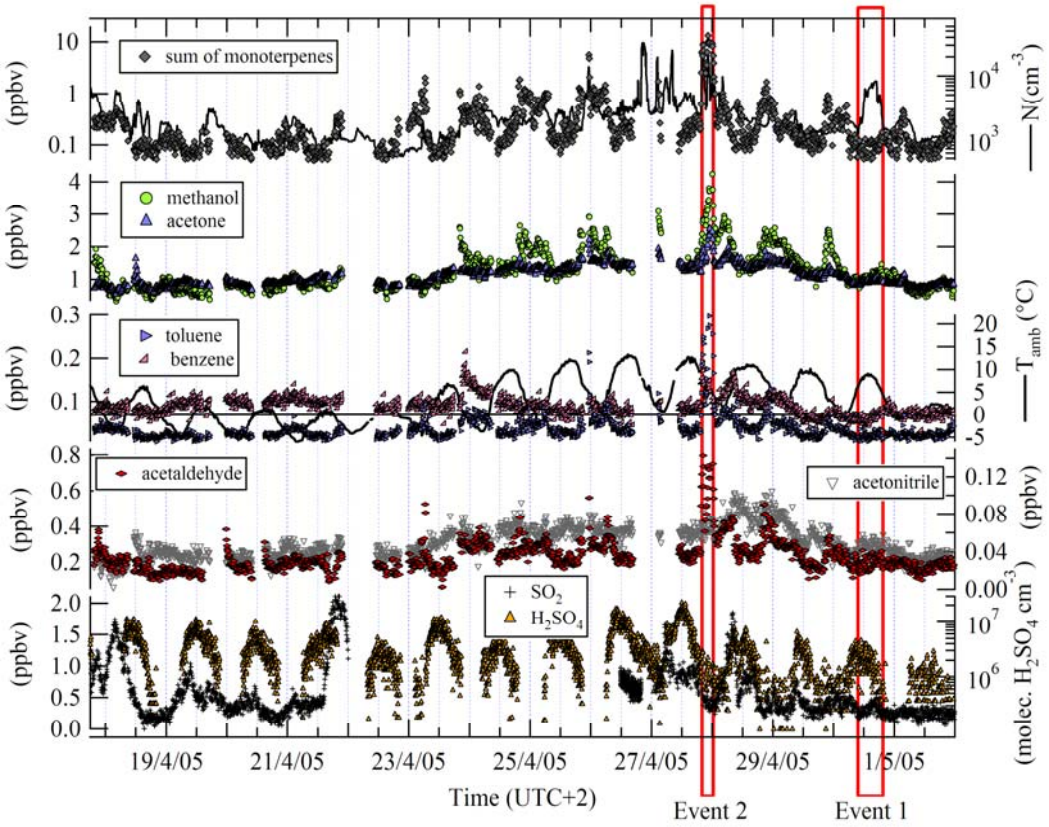

Figure 5-3: Inorganic and organic trace gases (10 min. avg.), total aerosol particle concentration (3 - 850 nm) measured for the springtime BACCI/QUEST IV campaign at Hyytiälä. Indicated are the windows for Event 1 and Event 2.

Analysis of the concentration ratio acetone/CO as discussed in de Reus et al., (2003) clearly shows in Figure 5-4 a strong correlation with acetonitrile. For acetonitrile mixing ratios of higher than 50 pptv, acetone/co values higher than ~7-8 pptv/ppbv have been observed. Within the period from early morning 23 April to morning 30 April 2005, large particles (20 - 200 nm) have been present day and night.

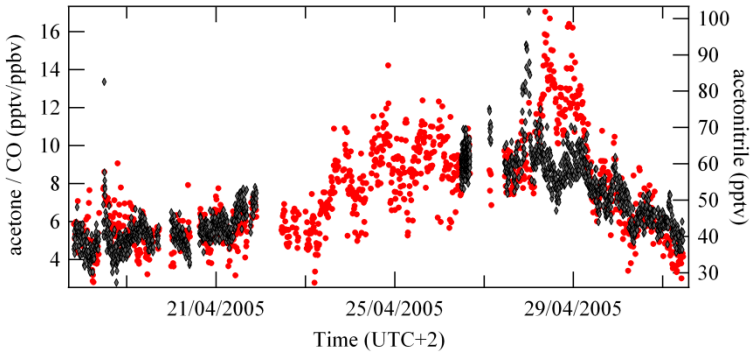

Figure 5-4: Concentration ratio of acetone over CO in connection with levels of acetonitrile.

Acetonitrile mixing ratios were generally low (53 ± 18 pptv) compared to measurements over the tropical and temperate forests (chapter 3 and 4). Higher than campaign average values were observed on April 28 and April 29 with an average of 90 ± 17 pptv and a maximum of 130 pptv. Acetonitrile was in agreement with studies by Sellegri et al., (2005a) and Ruuskanen et al., (2009). Levels of the anthropogenic tracers benzene and toluene are similarly low (medians 96 pptv and 69 pptv, respectively) but show occasionally short term increases. Benzene mixing ratios are generally low in this region during spring, summer and autumn but higher during wintertime (Taipale et al., 2008; Ruuskanen et al., 2009).

The results for acetaldehyde presented here are in good agreement with 24 hour cartridge samples for March and April taken in 2003 by Hellén et al., (2004) who reported acetaldehyde mixing ratios between 0.09 and 0.28 ppbv with an average of ~0.18 ppbv and to those reported by Ruuskanen et al., (2009) for springtime 2006-2007. Sellegri et al., (2005a) reported lower mixing ratios as shown in Table 5-1.

Ruuskanen et al., (2009) showed that the boreal forest is only a weak emitter of isoprene in springtime, approximately 10 times less than levels typically measured over the rainforest (Helmig et al., 1998; Zimmerman et al., 1988) and chapter 3, and our data confirm these very low isoprene mixing ratios.

From Figure 5-2 we note that the warmer period was characterised by elevated particle background concentrations in comparison to the cold period. The warmer period also exhibited comparatively more methanol relative to acetone than in the cold period.

From Figure 5-2 we may compare the total particle concentration in the range of 3 - 850 nm detected by the DMPS and the inverse value of the condensational sink (CS, i.e. pre-existing aerosol particle surface) calculated for sulphuric acid according to Kulmala et al., (2001a) with the meteorological parameters. 1/CS describes the time, which a sulphuric acid molecule has until it collides with the next aerosol surface area. The diel cycle of 1/CS is characterised by lower values after midnight and a pronounced increase between sunrise and about 10:00 LT. Campaign median values of 1/CS varied between 300 and 400 seconds with higher variability during daytime (250 - 550 s, 25p - 75p). Values have clearly been much lower (<300 s) between dusk on April 25 and dawn on April 29 still showing the same characteristic diel profile. Median values of 1/CS varied between 100 and 150 seconds. This period shows elevated aerosol particle concentrations with several distinct events, defined as strong deviations from the underlying background. In particular, there is a broad event on the 30th of April (hereafter termed Event 1) during which particle concentrations increased from circa 1200 to 6000 particles/cm^3 for approximately 6 hours. Between the 25th and the 28th of April a series of short, intense particle bursts

occurred. In such events (hereafter collectively termed Event 2), particle concentrations were observed to increase by an order of magnitude over the background (circa 30000 cm^{-3} over 3000 cm^{-3}).

Mixing ratios SO_2 whose predominant regional source is anthropogenic (e.g. fossil fuel burning) were highly variable exhibiting both daytime and nighttime maxima up to 2 ppbv or $4.2x10^{10}$ molec. SO_2 /cm³. This is in contrast to H_2SO_4 which showed a distinct diurnal cycle, see Figure 5-3, with maxima up to $2x10^7$ H_2SO_4 molec./cm³ for the period between the 17th of April and the 2nd of May.

Figure 5-5 shows the average 24 hour or diel cycle in the net radiation, the potential temperature gradient and the mixing ratios of monoterpenes, methanol, acetaldehyde and sulphuric acid during the warmer period which is also the period with the strongest nocturnal inversions during this campaign. Although monoterpene emissions have been shown previously to be a function of the ambient temperature, with higher emission rates during the day (Janson, 1992; Janson and De Serves, 1999, 2001; Spanke et al., 2001), the monoterpene mixing ratios observed at Hyytiälä during spring were found to be higher at night. This is likely due to the formation of a shallow nocturnal inversion layer at night over the continuously emitting vegetation. Also Taipale et al., (2008) measured occasional higher night-time mixing ratios for monoterpenes, though these increases were much weaker than observed during this campaign. These short term peaks in the monoterpenes do not correlate well with the slowly changing temperature profile and will be studied in depth in the following section.

Sellegri et al., (2005a) reported that the VOC mixing ratios were driven by boundary layer dynamics. They showed diel cycles for many VOCs with higher night time mixing ratios.

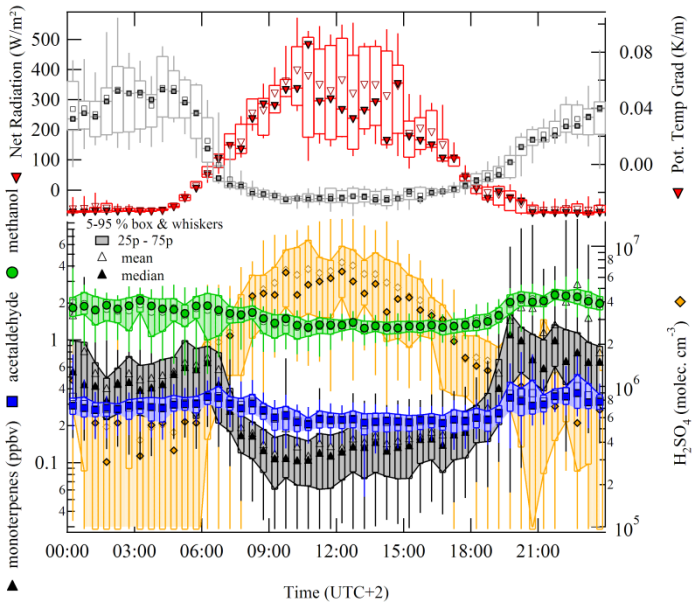

Figure 5-5: Diel profiles of the net radiation, the potential temperature gradient, methanol, acetaldehyde, monoterpenes and sulphuric acid for the period between April 23 and April 30, 2005 presented as 5-95 box & whisker plots.

Methane mixing ratios (not shown) ranged between 1.78 - 1.88 ppmv during the campaign with clear trends in the diel cycle. However, the diel cycle was different from that of any of the aforementioned VOCs and was not correlated with the strength of the nocturnal inversion. Mixing ratios increased at the onset of the NBL until the morning reaching maximum mixing ratios between 06:00 LT and 09:00 LT after which they declined to minimum values between ~15:00 LT and ~18:00 LT. Higher methane mixing ratios were generally observed when the wind blew from northwest to northeast.

5.4.2 Vertical distribution of VOCs

Vertical profiles of the VOCs were obtained by sampling over the 4 sampling levels previously described, from the evening of April 17 and before sunrise on April 23.

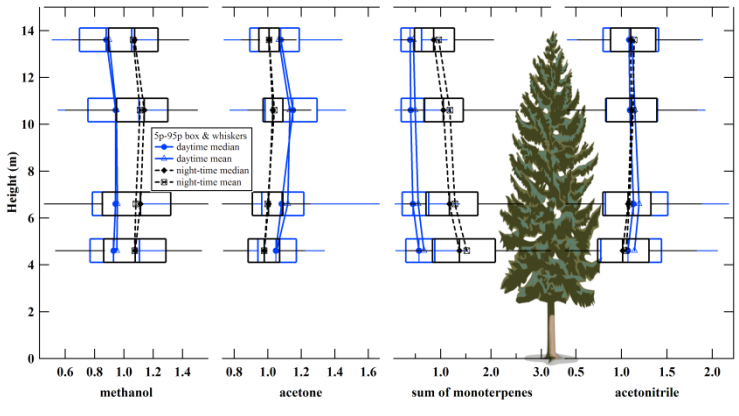

a

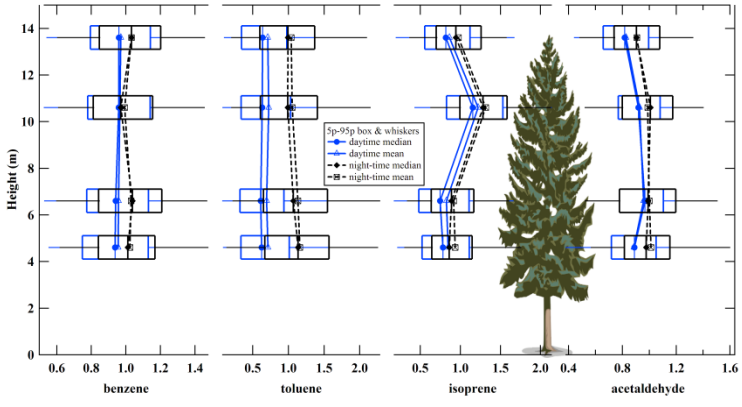

b

Figure 5-6: vertical profiles within the canopy for VOCs normalised to their daily average mixing ratio in 5p-95p box & whiskers for the period April 17-23, 2005.

They are presented in Figure 5-6 as 5p - 95p box and whisker plots a) for methanol, acetone, the sum of monoterpenes and acetonitrile b) benzene, toluene, isoprene and acetaldehyde with separate daytime (solid lines) and night-time (dashed lines) vertical profiles normalised to their daily average mixing ratios. The vertical gradients within the forest were not strong (<15%) and were not really substantially different for day and night time, except for monoterpenes. Interestingly, acetone was the only tracer within this selected group of VOCs with higher mixing ratios on average during the day than during the night for the aforementioned period. VOC mixing ratios have mostly been correlated with a positive temperature gradient and thus controlled by the suppressed mixing during the night. Fallen needles may be the possible source of monoterpenes close to the ground. The concentration differences between below canopy and above is expected to be larger.

5.4.3 VOCs and other trace gases during the particle events

Two distinct particle events were selected for examination in this study: Event 1 (daytime: April 30) was a threefold increase in particles lasting several hours; Event 2 (night-time: April 27-28) was a series of short duration pulses, ~10 fold increases in the monoterpene mixing ratios and ~10 fold increases in the total particle concentration. In this section we examine the relationship between organic and inorganic compounds, and particles during these events.

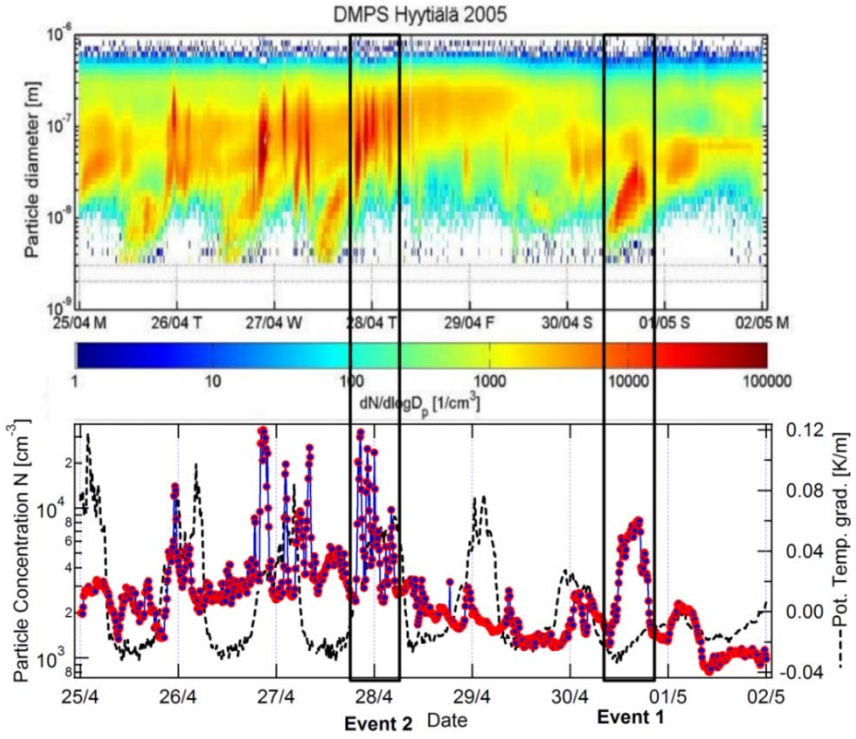

Figure 5-7: Differential mobility size spectra between 3nm and 850nm for one week during which Event 1 & 2 occurred. Event 1 is a broad event on April 30; Event 2 is a series of shorter, more intense particle bursts during the night of 27th to 28th of April. Bottom panel shows the occurrence of the strong short-term increases in the total aerosol particle concentration (right-axis) with the potential temperature inversions.

Prior to the start of the VOC measurements, relatively strong nucleation events were observed almost every day in daylight between March 28 and April 17, clearly discernible in DMPS spectra as the aerosol particle size distribution shifts from small (<3 nm) to larger aerosol particles (usually up to 100 nm). Some of these events have been discussed in detail by Riipinen et al., (2007). Occasionally, a nucleation event extended into the following day. This resulted in a size distribution with two independent size modes. Between April 19 and April 24, there was an absence of nucleation events and considerably fewer particles were counted in the range of 3 nm to 850 nm. Back trajectories for this period indicate relatively steady Arctic winds crossing Finland. Daytime and night time temperatures did not differ much during this period preventing the formation of a strong temperature inversion in the surface layer. The vertical potential temperature gradients (indicated by the black dashed line scaled on the bottom right axis of Figure 5-7) were 0.1 K per meter between the top of the canopy and 50 meter measurement height in the night being strongest during the night of April 25.

In the upper panel of Figure 5-7, the number of particles counted for a certain size interval is quantitatively colour marked for intensities between 1 and 10^5 particles per cm³ for 1 week of measurements in which Event 1 and Event 2 took place. A clear increase in intensity (N >3000 particles/cm³) for particles between 20 nm and 300 nm is visible between April 25 and April 29 noontime. During this period acetonitrile mixing ratios were 60 ± 11 pptv and thereby higher than 35 ± 10 pptv observed between April 17 and April 23, indicating a minor influence of wood combustion. However, these low mixing ratios indicate that the source must have been distant to the site.

5.4.4 **Event 1 (daytime)**

Event 1 (April 30, ~8:20 LT - ~19:00 LT), shows clear particle growth starting above the smallest size classes in contrast to the nucleation events on April 25, 26 and 27, the latter being discussed in Riipinen

et al., (2007). Although these 3 nucleation events have been characterised by growth, from particles <3nm rather than from 4 nm onward like Event 1, their particle number concentrations were less than observed during Event 1.

Nucleation already started approximately 1 hour before the slow increase in the total particle number concentration at 9:35 LT followed by very strong increase to a maximum of about 6000 cm^{-3} at 11:10 LT. Between 12:30 LT and 17:00 LT, the increase in the particle concentration was considerably less. Daytime temperatures were higher at the surface than at the highest measurement level (74m) (Figure 5-8a) from which we may assume well mixed boundary layers.

Figure 5-7 shows that all nucleation events mentioned above have been clearly influenced by boundary layer conditions, as the growth of the aerosol particles and the concentration flagged after the onset of the NBL in the evening. Monoterpene mixing ratios declined during the break-up of the NBL on April 30 to become rather constant around 0.2 ppbv for the rest of the day. Thus they do not show any correlation with particle concentration changes associated with Event 1 (Figure 5-8a).

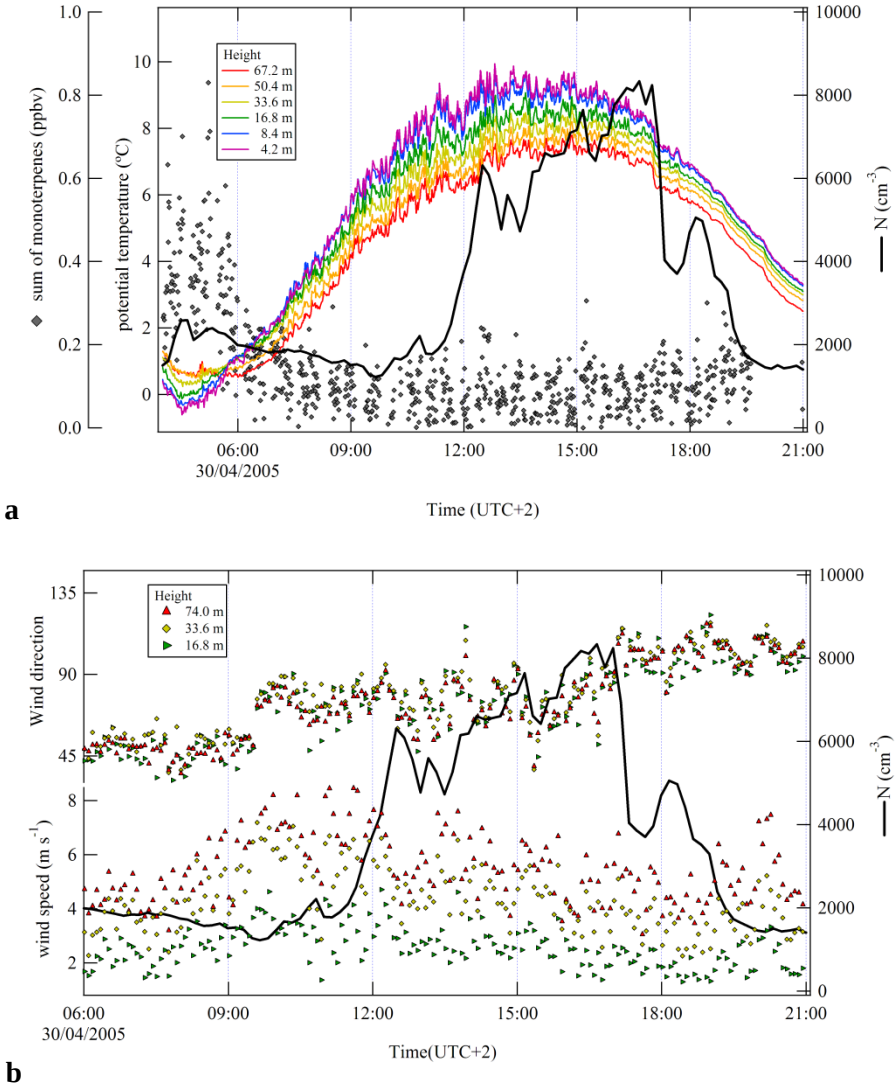

Figure 5-8: Aerosol total concentration (black solid lines) in relation to (a) the monoterpenes mixing ratios measured at 8.2 m and the potential temperature; (b) wind direction and wind speed measured at SMEAR II for Event 1.

Measured signals m/z 169 (pinonaldehyde), which could not be accurately converted into quantitative results due to a lack of a standard of monoterpenes oxidation products, have been shown to be mostly under the detection limit during Event 1. Uncalibrated signals for pinonaldehyde (m/z 169) measured at the time by the PTRMS instrument run by the University of Helsinki are presented in Figures 3 and 4 of Bonn et al., (2008b). Even though these measurements did not cover Event 1 in particular and mixing ratios were declining from elevated levels during the night preceding Event 1, it is probable that these low volatility products ended up in the particle phase.

Mixing ratios of methanol, acetone and acetaldehyde, were observed to increase only slightly (few hundred pptv) until the onset of the NBL. The toluene to benzene ratio (not shown) varied between 0.1 and 0.8 throughout the day except between 12:00 LT and 13:00 LT when it exceeded 1, indicating fresher anthropogenic pollution. Such fossil fuel combustion episodes may have introduced new aerosol particles for those formed by nucleation to collide with.

Methane mixing ratios decreased from 1.83 ppmv to 1.79 ppmv throughout Event 1. Owing to the low chemical reactivity of methane (lifetime ~9 years), it is unlikely to have played a significant role in the nucleation process and this is also the case for the aforementioned VOCs. However, for every peak in the particle concentration during Event 1, there is a peak in the methane mixing ratio as well.

During this campaign, the wind speed was variable by day (enhanced mixing) and more constant by night (suppressed mixing). Nearer the ground the wind speed was lower, consistent with a surface friction resistance and with a much higher wind deflection relative to the pressure gradient wind above. Shown in Figure 5-8b is the wind direction at different levels including a level (at 16.8m) just above the canopy and the highest level (at 67.2m) which is the least affected by wind shear. It should be noted that one hour after the start of nucleation at 8:30 LT, there was very abrupt change in wind direction (by ~25°) from North easterly during which nucleation took place, to North-North easterly on all measurement levels above the canopy. This suggests that SMEAR II had been located at the interface of two air masses and in one of these, new particle formation had occurred while the other air mass favoured particle growth. A slight shift in the air mass boundary relative to the location of SMEAR II could have made the difference between an event day and a non-event day. The particle growth in Event 1 appears to stop abruptly after about 8 hours coincident with the onset of the NBL, shortly before sunset and the wind veered further to become easterly wind.

Figure 5-8b also shows that at 9:35 LT wind speeds on all levels maximised (i.e. ~10 m/s at 67.2m, ~6 m/s at 16.8m) and halved over the course of Event 1 until 19:00 LT (= onset of the NBL). The highest total particle concentrations were observed when the wind direction was approximately 75±17°, and the enhanced particle event terminated when the wind direction shifted slightly to circa 100±17°. 4-day backward trajectories ending at Hyytiälä every three hours on the 30th indicate that the air mass originated from the north, but turned northeasterly so that it crossed central Finland two days before arrival at the site. According to the NOAA Hysplit model, the air mass stayed closer to the surface in the two days before arrival than on the days before. The model did not indicate any significant difference in trajectories arriving before and those arriving after the start of Event 1.

CO_2 is known to be removed from the atmosphere by vegetation during photosynthesis and a minimum in the daytime CO_2 mixing ratios is observed. CO_2 mixing ratios decreased from 404 ppmv at dawn to 394 ppmv at the end of Event 1, but CO_2 was not considered to be related to its occurrence (see Figure 5-9), in contrast to Event 2 discussed below. CO_2 mixing ratios were significantly higher within the canopy. Ozone mixing ratios were similar to those observed on the previous day when no nucleation event occurred. The difference in the ozone concentrations for more polluted to non-polluted airmasses measured during spring 2005 was about 50 ppbv to 25 ppbv, respectively. Carbon monoxide (CO) data did not show signs of diel variation on Friday the 29th and Saturday the 30th of April but varied between 130 and 160 ppbv. CO mixing ratios (not shown) were somewhat lower between 9:00 LT and 15:00 LT. A typical commuter traffic related NO peak (not shown) was observed between 04:30 LT and 7:00 LT

with maximum mixing ratios of 0.15 ppbv around 6:00 LT (corresponding to slightly higher CO mixing ratios) and occurring under a declining total aerosol number concentration. No such clear peak in NO has been observed in the afternoon. Only in the evening, between 19:00 LT and 20:00 LT a similar peak up to 0.15 ppbv NO was observed.

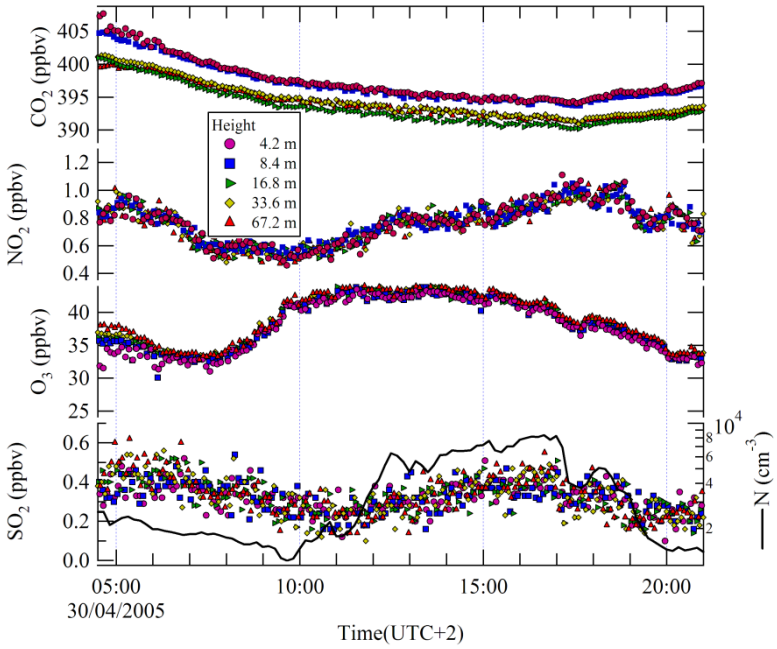

Figure 5-9: CO_2, O_3, NO_2 and SO_2 mixing ratios in relation to the aerosol particle total concentration for Event 1.

Several peaks in NO_2 (up to 1.2 ppbv) have been observed during the night of 29 to 30 of April, each lasting several hours and coinciding with increases in the particle concentration of 1200 cm^{-3}. The daytime NO_2 peak (up to 1 ppbv) was not as narrow as the night time peaks and closely resembled the aerosol particle concentration (see Figure 5-9). New particle formation by nucleation took place under a decline in NO_2 whereas faster increase in the particle concentration took place under constantly increasing NO_2 mixing ratios.

Radiative measurements (see top panel Figure 5-10a) indicated that Event 1 took place under mostly clear sky conditions until 11:10 with a very brief disturbance slightly reducing the direct sunlight around 9:35LT. Thereafter, the sky became overcast affecting both temperature and humidity. The relative humidity just above the canopy generally decreased from 84% at 04:35 LT to 44% at 13:30 LT, after which RH remained rather constant until 15:30 LT. The difference in RH from the lowest to the highest measurement level of SMEARII was about 5% over the entire day. The number concentration of particles between 6 nm and 25 nm increased right after nucleation. For the rest of the day there was little direct sunlight, and predominantly the number concentration of particles larger than 12 nm increased, whereas the number concentration of particles smaller than 12 nm decreased by scavenging.

At 17:00 LT, a sudden increase in RH by 5% and a change in the wind direction to the East occurred together with the large decrease in the number concentration of particles in the range 12-90 nm.

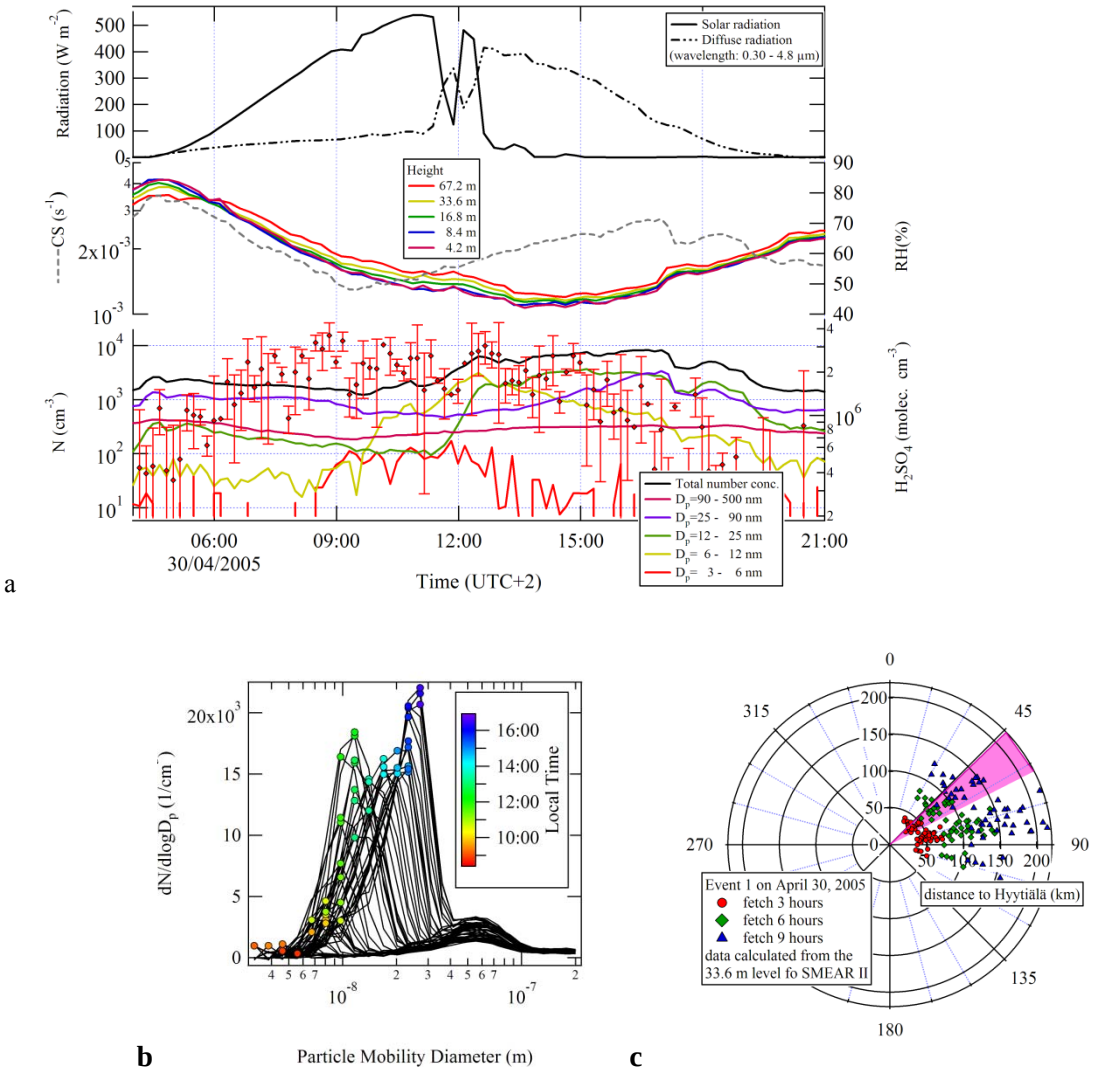

Figure 5-10: RH, CS and monoterpenes mixing ratios (±1σ over the measurement interval of the DMPS) as function of time for (a) Event 2 and (b) the second selected nighttime event. (c) Particle size distribution for the 3 intense peaks of Event 2 in red, blue and green and (d) the corresponding 15, 30 and 60 minutes plain fetch calculated from the 33.6 m SMEAR II wind data in kilometres to the site. Highlighted is the direction in which the Korkeakoski saw mill is located.

The observed concentration of SO_2 (mixing ratios 0.3-0.6 ppbv prior to nucleation shown in the bottom panel in Figure 5-9) were 10000 - 60000 times higher than the concentration of its photo-oxidation product H_2SO_4 during the night, and 1000 - 10000 times higher during daytime of April 30. H_2SO_4 showed maximum concentrations of $3.6x10^6$ molecules H_2SO_4 /cm³ just before 9:00LT, followed by a decline during nucleation to $1.5x10^6$ molecules H_2SO_4 /cm³ until noontime. Ammonia (not shown) was only measured until April 23 as described by Riipinen et al., (2007) and references therein. They found no significant relation between the particle concentrations and ammonia for the nucleation events prior to the VOC measurements at Hyytiälä.

Figure 5-10a also shows a continuous decrease in the condensational sink (CS) prior to Event 1 followed by a continuous increase during and after nucleation with only minor fluctuations under overcast conditions. CS values decline during Event 1 from 3.3×10^{-3} s^{-1} to 1.3×10^{-3} $s^{-1}s^{-1}$ and thus a lifetime of about 400 s which is commonly observed at Hyytiälä (median daytime values for first half of 2005 were $(3.5\pm2.0)\times10^{-3}$ s^{-1}). Even though there is no direct comparison with the growth rate for the

smaller particles, the observed growth rate at size from 5 nm to 10 nm was 8.4 nm/h, which is in agreement with values indicated by Kulmala et al., (2004) and Dal Maso et al., (2005).

The contribution of sulphuric acid on the growth rate can be approximated to be around 5 % using the methods described by Kulmala et al., (2001b). In practise this indicates large organic contribution on the growth. On the other hand it seems to be probable that sulphuric acid will participate in the atmospheric nucleation process, since the concentration of ultrafine particles is closely related to sulphuric acid concentration. Recently the atmospheric nucleation has been shown to occur around the size of 1.5 nm in Millikan diameter (Kulmala et al., 2007).

As a first approximation and in absence of real-time wind fields, plain fetch calculations were done for Event 1 on the assumption that the monitored air mass had been transported towards the site from the measured wind direction and speed. This assumption was supported by the 2-day steady back trajectories consistently following the same path on 3 levels (100m, 250m and 500m) prior to arrival. Figure 5-10c shows that a tracer released three, six and nine hours back in time, could have been influenced by sources between respectively 15 to 30 km, 30 to 90 km, and 60 to 130 km distant to the site. Clean air masses coming from the East-North East will have been impacted by emissions to some extent including organic and inorganic tracers such as SO_2 that converts into H_2SO_4. The organic mixing ratios in these air masses were low. The air mass back-trajectory crosses the city of Jyväskylä and its industrial region at ca. 60°, and its airport at 49° approximately 88 km and 95 km respectively away from Hyytiälä. We assume these to be emission sources of SO_2 in the case of continuous transport of air masses from the NE sector.

In summary we note that Event 1 occurred by day in the absence of a temperature inversion. The event was very sensitive to changes in wind direction and to a lesser extent on wind speed. Event 1 took place under relatively elevated levels of ozone and slightly elevated NO_x, under slightly increased CO, and under naturally declining CO_2. Event 1 is characterised by an anti correlation of the particle number concentration with sulphuric acid, which in turn depends on the solar radiation and SO_2 levels. No correlation with monoterpenes or other VOCs was found.

The production of the small particle (<4 nm) has occurred at some point upwind of the measurement station, but Event 1 still shows the remaining characteristics of a nucleation event.

5.4.5 **Event 2 (night-time)**

Event 2 refers to the series of intense particle bursts which occurred during the night of 27th to 28th of April 2005 under unusual meteorological conditions. Similar bursts to those observed in Event 2 occurred during the nights prior to Event 2 but could not be investigated in detail as the meteorological and trace gas dataset was incomplete.

The remarkably intense bursts were observed only a few hours after the onset of the NBL (~0.2 ppbv). Monoterpene mixing ratios increased to ~7.1 ppbv, ~ 10 ppbv and 15.9 ppbv and the corresponding particle concentrations were 18000, 32000 and 25000 particles/cm³ respectively (Figure 5-11a). The absence of monoterpene mixing ratios during the next peak of 23500 particles/cm³ was due to PTR-MS system calibration. Subsequent peaks were much lower in particle concentration (< 10000 particle /cm³) and in monoterpenes (< 1.5 ppbv) around 1, 3 and 4 o'clock.

The bursts of aerosol particles were strongly correlated with exceptionally high concentrations of monoterpenes as the squared correlation coefficient (R^2) for the first peak was 0.79, and 0.70 for the head of the second peak. An R^2 value of 0.80 has been obtained for the tailing part of the third peak. The head of this peak could not be analysed due to a gap in the monoterpene mixing ratio data. The R^2-value for the peak around 04:00 LT was 0.65. Minor peaks in the monoterpene mixing ratios during the second half of the night were not accompanied by peaks in the total particle number concentration.

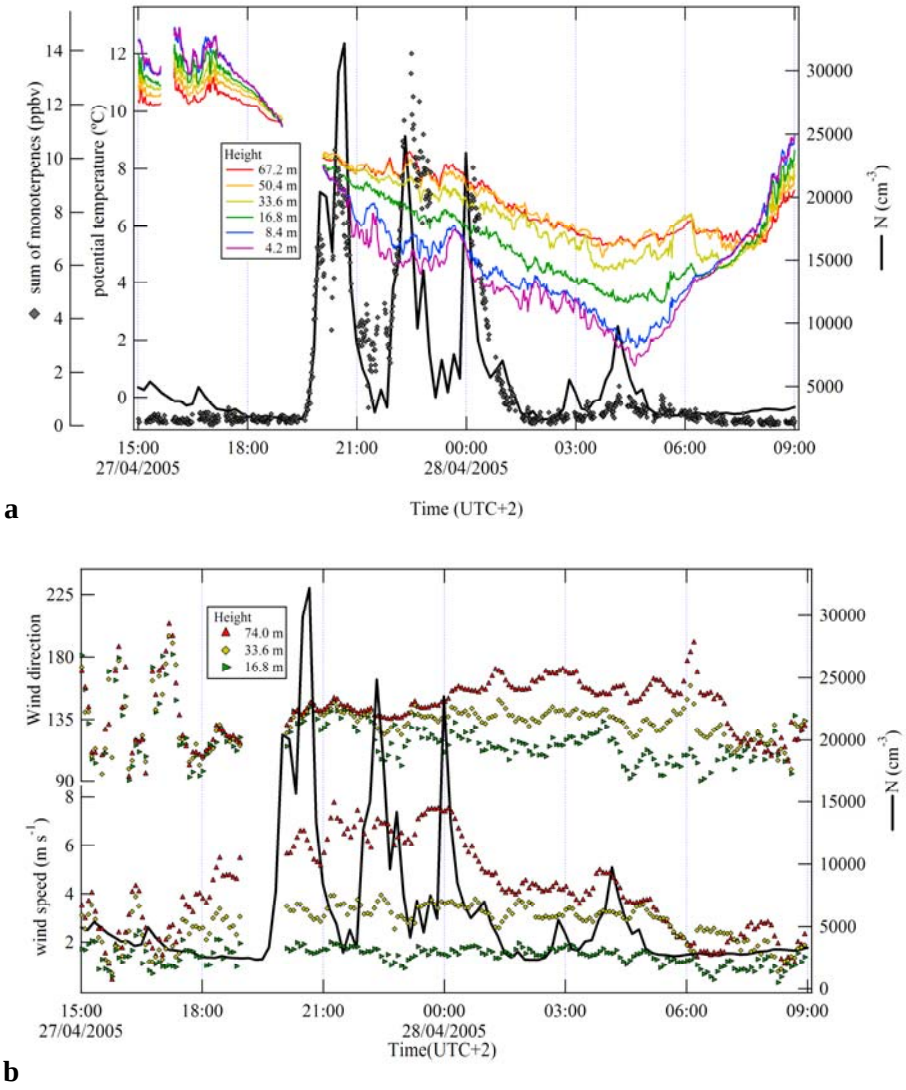

Figure 5-11: Total aerosol number concentration (black solid lines) in relation to the potential temperature and monoterpenes (a) wind direction and wind speed (b), measured at SMEAR II during Event 2.

The stratification of the nocturnal surface layer under investigation was apparent in the ambient temperature, humidity, wind speed and wind direction measured at SMEARII (see Figures 10 a and b). Even though ambient temperatures remained positive, they dropped by 9 °C at 4.2 m and by 5°C at 67.2 m over the course of the night. The first particle burst of Event 2 occurred when the inversion was formed. In between the particle bursts, there were short gusts of somewhat warmer air interspersed with the cooling of the air within the canopy.

The wind blew fairly steadily from the South-East above 16.8 m over the course of Event 2. The angular deviation of the wind above the canopy with height became more apparent after midnight with deviations of 15-30° between the different levels (Figure 5-11b). Wind speeds below 33.6 m have been fairly constant throughout the night and were significantly different in between all levels. Average wind speeds were 0.6, 1.6, and 3.3 m/s at 8.4 m 16.8 m and 33.6 m, respectively.

In contrast to the other VOCs (discussed below) methane mixing ratios clearly increased from 1.78 ppmv to 1.81 ppmv at the onset of the NBL and remained above 1.79 ppmv for the rest of the night, only increasing again in the early morning to 1.81 ppmv (Figure 5-12b).

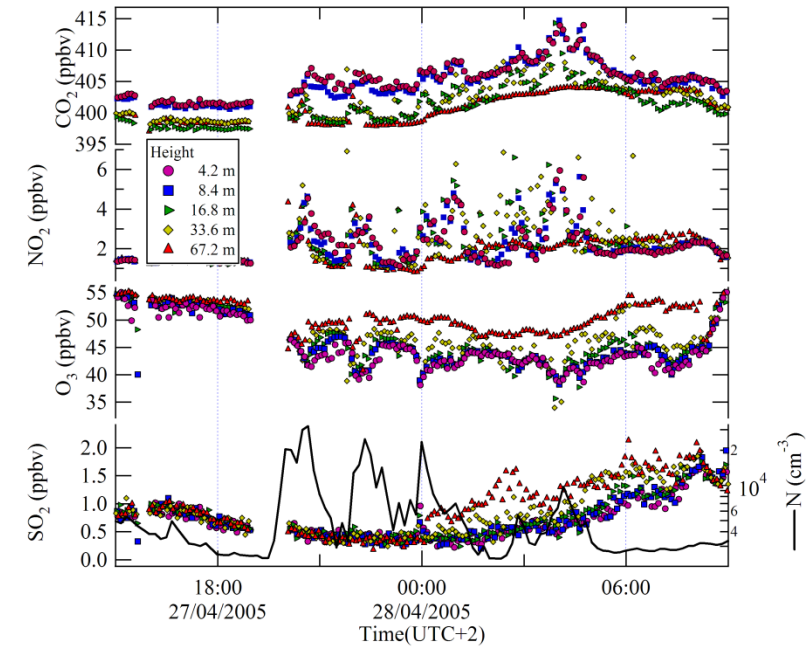

a

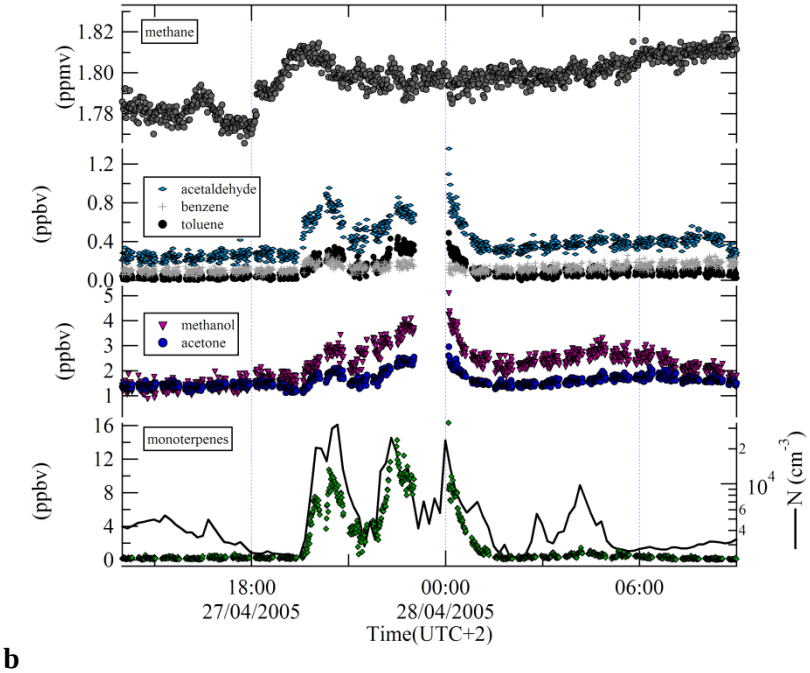

b

Figure 5-12: (a) CO_2, O_3, NO_2, SO_2, and (b) VOC mixing ratios in relation to the aerosol particle total concentration for Event 2.

The prevailing CO mixing ratios were 140-160 ppbv (not shown). Due to a data recording failure, only the end of the peak in CO has been captured showing a drastic change of ~50 ppbv during the first part of the first burst in Event 2. CO mixing ratios gradually increased from 160 to 180 ppbv between 03:00 LT and 09:00 LT.

SO_2 mixing ratios declined during the first 2 bursts of Event 2 strongly suggesting that it has no role in this event (Figure 5-12a). Gradual but substantial increases in SO_2 mixing ratios from ~0.3 ppbv up to 1.8 ppbv at canopy level but most substantially above 30m have been observed on all measurement levels after midnight (around the occurrence of the third peak), maximising at 09:00 LT.

Each particle burst was marked by exceptional increases in CO_2 and NO_x and drops in O_3 on all measurement levels. Peaks in the CO_2 mixing ratios extended well beyond the natural fluctuation. Similar peaks have also been observed on several occasions during this campaign together with peaks in monoterpenes, particles and NO_2 and drops in O_3. Between dusk and dawn, there was a clear vertical gradient in ozone with mixing ratios within the forest consistent with a surface or chemical loss. The gradient in ozone during Event 2 was as strong as 5 - 12 ppbv, much stronger than the gradient of less than 2 ppbv seen on nights without particle concentration increases. The highest peak in NO_2 was observed coincidently with the peak in the particle concentration around 04:00 LT with NO_2 mixing ratios up to 7.5 ppbv within the canopy and occasionally spiking up to 14 ppbv of NO_x at the 33.6 m (off scale in Figure 5-12a).

VOC mixing ratios generally were not well correlated with each other during this campaign with the exception of methanol, acetaldehyde and acetone. Methanol, acetaldehyde and acetone are too volatile to take part in particle formation or growth but may be emitted directly or be formed as oxidation products. Biomass burning can be eliminated as a source as there was no substantial increase in acetonitrile during Event 2.

Strong increases in compounds like benzene, toluene, C_2- and C_3-benzenes during each peak of Event 2 points to fossil fuel combustion processes. The ratio [toluene]/[benzene] went up to 5, and was found to increase from the first to the third peak. The ratio was on average 2 between 19:30 and 1:00 and was calculated to be 0.5 for the rest of the night. Although toluene declined at daybreak, benzene increased until 9:00, similar to CO (discussed below). R^2 for Event 2 data for toluene and acetone was 0.74. Acetone and toluene are known to be often emitted by anthropogenic sources.

Although there has not been additional proof from the TD-GCMS measurements, we strongly believe that the increases in m/z 69 and m71 during Event 2 were very unlikely related to natural emission of isoprene and its oxidation products given the time of the emissions and squared correlation coefficients for m/z 71 and m/z 69 with toluene (m/z 93) were 0.61 and 0.59, respectively. Therefore it seems more likely that isobaric compounds or fragments of compounds at m/z 87 have caused the increase in the signal at m/z 69. Our measurements indicate that there has been a stronger contribution the second and third peak of Event 2 onto m/z 69 than to m/z 87 compared to the first peak in the series.

Without further identification we note that there have been synchronous increases in the signals at m/z 73, 75, 83, 95, 117, 141 but not at m/z 77, 85, 105. Figures 3 and 4 in Bonn et al., 2008b show elevated pinonaldehyde mixing ratios between April 25 and April 29 matching the elevated monoterpene mixing ratios presented here.

The overall contribution of carbonaceous compounds to the ambient air was about 100 ppbC as measured by the total hydrocarbon analyser.

The RH of the air closer to the forest floor was higher than above and generally increased from dusk (18:00) to dawn (04:30) on all levels with a stronger rate of increase after midnight (Figure 5-13a). The RH increased from 44 to 53 % before midnight and increased further to 68 % at 4:30 at 4.2 m above the forest floor, whereas at 67.2 m RH was around 39% before midnight and increased only to 50 % just before sunrise.

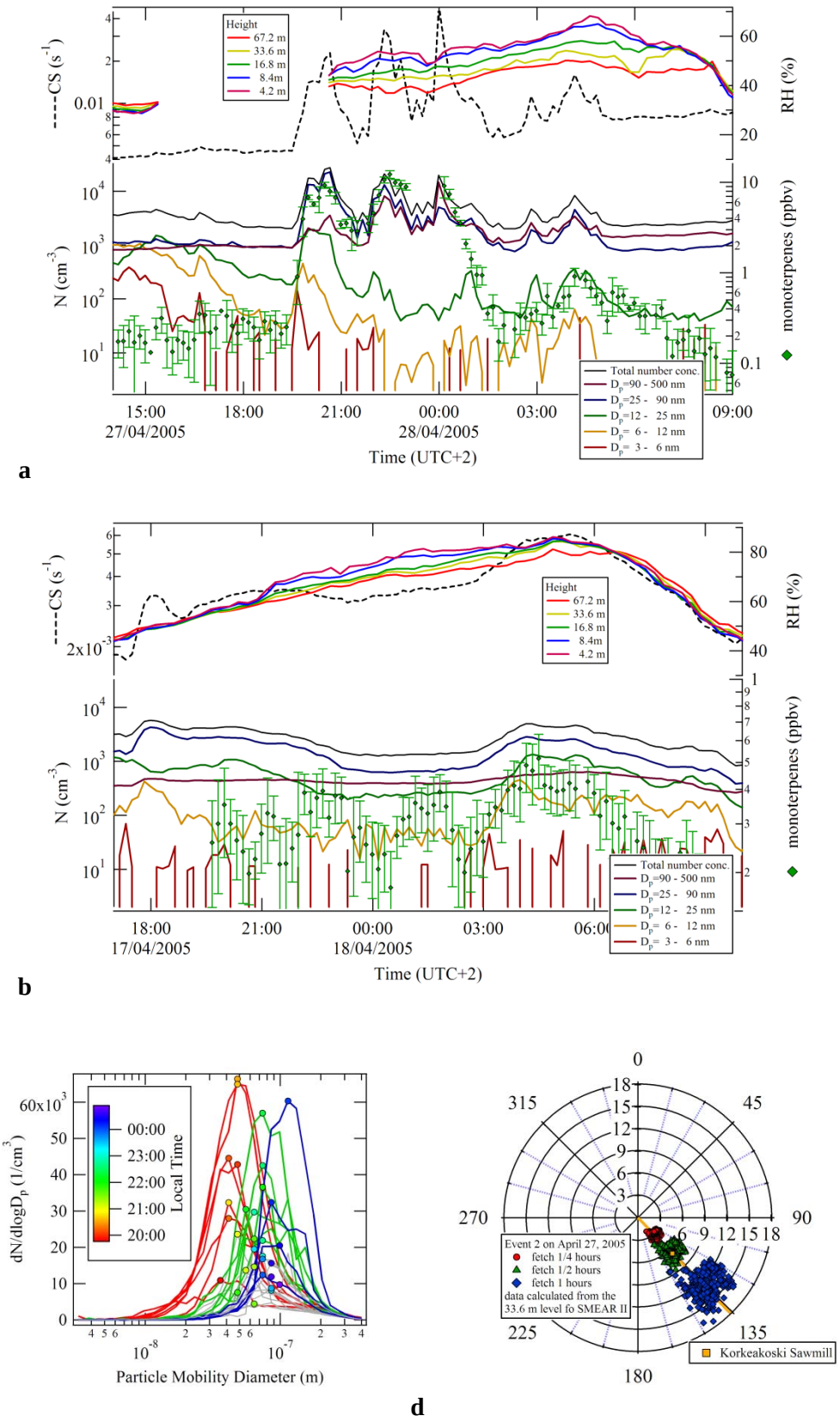

Figure 5-13: (a) RH, CS and monoterpenes mixing ratios (±1σ over the measurement interval of the DMPS) as function of time for Event 2 and the second selected night time event. (b) shift in the particle size distribution for the different peaks (c) wind direction dependence of monoterpenes for the period April 17 to May 1 at the SMEAR II at different heights.

In contrast to Event 1, small and large particles were present right from the beginning of the first burst of Event 2 suggesting that this was not a nucleation event. The condensational sink (typically examined for sulphuric acid, may serve as well for other molecules in a similar size range) for Event 2. It is shown in Figure 5-13a and indicates very short lifetimes of molecules which have an affinity with particle surfaces. Peak values of CS were 0.023, 0.034 and 0.051 s^-1 (corresponding to lifetimes of 43, 29 and barely 20 s). Even for the fourth burst the lifetime was only 62 seconds. Most vapours with low vapour pressure will probably end up on pre-existing aerosol particles.

4-day backward trajectories indicated that for Event 2, the air came from Central and Southern Finland between April 26 and 28 and show that the air mass has remained close to the surface (> 500m) for several days. The lifetime of e.g. α-pinene with respect to ozone under the conditions of Event 2 was 16 to 22 minutes. Empirical calculations, purely based on the measured wind speed and direction as measured at 16.8m, suggest that air parcels released 15, 30 and 60 minutes back in time would have covered a distance of approximately ~2 to ~4 km, ~4 to ~6 km, and ~6 to ~14 km (see Figure 5-13b).

At slightly more than 6 km distance and 136 degrees South-East of the SMEAR II station, the Korkeakoski sawmill is located in the town Juupajoki (the yellow square in Figure 5-13d represents the location of the Korkeakoski sawmill relative to the SMEAR II observatory at the origin). This sawmill has an annual production capacity of 330,000 cubic metres of softwood products, notably for the joinery industry and in this respect a very plausible source of the massive monoterpene emissions and other associated pollutants. However, intensive forest management activities carried out in the same section upwind of SMEAR II may also qualify.

Additional support for this source identification was obtained from the detailed analyses of the monoterpenes by TD-GC-MS which includes an enantiomeric separation. It has been shown previously that (+)-α-pinene, (+)-δ-3-carene, (-)-α-pinene and (-)-ß-pinene were the most abundant monoterpenes above the boreal forest. This monoterpene composition resembles that found in the emission of *P. sylvestris* with low (+)-δ-3-carene chemotype in the branch enclosure cuvette study (Yassaa and Williams, 2007).

Figure 5-14 shows that daytime enantiomeric ratios of [(+)-α-pinene]/[(-)-α-pinene] varied between 1.6 and 2 and that the night time ratio was usually higher (~2.5).

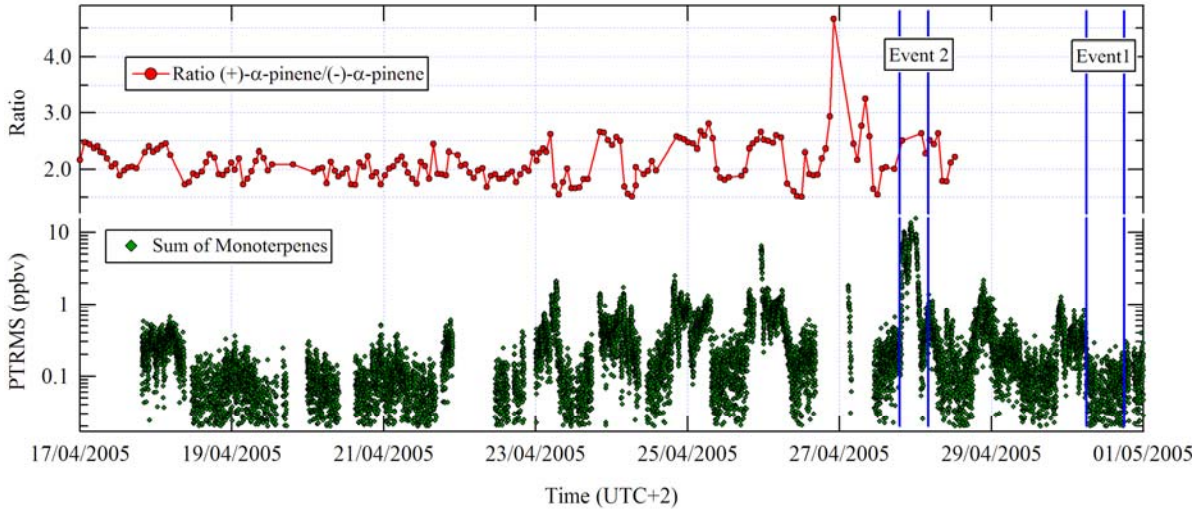

Figure 5-14: The enantiomeric ratio of (+)-α-pinene to (-)-α-pinene as function of time in connection to the sum of all monoterpenes for the entire period of investigation.

There have been several occasions during this campaign for which the enantiomeric ratio was significantly higher (3-5). Such significantly higher peaks on April 26 and 27 were believed to be of a similar kind as monitored by the PTR-MS during Event 2, during which the GCMS was being calibrated.

Subsequent study of the enantiomeric composition of monoterpenes from intact and damaged or wounded Scots pine has been conducted with solid-phase microextraction (SPME) combined with dynamic branch enclosure cuvettes and enantioselective GC-MS. The detached needles from *P. sylvetsris*, the dominant forest species, exhibited different enantiomeric emission patterns for the most abundant chiral monoterpene α-pinene. Damaging the plants seems to induce modifications not only to the emission rate of monoterpenes but also on their enantiomeric compositions. In the wounded plant materials, while the emission rates of monoterpenes increase by several orders of magnitude, the [(+)-α-pinene/(-)-α-pinene] enantiomeric ratios pass from ~2 for intact plants to ~6 for damaged trees, similar to what was observed in the Event 2. Therefore, the substantial increase in the mixing ratios of monoterpenes together with the [(+)-α-pinene/(-)-α-pinene] enantiomeric ratios observed during the Event 2 strongly supports the hypothesis that the wood industry is the very likely source of monoterpenes during the Event 2 and according to this line of reasoning also be responsible for all increased levels of monoterpenes.

To support our analysis and to summarise the conditions typical for these night time events, a second, less intense night time event has been selected. Nine days prior to Event 2 (on April 18, about 03:00 LT) generally showing the main characteristics of Event 2. The nocturnal surface layer had been stratified expressed by a potential gradient reaching 0.05K/m as well as a strong gradient in the relative humidity (here up to 8%) with the air near the forest floor being more moist. Ambient air temperatures on all measurement levels declined to -2 °C around 06:00LT and were about 0°C at the start of the event. The wind speeds were very constant and distinct at the different levels (2.0 ± 0.4 m/s, 3.6 ± 0.4 m/s and 6.6 ± 0.4 m/s at 16.8 m, 33.6 m and 74.0 m respectively). Only this time, the wind blew northeast at 74 m just after the onset of the NBL and veered to north northeast over the course of the night. Wind directions measured below deviated again by 10°-15° and indicate the stratification. Figure 5-13b shows the positive correlation between the monoterpenes mixing ratio (maximising around 0.6 ppbv at 04:15 LT) and the particle number concentrations (total ~4900 cm^{-3}). Important to note is that this event involves particle formation characterised by a shift in particle size and an increase in number concentration over the course of time.

This night time event is characterised by similar changes in monoterpenes and other trace gases as discussed previously. Peaks in the monoterpene mixing ratios match peaks in the CO_2 (ΔCO_2: 2-4 ppmv) on top of the natural respiration profile (increase 395 - 405 ppmv at 8.4 m over the course of the night). They correspond to simultaneous drops in ozone (ΔO_3: 2-7 ppbv) on top of the nocturnal decline in ozone from 40 to 30 ppbv. NO mixing ratios were low (<0.1 ppbv) but NO_2 mixing ratios increased 3 hours prior to the night time event up to 1.2 ppbv at 4.2m and 2.5 ppbv at 74 m at 09:00 LT. A similar change over the course of time has been found for SO_2. Mixing ratios increased from 0.5 to 1.8 ppbv at 4.2 m and even stronger increases at the top level 0.7 ppbv - 2.5 ppbv, maximising at 09:00 LT. Elevated levels of SO_2 were only observed during the second part of the night of April 28, not during the most intense bursts in particles and in monoterpenes. The ratio of [(+)-α-pinene]/[(-)-α-pinene] was 2.3-2.5 during the night of April 18 corresponding to damaged needles as observed during Event 2.

5.5 Discussion and conclusions

Rural background mixing ratios for the boreal forest have been determined for several VOCs during the transitional period between winter and spring when air masses come from the North crossing Finland. Most of the analysed non methane hydrocarbons in this generally clean air did not show distinct diel profiles. Of the VOCs measured, methanol, acetone and acetaldehyde were the most abundant daytime organic species present. The biogenic VOCs observed during this study predominantly result from coniferous trees as the deciduous trees were still leafless at this time of the year.

Elevated levels of anthropogenic pollutants were observed typically in the morning and the evening, presumably by commuter traffic or on occasions when air masses had passed over urbanized areas, marked by e.g. peaks in NO_2 and SO_2.

Elevated levels of monoterpenes were observed during night time presumably through the formation of a shallow nocturnal inversion layer at night over the continuously emitting vegetation. However, the levels were sometimes too high to be explained by this effect alone and are possibly supplemented by emissions into the NBL by forest management activities.

In this study, a daytime and a night-time aerosol event exhibiting high particle concentrations, were analysed using the available meteorological, organic and inorganic trace gases measurements. Figure 5-7 shows that Event 1 (daytime; April, 30) was characterised by a fivefold increase in the total aerosol concentration (N) lasting several hours and Event 2 (night-time, April, 27-28) was of short duration with 11 fold increase in N.

Event 1 is characterised by an abrupt start with clear particle growth starting above the smallest size classes. We have shown that the occurrence of the event was very sensitive to the wind direction. We believe that the location of the edges of air masses qualify whether a particular day at SMEAR II can be archived as event day or non-event day.

Event 1 is characterised by an anti correlation of particle growth with sulphuric acid during nucleation. H_2SO_4 is known as the most important key player atmospheric new particle formation which is generally thought to occur due to homogeneous or ion-induced nucleation of sulphuric acid (Kulmala, 2003; Lovejoy et al., 2004). Recently, Laaksonen et al., (2008) and Berndt et al., (2008) suggested a new particle formation mechanism in which the free HSO_5 radicals are formed prior to the H_2SO_4 formation. They suggest that at temperatures above 250 K these radicals produce nuclei of new aerosols much more efficiently than H_2SO_4 as well as that the HSO_5 radicals will react with other trace species, and that the resulting molecules act as nuclei for heterogeneous nucleation of H_2SO_4 vapour which will initiate the growth of the new particles. Recently Kulmala et al., (2006) suggested that activation of existing clusters might be the actual atmospheric nucleation mechanism. The existence of those clusters has later been shown (Kulmala et al. 2007). On the other hand, a study by Väkeva et al., (2000) indicated that somewhat larger deviations in the wind direction may interrupt the conditions favourable for the growth of particles which might have been also the case for Event 1. However, the growth of the particles by this mechanism may have been interrupted, by a reduced number of HSO_5 radicals formed after the sudden overcast, with a clear relapse in the concentration of H_2SO_4.

The event was found to be sensitive to changes humidity for instance due to the appearance of clouds. The latter reduces the instantaneous production of H_2SO_4 via OH (reduced gas-phase oxidation chemistry) but also enhances the water content in the air (increase of the condensation sink of condensable gases due to hygroscopic growth of pre-existing particles). It has been observed in different continental locations that nucleation events take preferentially place at low relative humidity (e.g. Hyvönen et al., 2005; Hamed et al., 2007; Laaksonen et al., 2008b) as a higher humidity implements a larger possibility of enhanced coagulation of sub 3nm clusters.

From all nucleation events arising during this campaign, we conclude that there is a certain condition upon which nucleation occurs and the strength of a nucleation event is not equivalent to the locally measured mixing ratio of H_2SO_4. This could possibly be explained by the competition between the growth of freshly formed particles and their loss by scavenging, rather than a limit in the initial particle production by nucleation of sulphuric acid (Riipinen et al., 2007).

No evidence was found that monoterpenes or other volatile organic compounds measured during this campaign were involved in the growth of particles during nucleation Event 1. Future work should include measuring condensable organics e.g. oxidation products of all terpenes.

In contrast, particle Event 2 is characterised by a very clear correlation with monoterpenes and no correlation with sulphuric acid. During Event 2, sulphuric acid concentrations were found to be relatively low and SO_2 mixing ratios declined during the intensive night-time bursts in aerosol particles before midnight. The source was characterised as releasing more toluene relative to benzene; more methanol relative to acetone; and above all, releasing massive amounts of aerosol particles, CO_2 , monoterpenes and NO_2. The latter two are known to be very reactive towards ozone explaining the drops in the ozone mixing ratios.

For event 2 the wood industry is suggested as the likely source. Monoterpenes and many other VOCs may have come directly from the cut wood whereas the NO_x and BTEX compounds come from the generators/cutting tools used. Recently Junninen et al., (2008) investigated night-time particle production events. Typically strong night particle production in Aitken and accumulation modes was connected to local pollution.

A study by Schade and Goldstein, (2003) also reported 10-fold increases of monoterpene emissions from a pine plantation as a result of mechanical disturbances. During the period of measurements we noted some deforestation activities nearby, to the south west of the measurement location and although we did not notice any burning during the campaign. Thinning is a routine forest management operation that changes tree spacing, number, and size distribution which can affect the emission of VOCs from vegetation to the atmosphere. A study by Vesala et al., (2005) has shown some effects of thinning on physical processes like wind speed normalized by the friction velocity, light penetration, and particle deposition. Some of these forest management activities undoubtedly can have implications for regional air quality management, likely both in terms of ozone chemistry and secondary aerosol formation (Goldstein et al., 2004). However, in this case the strong dependence on the wind direction strongly suggests that the sawmill was the source of these bursts.

It is well established that secondary aerosol particles can be formed during monoterpene oxidation, but is this process sufficient enough to deliver more than 20000 particles/cm³ in half an hour under atmospheric conditions? The second night time event addressed did not involve such enormous particle concentrations but it has been characterised by nucleation.

To begin with, nucleation in the monoterpene/ozone system could not be explained by classical nucleation theory involving sulphuric acid. According to Bonn et al., (2007) it involves 1) the formation of nucleation inducing molecules; 2) the activation and initial growth by reactive trace gases such as RO_2; 3) above about 3 nm in diameter condensation of oxidised compounds such as acids, nitrates, hydroperoxides etc provide for further growth.

Primary ozonides of monoterpenes are formed first, and these then decompose into Criegee biradical and carbonyl compounds as discussed in e.g. Koch et al., (2000). The carboxylic acids which can be formed from the Criegee biradical will have a lower yield over the carbonyl compounds (Calogirou et al., 1999). Bonn and Moortgat, (2002) following the reaction of α- and ß-pinene with ozone (each 500 ppbv) observed various products of different volatility non-, semi- and volatiles. The non-volatile products reached their saturation vapour pressure and started to nucleate homogeneously. This was observed during the ozonolysis reaction in an intense nucleation during the first four minutes of the experiment. At this stage of the reaction, the more volatile products (semi-volatile) were able to condense on the surface of the pre-formed particles and cause an increase in particle size and aerosol volume. This behaviour was observed in a broadening, and a shift of the particle size distribution to larger diameters (centred around 60nm in diameter at 50 min reaction time) due to both the coagulation as well as the condensation. The authors measured a N of 10^6 particles/cm^3 distributed around 20 nm after 4 minutes, and 7.10^5 particles/cm^3 distributed around 60 nm after 12 minutes. However, under ambient conditions as in Koch et al., (2000) and Bonn and Moortgat, (2003), the nucleation threshold was found to be ~2 ppbv of monoterpenes but the calculated atmospheric nucleation time eliminates the possibility of nucleation by reaction of monoterpenes with ozone. This, however, becomes possible if sesquiterpenes were to be

involved which is very well possible but cannot be proven here by measurements. Sesquiterpenes are much more reactive than monoterpenes and the nucleation threshold and the atmospheric nucleation time is much lower. 2.5 pptv of sesquiterpenes could be exceeded in Hyytiälä in less than 3 minutes (Hakola et al., 2000).

Signatures of the sawmill have not always been as intense as during the nights of April 25 - April 29. Accepting a threshold of 2.4 (1σ) for the ratio of [(+)-α-pinene]/[(-)-α-pinene] results in 8 out of 14 days of measurements for which the ratio has been above 2.4. It is very well possible that even more sesquiterpenes are emitted during forestry activities than under natural conditions leading to atmospheric biogenic SOA which in a later stage (for example during transport to the site) can grow by compounds arising from monoterpenes ozonolysis. This could possibly explain the similarity in the observed size distribution from Event 2 with those from the laboratory experiment of Bonn and Moortgat, (2002).

We may conclude from this study that Event 1 (April 30) is typical nucleation event and Event 2 (April 27) is a pollution episode. However, we have shown that new particle formation can occur at night under similar conditions as Event 2 (e.g. April 18). Forestry activities and the sawmill industry can under certain meteorological circumstances substantially influence air chemistry and the aerosol burden over Hyytiälä, especially under stable meteorological conditions.

For future studies, it would be advisable to perform high resolution observations of mono- and sesquiterpenes and their oxidation products in combination with measurement on the physico-chemical characteristics of aerosol particles and boundary layer meteorological measurements over boreal forests to better constrain the role of organics in daytime and night time new particle formation.

6 Inter-campaign comparison

In this final summary chapter a comparison is made of the boundary layer measurements of the oxygenated VOCs methanol, and acetone from the 3 campaigns namely: HOHPEX04 (Southern Germany, temperate latitude, 2 weeks continuous summertime measurements), BACCI-QUEST IV (Southern-Finland, high latitude, 3 weeks continuous springtime measurements) and GABRIEL (Northern South-America, low latitude, 8 days discontinuous and 6 days continuous dry season measurements).

Ratios of oVOCs against CO and other anthropogenic tracers have been used previously either for source allocations (de Gouw et al., 2005) or for classification of air masses (de Reus et al., 2003). CO is a well known tracer for anthropogenic pollution and biomass burning, since it is produced by incomplete combustion processes.

The slope and intercept in the correlation of acetone against CO (pptv/ppbv) has been a useful tool for data screening for distinct regimes as exemplified in Figure 4-4 and Figure 5-4 in which higher than average ratios point at pollution events. These data have not been considered when summarising in Table 6-1 the correlations between acetone and methanol for the three ecosystems at the end of this chapter.

The correlation of acetone vs. methanol from the three campaigns covering the Topics to the Arctic circle is shown in Figure 6-1a. Guidelines in different proportions are shown as dashed lines.

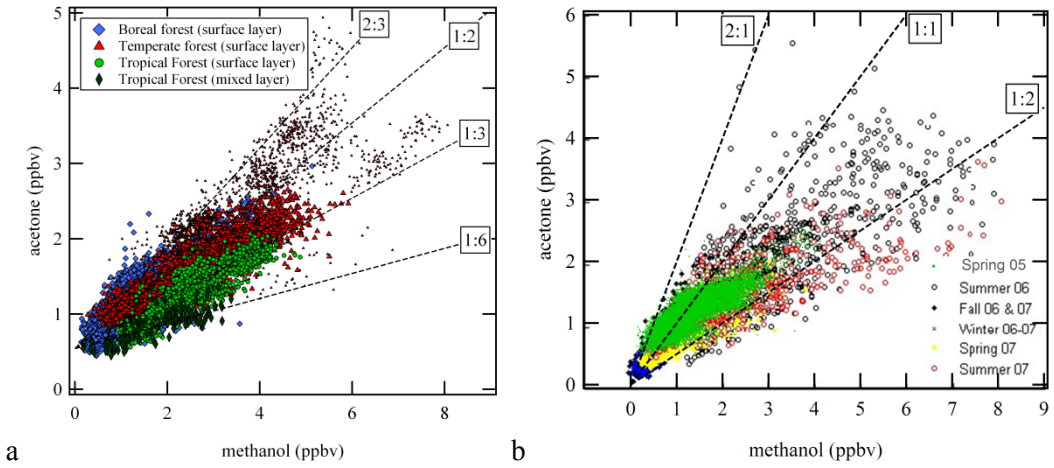

Figure 6-1: (a) Correlation between acetone and methanol for tropical, temperate and boreal forest. (b) Comparison of acetone and methanol measured over several years at SMEAR II Hyytiälä (Ruuskanen et al., 2009) including BACCI-QUEST IV of spring 2005.

On first inspection it is clear that the acetone/methanol ratio is remarkably similar between the three campaigns with the exception of one small group of points from the HOHPEX04 dataset between 4 and 6 ppbv methanol located above the 1:2 line. As discussed in section 4.4.6, these data points reflect the characteristics of air masses that have been enriched in acetone by anthropogenic emissions from Munich in Germany or the Po-valley in Northern Italy. As discussed previously, this period of distinct correlation has also been characterised by higher temperature, has also been found to be enriched in CO and corresponds to a period (7 June, 15:00LT - 8 June, 18:00LT) in which the Hohenpeißenberg region is located in the warm sector of the low pressure system.

The upper half of Figure 6-2 shows, the ratio of the mixing ratios of acetone and methanol for 2 hourly intervals for the temperate latitude and the bottom half shows the corresponding slope and the intercept for each interval. There have been many intervals with and without linear correlation between acetone and methanol. The pattern in the intercepts (offset on the y-axis) clearly shows exceptionally high intercept values attributed to the warm sector (marked on 7 and 8 July) connected to a low pressure system and no clear correlation has been found for equally high mixing ratios of acetone and methanol for periods for which the wind blew from the metropolitan area of Munich and Augsburg or from the south east towards Hohenpeißenberg. Rainfall and associated washout, affects methanol mixing ratios more than those of acetone mostly resulting in much weaker correlation but can be easily noticed by increases in the concentration ratio in Figure 6-2.

Excluding this data and focussing on well mixed conditions as assumed during daytime, we obtain a slope for acetone vs. methanol of 0.35 and an intercept of 0.64 with an R^2 of 0.84. However, instant ratios of [acetone]/[methanol] varied between 0.55 (25p) and 0.76 (75p) with a median of 0.66. The proportionality is comparable to that observed for the tropical rainforest.

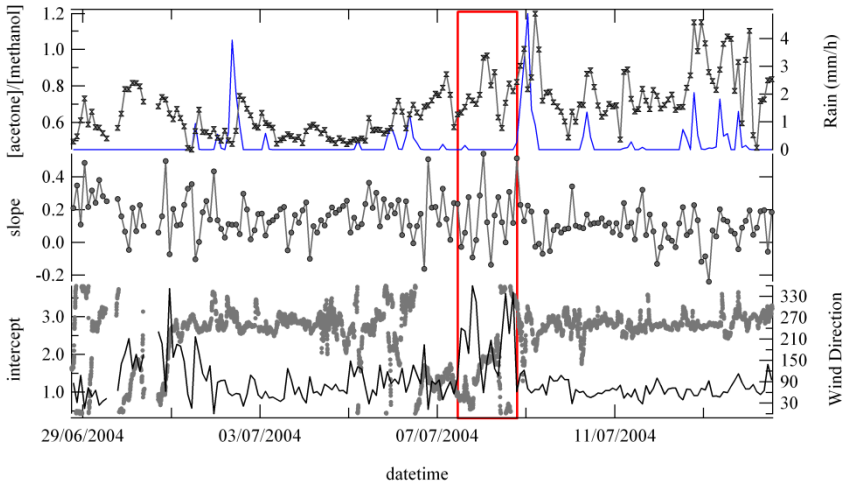

Figure 6-2: A comparison of the instantaneous ratio of acetone over methanol with linear correlation coefficients, slope and intercept (2 hourly intervals). Indicated on the right axis are the rain intensity and the wind direction for the HOHPEX04-campaign. Marked in red the period during which Hohenpeißenberg was situated in the warm sector of a low pressure system.

A good linear correlation (R^2=0.86) has been found for surface layer data at canopy level of the tropical rain forest with a slope of 0.32 and an offset of 0.36. Mixed layer data above the rainforest, taken by plane, exhibit a slightly smaller slope of 0.29 and an offset of 0.43 (R^2=0.60). Data above the mixed layer but below the free troposphere exhibit a very similar slope 0.21 of and an offset of 0.29 (R^2= 0.53). Methanol was in all cases measured at higher mixing ratios to that of acetone.

One explanation for the differences in the relationship between these tropical surface and aircraft data would be the production of acetone from the oxidation of monoterpenes close to the canopy.

Another explanation would be that a fraction of the signal measured within the boundary layer at mass 59, assumed to be acetone, is in fact the more reactive isobaric compound propanal. These tropical correlations are assumed to be representative of pristine biogenic emissions with minimal anthropogenic influence. This assumption is based on the back trajectories that indicate that the airmasses sampled had been advected over the Atlantic Ocean and had not crossed other pollution sources over the previous 5 days. Acetonitrile mixing ratios, which indicate an influence of biomass burning, were low within the boundary layer (0.18-0.20 ppbv) consistent with a negligible influence from the biomass burning source. Biomass burning emissions have been shown previously to be relatively rich in methanol compared to acetone (Andreae and Merlet, 2001). Thus a small influence from a distant biomass burning event

present in the mixed layer (i.e. above the mixed layer) is a second possible explanation for the small ratio difference between the mixed and boundary layer measurements. Direct emissions from vegetation and a more minor input from plant decay are considered to be the main sources here.

The level of acetonitrile over the tropical forest is much more significant than observed over the boreal forest, although in the tropical case this is likely due to the largescale hemisphere wide burning rather than local events. Both regions are known for biomass burning albeit for different purposes. Biomass is burnt in the Tropics mainly for cooking and land reclamation, whereas in the boreal zone the annual heating demand is high. In Finland, energy-intensive industries play an important role in the economy and have spurred the development of efficient energy systems in contrast to the less efficient energy consumption by for example intensive ore-mining industries scattered in the Tropics. Finland produces about 26% of total primary energy from biomass fuels and peat of which 50 % is used for primary or secondary heating systems (statistics Finland 2008). The extent and efficiency of the burning process has an effect on the release of oxygenated compounds.

During the BACCI QUEST IV campaign, the observed mixing ratios of acetonitrile were on average 50 pptv and below 110 pptv. Nonetheless, mixing ratios during the warmer period stood out by a factor 1.5 - 2.5 over the cold period, thus opposite to the domestic heating demands.

Data from the boreal site shows a higher slope between acetone and methanol than observed over the Tropics even though the range of values measured for acetone and methanol were similar for both sites. Daytime data were correlated by a slope of 0.32, an offset of 0.67 and an R^2 of 0.51 and night time data were by a slope of 0.35 and an offset of 0.53 but with a much higher degree of linear correlation, namely an R^2= 0.83 and most likely due to the suppressed mixing. This lower slope is most likely due to biomass burning emissions with the larger relative contribution of methanol.

A comparison of acetone and methanol mixing ratios measured at Hyytiälä over the past years is shown in Figure 6-1b in which the BACCI-QUEST IV data (green dots) have been superimposed onto data obtained by Ruuskanen et al., (2009). Important remains a thorough examination of the prevailing conditions upon sampling including the origin of the airmasses and meteorology. Ruuskanen et al., (2009) have concluded from this graph that acetone and methanol have been controlled by similar source and sink processes. The similarity of the correlations reported here, Figure 6-1 supports this view.

The agreement with springtime 2007 data is reasonably good. However, we note the somewhat higher offset for the BACCI-QUEST IV campaign. Summertime biogenic emissions have been observed to be much higher and more variable compared to the emissions during the rest of the year (Ruuskanen et al., 2009). Coniferous and deciduous leaves both emit these compounds in different proportions. Their leaves and thus their emissions go through a number of stages as there are sprouting, growth, senescence and decay following a different biorhythm causing a natural variability in the mixing ratios and in the proportionality of acetone and methanol. Higher mixing ratios during summer are most likely due to more intense leaf formation from deciduous trees which sprout later in the season than conifer trees. On top of that are the processes producing these compounds by oxidation or by direct emission.

Figure 6-3 shows that the ratio variations in the boreal latitude dataset for 2 hourly intervals varied between 0.5 and 1.3. Acetone was well correlated with methanol during daytime for all wind directions ([acetone]/[methanol] 25p/median/75p: 0.753, 0.864, 0.990). During the night, substantially lower ratios of [acetone]/[methanol] have been observed for the southern sector (25p/median/75p: 0.532, 0.595, 0.627). Figure 6-3 shows much higher intercepts for the warm period (23 - 29 April, as discussed in Chapter 5) than during the cold period when airmasses have been aged as well as loaded acetone from monoterpenes oxidation during transport from the very North to Hyytiälä in southern Finland with one exception of Event 2 (noted in Chapter 5).

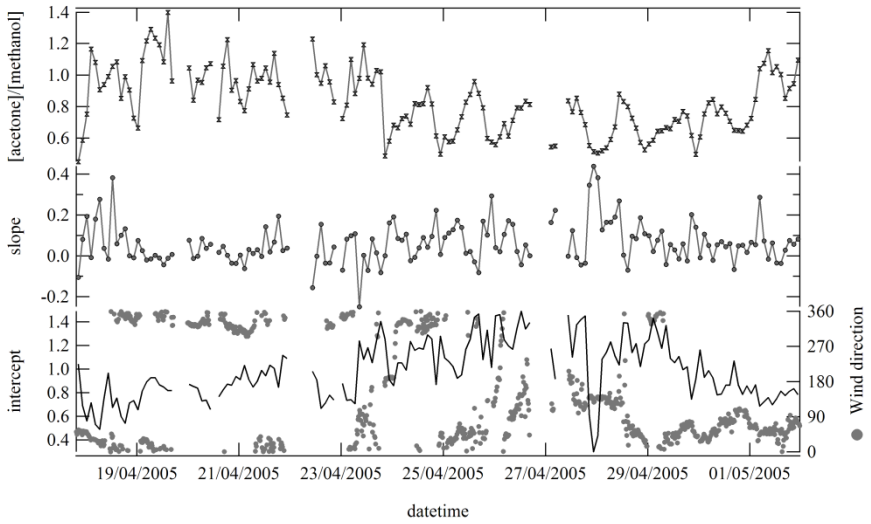

Figure 6-3: Comparison of the instant ratio of acetone over methanol with linier correlation coefficients, slope and intercept (2 hourly intervals). Indicated on the right axis is the wind direction for the BACCI-QUEST IV-campaign.

It is concluded that the proportionality of acetone over methanol does include information about the biogenic and anthropogenic content of an airmass. In order to understand their relationship, temporal variations have to be examined along with basic meteorological and trace gas related parameters. Typically for biogenically influenced air masses, one may expect a ratio of acetone over methanol of 1:3. Biomass burning releases more methanol than acetone resulting in a smaller slope. Additional compounds adding to the signal of m/z 59 or anthropogenic processes that emit much more acetone directly but little methanol may have been responsible for the extraordinarily higher slopes.

Table 6-1: Overview of the linear correlation between acetone and methanol and the ratio of acetone and CO for the 3 latitudes tropical, temperate and boreal after taking out pollution events.

	acetone vs methanol			**Acetone / CO (pptv/ppbv)**
	slope	intercept	R^2	25p - median - 75p
Tropical rainforest Mixed layer Brownsberg	 0.288 0.322	 0.431 0.359	 0.863 0.861	 6.1 - 8.1 - 8.5 -
Temperate forest	0.352	0.628	0.793	12.3 - 14.0 - 16.6
Boreal forest	0.324	0.674	0.505	5.2 - 5.8 - 6.4

7 List of tables

8 List of figures

9 Bibliography

Aalto, P. P., Hämeri, K., Becker, E., Waber, R., Salm, J., Mäkelä, J., Hoell, C., O'Dowd, C. D., Karlsson, H., Hansson, H., Väkevä, M., Koponen, I. K., Buzorius, G., and Kulmala, M.: Physical characterization of aerosol particles during nucleation events, Tellus B, 53, 344-358, 2001.

Acker, K., Möller, D., Wieprecht, W., Meixner, F. X., Bohn, B., Gilge, S., Plass-Dülmer, C., and Berresheim, H.: Strong daytime production of OH from HNO_2 at a rural mountain site., Geophys. Res. Lett., 33, L02809, doi:10.1029/2005GL024643, 2006.

Alapaty, K., and Mathur, R.: Effects of boundary layer mixing representations on vertical distribution of passive and reactive tracers., Meteorol. Atmos. Phys. , 69, 101-118, 1998.

Andreae, M. O., and Merlet, P.: Emission of trace gases and aerosols from biomass burning, Global Biogeochem. Cycles, 15, 955-966, 2001.

Anttila, P., Rissanen, T., Shimmo, M., Kallio, M., Hyotylainen, T., Kulmala, M., and Riekkola, M. L.: Organic compounds in atmospheric aerosols from a Finnish coniferous forest, Boreal Environment Research, 10, 371-384, 2005.

Apel, E. C., Riemer, D. D., Hills, A., Baugh, W., Orlando, J., Faloona, I., Tan, D., Brune, W., Lamb, B., Westberg, H., Carroll, M. A., Thornberry, T., and Geron, C. D.: Measurement and interpretation of isoprene fluxes and isoprene, methacrolein, and methyl vinyl ketone mixing ratios at the PROPHET site during the 1998 Intensive, J. Geophys. Res., 107, 4034, DOI: 10.1029/2000JD000225, 2002.

Arnold, F., Schneider, J., Gollinger, K., Schlager, H., Schulte, P., Hagen, D. E., Whitefield, P. D., and van Velthoven, P.: Observations of upper tropospheric sulfur dioxide and acetone pollution: Potential implications for hydroxyl radical and aerosol formation, Geophys. Res. Lett., 24, 57-60, 1997.

Arya, S. P.: Introduction to Micrometeorology, Academic Press, San Diego, Calif., 1988.

Atkinson, R.: Gas-Phase Tropospheric Chemistry of Organic-Compounds - a Review, Atmospheric Environment Part a-General Topics, 24, 1-41, 1990.

Atkinson, R.: Atmospheric chemistry of VOCs and NOx, Atmospheric Environment, 34, 2063-2101, 2000.

Atkinson, R., and Arey, J.: Gas-phase tropospheric chemistry of biogenic volatile organic compounds: a review, Atmospheric Environment, 37, S197-S219, 2003.

Atkinson, R., Baulch, D. L., Cox, R. A., Crowley, J. N., Hampson, R. F., Hynes, R. G., Jenkin, M. E., Rossi, M. J., and Troe, J.: Evaluated kinetic and photochemical data for atmospheric chemistry: Volume II - gas phase reactions of organic species, Atmos. Chem. Phys., 6, 3625-4055, 2006a.

Atkinson, R., Baulch, D. L., Cox, R. A., Crowley, J. N., Hampson, R. F., Hynes, R. G., Jenkin, M. E., Rossi, M. J., and Troe, J.: Evaluated kinetic and photochemical data for atmospheric chemistry: Volume II – gas phase reactions of organic species, Atmospheric Chemistry and Physics, 6, 3625-4055, 2006b.

Attmannspacher, W., and Riedl, J.: Ein Ombrometer im Baukastenprinzip zur Erfassung und digitalen Ausgabe der Niederschlagsdauer und -menge, Berichte des Deutschen Wetterdienstes, 131, 1-19, 1973.

Bäck, J., Hari, P., Hakola, H., Juurola, E., and Kulmala, M.: Dynamics of monoterpene emissions in Pinus sylvestris during early spring, Boreal Enivironment Research, 10 409-424, 2005.

Baldocchi, D., Guenther, A. B., Harley, P. C., Klinger, L., Zimmerman, P., Lamb, B., and Westberg, H.: The fluxes and air chemistry of isoprene above a deciduous hardwood forest., Philosophical Transactions of the Royal Society of London Series A-Mathematical Physical and Engineering Sciences, 351, 279-296, 1995.

Bartenbach, S.: Application of comprehensive gas chromatography (GCxGC) to measurements of volatile organic species in ambient air, Doktor, Fachbereich Chemie, Pharmazie und Geowissenschaften, Johannes Gutenberg-Universität, Mainz, Germany, 2005.

Bartenbach, S., Williams, J., Plass-Dülmer, C., Berresheim, H., and Lelieveld, J.: In-situ measurements of reactive hydrocarbons at Hohenpeissenberg with comprehensive gas chromatography (GCxGC-FID): use in estimating HO and NO_3, Atmospheric Chemistry and Physics, 7, 1-14, 2007.

Benkelberg, H.-J., Böge, O., Seuwen, R., and Warneck, P.: Product distributions from the OH radical-induced oxidation of but-1-ene, methyl-substituted but-1-enes and isoprene in NOx-free air, Phys. Chem. Chem. Phys., 2, 4029 - 4039, 2000.

Berman, S., Ku, J. Y., and Rao, S. T.: Spatial and temporal variation of the mixing depth over the northeastern United States during the summer of 1995., J. Appl. Meteorol. , 38, 1661- 1673, 1999.

Berndt, T., Stratmann, F., Bräsel, S., Heintzenberg, J., Laaksonen, A., and Kulmala, M.: SO_2 oxidation products other than H_2SO_4 as a trigger of new particle formation – Part 1: Laboratory investigations, Atmospheric Chemistry and Physics, 8, 6365-6374, 2008.

Berresheim, H., Elste, T., Plass-Dülmer, C., Eisele, F. L., and Tanner, D. J.: Chemical ionization mass spectrometer for long-term measurements of atmospheric OH and H2SO4., International Journal of Mass Spectrometry, 202, 91-109, 2000.

Bethan, S., Vaughan, G., Gerbig, C., Volz-Thomas, A., Richer, H., and Tidderman, D. A.: Chemical Air mass differences near fronts, Journal of Geophysical Research - Atmospheres, 103, 13413-13434, 1998.

Bevington, P. R., and Robinson, D. K.: Data Reduction and Error Analysis for the Physical Sciences., 2nd edition ed., McGraw-Hill, New York, 2002.

Biesenthal, T. A., Bottenheim, J. W., Shepson, P. B., Li, S. M., and Brickell, P. C.: The chemistry of biogenic hydrocarbons at a rural site in eastern Canada., Journal of Geophysical Research - Atmospheres, 103, 25487-25498, 1998.

Birmili, W., Wiedensohler, A., Plass-Dülmer, C., and Berresheim, H.: Evolution of newly formed aerosol particles in the continental boundary layer: A case study including OH and H_2SO_4 measurements, J. Geophys. Res., 27, 2205-2208, 2000.

Birmili, W., Berresheim, H., Plass-Dülmer, C., Elste, T., Gilge, S., Wiedensohler, A., and Uhrner, U.: The Hohenpeissenberg aerosol formation experiment (HAFEX): a long-term study including size-resolved aerosol, H_2SO_4, OH, and monoterpenes measurements., Atmos. Chem. Phys., 3, 361-376, 2002.

Blake, R. S., Whyte, C., Hughes, C. O., Ellis, A. M., and Monks, P. S.: Demonstration of Proton-Transfer Reaction Time-of-Flight Mass Spectrometry for Real-Time Analysis of Trace Volatile Organic Compounds., Anal. Chem., 76, 3841-3845, 2004.

Blake, R. S., Monks, P. S., and Ellis, A. M.: Proton-Transfer Reaction Mass Spectrometry, Chemical Reviews, 109, 861-896, doi:10.1021/cr800364q, 2009.

Blitz, M. A., Heard, D. E., and Pilling, M. J.: Pressure and temperature-dependent quantum yields for the photodissociation of acetone between 279 and 327.5 nm., Geophys. Res. Lett., 31, doi:10.1029/2003GL018793, 2004.

Bolton, D.: Computation of equivalent potential temperature., Montly Weather Reviews, 108, 1046-1053, 1980.

Bonn, B., and Moortgat, G. K.: New particle formation during α- and ß-pinene oxidation by O_3, OH and NO_3, and the influence of water vapour: particle size distribution studies, Atmospheric Chemistry and Physics, 2, 183-196, 2002.

Bonn, B., and Moortgat, G. K.: Sesquiterpene ozonolysis: Origin of atmospheric new particle formation from biogenic hydrocarbons, Geophys. Res. Lett., 30, 4, 1585 10.1029/2003gl017000, 2003.

Bonn, B., Boy, M., Dal Maso, M., Hakola, H., Hirsikko, A., Kulmala, M., Kurtén, T., Laakso, L., Mäkelä, J., Riipinen, I., Rannik, Ü., Sihto, S.-L., and Ruuskanen, T. M.: Biogenic Sesquiterpenes and Atmospheric New Particle Formation: A Boreal Forest Site Investigation, Nucleation and Atmospheric Aerosols;, 17th International Conference,, Galway, Ireland, 2007a, 344-349,

Bonn, B., Korhonen, H., Petäjä, T., Boy, M., and Kulmala, M.: Understanding the formation of biogenic secondary organic aerosol from alpha-pinene in smog chamber studies: role of organic peroxy radicals., Atmos. Chem. Phys. Discuss., 7, 3901-3939, 2007b.

Bonn, **B.**, Boy, M., Dal Maso, M., Hakola, H., Hirsikko, A., Kulmala, M., Kurtén, T., Laakso, L., Mäkelä, J., Riipinen, I., Rannik, Ü., Sihto, S.-L., and Ruuskanen, T. M.: Biogenic Sesquiterpenes and Atmospheric New Particle Formation: A Boreal Forest Site Investigation, Nucleation and Atmospheric Aerosols; 17th International Conference, Galway, Ireland, 2007, 2008a, 344-349,

Bonn, B., Kulmala, M., Riipinen, I., Sihto, S.-L., and Ruuskanen, T. M.: How biogenic terpenes govern the correlation between sulfuric acid concentrations and new particle formation, J. Geophys. Res., 113, D12209, doi:10.1029/2007JD009327, 2008b.

Butler, T. M., Taraborrelli, D., Brühl, C., Fischer, H., Harder, H., Martinez, M., Williams, J., Lawrence, M. G., and Lelieveld, J.: Improved simulation of isoprene oxidation chemistry with the ECHAM5/MESSy chemistry-climate model: lessons from the GABRIEL airborne field campaign, Atmos. Chem. Phys., 8, 4529–4546, 2008.

Calogirou, A., Larsen, B. R., and Kotzias, D.: Gas phase terpene oxidation products: A review, Atmospheric Environment, 33A, 1352-2310, 1999.

Canagaratna, M. R., Jayne, J. T., Jimenez, J. L., Allan, J. D., Alfarra, M. R., Zhang, Q., Onasch, T. B., Drewnick, F., Coe, H., Middlebrook, A., Delia, A., Williams, L. R., Trimborn, A. M., Northway, M. J., DeCarlo, P. F., Kolb, C. E., Davidovits, P., and Worsnop, D. R.: Chemical and microphysical characterization of ambient aerosols with the aerodyne aerosol
mass spectrometer, Mass Spectrom. Rev., 26, 185-222, 2007.

Carter, W. P. L., and Atkinson, R.: Development and evaluation of a detailed mechanism for the atmospheric reactions of isoprene and NOx, International Journal of Chemical Kinetics, 28, 497-530, 1996.

Chameides, W. L., Lindsay, R. W., Richardson, J., and Kiang, C. S.: The role of biogenic hydrocarbons in urban photochemical smog: Atlanta as a case study, Science, 241, 1473-1475, 1988.

Christian, T. J., Kleiss, B., Yokelson, R. J., Holzinger, R., Crutzen, P. J., Hao, W. M., Shirai, T., and Blake, D. R.: Comprehensive laboratory measurements of biomass-burning emissions: 2. First intercomparison of open-path FTIR, PTR-MS, and GC- MS/FID/ECD, J. Geophys. Res.-Atmos., 109, D02311
10.1029/2003jd003874, 2004.

Clarkson, T. S., Martin, R. J., Rudolph, J., and Graham, B. W. L.: Benzene and toluene in New Zealand air, Atmospheric Environment, 30, 569-577, 1996.

Colomb, A., Williams, J., Crowley, J., Gros, V., Hofmann, R., Salisbury, G., Klüpfel, T., Kormann, R., Stickler, A., Forster, C., and Lelieveld, J.: Airborne measurements of trace organic species in the upper troposphere over Europe: the impact of deep convection, Environmental Chemistry, 3, 244-259, 2006.

Conn, E. E.: The metabolism of a natural product - lessons learned from cyanogenic glycosides, Planta Med., 57, S1, 1991.

Custer, T., and Schade, G.: Methanol and acetaldehyde fluxes over ryegrass, Tellus Series B-Chemical and Physical Meteorology, 59, 673-684, 10.1111/j.1600-0889.2007.00294.x, 2007.

Custer, T. G., Kato, S., Fall, R., and Bierbaum, V. M.: Negative-ion CIMS: analysis of volatile leaf wound compounds including HCN, International Journal of Mass Spectrometry, 1-20, 12272, 2002.

Dal Maso, M., Kulmala, M., Riipinen, I., Wagner, R., and Hussein, T.: Formation and growth of fresh atmospheric aerosols: eight years of aerosol size distribution data from SMEAR II, Hyytiälä , Finland, Boreal Environ. Res., 10, 323-336, 2005.

de Gouw, J., Warneke, C., Karl, T., Eerdekens, G., van der Veen, C., and Fall, R.: Sensitivity and specificity of atmospheric trace gas detection by proton-transfer-reaction mass spectrometry, International Journal of Mass Spectrometry, 223-224, 365-382, 2003a.

de Gouw, J., and Warneke, C.: Measurements of volatile organic compounds in the earths atmosphere using proton-transfer-reaction mass spectrometry, Mass Spectrometry Reviews, 26, 223-257, 2007.

de Gouw, J. A., Goldan, P. D., Warneke, C., Kuster, W. C., Roberts, J. M., Marchewka, M., Bertman, S. B., Pszenny, A. A. P., and Keene, W. C.: Validation of Proton-Transfer-Reaction Mass Spectrometry (PTR-MS) Measurements of Gas-Phase Organic Compounds in the Atmosphere During the New England Air Quality Study (NEAQS) in 2002, J. Geophys. Res., 108, 2003b.

de Gouw, J. A., Warneke, C., Holzinger, R., Klüpfel, T., and Williams, J.: Inter-comparison between airborne measurements of methanol, acetonitrile and acetone using two different configured PTR-MS instruments, International Journal of Mass Spectrometry, 239, 129-137, 2003c.

de Gouw, J. A., Middlebrook, A. M., Warneke, C., Goldan, P. D., Kuster, W. C., Roberts, J. M., Fehsenfeld, F. C., Worsnop, D. R., Canagaratna, M. R., Pszenny, A. A. P., Keene, W. C., Marchewka, M., Bertman, S. B., and Bates, T. S.: Budget of organic carbon in a polluted atmosphere: results from the New England Air Quality Study in 2002, Journal of Geophysical Research-Part D-Atmospheres, 110, 22 pp., 10.1029/2004jd005623, 2005.

de Gouw, J. A., and Jimenez, J. L.: Organic Aerosols in the Earth's Atmosphere, Environ. Sci. & Technol., 43, 7614-7618, DOI:10.11021/es9006004, 2009.

de Reus, M., Fischer, H., Arnold, F., de Gouw, J. A., Holzinger, R., Warneke, C., and Williams, J.: On the relationship between acetone and carbon monoxide in air masses of different origin, Atmos. Chem. Phys., 3, 1709-1723, 2003.

Delwiche, C. F., and Sharkey, T. D.: Rapid appearance of ^{13}C in biogenic isoprene when $^{13}CO_2$ is fed to intact leaves, Plant, Cell Environ., 16, 587-591, 1993.

Derwent, R. G., Jenkin, M. E., and Saunders, S. M.: Photochemical ozone creation potentials for a large number of reactive hydrocarbons under European conditions, Atmospheric Environment, 30, 181-199., 1996.

Dong, S., and Dasgupta, P. K.: Solubility of Gaseous Formaldehyde in Liquid Water and Generation of Trace Standard Gaseous Formaldehyde, Environ. Sci. Technol., 20, 637-640, 1986.

Dotan, I., Albritton, D. L., Lindinger, W., and Pahl, M.: Mobilities of CO_2^+, N_2H^+, H_3O^+ and $H_3O^+(H_2O)_2$ ions in N_2, J. Chem. Phys., 65, 5028-5030, 1976.

Eerdekens, G.: Investigation of the possible interferences in the PTR-MS measurements of ambient air by use of GC-PTR-MS. Development of an all-Teflon® injection system for GC-PTR-MS., Master of Chemistry, Institute for Marine and Atmospheric research Utrecht, Faculty of Physics and Astronomy, University of Utrecht, Utrecht, 2002.

Ehhalt, D., and Prather, M.: Atmospheric Chemistry and Greenhouse Gases, Climate Change 2001; Working Group 1: The Scientific Basis, edited by: Houghton, J., Ding, Y., Griggs, D., Noguer, M., van der Linden, P., and Xiaosu, D., Cambridge University Press, 2001.

Ehhalt, D. H., Dorn, H.-P., and Poppe, D.: The chemistry of the hydroxyl radical in the troposphere, Proc. R. Soc. Edinburgh, Sect. B: Biol. Sci., 97, 17- 34, 1991.

Elperin, T., Fominykh, A., and Krasovitov, B.: Scavenging of soluble trace gases by falling rain droplets in inhomogeneous atmosphere, Atmospheric Environment, 44, 2133-2139, 2010.

Eva, H. D., Belward, A. S., De Miranda, E. E., Di Bella, C. M., GOND, V., Huber, O., Jones, S., Sgrenzaroli, M., and Fritz, S.: A Land Cover Map of South-America, Global Change Biology, 10, 731-744, doi: 10.1111/j.1529-8817.2003.00774.x, 2004.

Fall, R., and Benson, A. A.: Leaf methanol-the simplest natural product from plants., Trends in Plant Sciences, 1, 296-301, 1996.

Fall, R.: Biogenic emissions of volatile organic compounds from higher plants, in: Reactive Hydrocarbons in the Atmosphere, edited by: Hewitt, C. N., Academic Press, San Diego, 43-96, 1999.

Fall, R., Karl, T., Hansel, A., Jordan, A., and Lindinger, W.: Volatile organic compounds emitted after leaf wounding: On-line analysis by proton-transfer-reaction mass spectrometry J. Geophys. Res., 104, 15963-15974, 1999.

Fall, R., Karl, T., Jordan, A., and Lindinger, W.: Biogenic C5-VOCs: release from leaves after freeze-thaw wounding and occurrence in air at a high mountain observatory Atmospheric Environment, 35, 3905-3916, 2001.

Fall, R.: Abundant oxygenates in the atmosphere: A biochemical perspective, Chemical Reviews, 103, 4941- 4495, 2003.

Fehsenfeld, F., Calvert, J., Fall, R., Goldan, P., Guenther, A. B., Hewitt, C. N., Lamb, B., Liu, S., Trainer, M., Westberg, H., and Zimmerman, P.: Emissions of volatile organic compounds from vegetation and the implications for atmospheric chemistry, Global Biogeochem. Cycles, 6, 389-430, 1992.

Fenger, J.: Urban air quality, Atmospheric Environment, 33, 4877-4900, 1999.

Fiedler, V., Dal Maso, M., Boy, M., Aufmhoff, H., Hoffmann, J., Schuck, T., Birmili, W., Hanke, M., Uecker, J., Arnold, F., and Kulmala, M.: The contribution of sulphuric acid to atmospheric particle formation and growth: a comparison between boundary layers in Northern and Central Europe, Atmos. Chem. Phys., 5, 1773-1785, 2005.

Fishera, A. J., Grimesb, H. D., and Fall, R.: The biochemical origin of pentenol emissions from wounded leaves, Phytochemistry, 62, 159-163, 2003.

Frey, A. K., Tissary, J., Saarnio, K. M., Timonen, H. J., Tolonen - Kivimäki, O., Aurela, M. A., Saarikoski, S. K., Makkonen, U., Hytönen, K., Jokiniemi, J., Solonen, R. O., and Hillamo, R. E. J.: Chemical composition and mass size distribution of the fine particulate matter emitted by a small masonry heater, Boreal Environment Research, 14, 255-271, 2009.

Fuentes, J. D., Lerdau, M., Atkinson, R., Baldocchi, D., Bottenheim, J. W., Ciccioli, P., Lamb, B., Geron, C., Gu, L., Guenther, A., Sharkey, T. D., and Stockwell, W.: Biogenic hydrocarbons in the atmospheric boundary layer: A review, Bulletin of the American Meteorological Society, 81, 1537-1575, 2000.

Galbally, I. E., and Kirstine, W.: The production of methanol by flowering plants and the global cycle of methanol, J. Atmos. Chem., 43, 195-229, 2002.

Ganzeveld, L., Valverde-Canossa, J., Moortgat, G. K., and Steinbrecher, R.: Evaluation of Peroxide Exchanges over Coniferous Forest in a Single-Column Chemistry-Climate Model., Atmospheric Environment, 40, S68-S80 Suppl. 61, 2006.

Ganzeveld, L., Eerdekens, G., Feig, G., Fischer, H., Harder, H., Königstedt, R., Kubistin, D., Martinez, M., Meixner, F. X., Scheeren, B., Sinha, V., Williams, J., Vilà, J., and Lelieveld, J.: Surface and Boundary Layer Exchanges of Volatile Organic Compounds, Nitrogen Oxides and Ozone during the GABRIEL Campaign, Atmos. Chem. Phys., 8, 6223-6243, ISI:000260558500016, 2008.

Gebhardt, S., Colomb, A., Hofmann, R., Williams, J., and Lelieveld, J.: Halogenated organic species over the tropical rainforest, Atmos. Chem. Phys., 8, 3185-3197, 2008.

Geron, C., Guenther, A., Greenberg, J., Loescher, H., Clark, D., and Baker, B.: Biogenic Volatile Organic Compound Emissions from a Rain Forest in Costa Rica, Atmospheric Environment, 36, 3793-3802, 2002.

Goldan, P. D., Kuster, W. C., Fehesenfeld, F. C., and Montzka, S. A.: Hydrocarbon measurements in the southeastern United States: The Rural Oxidants in the Southern Environment (ROSE) program 1990, Journal of Geophysical Research - Atmospheres, 103, 31045-31056, 1995.

Goldan, P. D., Kuster, W. C., and Fehsenfeld, F. C.: Nonmethane hydrocarbon measurements during the tropospheric OH photochemistry experiment, 102, 6315-6324, 1997.

Goldstein, A. H., McKay, M., Kurpius, M. R., Schade, G. W., Lee, A., Holzinger, R., and Rasmussen, R. A.: Forest thinning experiment confirms ozone deposition to forest canopy is dominated by reaction with biogenic VOCs, Geophys. Res. Lett., 31, L22106, doi:10.1029/2004GL021259, 2004.

Goulden, M. L., Miller, S. D., da Rocha, H. R., Menton, M. C., de Freitas, H. C., Figueira, A. M. E. S., and de Sousa, C. A. D.: Diel and seasonal patterns of tropical forest CO2 exchange, Ecological Applications, 14, S42-S54, 2004.

Greenberg, J. P., and Zimmerman, P.: Nonmethane hydrocarbons in remote tropical, continental, and marine atmospheres, Journal of Geophysical Research - Atmospheres, 89, 4767-4778, 1984.

Greenberg, J. P., Guenther, A. B., Petron, G., Wiedinmyer, C., Vega, O., Gatti, L. V., Tota, J., and Fisch, G.: Biogenic VOC emissions from forested Amazonian landscapes, Global Biogeochem. Cycles, 10, 651-662, 2004a.

Greenberg, J. P., Guenther, A. B., Petron, G., Wiedinmyer, C., Vega, O., Gatti, L. V., Tota, J., and Fisch, G.: Biogenic VOC emissions from forested Amazonian landscapes, Global Change Biology, 10, 651-662, 2004b.

Greenberg, J. P., Friedli, H., Guenther, A. B., Hanson, D., Harley, P., and Karl, T.: Volatile organic emissions from the distillation and pyrolysis of vegetation, Atmos. Chem. Phys., 6, 81-91, 2006.

Grosjean, E., and Grosjean, D.: The reaction of unsaturated aliphatic oxygenates with ozone, J. Atmos. Chem., 35, 205-232, 1999.

Guenther, A., Zimmerman, P., and Wildermuth, M.: Natural volatile organic compound emission rates for U.S. woodland landscapes., Atmospheric Environment, 28, 1197-1210, 1994.

Guenther, A., Nicolas Hewitt, C., Erickson, D., Fall, R., Geron, C., Graedel, T., Harley, P., Klinger, L., Lerdau, M., McKay, W. A., Pierce, T., Scholes, B., Steinbrecher, R., Tallamraju, R., Taylor, J., and Zimmerman, P.: A global model of natural volatile organic compound emissions, J. Geophys. Res., 100, 8873-8892, 1995.

Guenther, A., and Hills, A.: Eddy covariance measurement of isoprene fluxes, J. Geophys. Res., 103, 13145-13152, 1998.

Guenther, A.: The contribution of reactive carbon emissions from vegetation to the carbon balance of terrestrial ecosystems, Chemosphere, 49, 837-844, 2002.

Guenther, A., Karl, T., Harley, P., Wiedinmyer, C., Palmer, P. I., and Geron, C.: Estimates of global terrestrial isoprene emissions using MEGAN (Model of Emissions of Gases and Aerosols from Nature), Atmospheric Chemistry and Physics, 6, 3181-3210, 2006.

Guenther, A. B., Baugh, B., and Brasseur, G.: Isoprene emission estimates and uncertainties for the central African EXPRESSO study domain, J. Geophys. Res., 104, 30625-30639, 1999.

Gurk, C.: Untersuchungen zur Verteilung von Kohlendioxid in der Tropopausenregion., MSc, Diploma thesis, Johannes-Gutenberg University, Mainz, 2003.

Haagen-Smit, A. J., and Bradley, C. E.: Ozone formation in photochemical oxidation of organic substances, Ind. Eng. Chem., 45, 2086-2089, 1953.

Haapanala, S., Rinne, J., Hakola, H., Hellén, H., Laakso, L., Lihavainen, H., Janson, R., O'Dowd, C., and Kulmala, M.: Boundary layer concentrations and landscape scale emissions of volatile organic compounds in early spring, Atmos. Chem. Phys., 7, 1869-1878, 2007.

Hager: A new linear ion trap mass spectrometer, Rapid Communication in Mass Spectrometry, 16, 512, 2002.

Hakola, H., Laurila, T., Rinne, J., and Puhto, K.: The ambient concentrations of biogenic hydrocarbons at a northern European, boreal site, Atmospheric Environment, 34, 4971-4982, 2000.

Hakola, H., Tarvainen, V., Laurila, T., Hiltunen, V., Hellen, H., and Keronen, P.: Seasonal variation of VOC concentrations above a boreal coniferous forest, Atmospheric Environment, 37, 1623-1634, 2003.

Hamed, A., Joutsensaari, J., Mikkonen, S., Sogacheva, L., Dal Maso, M., Kulmala, M., Cavalli, F., Fuzzi, S., Facchini, M. C., Decesari, S., Mircea, M., Lehtinen, K. E. J., and Laaksonen, A.: Nucleation and growth of new particles in Po Valley, Italy, Atmospheric Chemistry and Physics, 7, 355-376, 2007.

Hamm, and Warneck: The Interhemispheric Distribution and the Budget of Acetonitrile in the Troposphere., Journal of Geophysical Research - Atmospheres, 95, 20593-20606, 1990.

Hamm, S., Hahn, J., Helas, G., and Warneck, P.: Acetonitrile in the troposphere - residence time due to rainout and uptake by the ocean, Geophys. Res. Lett., 11, 1207-1210, 1984.

Handisides, G. M., Plaß-Dülmer, C., Gilge, S., Bingemer, H., and Berresheim, H.: Hohenpeissenberg Photochemical Experiment (HOPE 2000): Measurements and photostationary state calculations of OH and peroxy radicals. , Atmos. Chem. Phys., 3, 1565-1588, 2003.

Hanke, M., Uecker, J., Reiner, T., and Arnold, F.: Atmospheric peroxy radicals: ROXMAS, a new mass-spectrometric methodology for speciated measurements of HO_2 and Sigma RO_2 and first results, International Journal of Mass Spectrometry, 213, 91-99, 2002.

Hansel, A., Jordan, A., Holzinger, R., Prazeller, P., Vogel, W., and Lindinger, W.: Proton-transfer reaction mass-spectrometry - online trace gas-analysis at the ppb level, Int. J. of Mass Spectrometry and Ion Processes, 149/150, 609-619, 1995.

Hansel, A., Singer, W., Wisthaler, A., Schwarzmann, M., and Lindinger, W.: Energy dependencies of the proton transfer reactions $H_3O^+ + CH_2O$ double left right arrow $CH_2OH^+ + H_2O$ International Journal of Mass Spectrometry, 167/168, 697, 1997.

Hari, P., and Kulmala, M.: Station for Measuring Ecosystem-Atmosphere Relations (SMEAR II). Boreal Environ. Res., 10, 315-322, 2005.

Harisson, A. G.: Chemical Ionization Mass Spectrometry., CRC Press, London, 1992.

Harley, P. C., Monson, R. K., and Lerdau, M. T.: Ecological and evolutionary aspects of isoprene emission from plants, Oecologia Berlin, 118, 109-123, 1999.

Hatanaka, A.: The Biogeneration of green odor by green leaves, Phytochemistry, 34, 1201, 1993.

Heikes, B. G., Chang, W., Pilson, M. E. Q., and Swift, E.: Atmospheric Methanol Budget and Ocean Implication, Global Biogeochem. Cycles, 16, 1133, doi:10.1029/2002GB001895., 2002.

Hellén, H., Hakola, H., Reissell, A., and Ruuskanen, T. M.: Carbonyl compounds in boreal coniferous forest air in Hyytiälä, Southern Finland, , Atmos. Chem. Phys., 4, 1771-1780, SRef-ID: 1680-7324/acp/2004-4-1771., 2004.

Helmig, D., Greenberg, J., Guenther, A., Zimmerman, P., and Geron, C.: Volatile organic compounds and isoprene oxidation products at a temperate deciduous forest site Journal of Geophysical Research - Atmospheres, 103, 22397-22414, 1998.

Holzinger, R., Warneke, C., Hansel, A., Jordan, A., Lindinger, W., Scharffe, D. H., Schade, G., and Crutzen, P. J.: Biomass burning as a source of formaldehyde, Acetaldehyde, Methanol, Acetone Acetonitrile, and hydrogen cyanide, Geophys. Res. Lett., 26, 1161-1164, 1999.

Holzinger, R., Jordan, A., Hansel, A., and Lindinger, W.: Automobile emissions of Acetonitrile: assessment of tis contribution to the global source, J. Atmos. Chem., 38, 187-193, 2001.

Houweling, S., Dentener, F. J., and Lelieveld, J.: The impact of non-methane hydrocarbon compounds on tropospheric photochemistry, J. Geophys. Res., 103, 10673 -10696, 1998.

Hunter, E. P., and Lias, S. G.: Evaluated gas phase basicities and proton affinities of molecules: An update, Journal of Physical and Chemical Reference Data, 27, 413-656, 1998.

Hurst, J. M., Barcket Jr., D. J., Herrera-Gomez, O., Couch, T. L., Shepson, P. B., Faloona, I., Tan, D., Brune, W., Westberg, H., Lamb, B., Biesenthal, T., Young, V., Goldstein, A., Munger, J. W., Thornberry, T., and Carroll, M. A.: Investigation of the nighttime decay of isoprene, J. Geophys. Res., 106, 24335-24346, 2001.

Hüve, K., Christ, M. M., Kleist, E., Niinemets, Ü., Uerlings, R., Walter, A., and Wildt, J.: Simultaneous growth and emission measurements demonstrate an interactive control of methanol release by leaf expansion and stomata, , J. Exp. Bot., 58, 1783-1793, 2007.

Hyvönen, S., Junninen, H., Laakso, L., Dal Maso, M., Gronholm, T., Bonn, B., Keronen, P., Aalto, P., Hiltunen, V., Pohja, T., Launiainen, S., Hari, P., Mannila, H., and Kulmala, M.: A look at aerosol formation using data mining techniques, Atmospheric Chemistry and Physics, 5, 3345-3356, 2005.

Jacob, D. J., Field, B. D., Jin, E. M., Bey, I., Li, Q., Logan, J. A., Yantosca, R. M., and Singh, H. B.: Atmospheric budget of acetone, J. Geophys. Res., 107, 4100, doi:10.1029/2001JD000694, 2002.

Jacobson, M. Z.: Effects of ethanol versus gasoline vehicles on cancer and mortality in the United States, Environ. Sci. Technol., 41, 4150-4157, 10.1021/es062085v, 2007.

Janson, R.: Monoterpene concentrations in and above a forest of Scots pine, J. Atmos. Chem., 14, 385-394, 1992.

Janson, R., and De Serves, C.: Emissions of Biogenic VOCs from Boreal Ecosystems, in: Biogenic VOC emissions and photochemistry in the boreal regions of Europe – Biphorep, edited by: Lindfors, T. L. a. V., European Commission, 45-56, 1999.

Janson, R., and De Serves, C.: Acetone and monoterpene emissions from the boreal forest in northern Europe, Atmospheric Environment, 35, 4629-4637, 2001.

Jardine, K., Harley, P., Karl, T., Guenther, A., Lerdau, M., and Mak, J. E.: Plant physiological and environmental controls over the exchange of acetaldehyde between forest canopies and the atmosphere, Biogeosciences, 5, 1726-4170, 2008.

Jianzhen, Y., Griffin, R. J., Cocker, D. R., Flagan, R. C., H., S. J., and Blanchard, P.: Observation of gaseous and particulate products of monoterpene oxidation in forest atmospheres, Geophys. Res. Lett., 26, 1145-1148, 1999.

Jöckel, P., Tost, H., Pozzer, A., Brühl, C., Buchholz, J., Ganzeveld, L., Hoor, P., Kerkweg, A., Lawrence, M. G., Sander, R., Steil, B., Stiller, G., Tanarhte, M., Taraborrelli, D., van Aardenne, J., and Lelieveld, J.: The atmospheric chemistry general circulation model ECHAM5/MESSy: Consistent simulation of ozone from the surface to the mesosphere, Atmos. Chem. Phys., 6, 5067-5104, 2006.

Junninen, H., Hulkkonen, M., Riipinen, I., Nieminen, T., Hirsikko, A., Suni, T., Boy, M., Lee, S.-H., Vana, M., Tammet, H., Kerminen, V.-M., and Kulmala, M.: Observations on nocturnal growth of atmospheric clusters, Tellus B, 60, 365-371, 2008.

Kamens, R. M., and Jaoui, M.: Modeling aerosol formation from alpha-pinene plus NOx in the presence of natural sunlight using gas-phase kinetics and gas-particle partitioning theory Environ. Sci. Technol., 35, 1394-1405, 2001.

Karl, T., Fall, R., Crutzen, P. J., Jordan, A., and Lindinger, W.: High concentrations of reactive biogenic VOCs at a high altitude site in late autumn., Geophys. Res. Lett., 28, 507-510, 2001a.

Karl, T., Guenther, A. B., Jordan, A., Fall, R., and Lindinger, W.: Eddy covariance measurement of biogenic oxygenated VOC emissions from hay harvesting, Atmospheric Environment, 35, 491-495, 2001b.

Karl, T., Potosnak, M., Guenther, A., Clark, D., Walker, J., Herrick, J. D., and Geron, C.: Exchange processes of volatile organic compounds above a tropical rain forest: Implications for modeling tropospheric chemistry above dense vegetation., J. Geophys. Res., 109, D18306, DOI: 10.1029/2004JD004738, 2004a.

Karl, T., Potosnak, M., Guenther, A., Clark, D., Walker, J., Herrick, J. D., and Geron, C.: Exchange processes of volatile organic compounds above a tropical rain forest: Implications for modeling tropospheric chemistry above dense vegetation, J. Geophys. Res., 109, D18306, doi:18310.11029/12004JD004738, 2004b.

Karl, T., Guenther, A., Yokelson, R. J., Greenberg, J., Potosnak, M., Blake, D. R., and Artaxo, P.: The tropical forest and fire emissions experiment: Emission, chemistry, and transport of biogenic volatile organic compounds in the lower atmosphere over Amazonia, J. Geophys. Res.-Atmos., 112, 17, D18302 10.1029/2007jd008539, 2007.

Karl, T. G., Spirig, C., Rinne, J., Stroud, C., Prevost, P., Greenberg, J., Fall, R., and Guenther, A.: Virtual disjunct eddy covariance measurements of organic compound fluxes from a subalpine forest using proton transfer reaction mass spectrometry, Atmos. Chem. Phys., 2, 279-291, 2002.

Kelly, T. J., and Fortune, C. R.: Continuous monitoring of gaseous formaldehyde using an improved fluorescence approach., Intern. Environ. Anal. Chem., 54, 249-263, 1994.

Kesselmeier, J., and Staudt, M.: Biogenic Volatile Organic Compounds (VOC): An Overview on Emission, Physiology and Ecology, J. Atmos. Chem., 33, 23–88, 1999.

Kesselmeier, J.: Exchange of Short-Chain Oxygenated Volatile Organic Compounds (VOCs) between Plants and the Atmosphere: A Compilation of Field and Laboratory Studies, J. Atmos. Chem., 39, 219–233, 2001.

Kesselmeier, J. K., and al., e.: The BEMA Project: Emission of short-chained organic acids, aldehydes, and monoterpenes, from Quercus ilex L. and Pinus pinea L. in relation to physiological activities, carbon budget, and emission algorithms, , Atmospheric Environment, 31, 119- 133, 1997.

Kieber, R. J., Zhou, X. L., and Mopper, K.: Formation of carbonyl compounds from UV-induced photodegradation of humic substances in natural waters: Fate of riverine carbon in the sea, Limnology and Oceanography, 35, 1503-1515, 1990.

Koch, S., Winterhalter, R., Uherek, E., Kolloff, A., Neeb, P., and Moortgat, G. K.: Formation of new particles in the gas-phase ozonolysis of monoterpenes, Atmospheric Environment, 34, 4031-4042, 2000.

Koppmann, R.: Volatile organic compounds in the atmosphere, Wiley-Blackwell, 2007.

Krejci, R., Strom, J., de Reus, M., Williams, J., Fischer, H., Andreae, M. O., and Hansson, H. C.: Spatial and temporal distribution of atmospheric aerosols in the lowermost troposphere over the Amazonian tropical rainforest, Atmos. Chem. Phys., 5, 1527-1543, 2005.

Kreuzwieser, J., Harren, F. J. M., Laarhoven, L. J. J., Boamfa, I., Lintel-Hekkert, S., Scheerer, U., Hüglin, C., and H., R.: Acetaldehyde emission by leaves of trees – correlation with physiological and environmental parameters., Physiologia Plantarum, 113, 41-49, 2001.

Kubistin, D., Harder, H., Martinez, M., Rudolf, M., Sander, R., Bozem, H., Eerdekens, G., Fischer, H., Gurk, C., Klüpfel, T., Königstedt, R., Parchatka, U., Schiller, C. L., Stickler, A., Taraborrelli, D., Williams, J., and Lelieveld, J.: Hydroxyl radicals in the tropical troposphere over the Suriname rainforest: comparison of measurements with the box model MECCA, Atmos. Chem. Phys. Discuss., 8, 15239-15289, 2008.

Kuhn, U., Andreae, M. O., Ammann, C., Araújo, A. C., Brancaleoni, E., Ciccioli, P., Dindorf, T., Frattoni, M., Gatti, L. V., Ganzeveld, L., Kruijt, B., Lelieveld, J., Lloyd, J., Meixner, F. X., Nobre, A. D., Pöschl, U., Spirig, C., Stefani, P., Thielmann, A., Valentini, R., and Kesselmeier, J.: Isoprene and Monoterpene Fluxes from Central Amazonian Rainforest Inferred from Tower-based and Airborne Measurements, and Implications on the Atmospheric Chemistry and the Local Carbon Budget, Atmos. Chem. Phys., 7, 2855-2879, 2007.

Kulmala, M., Toivonen, A., Mäkelä, J. M., and Laaksonen, A.: Analysis of the growth of nucleation mode particles observed in Boreal forest, Tellus B, 50, 449-462, 1998.

Kulmala, M., Hämeri, K., Mäkelä, J. M., Aalto, P. P., Pirjola, L., Väkevä, M., Nilsson, E. D., Koponen, I. K., Buzorius, G., Keronen, P., Rannik, Ü., Laakso, L., Vesala, T., Bigg, K., Seidl, W., Forkel, R., Hoffmann, T., Spanke, J., Janson, R., Shimmo, M., C., H. H.-., O'Dowd, C., Becker, E., Paatero, J., Teinilä, K., Hillamo, R., Viisanen, Y., Laaksonen, A., Swietlicki, E., Salm, J., Hari, P., Altimir, N., and Weber, R.: Biogenic aerosol formation in the boreal forest, Boreal Enviroment Research, 5, 281-297, 2000.

Kulmala, M., Dal Maso, M., Mäkelä, J. M., Pirjola, L., Väkevä, M., and Aalto, P. P.: On the formation, growth and composition of nucleation mode particles, Tellus, 53B, 479-490, 2001a.

Kulmala, M., Hämeri, K. K., Aalto, P., Mäkelä, J., Pirjola, L., Nilsson, E. D., Buzorius, G., Rannik, Ü., Dal Maso, M., Seidl, W., Hoffmann, T., Jansson, R., Hansson, H.-C., O'Dowd, C., and Viisanen, Y.: Overview of the international project on biogenic aerosol formation in the boreal forest (BIOFOR), Tellus B, 53, 324-342, 2001b.

Kulmala, M.: How particles nucleate and grow, Science, 302, 1000-1001,, 2003.

Kulmala, M., Vehkamäki, H., Petäjä, T., Dal Maso, M., Lauri, A., Kerminen, V.-M., Birmili, W., and McMurry, P. H.: Formation and growth rates of ultrafine atmospheric particles: A review of observations, J. Aerosol Sci., 35, 143-176, 2004.

Kulmala, M., Lehtinen, K. E. J., and Laaksonen, A.: Cluster activation theory as an explanation of the linear dependence between formation rate of 3 nm particles and sulphuric acid concentration. , Atmos. Chem. Phys., 6, 787-793, 2006.

Kulmala, M., Riipinen, I., Sipilä, M., Manninen, H. E., Petäjä, T., Junninen, H., Dal Maso, M., Mordas, G., Mirme, A., Vana, M., Hirsikko, A., Laakso, L., Harrison, R. M., Hanson, I., Leung, C., Lehtinen, K. E. J., and Kerminen, V.-M.: Toward direct measurement of atmospheric nucleation, Science, 318, 89-92, 10.1126/science.1144124, 2007.

Kulmala, M., and Kerminen, V.-M.: On the formation and growth of atmospheric nanoparticles. , Atmospheric Research, 90, 132-150, doi:10.1016/j.atmosres.2008.01.005, 2008.

Kurten, T., Kulmala, M., Dal Maso, M., Suni, T., Reissell, A., Vehkamäki, H., Hari, P., Laaksonen, A., Viisanen, Y., and Vesala, T.: Estimations of different forest-related contributions to the radiative balance using observations in Southern Finland., Boreal Environment Research, 8, 275-285, 2003.

Kwan, A. J., Crounse, J. D., Clarke, A. D., Shinozuka, Y., Anderson, B. E., Crawford, J. H., Avery, M. A., McNaughton, C. S., Brune, W. H., Singh, H. B., and Wennberg, P. O.: On the flux of oxygenated volatile organic compounds from organic aerosol oxidation, Geophys. Res. Lett., 33, L15815, doi:10.1029/2006GL026144, 2006.

Laaksonen, A., Kulmala, M., Berndt, T., Stratmann, F., Mikkonen, S., Ruuskanen, A., Lehtinen, K. E. J., Dal Maso, M., Aalto, P. P., Petäjä, T., Riipinen, I., Sihto, S.-L., Janson, R., Arnold, F., Hanke, M., Ücker, J., Umann, B., Sellegri, K., O'Dowd, C. D., and Viisanen, Y.: SO_2 oxidation products other than H_2SO_4 as a trigger of new particle formation – Part 2: Comparison of ambient and laboratory measurements, and atmospheric implications, Atmospheric Chemistry and Physics, 8, 7255-7264, 2008a.

Laaksonen, A., Kulmala, M., O'Dowd, C. D., Joutsensaari, J., Vaattovaara, P., Mikkonen, S., Lehtinen, K. E. J., Sogacheva, L., Dal Maso, M., Aalto, P., Petaja, T., Sogachev, A., Yoon, Y. J., Lihavainen, H., Nilsson, D., Facchini, M. C., Cavalli, F., Fuzzi, S., Hoffmann, T., Arnold, F., Hanke, M., Sellegri, K., Umann, B., Junkermann, W., Coe, H., Allan, J. D., Alfarra, M. R., Worsnop, D. R., Riekkola, M. L., Hyotylainen, T., and Viisanen, Y.: The role of VOC oxidation products in continental new particle formation, Atmospheric Chemistry and Physics, 8, 2657-2665, 2008b.

Lagg, A., Taucher, J., Hansel, A., and Lindinger, W.: Applications of proton-transfer reactions to gas-analysis, Int. J. of Mass Spectrometry and Ion Processes, 134, 55-66, 1994.

Lamb, B., Gay, D., Westberg, H., and Pierce, T.: A biogenic hydrocarbon emission inventory for the USA using a simple Forest Canopy Model Atmospheric Environment Part A-General Topics, 27, 1673-1690, 1993.

Lee, S. H., Young, L. H., Benson, D. R., Suni, T., Kulmala, M., Junninen, H., Campos, T. L., Rogers, D. C., and Jensen, J.: Observations of nighttime new particle formation in the troposphere, J. Geophys. Res.-Atmos., 113, 7, D10210
10.1029/2007jd009351, 2008.

Lee, W., Baasandorj, M., Stevens, P. S., and Hites, R. A.: Monitoring OH-initiated oxidation kinetics of isoprene and its products using online mass spectrometry, Environ. Sci. Technol., 39, 1030-1036, DOI: 10.1021/es049438f, 2005.

Lelieveld, J., and Crutzen, P.: The role of clouds in tropospheric photochemistry, J. Atmos. Chem., 12, 229-267, 1991.

Lelieveld, J., Dentener, F. J., Peters, W., and Krol, M. C.: On the role of hydroxyl radicals in the self-cleansing capacity of the troposphere, Atmos. Chem. Phys., 4, 2337-2344, 2004.

Lelieveld, J., Butler, T. M., Crowley, J., Dillon, T., Fischer, H., Ganzeveld, L., Harder, H., Kubistin, D., Lawrence, M. G., Martinez, M., Taraborrelli, D., and Williams, J.: Tropical forest sustains atmospheric oxidation capacity, Nature, 452, 737-740 2008.

Lerdau, M., Guenther, A. B., and Monson, R. K.: Plant production and emission of volatile organic compounds, Bioscience, 47, 373-383, 1997.

Levy, H., II: Photochemistry of the lower troposphere, Planet. Space Sci., 20, 919- 935, 1972.

Levy, H., II Photochemistry of the troposphere, Adv. Photochem., 9, 369- 523, 1974.

Lindinger, W., Hansel, A., and Jordan, A.: On-line monitoring of volatile organic compounds at pptv levels by means of Proton-Transfer-Reaction Mass Spectrometry (PTR-MS): Medical Applications, food control and environmental research., Int. J. of Mass Spectrometry and Ion Processes, 173, 191-241, 1998.

Lopez, S., Topalian, J. H., Mitra, S. K., and Montague, D. C.: Absorption and desorption of dichloromethane vapor by water drops in air. An experimental test of scavenging theory, J. Atmos. Chem., 8, 175-188, 1989.

Loreto, F., and Sharkey, T. D.: Isoprene emission by plants is affected by transmissible wound signals., Plant, Cell Environ., 16, 563-570, 1993.

Loreto, F., Nascetti, P., Graverini, A., and Mannozzi, M.: Emission and content of monoterpenes in intact and wounded needles of the Mediterranean Pine, Pinus pinea, Functional Ecology, 14, 589-595, 2000.

Lovejoy, E. R., Curtius, J., and Froyd, K. D.: Atmospheric ion-induced nucleation of sulphuric acid and water, J. Geophys. Res., 109, 11 pp., 10.1029/2003dj004460, 2004.

Mäkelä, J., Aalto, P., Jokinen, V., Pohja, T., Nissinen, A., Palmroth, S., Markkanen, T., Seitsonene, K., Lihavainen, H., and Kulmala, M.: Observations of ultrafine aerosol particle formation and growth in boreal forest, Geophys. Res. Lett., 24, 1219-1222, 1997.

Marandino, C. A., De Bruyn, W. J., Miller, S. D., Prather, M. J., and Saltzman, E. S.: Oceanic uptake and the global atmospheric acetone budget, Geophys. Res. Lett., 32, L15806, DOI: 10.1029/2005GL023285, 2005.

Marti, J. J., Weber, R. J., McMurry, P. H., Eisele, F. L., Tanner, D. J., and Jefferson, A.: New particle formation at a remote continental site: Assessing the contributions of SO_2 and organic precursors Journal of Geophysical Research, 102, 6331-6339, 1997.

Martin, C. L., Fitzjarrald, D., Garstang, M., Oliveira, A. P., Greco, S., and Browell, E.: Structure and growth of the mixing layer over the Amazonian rain forest., J. Geophys. Res., 93, 1361-1375, 1988.

Martinez, M., Harder, H., Kubistin, D., M., R., Bozem, H., Butler, T., Eerdekens, G., Fischer, H., Gurk, C., Königstedt, R., Klüpfel, T., Lawrence, M., Parchatka, U., Schiller, C., Stickler, A., Williams, J., and Lelieveld, J.: Hydroxyl Radicals in the Tropical Troposphere over the Suriname rain forest: Airborne Measurements, Atmos. Chem. Phys. Discuss., 8, 15491-15536, 2008.

Martius, C., Höfer, H., Garcia, M. V. B., Römbke, J., and Hanagarth, W.: Litter fall, litter stocks and decomposition rates in rainforest and agroforestry sites in central Amazonia, Nutrient Cycling in Agroecosystems 68, 137-154, 2004.

Mason, E. A., and McDaniel, E. W.: Transport Properties of Ions in Gases, John Wiley & Sons, New York, 1988.

McMurry, P. H.: A review of atmospheric aerosol measurements, Atmospheric Environment 34, 1959-1999, 2000.

Millet, D. B., Guenther, A., Siegel, D. A., Nelson, N. B., Singh, H. B., de Gouw, J. A., Warneke, C., Williams, J., Eerdekens, G., Sinha, V., Karl, T., Flocke, F., Apel, E. C., Riemer, D. D., Palmer, P. I., and Barkley, M.: Global atmospheric budget of acetaldehyde: 3D model analysis and constraints from in-situ and satellite observations, Atmos. Chem. Phys. Discuss., 2009.

Miyoshi, A., Hatakeyama, S., and Washida, N.: OH radical-initiated photooxidation of isoprene: An estimate of global CO production, J. Geophys. Res., 99, 18787- 18799, 1994.

Monod, A., Chebbi, A., Durand-Jolibois, R., and Carlier, P.: Oxidation of methanol by hydroxyl radicals in aqueous solution under simulated cloud droplet conditions., Atmospheric Environment, 34, 5283-5294, 2000.

Monson, R. K., and Fall, R.: Isoprene emission from aspen leaves: Influence of environment and relation to photosynthesis and photorespiration., Plant Physiology, 90, 267-274, 1989.

Monson, R. K., Jaeger, C. H., Adams III, W., Driggers, E. M., Silver, G. M., and Fall, R.: Relationships among isoprene emission rate, photosynthesis, and isoprene synthase activity as influenced by temperature, Plant Physiology, 98, 1175-1180, 1992.

Montzka, S. A., Trainer, M., Goldan, P. D., Kuster, W. C., and Fehsenfeld, F. C.: Isoprene and its oxidation-products, methyl vinyl ketone and methacrolein, in the rural troposphere., Journal of Geophysical Research - Atmospheres, 98, 1101-1111, 1993.

Müller, J.-F.: Geographical distribution and seasonal variation of surface emissions and deposition velocities of atmospheric trace gases., J. Geophys. Res., 97, 3787-3804, 1992.

Müller, J.-F., Stavrakou, T., Wallens, S., De Smedt, I., Van Roozendael, M., Potosnak, M. J., Rinne, J., Munger, B., Goldstein, A., and Guenther, A. B.: Global isoprene emissions estimated using MEGAN, ECMWF analyses and a detailed canopy environment model, Atmos. Chem. Phys., 8, 1329–1341, 2008.

Murphy, D. M.: The design of single particle laser mass spectrometers, , Mass Spectrom. Rev., 26, 150-165, 2007.

Naresh, R., Sundar, S., and Shukla, J. B.: Modeling the removal of primary and secondary pollutants from the atmosphere of a city by rain, Applied Mathematics and Computation, 179, 282–295, 2006.

Niinemets, U., Loreto, F., and Reichstein, M.: Physiological and physico-chemical controls on foliar volatile organic compound emissions, Trends Plant Sci., 9, 180-186, 2004.

Nozière, B., Barnes, I., and Becker, K.-H.: Product study and mechanisms of the reactions of a-pinene and pinonaldehyde with OH radicals. , J. Geophys. Res., 104, 23645-23656, 1999.

O'Dowd, C. D., Geever, M., and Hill, M. K.: New particle formation: Nucleation rates and spatial scales in the clean marine coastal environment Geophys. Res. Lett., 25, 1661-1664, 1998.

O'Dowd, C. D., Hameri, K., Makela, J., Vakeva, M., Aalto, P. P., de Leeuw, G., Kunz, G. J., Becker, E., Hansson, H. C., Allen, A. G., Harrison, R. M., Berresheim, H., Geever, M., Jennings, S. G., and Kulmala, M.: Coastal new particle formation: Environmental conditions and aerosol physicochemical characteristics during nucleation bursts Journal of Geophysical Research - Atmospheres, 107, 17, 8107 10.1029/2000jd000206, 2002.

Palmer, P. I., Jacob, D. J., Fiore, A. M., Martin, R. V., Chance, K., and Kurosu, T. P.: Mapping isoprene emissions over North America using formaldehyde column observations from space, J. Geophys. Res., 108, 4180, 2003.

Paulson, S. E., and Seinfeld, J. H.: Development and evaluation of a photooxidation mechanism for isoprene. , J. Geophys. Res., 97, 20703-20715, 1992.

Pena, R. M., Garcia, S., Herrero, C., Losada, M., Vazguez, A., and Lucas, T.: Organic acids and aldehydes in rainwater in a northwest region of Spain, Atmos. Environ., 36, 5277-5288, 2002.

Piccot, S. D., Watson, J. J., and Jones, J. W.: A global inventory of volatile organic compound emissions from anthropogenic sources, J. Geophys. Res., 97, 9897-9912, 1992.

Plaß-Dülmer, C., Michl, K., Ruf, R., and Berresheim, H.: C_2 - C_8 hydrocarbon measurement and quality control procedures at the Global Atmosphere Watch Observatory Hohenpeissenberg., J. Chromatogr. A, 953, 175-197, 2002.

Plass-Dülmer, C., Michl, K., Ruf, R., and Berresheim, H.: C_2 - C_8 hydrocarbon measurement and quality control procedures at the Global Atmosphere Watch Observatory Hohenpeissenberg., J. Chromatogr. A, 953, 175-197, 2002.

Prazeller, P., Palmer, P. T., Boscaini, E., Jobson, T., and Alexander, M.: Proton transfer reaction ion trap mass spectrometry, Rapid Communication in Mass Spectrometry, 17, 1593-1599, 2003.

Raes, F., Van Dingenen, R., Cuevas, E., VanVelthoven, P. F. J., and Prospero, J. M.: Observations of aerosols in the free troposphere and marine boundary layer of the subtropical Northeast Atlantic: Discussion of processes determining their size distribution journal of Geophysical Research - Atmospheres, 102, 21315-21328, 1997.

Räisänen, T., Ryyppö, A., and Kellomäki, S.: Monoterpene emission of a boreal Scots pine (Pinus sylvestris L.) forest, Agricultural and forest meteorology, 149, 808 - 819, 2009.

Rao, S. T., Ku, J. Y., Berman, S., Zhang, K., and Mao, H.: Summertime characteristics of the atmospheric boundary-layer and relationships to ozone levels over the eastern U.S., Pure and Applied Geophysics, 160, 21 - 55 2003.

Rasmussen, R. A., and Khalil, M. A. K.: Atmospheric benzene and toluene, Geophys. Res. Lett., 10, 1096-1099, 1983.

Riemer, D., and al., e.: Observations of nonmethane hydrocarbons and oxygenated volatile organic compounds at a rural site in the southeastern United States, J. Geophys. Res., , ,. J. Geophys. Res., 103, 28111 - 28128, 1998.

Riipinen, I., Sihto, S.-L., Kulmala, M., Arnold, F., Dal Maso, M., Birmili, W., Saarnio, K., Teinilä, K., Kerminen, V.-M., Laaksonen, A., and Lehtinen, K. E. J.: Connections between atmospheric sulphuric acid and new particle formation during QUEST III-IV campaigns in Heidelberg and Hyytiälä, Atmospheric Chemistry and Physics, 7, 1899-1914, 2007.

Rinne, H. J. I., Guenther, A. B., Greenberg, J. P., and Harley, P. C.: Isoprene and monoterpene fluxes measured above Amazonian rainforest and their dependence on light and temperature, Atmospheric Environment, 36, 2421-2426, 2002.

Rinne, J., Ruuskanen, T. M., Reissell, A., Taipale, R., Hakola, H., and Kulmala, M.: On-line PTR-MS measurements of atmospheric concentrations of volatile organic compounds in a European boreal forest ecosystem, Boreal Environment Research, 10, 425-436, 2005.

Roberts, J. M.: The atmospheric chemistry of organic nitrates, Atmospheric Environment, 24A, 243-287, ISI:A1990CX36000001, 1990.

Roelofs, G.-J., and Lelieveld, J.: Tropospheric ozone simulation with a chemistry-general circulation model: Influence of higher hydrocarbon chemistry., J. Geophys. Res., 105, 22697-22712, 2000.

Roshchina, V. V., and Roshchina, V. D.: The Excretory Function of Higher Plants, Springer-Verlag, Berlin, 1993.

Rottenberger, S., Kuhn, U., Wolf, A., Schebeske, G., Oliva, S. T., Tavares, T. M., and Kesselmeier, J.: Exchange of short-chain aldehydes between amazonian vegetation and the atmosphere., Ecological Applications 14, S247-S262, 2004.

Ruppert, L., and Becker, K. H.: A product study of the OH radical-initiated oxidation of isoprene: formation of C_5-unsaturated diols, Atmospheric Environment, 34, 1529-1542, 2000.

Ruuskanen, T. M., Taipale, R., Rinne, J., Kajos, M. K., Hakola, H., and Kulmala, M.: Quantitative long-term measurements of VOC concentrations by PTR-MS: annual cycle at a boreal forest site, Atmos. Chem. Phys. Discuss., 9, 81-134, 2009.

Sander, S. P., Friedl, R. R., Golden, D. M., Kurylo, M. J., Moortgat, G. K., Wine, P. H., Ravishankara, A. R., Kolb, C. E., Molina, M. J., Finlayson-Pitts, B. J., Huie, R. E., and Orkin, V. L.: Chemical kinetics and photochemical data for use in atmospheric studies: Evaluation number 15, JPL Publication 02-25, Jet Propulsion Laboratory, Pasadena, 2006.

Sato, E., Matsumoto, K., Okochi, H., and Igawa, M.: Scavenging Effect of Precipitation on Volatile Organic Compounds in Ambient Atmosphere, Bulletin of the Chemical Society of Japan, 79, 1231-1233, 2006.

Schade, G. W., and Goldstein, A. H.: Fluxes of oxygenated volatile organic compounds from a ponderosa pine plantation,, J. Geophys. Res., 106, 3111- 3124, 2001.

Schade, G. W., and Goldstein, A. H.: Increase of monoterpene emissions from a pine plantation as a result of mechanical disturbances, Geophys. Res. Lett., 30, 1380, doi:10.1029/2002GL016138, 2003.

Scheeren, B., Becker, C., and Warsodikromo, T.: The climatology of Suriname with emphasis on the October 2005 GABRIEL campaign, Internal report Max Planck Institute for Chemistry, Mainz, Germany, 2007.

Schumann, U., Dörnbrack, A., and Mayer, B.: Cloud-shadow effects on the stracture of the convective boundary layer, Meteorologische Zeitschrift, 11, 285-294, doi: 10.1127/0941-2948/2002/0011-0285, 2002.

Schwartz, S. E., and Slinn, W. G. N.: Precipitation Scavenging and Atmosphere-Surface Exchange, Precipitation Scavenging and Atmosphere-Surface Exchange, edited by: Schwartz, S. E., and Slinn, W. G. N., Hemisphere Publishing, Washington, D.C., 1992.

Seibert, P., Kromp-kolb, H., Kasper, A., Kalina, M., Puxbaum, H., Jost, D. T., Schwikowski, M., and Baltensperger, U.: Transport of polluted boundary layer air from the Po Valley to high-alpine sites, Atmospheric Environment, 32, 3953-3965, 1998.

Seinfeld, J. H., and Pandis, S. N.: Atmospheric Chemistry and Physics, in, John Wiley & Sons, Inc. , 343-344, 1998.

Sellegri, K., Umann, B., Hanke, M., and Arnold, F.: Deployment of a ground-based CIMS apparatus for the detection of organic gases in the boreal forest during the QUEST campaign, Atmos. Chem. Phys., 5, 357-372, 2005a.

Sellegri, K., Umann, B., Hanke, M., Arnold, F., and Kulmala, M.: Measurements of organic gases during aerosol formation events in the boreal forest atmosphere during QUEST, Atmos. Chem. Phys., 5, 373–384, 2005b.

Sharkey, T. D., Loreto, F., and Delwiche, C. F.: The biochemistry of isoprene emission from leaves during photosynthesis. , in: Trace Gas Emissions by Plants, edited by: Sharkey, T. D., Holland, E. A., and Mooney, H. A., Academic Press, 153-184., 1991.

Sharkey, T. D., and Singsaas, E.: Why plants emit isoprene., Nature, 374, 769, 1995.

Shimmo, M., Jäntti, J., Aalto, P., Hartonen, K., Hyötyläinen, T., Kulmala, M., and Riekkola, M.-L.: Characterisation of organic compounds in aerosol particles from a Finnish forest by on-line coupled supercritical fluid extraction–liquid chromatography–gas chromatography–mass spectrometry, Analytical and Bioanalytical Chemistry, 378, 1982-1990, 2004.

Shu, Y., and Atkinson, R.: Atmospheric lifetimes and fates of a series of sesquiterpenes, J. Geophys. Res., 100, 7275-7281, 1995.

Siebesma, A. P., Christopher, B., Bretherton, S., Brown, A., Chlond, A., Cuxart, J., Duynkerke, P. G., Jiang, H., Khairoutdinov, M., Lewellen, D., Moeng, C.-H., Sanchez, E., Stevens, B., and Stevens, D. E.: A Large Eddy Simulation Intercomparison Study of Shallow Cumulus Convection, Journal of the Atmospheric Sciences, 60, 1201-1219, 2003.

Silver, G., and Fall, R.: Enzymatic synthesis of isoprene from dimethylallyl diphosphate in aspen leaf extracts., Plant Physiology, 97, 1588-1691, 1991.

Simcik, M. F.: The importance of surface adsorption on the washout of semivolatile organic compounds by rain, Atmospheric environment, 38, 491-501, 2004.

Simpson, D., Winiwarter, W., Börjesson, G., Cinderby, S., Ferreiro, A., Guenther, A., Hewitt, C. N., Janson, R., Aslam, M., Khalil, K., Owen, S., Pierce, T. E., Puxbaum, H., Shearer, M., Skiba, U., Steinbrecher, R., Tarraso´n, L., and Öquist, M. G.: Inventorying emissions from nature in Europe, J. Geophys. Res., 104, 8113-8152, 1999.

Singh, H. B., Salas, L. J., Cantrell, B. K., and Redmont, R. M.: Distribution of aromatic hydrocarbons in the ambient air, Atmospheric Environment, 19, 1911-1919, 1985.

Singh, H. B., and Zimmerman, P.: Atmospheric distribution and sources of nonmethane hydrocarbons. , Gaseous Pollutants: Characterization and Cycling, edited by: Nriagu, J. O., John Wiley and Sons, 155-174 pp., 1992.

Singh, H. B., O'Hara, D., Herlth, D., Sachse, W., Blake, D. R., Bradshaw, J. D., Kanakidou, M., and Crutzen, P. J.: Acetone in the atmosphere: distribution, sources and sinks, J. Geophys. Res., 99, 1805-1819, 1994.

Singh, H. B., Kanakidou, M., Crutzen, P. J., and Jacob, D. J.: High concentrations and photochemical fate of oxygenated hydrocarbons in the global troposphere, Nature, 378, 50 - 54, 1995.

Singh, H. B., Chen, Y., Tabazadeh, A., Fukui, Y., Bey, I., Yantosca, R., Jacob, D., Arnold, F., Wohlfrom, K., Atlas, E., Flocke, F., Blake, D., Blake, N., Heikes, B., Snow, J., Talbot, R., Gregory, G., Sachse, G., Vay, S., and Kondo, Y.: Distribution and fate of selected oxygenated organic species in the troposphere and lower stratosphere over the Atlantic, J. Geophys. Res., 105, 3795-3805, 2000.

Singh, H. B., Chen, Y., Staudt, A., Jacob, D., Blake, D., Heikes, B., and Snow, J.: Evidence from Pacific troposphere for large global sources of oxygenated organic compounds, Nature, 410, 1078-1081, 2001.

Singh, H. B., Salas, L. J., Chatfield, R. B., Czech, E., Fried, A., Walega, J., Evans, M. J., Field, B. D., Jacob, D. J., Blake, D. R., Heikes, B. G., Talbot, R., Sachse, G., Crawford, J. H., Avery, M. A., Sandholm, S., and Fuelberg, H.: Analysis of the atmospheric distribution, sources, and sinks of oxygenated volatile organic chemicals based on measurements over the Pacific during TRACE-P, J. Geophys. Res., 109, S07, doi:10.1029/2003JD003883, 2004.

Sinha, V., Williams, J., Crutzen, P., and Lelieveld, J.: Methane emissions from boreal and tropical forest ecosystems derived from in-situ measurements, Atmos. Chem. Phys. Discuss., 7, 14011- 14039, 2007a.

Sinha, V., Williams, J., Meyerhofer, M., Riebesell, U., Paulino, A. I., and Larsen, A.: Air-sea fluxes of methanol, acetone, acetaldehyde, isoprene and DMS from a Norwegian fjord following a phytoplankton bloom in a mesocosm experiment Atmospheric Chemistry and Physics, 7, 739-755, 2007b.

Sinha, V., Williams, J., Crowley, J., and Lelieveld, J.: The Comparative Reactivity Method - A new tool to measure the total OH Reactivity of ambient air, Atmos. Chem. Phys., 8, 2213-2227, 2008.

Smith, P. L.: Raindrop size distributions: Exponential or gamma - does the difference matter?, J. Appl. Meteorol., 42, 1031-1034, 2003.

Spanke, J., Rannik, U., Forkel, R., Nigge, W., and Hoffmann, T.: Emission fluxes and atmospheric degradation of Monoterpenes above a boreal forest: field measurements and modeling, Tellus B, 53, 406-422, 2001.

Stickler, A., Fischer, H., Bozem, H., Gurk, C., Schiller, C., Martinez-Harder, M., Kubistin, D., Harder, H., Williams, J., Eerdekens, G., Yassaa, N., Ganzeveld, L., Sander, R., and Lelieveld, J.: Chemistry, transport and dry deposition of trace gases in the boundary layer over the tropical Atlantic Ocean and the Guyanas during the GABRIEL field campaign, Atmospheric Chemistry and Physics, 7, 3933-3956, 2007.

Stroud, C. A., Roberts, J. M., Goldan, P. D., Kuster, W. C., Murphy, P. C., Williams, E. J., Hereid, D., Parrish, U. D., Sueper, D., Trainer, M., Fehsenfeld, F. C., Apel, E. C., Riemer, D., Wert, B., Henry, B., Fried, A., Martinez-Harder, M., Harder, H., Brune, W. H., Li, G., Xie, H., and Young, V. L.: Isoprene and its oxidation products, methacrolein and methyl vinyl ketone, at an urban forested site during the 1999 Southern Oxidants Study, J. Geophys. Res., 106, 8034- 8046, 2001.

Stull, R. B.: An introduction to boundary layer meteorology., Kluwer Academic Publishers, Dordrecht, 1988.

Su, T., and Chesnavich, W. J.: Parametrization of the ion-polar molecule collision rate-constant by trajectory calculations, J. Chem. Phys., 76, 5183-5185, 1982.

Taipale, R., Ruuskanen, T. M., Rinne, J., Kajos, M. K., Hakola, H., Pohja, T., and Kulmala, M.: Technical Note: Quantitative long-term measurements of VOC concentrations by PTR-MS – measurement, calibration, and volume mixing ratio calculation methods, Atmos. Chem. Phys., 8, 6681–6698, 2008.

Tang, Y., Carmichael, G. R., Uno, I., Woo, J.-H., Kurata, G., Lefer, B., Shetter, R. E., Huang, H., Anderson, B. E., Avery, M. A., Clarke, A. D., and Blake, D. R.: Impacts of aerosols and clouds on photolysis frequencies and photochemistry during TRACE-P: 2. Three-dimensional study using a regional chemical transport model, J. Geophys. Res., 108, 8822, DOI: 10.1029/2002JD003100, 2003.

Tie, X., Guenther, A., and Holland, E.: Biogenic methanol and its impacts on tropospheric oxidants, Geophys. Res. Lett., 30, 1881, doi:10.1029/2003GL01716, 2003.

Trainer, M., Williams, E. J., Parrish, D. D., Buhr, M. P., and Allwine, E. J.: Models and observations of the impact of natural hydrocarbons on rural ozone, Nature, 329, 705–707, 1987.

Trainer, M., Ridley, B. A., Buhr, M. P., Kok, G., Walega, J., Hübler, G., Parrish, D. D., and Fehsenfeld, F. C.: Regional ozone and urban plumes in the southeastern United States: Birmingham, a case study., J. Geophys. Res., 100, 18823-18834, 1995.

Tunved, P., Hansson, H.-C., Kerminen, V.-M., Ström, J., Dal Maso, M., Lihavainen, H., Viisanen, Y., Aalto, P. P., Komppula, M., and Kulmala, M.: High Natural Aerosol Loading over Boreal Forests, Science, 312, 261-263, 2006.

Tyndall, G. S., Cox, R. A., Granier, C., Lesclaux, R., Moortgat, G. K., Pilling, M. J., Ravishankara, A. R., and Wallington, T. J.: Atmospheric chemistry of small organic peroxy radicals, J. Geophys. Res., 106, 12,157- 112,182, 2001.

UNEP-WCMC, Forest Protection Analysis June 2000: http://www.unep-wcmc.org/forest/datasets_maps.htm, access: November, 2006, 2000.

Väkeva, M., Hämeri, K., Puhakka, T., Nilsson, E. D., Hohti, H., and Mäkela, J. M.: Effects of meteorological processes on aerosol particle size distribution in an urban background area., J. Geophys. Res., 105, 9807-9821, 2000.

Valverde-Canossa, J.: Sources and Sinks or Organic Peroxides in the Planetary Boundary Layer., PhD, Johannes Gutenberg, Mainz, Germany, 2004.

Vana, M., Kulmala, M., Dal Maso, M., Horrak, U., and Tamm, E.: Comparative study of nucleation mode aerosol particles and intermediate air ions formation events at three sites, Journal of Geophysical Research - Atmospheres, 109, 201, 2004.

Vesala, T., Haataja, J., Aalto, P., Altimir, N., Buzorius, G., Garam, E., Hämeri, K., Ilvesniemi, H., Jokinen, V., Keronen, P., Lahti, T., Markkanen, T., Mäkelä, J. M., Nikinmaa, E., Palmroth, S., Palva, L., Pohja, T., Pumpanen, J., Rannik, U., Siivola, E., Ylitalo, H., Hari, P., and Kulmala, M.: Long-term field measurements of atmospheresurface interactions in boreal forest combining forest ecology, micrometeorology, aerosol physics and atmospheric chemistry., Trends in Heat, Mass, Momentum Transfer, 4, 17-35, 1998.

Vesala, T., Suni, T., Rannik, Ü., Keronen, P., Markkanen, T., Sevanto, S., Grönholm, T., Smolander, S., Kulmala, M., Ilvesniemi, H., Ojansuu, R., Uotila, A., Levula, J., Mäkelä, A., Pumpanen, J., Kolari, P., Kulmala, L., Altimir, N., Berninger, F., Nikinmaa, E., and Hari, P.: Effect of thinning on surface fluxes in a boreal forest, Global Biogeochem. Cycles, 19, 1-11, 2005.

Viehland, L. A., and Mason, E. A.: Transport properties of gaseous ions over a wide energy range., At. Data Nucl. Data Tables, 60, 1995.

Viggiano, A. A., and Morris, R. A.: Rotational and Vibrational Energy Effects on Ion-Molecule Reactivity As Studied by the VT-SIFDT Technique, J. Phys. Chem., 100, 19227, 1996.

Vilà-Guerau de Arellano, J., Kim, S.-W., Barth, M. C., and Patton, E. G.: Transport and chemical transformations influenced by shallow cumulus over land, Atmos. Chem. Phys., 5, 3219-3231, 2005.

Vilà-Guerau de Arellano, J.: Role of nocturnal turbulence and advection in the formation of shallow cumulus over land, Quaterly Journal Of The Royal Meteorological Society, 133, 1615-1627, 2007.

Vilà-Guerau de Arellano, J., van den Dries, K., and Pino, D.: On inferring isoprene emission surface flux from atmospheric boundary layer concentration measurements, Atmos. Chem. Phys., 9, 3629-3640, 2009.

von Kuhlmann, R., Lawrence, M. G., Pöschl, U., and Crutzen, P. J.: Sensitivities in global scale modeling of isoprene, Atmos. Chem. Phys., 4, 1-17, 2004.

Walcek, C. J., and Pruppacher, H. R.: On the scavenging of SO_2 by cloud and raindrops: I. A theoretical study of SO_2 absorption and desorption for water drops in air, J. Atmos. Chem., 1, 269-289, 1984.

Warneke, C., Karl, T., Judmaier, H., Hansel, A., Jordan, A., and Lindinger, W.: Acetone, methanol, and other partially oxidized volatile organic emissions from dead plant matter by abiological processes: Significance for atmospheric HOx chemistry, Global Biogeochem. Cycles, 13, 9 -17, 1999.

Warneke, C., Holzinger, R., Hansel, A., Jordan, A., Lindinger, W., Pöschl, U., Williams, J., Hoor, P., Fischer, H., Crutzen, P. J., Scheeren, H. A., and Lelieveld, J.: Isoprene and its oxidation products methyl vinyl ketone, methacrolein, and isoprene related peroxides measured online over the tropical rain forest of Surinam in March 1998., J. Atmos. Chem., 38, 167-185, 2001a.

Warneke, C., van der Veen, C., Luxembourg, S., de Gouw, J. A., and Kok, A.: Measurements of benzene and toluene in ambient air asing Proton-Transfer-Reaction Mass Spectrometry: calibration, humidity dependence, and field intercomparison, International Journal of Mass Spectrometry, 207, 167-182, 2001b.

Warneke, C., Luxembourg, S. L., de Gouw, J. A., Rinne, H. J. I., Guenther, A. B., and Fall, R.: Disjunct eddy covariance measurements of oxygenated volatile organic compounds fluxes from an alfalfa field before and after cutting, J. Geophys. Res., 107, 4067, 4010.1029/2001JD000594, 2002.

Warneke, C., de Gouw, J. A., Goldan, P. D., Kuster, W. C., and Fall, R.: Validation of atmospheric measurements by proton-transfer-reaction mass spectrometry using a gas-chromatographic pre-separation method, Environ. Sci. Tech., 37, 2494-2501, 2003.

Warneke, C., Rosen, S., Lovejoy, E. R., de Gouw, J. A., and Fall, R.: Two Additional Advantages of Proton Transfer Ion Trap Mass Spectrometer (PT-ITMS), Rapid Communication in Mass Spectrometry, 18, 133-134, 2004.

Warneke, C., de Gouw, J. A., Lovejoy, E. R., Murphy, P., Kuster, W. C., and Fall, R.: Development of Proton Transfer Ion Trap - Mass Spectrometry (PIT-MS): On-line Detection and Identification of Volatile Organic Compounds in Air, Environ. Sci. Technol., 2005, 5390, 2005.

Weber, R. J., Marti, J. J., McMurry, P. H., Eisele, F. L., Tanner, D. J., and Jefferson, A.: Measurements of new particle formation and ultrafine particle growth rates at a clean continental site Journal of Geophysical Research - Atmospheres, 102, 4375-4385, 1997.

Weber, R. J., McMurry, P. H., Mauldin, R. L., Tanner, D. J., Eisele, F. L., Clarke, A. D., and Kapustin, V. N.: New particle formation in the remote troposphere: A comparison of observations at various sites, Geophys. Res. Lett., 26, 307-310 1999.

Williams, J., Pöschl, U., Crutzen, P. J., Hansel, A., Holzinger, R., Warneke, C., Lindinger, W., and Lelieveld, J.: An atmospheric chemistry interpretation of mass scans obtained from a proton transfer mass spectrometer flown over the tropical rainforest of Surinam, J. Atmos. Chem., 38, 133-166, 2001.

Williams, J., Holzinger, R., Gros, V., Xu, X., Atlas, E., and Wallace, D. W. R.: Measurements of organic species in air and seawater from the tropical Atlantic, Geophys. Res. Lett., 31, 5, 2004.

Williams, J., Yassaa, N., Bartenbach, S., and Lelieveld, J.: Mirror image hydrocarbons from Tropical and Boreal forests, Atmospheric Chemistry and Physics, 6, 973–980, 2007.

Xu, X., Williams, J., Plaß-Dülmer, C., Berresheim, H., Salisbury, G., Lange, L., and Lelieveld, J.: GC×GC measurements of C_7- C_{11} aromatic and n-alkane hydrocarbons on Crete, in air from Eastern Europe during the MINOS campaign, Atmos. Chem. Phys., 3, 1461-1475, 2003.

Yassaa, N., and Williams, J.: Analysis of enantiomeric and non-enantiomeric monoterpenes in plant emissions using portable dynamic air sampling/solid-phase microextraction (PDAS-SPME) and chiral gas chromatography/mass spectrometry Atmospheric Environment, 39, 4875-4884, 2005.

Yassaa, N., and Williams, J.: Enantiomeric monoterpene emissions from natural and damaged Scots pine in a boreal coniferous forest measured using solid-phase microextraction and gas chromatography/mass spectrometry, Journal of Chromatography A 1141, 138-144 2007.

Yienger, J. J., and Levy, I., H.: Global inventory of soil-biogenic NOx emissions., J. Geophys. Res., 100, 11447-11646, 1995.

Yokouchi, Y.: Seasonal and diurnal variation of isoprene and its reaction products in a semirural area, Atmospheric Environment, 28, 2651-2658, 1994.

Yu, F. Q., and Turco, R. P.: Ultrafine aerosol formation via ion-mediated nucleation Geophys. Res. Lett., 27, 883-886, 2000.

Yu, J. Z., Griffin, R. J., Cocker, D. R., Flagan, R. C., Seinfeld, J. H., and Blanchard, P.: Observation of gaseous and particulate products of monoterpene oxidation in forest atmospheres, Geophys. Res. Lett., 26, 1145-1148, 1999.

Zhang, K., Mao, H., Civerolo, K., Berman, S., Ku, J.-Y., Rao, S. T., Doddridge, B., Philbrick, C. R., and Clark, R.: Numerical investigation of boundary layer evolution and nocturnal low-level jets: local versus non-local PBL schemes, Environ. Fluid Mech., 1, 171-208, 2001.

Zhang, R., Suh, I., Zhao, J., Zhang, D., Fortner, E. C., Tie, X., Molina, L. T., and Molina, M. J.: New particle formation enhanced by organic acids, Science, 304, 1487-1490, DOI: 10.1126/science.1095139, 2004.

Zimmerman, P. R., Greenberg, J. P., and Westberg, C. E.: Measurements of atmospheric hydrocarbons and biogenic emission fluxes in the Amazon boundary layer, J. Geophys. Res., 93, 1407–1416, 1988.